

A GLOBAL FREE-RADICAL MECHANISM FOR NITROGEN RELEASE DURING
COAL DEVOLATILIZATION BASED ON CHEMICAL STRUCTURE

by
Steven T. Perry

A dissertation submitted to the faculty of
Brigham Young University
in partial fulfillment of the requirements for the degree of
Doctor of Philosophy

Department of Chemical Engineering
Brigham Young University
December 1999

BRIGHAM YOUNG UNIVERSITY

GRADUATE COMMITTEE APPROVAL

of a dissertation submitted by

Steven T. Perry

This dissertation has been read by each member of the following graduate committee and by majority vote has been found to be satisfactory.

Date

Thomas H. Fletcher, Chair

Date

Ronald J. Pugmire

Date

John N. Harb

Date

William C. Hecker

Date

John L. Oscarson

BRIGHAM YOUNG UNIVERSITY

As chair of the candidate's graduate committee, I have read the dissertation of Steven T. Perry in its final form and have found that (1) its format, citations, and bibliographical style are consistent and acceptable and fulfill the university and department style requirements; (2) its illustrative materials including figures, tables, and charts are in place; and (3) the final manuscript is satisfactory to the graduate committee and is ready for submission to the university library.

Date

Thomas H. Fletcher
Chair, Graduate Committee

Accepted for the Department

Kenneth A. Solen
Department Chair

Accepted for the College

Douglas M. Chabries
Dean, College of Engineering and Technology

ABSTRACT

A GLOBAL FREE-RADICAL MECHANISM FOR NITROGEN RELEASE DURING COAL DEVOLATILIZATION BASED ON CHEMICAL STRUCTURE

Steven T. Perry

Department of Chemical Engineering

Doctor of Philosophy

As the pulverized coal combustion industry faces increasingly stringent NO_x emission regulations, cost-effective low-NO_x strategies like local fuel/air staging are important. Although most coal combustion NO_x originates from nitrogen in the coal, the rate of nitrogen release from coal is currently treated empirically when modeling these low-NO_x techniques. The objective of this research was to develop a model that relates nitrogen release from coal during devolatilization to the changes in the chemical structure of the char.

Thirty-four rapid pyrolysis tests were performed using coals from around the world ranging in rank from brown coal to low volatile bituminous. Trends in measured tar yields and total volatiles yields as a function of temperature between 900 and 1650 K were distinctly different for different ranks of coal.

Matched tar/char sets from both lignite and bituminous coals pyrolyzed at increasingly severe conditions were analyzed by solid-state ¹³C NMR. At about 1250 K,

tars and chars showed evidence of both ring opening and cluster growth reactions, neither of which appeared to accelerate nitrogen release via ring rupture. Several ^{13}C NMR chemical structural parameters from these experiments and from published studies showed a strong correlation with light gas nitrogen release, suggesting a mechanism other than the pure thermal decomposition seen in pyrolysis of model compounds (i.e. pyridine or pyrrole). Accordingly, a nitrogen model using a three-step free-radical global mechanism was developed to model light gas nitrogen release. This nitrogen model requires only a network devolatilization model and coal-specific chemical structural input data to adequately predict the nitrogen distribution among pyrolysis products. Because the model is based on char chemical structure it is very robust, accurately describing nitrogen release characteristics even for conditions far different from those used in the model development. The model is the first to describe the rank dependence of nitrogen release as light gas without the use of correlations. The model is also the first to offer reasonable explanations for the observed release of ring nitrogen at relatively low temperatures and the inherent stability of much of the char nitrogen during pyrolysis; observations not easily explained by a simple thermal decomposition model alone.

ACKNOWLEDGMENTS

I would like to thank my wife Teresa for her unwavering support and encouragement throughout the pursuit of yet another degree. I believe this degree will continue to be a blessing to Teresa and our family. I would like to thank Dr. Thomas H. Fletcher for his guidance, friendship, and significant investment of time and resources on my behalf. I have learned many things through his daily conduct and leadership. Special thanks to Dr. Mark Solum and Dr. Ronald J. Pugmire at the University of Utah who performed all the ^{13}C NMR analyses upon which this project heavily relied. I gratefully acknowledge Jon and Karen Huntsman for a generous fellowship. Thanks to NEDO (Japan) for sponsoring this project. Funding contributed by ACERC is also appreciated.

I would like to thank those with whom I have exchanged so many ideas from which this work been refined and has blossomed, namely Dominic Genetti, Eric Hambly, Haifeng Zhang, Jianhui Hong, Jared Parker, Paul and Mary Goodman, Todd Salisbury, and Josh Wang. Thanks to Dan Clayton who helped perform the flat flame reactor pyrolysis experiments. I am especially indebted to Jared Parker, who is destined for great things, for his help with drop tube pyrolysis tests and the sample splitter, and for caring as much as I do about discovering truth. Lastly I thank God, from whom, I believe, all good or creative things in this dissertation were given.

Table of Contents

List of Figures.....	xi
List of Tables.....	xvii
Nomenclature.....	xix
1. Introduction	1
Background.....	1
Organization of this Dissertation.....	3
2. Literature Review.....	5
Coal Chemical Structural Evolution During Devolatilization	6
Bridge Breaking and Tar Release.....	8
Cross-linking.....	8
Early Light Gas Release.....	9
Severe Pyrolysis.....	9
Nitrogen Speciation in Coal	10
Nitrogen Speciation Progression During Pyrolysis.....	11
Nitrogen Release From Coal Char.....	12
Nitrogen release by tar transport.....	12
Nitrogen release by ring rupture	13
Total Pyrolytic Nitrogen Release.....	14
Nitrogen Release Modeling.....	15
3. Objectives and Approach	21
4. Description of Experiments.....	23
Drop Tube Reactor.....	23

Flat-Flame Reactor (FFR)	26
Coal Selection.....	26
Sample Preparation, Storage and Analysis	29
Sample Characterization.....	29
Determination of Elemental Composition.....	30
Determination of Ash, Moisture, and Volatile Matter.....	30
Determination of Total Mass Release by Tracer.....	31
¹³ C NMR Chemical Structure Determination.....	31
HCN and NH ₃ Quantification.....	32
Experimental Test Matrix	33
5. Experimental Results and Discussion.....	37
Proximate/Ulimate Results.....	37
Error Analysis.....	42
Chemical Structure Results (¹³ C NMR).....	46
Analysis of Mass Release and Tar Data.....	46
Analysis of Nitrogen Distribution Data.....	56
Analysis of Chemical Structure Data	60
6. Nitrogen Chemical Structure Analysis.....	67
Definition of N _{site}	67
Justification of the use of N _{site}	69
Nitrogen Functionality Analysis	73
Relationship of N _{site} and M _{cl}	74
7. Nitrogen Release Model	81
Model Development	81
Free-Radical Global Mechanism.....	84
Discussion of Free-Radical Mechanism.....	85
Fast Light Gas Nitrogen Release.....	87

Slow Light Gas Nitrogen Release	90
Other Mechanisms.....	91
Nitrogen Distribution Calculation.....	91
Devolatilization Modeling Procedure.....	93
Rate Constant Regression for the Nitrogen Model.....	96
Evaluation of the Nitrogen Release Model.....	98
N_{site} Predictions	99
Nitrogen Distribution Predictions.....	106
8. Summary and Conclusions.....	121
Pyrolysis Tests.....	122
Char and Tar Chemical Structure	122
Nitrogen Release Model.....	124
9. Recommendations.....	125
Improving Precision and Usefulness of Pyrolysis Data.....	125
Ideas for Future Work.....	126
References.....	129
Appendices	137
Appendix A: Temperature Correction.....	139
Appendix B: Drop Tube Procedures.....	141
Appendix C: Experimental Pyrolysis Conditions	145
Appendix D: Tabulation of Experimental Data.....	147
Appendix E: Additional Pyrolysis Test Results and Discussion.....	161
Appendix F: Analysis of CPD Tar and Total Volatiles Predictions	167
Appendix G: Gas Field Simulations for Drop Tube Tests	171
Appendix H: Sample CPD Model Input Files	183
Appendix I: Nitrogen Model Predictions.....	185

List of Figures

Figure 2.1	Schematic of the devolatilization process	5
Figure 2.2	The structure of a hypothetical coal molecule.....	7
Figure 4.1.	Schematic of Drop Tube Reactor with pre-heater attached.....	24
Figure 4.2.	Schematic of Drop Tube Reactor configuration.....	25
Figure 4.3.	Schematic of Flat Flame Burner (FFB)	27
Figure 4.4.	Van Krevelen coalification diagram for coals used in this study.....	28
Figure 4.5	Matrix of experimental pyrolysis tests.....	33
Figure 5.1.	Tar yield and total mass release compared to Xu and Tomita.....	50
Figure 5.2.	Validation of % daf mass release from tracer measurements	52
Figure 5.3.	Comparison of ultimate mass release with daf ASTM volatile matter ...	53
Figure 5.4.	Comparison of total volatiles release by Ma and coals in this study.....	54
Figure 5.5.	Variation of measured total volatiles yields with pyrolysis severity.	55
Figure 5.6.	Variation of measured tar and soot yields with pyrolysis severity.....	57
Figure 5.7.	The fraction of coal nitrogen in the tar versus tar yield.....	60
Figure 5.8.	Trend with temperature of bridges and loops per cluster (B.L.)	61
Figure 5.9.	Trend with temperature of aromatic carbons per cluster.....	62
Figure 5.10.	Trend with temperature of side chains per cluster (S.C.)	62
Figure 5.11.	A hypothetical reaction for carboxyl formation in coal char	63
Figure 5.12.	Trend with temperature of fraction of carbon which is carbonyl.....	64
Figure 5.13.	Trend with temperature of the fraction of carbon which is aromatic (f_a)	64
Figure 6.1.	Parity plot comparing char N/AC and char N_{site}	69
Figure 6.2.	Balance on aromatic carbon for South Banko and Pittsburgh.....	70

Figure 6.3.	Estimated aromatic mass balance at the 1100 K condition.....	71
Figure 6.4.	N/C ratios for South Banko and Pittsburgh chars and tars	73
Figure 6.5.	Comparison of the change in N/AC by XPS N functionality.....	74
Figure 6.6.	Comparison of the trend with rank for char N_{site} and M_{cl}	76
Figure 6.7.	Comparison of the trend with pyrolysis time for N_{site} and M_{cl}	77
Figure 6.8.	Comparison of normalized N_{site} and M_{cl} for chars and tars	78
Figure 6.9.	Comparison of normalized N_{site} and M_{cl} for chars and tars	79
Figure 7.1.	Schematic showing the fate of coal N at various stages of pyrolysis....	83
Figure 7.2.	Particle trajectory assumed in modeling gas T and velocity profiles....	94
Figure 7.3.	Gas temperature profiles for the 900 K drop tube condition.....	95
Figure 7.4.	Gas temperature profiles for the 1000 K drop tube condition.....	95
Figure 7.5.	Predicted N_{site} compared to data published by Fletcher and Hardesty..	100
Figure 7.6.	Predicted N_{site} compared to data for chars at 1100 K condition.	101
Figure 7.7.	Trend with rank of N_{site} decay for chars at the 1100 K condition.....	102
Figure 7.8.	Trend with parent coal O/N ratio for chars at the 1100 K condition....	104
Figure 7.9.	Predicted N_{site} compared to data of Hambly at 1080 K and 820 K.....	105
Figure 7.10.	Predicted char N/AC values compared to values measured by XPS as reported by Kelemen.....	106
Figure 7.11.	Comparison of predicted total light gas N yields with data of Bassilakis et al. for 0.5 K/sec pyrolysis of the Argonne premium coals.....	107
Figure 7.12.	Comparison of predictions with predictions of Niksa and data of Friehtaut for light gas N and tar N yields.....	108
Figure 7.13.	Comparison of predicted and measured mass and nitrogen release for Curie point pyrolysis experiments reported by Nomura.....	109
Figure 7.14.	Comparison of predicted total light gas release and measured HCN release for Curie point pyrolysis at 943 K and 1313 K by Nomura....	110
Figure 7.15.	Predicted and measured tar and tar nitrogen yields for drop tube data of Hambly at 1080 K.....	111
Figure 7.16.	Predicted and measured mass and nitrogen release for drop tube data of Hambly at 1080 K.....	111
Figure 7.17.	Parity plot of predicted, measured char N content for data of Hambly.	112

Figure 7.18.	Predicted and measured char nitrogen content and char N_{site} for a North Dakota lignite pyrolyzed in a drop tube reactor at Sandia.....	113
Figure 7.19.	Predicted and measured nitrogen release for a lignite and a bituminous coal in drop tube of Pohl and Sarofim.....	114
Figure 7.20.	Predicted nitrogen release for a bituminous coal pyrolyzed in a crucible at 2100 K and 1750 K for very long residence times.....	114
Figure 7.21.	Predicted and measured mass and nitrogen release for flat flame reactor pyrolysis data of Genetti at 1650 K and 78 ms.....	115
Figure 7.22.	Predicted and measured tar and tar nitrogen yields and mass and nitrogen release for drop tube and FFR pyrolysis test of this study.....	116
Figure 7.23.	Predicted and measured tar and tar nitrogen yields and mass and nitrogen release at 1100 K and 1650 K using correlation of Genetti et al.....	118
Figure 7.24.	Predicted and measured char nitrogen contents for drop tube and flat flame reactor pyrolysis experiments.....	119
Figure E.1.	Nitrogen release and mass release for preliminary FFR tests.....	164
Figure E.2.	Correlation of daf mass and N yields in soot for preliminary FFR tests	165
Figure E.3.	Light gas N release and mass release for preliminary FFR tests.....	165
Figure F.1.	Comparison of measured and predicted tar release for drop tube tests.	168
Figure F.2.	Comparison of measured and predicted total volatiles release for drop tube and FFR tests	170
Figure G.1.	Schematic of drop tube flow straightener and dimensions.....	172
Figure G.2.	Axi-symmetric schematic of drop tube and dimensions.....	173
Figure G.3.	Schematic of drop tube collection probe and dimensions.....	174
Figure G.4.	Schematic showing drop tube injection probe dimensions.....	175
Figure G.5.	Particle trajectory assumed in modeling gas field for drop tube tests...	177
Figure G.6.	Gas temperature profiles for the 900 K drop tube condition.....	177
Figure G.7.	Gas temperature profiles for the 1000 K drop tube condition.....	178
Figure G.8.	Gas temperature profiles for the 1100 K drop tube condition.....	178
Figure G.9.	Gas temperature profiles for the 1250 K drop tube condition.....	179
Figure G.10.	Gas velocity profiles for the 900 K drop tube condition.....	179
Figure G.11.	Gas velocity profiles for the 1000 K drop tube condition.....	180

Figure G.12.	Gas velocity profiles for the 1100 K drop tube condition.....	180
Figure G.13.	Gas velocity profiles for the 1250 K drop tube condition.....	181
Figure I.1.	Predicted tar, char, and light gas N compared to data of Chen for Dietz coal.....	186
Figure I.2.	Predicted tar, char, and light gas N compared to data of Chen for Illinois #6 coal.....	186
Figure I.3.	Predicted tar, char, and light gas N compared to data of Chen for Pittsburgh #8 coal.....	187
Figure I.4.	Predicted tar, char, and light gas N compared to data of Chen for Lower Kittanning coal.....	187
Figure I.5.	Predicted mass and N release compared to 1050 K Sandia data	188
Figure I.6.	Predicted mass and N release compared to 1250 K Sandia data	189
Figure I.7.	Predicted mass and N release compared to 1600 K Sandia data (FFR)	189
Figure I.8.	Predicted and measured char nitrogen content for a North Dakota lignite pyrolyzed at 1050 K at Sandia.....	190
Figure I.9.	Predicted and measured char nitrogen content and char N_{site} for a North Dakota lignite pyrolyzed at 1250 K at Sandia.....	190
Figure I.10.	Predicted and measured char nitrogen content and char N_{site} for Blue #1 coal pyrolyzed at 1050 K at Sandia	191
Figure I.11.	Predicted and measured char nitrogen content and char N_{site} for Blue #1 coal pyrolyzed at 1250 K at Sandia	191
Figure I.12.	Predicted and measured char nitrogen content for Illinois #6 coal pyrolyzed at 1050 K at Sandia.....	192
Figure I.13.	Predicted and measured char nitrogen content and char N_{site} for Illinois #6 coal pyrolyzed at 1250 K at Sandia	192
Figure I.14.	Predicted and measured char nitrogen content for Pittsburgh #8 coal pyrolyzed at 1050 K at Sandia.....	193
Figure I.15.	Predicted and measured char nitrogen content and char N_{site} for Pittsburgh #8 coal pyrolyzed at 1250 K at Sandia.....	193
Figure I.16.	Predicted and measured char nitrogen content and char N_{site} for Pocahontas #3 coal pyrolyzed at 1050 K at Sandia	194
Figure I.17.	Predicted and measured char nitrogen content and char N_{site} for Pocahontas #3 coal pyrolyzed at 1250 K at Sandia	194
Figure I.18.	Comparison of predicted total light gas N yields with data of Bassilakis et al. for 0.5 K/sec pyrolysis of the Argonne premium coals.....	195

Figure I.19.	Comparison of predictions with predictions of Niksa and data of Friehaut for light gas N and tar N yields.....	195
Figure I.20.	Comparison of predicted and measured mass and nitrogen release for Curie point pyrolysis experiments reported by Nomura.....	196
Figure I.21.	Comparison of predicted and measured total light gas N and tar N release for furnace pyrolysis (10 K/s) of 8 coals at 1273 K by Nomura.....	197
Figure I.22.	Comparison of predicted total light gas release and measured HCN release for Curie point pyrolysis at 943 K and 1313 K by Nomura....	197
Figure I.23.	Predicted and measured tar and tar nitrogen yields for drop tube data of Hambly at 1080 K.....	198
Figure I.24.	Predicted and measured mass and nitrogen release for drop tube data of Hambly at 1080 K.....	198
Figure I.25.	Parity plot of predicted, measured char N content for data of Hambly.	199
Figure I.26.	Predicted and measured nitrogen release for a lignite and a bituminous coal in drop tube of Pohl and Sarofim.....	199
Figure I.27.	Predicted nitrogen release for a bituminous coal pyrolyzed in a crucible at 2100 K and 1750 K for very long residence times.....	200
Figure I.28.	Predicted and measured mass and nitrogen release for flat flame reactor pyrolysis data of Genetti at 1650 K and 78 ms.....	200
Figure I.29.	Predicted and measured tar and tar nitrogen yields and mass and nitrogen release for drop tube and FFR pyrolysis test of this study.....	201
Figure I.30.	Predicted and measured tar and tar nitrogen yields and mass and nitrogen release at 1100 K and 1650 K using correlation of Genetti et al.....	202
Figure I.31.	Predicted and measured char nitrogen contents for drop tube and flat flame reactor pyrolysis experiments.....	203

List of Tables

Table 2.1	Summary of pyrolysis studies for investigation of nitrogen release.....	16
Table 4.1	Summary of drop tube and the flat flame reactor conditions.....	34
Table 5.1	Proximate/Ultimate analyses of the coals used in this study.....	37
Table 5.2	Summary of ultimate analyses, dry ash, and mass release (%MR).....	38
Table 5.3	Summary of ultimate analyses and yields of tars/soots.....	40
Table 5.4	Replicate sample characterization for chars from the 950 K condition ..	42
Table 5.5	Replicate elemental determination for char produced in the drop tube...	45
Table 5.6	¹³ C NMR measured parameters for chars from the drop tube and FFR.	47
Table 5.7	¹³ C NMR measured parameters for tars from the drop tube and FFR...	48
Table 5.8	¹³ C NMR derived parameters for chars from the drop tube and FFR ...	49
Table 5.9	¹³ C NMR derived parameters for tars from the drop tube and FFR	50
Table 5.10	Distribution of nitrogen in pyrolysis products.....	58
Table 7.1	Summary of free-radical mechanism parameters used in this study.	98
Table C.1	Summary of settings used in drop tube pyrolysis experiments.....	145
Table C.2	Summary settings used during FFR pyrolysis experiments.....	146
Table D.1	Measured drop tube centerline gas temperatures by condition.....	147
Table D.2	Measured FFR centerline gas temperatures and velocity.....	148
Table D.3	Preliminary proximate/ultimate analysis of Yallourn coal.....	149
Table D.4	Preliminary proximate/ultimate analysis of South Banko coal.....	149
Table D.5	Preliminary proximate/ultimate analysis of Taiheiyo coal.....	150
Table D.6	Preliminary proximate/ultimate analysis of Miike coal	150
Table D.7	Preliminary proximate/ultimate analysis of Hunter Valley coal.....	151

Table D.8	Summary of ultimate analyses and ash for preliminary FFR chars.....	151
Table D.9	Accuracy check of preliminary elemental analysis calibration.....	152
Table D.10	Summary of ultimate analyses, dry ash, and mass release (%MR).....	153
Table D.11	Summary of ultimate analyses and yields of tars/soots.....	155
Table D.12	¹³ C NMR measured parameters for chars from the drop tube/FFR.....	157
Table D.13	¹³ C NMR measured parameters for tars from the drop tube and FFR..	158
Table D.14	¹³ C NMR derived parameters for chars from the drop tube and FFR ..	159
Table D.15	¹³ C NMR derived parameters for tars from the drop tube and FFR	160
Table E.1	Dry elemental analysis of char and coal feeds pyrolyzed at 1250 K....	163
Table E.2	Mass and nitrogen release for preliminary FFR tests at 1650 K	164
Table G.1	Summary of boundary conditions assumed in drop tube FLUENT simulations.....	175
Table G.2	Summary of material properties assumed in drop tube FLUENT simulations.....	176

Nomenclature

A_i	Pre-exponential factor in rate constant for reaction i
AA	Atomic Absorption spectroscopy
AC	aromatic carbon
ACERC	Advanced Combustion Engineering Research Center
adj.	adjusted
Al	aluminum
AM	aromatic mass
<i>ANL</i>	Argonne National Laboratories
ASTM	American Society of Testing and Materials
atm	atmosphere
B.L.	number of bridges and loops per cluster
BYU	Brigham Young University
C	carbon
°C	degrees Celsius
C_{Cl}	aromatic carbons per cluster
c_0	fraction of initial bridges that are stable
CFD	Computational Fluid Dynamics
Cluster-R'	char free-radical
cm	centimeter
CPD	Chemical Percolation Devolatilization

cpdcp	chemical percolation devolatilization model- version which calculates particle temperature
CV	coefficient of variation
daf	dry, ash free
DECS	Department of Energy Coal Sample
diff.	Difference
dt	differential time step
E_i	activation energy for reaction i
f	fractional yield, daf mass basis
f_N	fractional nitrogen yield, mass basis
f_a	total percent of sp ² -hybridized carbon
f_a^*	percent of aromatic carbon
f_a^B	percent of bridgehead aromatic carbon
f_a^C	percent of carbonyl carbon
f_a^H	percent of aromatic carbon with proton attachment
f_a^N	percent of nonprotonated aromatic carbon
f_a^P	percent of phenolic or phenolic ether aromatic carbon
f_a^S	percent of alkylated aromatic carbon
f_{al}	total percent aliphatic carbon
f_{al}^*	percent aliphatic carbon that is nonprotonated or CH ₃
f_{al}^H	percent aliphatic carbon that is CH or CH ₂
f_{al}^O	percent aliphatic carbon that is bound to oxygen
f_{AM}	the fraction of mass which is aromatic
FFR	methane-air flat flame reactor
FTIR	fourier transform infrared spectroscopy
f_{char}	char yield
f_{stable}	fraction of M _{cl} decay before ring nitrogen release begins

g	gram
H	hydrogen
H/C	hydrogen to carbon molar ratio
HCN	hydrogen cyanide
hr	hour
hvAb	high volatile A bituminous
hvb	high volatile bituminous
hvCb	high volatile C bituminous
ICP	inductively coupled plasma
K	Kelvin
k_i	rate constant for reaction or step i
kcal	kilocalories
l	fraction of bridges which are labile
lvb	low volatile bituminous
m	meter
M_{Cl}	average molecular weight per cluster
M	average molecular weight of the cluster attachments
M_{site}	average aromatic mass per cluster
moist.	Moisture
mol	mole
ms	millisecond
mvb	medium volatile bituminous
N	nitrogen
n	total number of replicates
N_{site}	mass of nitrogen per mass of aromatic material
NCSR	non-catalytic selective reduction
NH_3	ammonia

NMR	nuclear magnetic resonance spectroscopy
NO _x	nitrogen oxides (NO, NO ₂ and N ₂ O)
NR	fraction of original nitrogen released during pyrolysis
O	oxygen
O/C	oxygen to carbon molar ratio
p_0	fraction of attachments that are bridges
PCGC - 3	Pulverized Coal Gasification and Combustion code (3 dimensions)
ppb	parts per billion, vol/vol
PSOC	Penn State Office of Coal Research
R	universal gas constant
R''	material which competes with ring N for char free-radicals
'R'	aliphatic free-radical (light gas precursor)
r_i	rate of reaction i
ring N	nitrogen contained within the aromatic structures of coal
S	sulfur
s	second
S.C.	number of side chains per cluster
SCR	selective catalytic reduction
sec	second
Si	silicon
sub	subituminous
T	temperature
T _p	particle temperature
Ti	titanium
t	time
TG-FTIR	thermogravimetric fourier transform infrared spectroscopy
VM	ASTM volatile matter

x_i	value of replicate I
\bar{x}	mean value of all replicates
XPS	X-ray photoelectron spectroscopy
y_C	daf mass fraction of carbon
y_N	daf mass fraction of nitrogen
y_O	daf mass fraction of oxygen
2-D	two-dimensional
	fraction of attachments which are metastable side chains
	bonding pi molecular orbital
*	anti-bonding pi molecular orbital
+1	total attachments per cluster
b	fraction of bridgehead carbons

1. Introduction

Current nitrogen release models empirically correlate nitrogen release rate constants with the ultimate analysis of the parent coal.¹⁻³ While this may work well for many coals, some coals with similar ultimate analyses exhibit large differences in chemical structure^{4, 5} and thus behave differently during devolatilization. In effect, existing models fail to acknowledge that the rate of nitrogen release during coal devolatilization, like any chemical reaction, is dependent on the chemical structure of the reactants. The purpose of this work is to better characterize and model how nitrogen release during rapid coal devolatilization depends on the chemical structure of the char.

Background

As pulverized coal combustion is used increasingly for power generation in developing countries around the world, pollutant emissions from coal combustion may impact the quality of life of more people than ever before. NO_x (nitrogen oxides), which cause a variety of environmental and health problems⁶, are particularly difficult to remove from the combustion products of coal, requiring expensive selective reduction techniques such as selective catalytic reduction (SCR) or non-catalytic selective reduction (NCSR). During pulverized coal combustion, the nitrogen in NO_x originates either in the fuel (fuel NO_x) or in the air (thermal NO_x). Fuel NO_x is more important than thermal NO_x during coal combustion, making up 60-95% of the total NO_x formed in typical coal flames.^{7, 8}

Fuel nitrogen released during coal combustion is of three types: (1) nitrogen released with the light gases (gaseous combustion products which do not condense at

ambient temperature and pressure); (2) nitrogen contained within the tar (volatile hydrocarbon compounds that condense at room temperature); and (3) nitrogen retained within the char (the solid remaining after devolatilization). All three forms of fuel nitrogen end up in the combustion products, but the nitrogen which is released during devolatilization, unlike char nitrogen, is amenable to removal through inexpensive techniques such as modification of combustion configuration hardware, which can reduce NO_x emissions by 50-80%.⁸ Furthermore, if nitrogen partitioning between char and volatiles can be quantified, power plants will be better able to model the effect of changes in burner design and configuration, operating conditions, and coal feed material on NO_x emissions without having to perform as many actual tests. Thus models have been developed to predict the rate of volatile nitrogen release using correlations to estimate rate constants from the parent coal elemental composition. However, because such models have no basis in coal chemical structure, they cannot reliably predict nitrogen release rates for conditions and coals outside the narrow limits within which they were developed. Any practical nitrogen model should be able to extrapolate from typical laboratory pyrolysis conditions used in model development (10³-10⁵ K/sec) to typical combustion conditions (up to 10⁶ K/sec). Hence there is a need for a nitrogen model based on correct chemical structures and reaction mechanisms. A preliminary nitrogen model based on measured changes in char chemical structure was developed by Genetti.^{3, 9} However, during the development of this model, only a limited amount of chemical structural data was available, and the model did not perform well at long residence times or for high rank coals.

Some excellent chemical structural data as characterized by ¹³C NMR already exist for chars produced from a few U.S. coals.^{5, 10-12} Furthermore, solid-state ¹³C NMR analyses of tars from each of 5 coals from one pyrolysis condition were reported by Hambly.¹¹ However, more chemical structural data are necessary for both chars and tars from a wider variety of coals to better characterize trends with rank and temperature.

This dissertation contains new chemical structural data for tars and chars produced from rapid pyrolysis of eight coals spanning a wide range of rank. Using these data along with other published data, a model that relates nitrogen release from coal during devolatilization to changes in chemical structure throughout devolatilization was developed and evaluated.

Organization of this Dissertation

First, literature pertinent to the chemical structure of coal and coal pyrolysis products, pyrolytic nitrogen release, and existing nitrogen release models is presented in Chapter 2. The objectives and approach used in this study are explained in Chapter 3, and the pyrolysis experiments and characterization techniques are subsequently described in detail in Chapter 4. The results of the pyrolysis tests are then presented and discussed in Chapter 5, with an emphasis on nitrogen release and chemical structure. Next, relationships between chemical structure and nitrogen release are examined in detail in Chapter 6, from which a nitrogen model is developed and evaluated in Chapter 7. Finally a summary is given in Chapter 8 and several recommendations are made (Chapter 9).

2. Literature Review

Coal devolatilization has been studied extensively in both slow and rapid pyrolysis studies. Devolatilization occurs when coal is heated in an inert environment, resulting in the release of much of the organic matter to the gas phase as a result of a set of complex chemical reactions.¹³ During pulverized coal combustion, devolatilization occurs rapidly (see Figure 2.1), followed by oxidation of the pyrolysis products. As tar and light gas are released, much of the nitrogen in the coal is also released. The rate of this nitrogen release, like the rate of any chemical reaction, depends on the temperature history and the chemical structure of the important reactants. The more accurately the chemical structure of the reactants (coal or char throughout devolatilization) is known, the easier it is to accurately model pyrolytic chemical reactions, including those responsible for the release of nitrogen from coal. Accordingly, the literature reviewed here will focus on the chemical structural changes which take place during devolatilization and how they influence nitrogen release

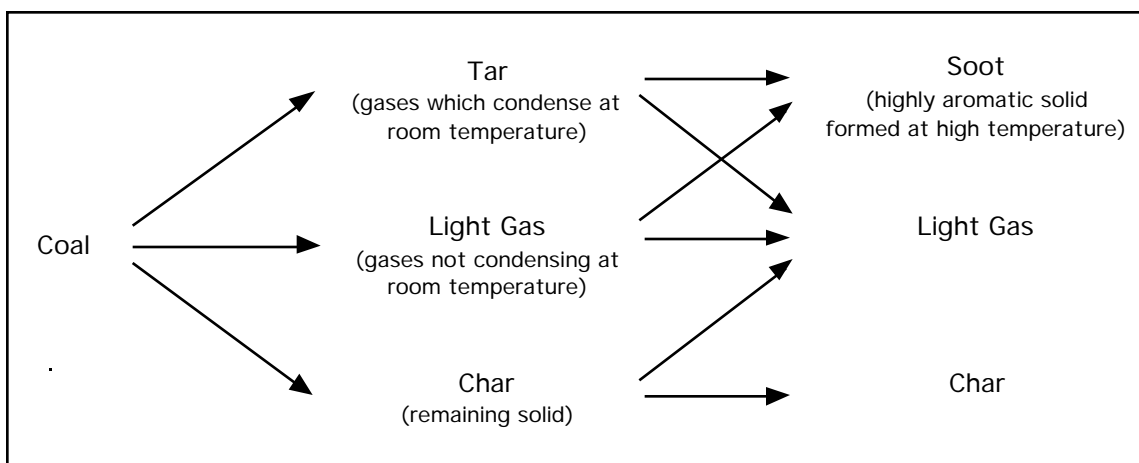


Figure 2.1 Schematic of the devolatilization process that occurs when coal is heated in an inert environment (adapted from Serio et al.¹⁴).

from the char. Computer models which quantitatively predict nitrogen release during devolatilization will also be reviewed.

Coal Chemical Structural Evolution During Devolatilization

Devolatilization behavior, like the behavior of any chemical reaction, is strongly influenced by the chemical structure of the coal.¹⁵ The chemical structure of a hypothetical high-volatile bituminous coal molecule is shown in Figure 2.2. The names used throughout this document for the general types of structures found in coal are also indicated in Figure 2.2. Any carbon double bonded to an oxygen atom will be referred to as carbonyl carbon. Actual coal structures may vary greatly from coal to coal due to differences in the way each coal was formed.^{16, 17} Coal is a very heterogeneous substance,¹⁸ exhibiting a large range of functional groups all attached to an aromatic backbone in a myriad of combinations.^{16, 17} Coal consists of a very large three-dimensional macromolecular network of aromatic sites, cross-linked by aliphatic carbon and oxygen bridges.¹⁹ These aromatic sites are groups of aromatic carbon atoms with typical average sizes of between two and six rings.¹⁹ Aromatic sites can have side chains and bridge type attachments (see Figure 2.2).⁴ A mobile "guest material", chemically unconnected to the coal matrix, is also thought to exist.^{20, 21} The aromatic structures in coal usually contain oxygen, nitrogen, and sulfur heteroatoms.¹⁶ Most nitrogen heteroatoms occur within clusters which contain at least one other heteroatom.²²

¹³C NMR has been used to characterize the average structural characteristics of several coals.^{4, 23, 24} A correlation has been developed which can be used to estimate the number of aromatic carbons per cluster based on the fraction of carbons which are bridgeheads (aromatic carbons bonded only to other aromatic carbons), as measured by ¹³C NMR.⁴ This technique has also been used to follow changes in the chemical structure of coal chars during primary devolatilization²⁵ which include:

- Bridge-breaking and tar release

- Crosslinking in the char throughout devolatilization, and
- Light gas release

These changes and their relation to nitrogen release will be discussed in more detail in the paragraphs that follow.

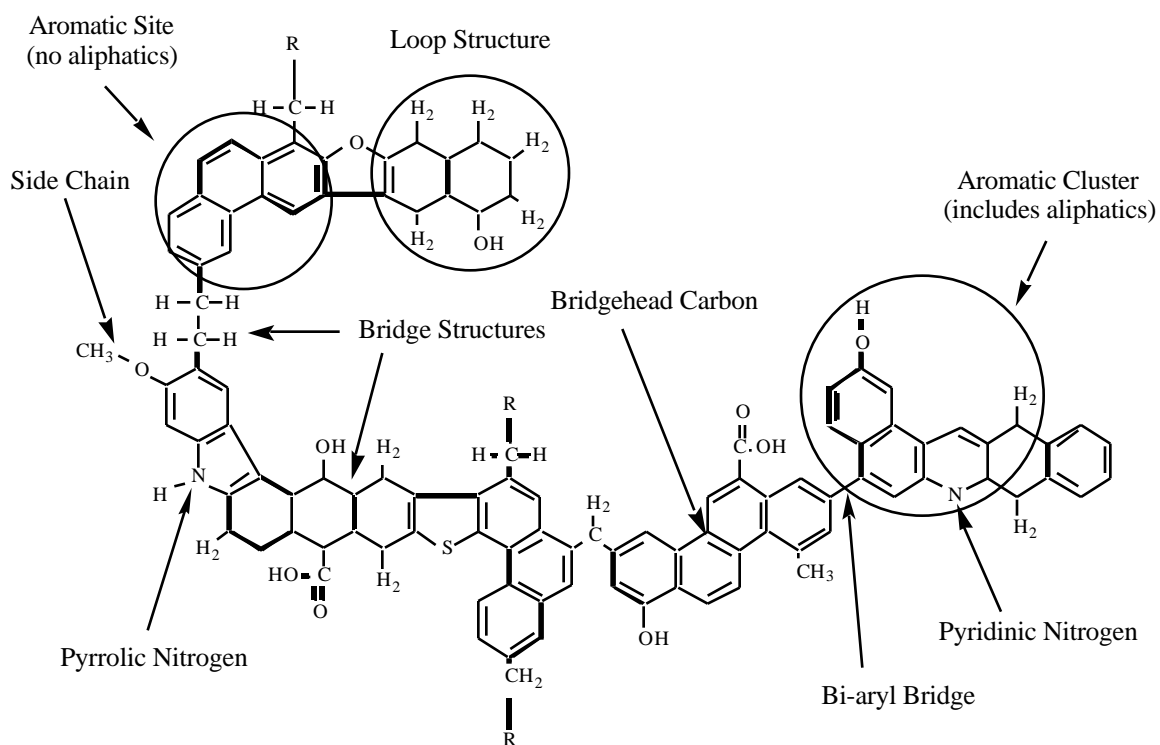


Figure 2.2 The structure of a hypothetical coal molecule, adapted from Solomon²⁰

Thermally initiated chemical reactions cause each of these changes to occur. Thermal decomposition of coal is thought to begin with bond dissociation reactions in the aliphatic bridges and side chains (see Figure 2.2).²⁶ Two free-radicals are formed as a bond is dissociated, which then react further in any of several ways: recombining with each other; adding to double bonds; adding to aromatic rings; and so on.²⁶ Non free-radical reactions such as condensation reactions of carboxyl and phenolic hydroxyl groups may also play a role in the thermal decomposition of coal. In this work, char refers to coal which has undergone any amount of thermal decomposition.

Bridge Breaking and Tar Release

As coal is heated above about 600-700 K, aliphatic bridges which connect aromatic clusters in the coal are broken, forming fragments which are detached from the network of interconnected clusters in the coal (or char).¹⁹ These fragments can either vaporize (as tar) or reconnect to the coal matrix. Tar release is predicted fairly well by network devolatilization models such as the Chemical Percolation Devolatilization (CPD) model.^{27, 28}

Primary (unreacted) tar produced from bituminous coal at a moderate heating rate (600°C/min) is similar to the parent coal in aromaticity and carbon and nitrogen content, while measuring slightly lower in oxygen and about 20% higher in hydrogen than the parent coal.^{16, 29} The structures of tars released from low and medium volatile bituminous (high rank) coals become more like that of the parent coals as devolatilization proceeds.³⁰ The structures of tars from lignites (low-rank coals) differ greatly from the initial parent coal structures, since extensive cross-linking occurs in the coal before and during tar release.^{16, 25, 29} Tar and char chemical structural differences are probably responsible for the much lower stability of ring nitrogen in tar as compared to char during conditions of severe pyrolysis (i.e. conditions at which soot forms). However, the chemistry responsible for this lower stability in tar nitrogen (as compared to char nitrogen) is not well understood and is the focus of research currently underway by Zhang.³¹

Cross-linking

Cross-linking occurs when two clusters chemically react to form an aliphatic linkage or bridge between the two aromatic clusters. Cross-linking is influenced by many factors and has a large effect upon char structure and volatiles release.³²⁻³⁴ In a study by Pugmire and coworkers,²⁵ early (low temperature) cross-linking in a North Dakota lignite was thought to have caused the structure of the tar to differ from that of the parent coal, while the structure in an Illinois bituminous coal tar was similar to that of the parent coal,

apparently because tar release occurred before substantial cross-linking took place. Low temperature cross-linking reduces tar yields and thus total volatiles yields.³⁴ Furthermore, low temperature cross-linking is most pronounced in low-rank coals and may be substantially reduced at high heating rates.³⁴ Hambly reported that for matched tars and chars from five coals produced in a drop tube at 1080 K and 282 ms, chars showed 34-100% increases in the average number of bridges and loops per cluster (and thus cluster interconnectedness) when compared to the parent coal structures, while tars showed only 0-34% increases.¹¹ It is possible that the more highly cross-linked nature of devolatilized char when compared to tar is related to the differences in light gas nitrogen release from tar and char by ring rupture.

Early Light Gas Release

During light gas release CH₄, H₂O, CO₂, CO, SO₂, NH₃, C₂H₄, and COS are all released, along with a few larger aliphatic hydrocarbons.³³ Early light gas release reportedly does not cause any nitrogen release from the coal.³⁵ This is probably because almost all nitrogen atoms in coal are found within aromatic rings³⁶⁻³⁸ (see Figure 2.2) which do not open at the low temperatures corresponding to early light gas release.²⁵

Severe Pyrolysis

Secondary reactions cause the release of aliphatic material from primary tar at moderate pyrolysis conditions³⁵ and cause ring opening and soot formation³⁹ in the tar at more severe pyrolysis conditions. It has been shown that during severe pyrolysis, secondary reactions convert most of the tar to soot, although less than a third of the tar nitrogen is retained within the soot structure.^{40, 41} This is in contrast to char, which typically retains at least half of the coal nitrogen under conditions severe enough to convert tar to soot.¹⁵ This is surprising considering the fact that solid-state ¹³C NMR of matching tars and chars from five parent coals (produced at 1083 K and 285 ms residence time)

showed the tar and char structures to be very similar except that the chars were much more interconnected by stable bridges.

Nitrogen Speciation in Coal

The coal chemical structure in the vicinity of each nitrogen atom will largely determine how that nitrogen atom will react during pyrolysis. Nitrogen in coal is almost exclusively found in the aromatic sites of the coal.³⁶⁻³⁸ Nitrogen speciation has been measured in coal and its pyrolysis products by X-ray Photoelectron Spectroscopy (XPS), X-ray Absorption Near-Edge Spectroscopy (XANES), ¹⁵N Nuclear Magnetic Resonance (NMR) Spectroscopy, and by Gas Chromatography (GC) for small tar molecules.^{38, 42}

High resolution X-ray Photoelectron Spectroscopy (XPS) is a surface technique that is the most well developed and most widely used method for quantitative analysis of nitrogen species. XPS studies show all the nitrogen in coal to be pyrrolic, pyridinic, or quaternary.³⁸ Pyrrolic and pyridinic nitrogen atoms are heteroatoms in five and six-membered aromatic rings, respectively (see Figure 2.2). It is not clear what quaternary nitrogen (as measured by XPS) really represents. It is possible that several different situations could cause a quaternary nitrogen signal, including protonated pyridinic, pyridinic nitrogen “associated with hydroxyl groups from carboxylic acids or phenols”,^{37, 43} or pyridinic nitrogen which has undergone “ionic or charge transfer interactions”.³⁵ A study of 182 UK bituminous coals (ranging from 79-95% C) showed that absolute dry mineral matter free (dmmf) coal nitrogen content peaks at about 85% carbon (dmmf).⁴⁴ XPS was used on 8 of these UK coals to show that the decrease in nitrogen above 84% C is due to reduced amounts of pyrrolic nitrogen. At the same time, absolute pyridinic nitrogen content continues to increase with increasing rank up to 90% C, at which point pyridinic nitrogen also declines. This seems to indicate an increased stability for pyridinic nitrogen over that of pyrrolic nitrogen during coalification. In the eight Argonne premium coals, which cover a wide range of rank, pyrrolic nitrogen is the most abundant nitrogen

species (55-65% of coal nitrogen), followed by pyridinic (25-33%), with 3-16% quaternary nitrogen and undetectable amounts (less than 5%) of amine nitrogen.³⁷ Qualitative agreement has been shown between the nitrogen speciation distributions of the Argonne Premium coals as measured by ¹⁵N NMR and those measured by XPS, although the signal to noise ratio in the ¹⁵N NMR experiments is low due to the low abundance of nitrogen in coal.⁴⁵

Nitrogen Speciation Progression During Pyrolysis

During pyrolysis, the functional forms of nitrogen (as measured by XPS) in the tar and char change in different ways. This may help explain why severe pyrolysis affects tar (which releases most of its nitrogen on conversion to soot) and char (which retains much of its nitrogen) in different ways. In one study⁴³, the char initially lost quaternary nitrogen, after which pyrrolic nitrogen was converted to quaternary nitrogen (possibly different than the type of quaternary nitrogen in the coal). The relative amount of quaternary nitrogen was found to increase to about 50% in the char at 1073 K, suggesting that the nitrogen in the char becomes entrapped as the aromatic carbon matrix completely surrounds the nitrogen atom.^{43, 46} The formation and stability of quaternary nitrogen was also observed in a model compound study by Stanczyk et al.⁴⁷, who reported very similar nitrogen functionality distributions after pyrolysis at 1073 K for model compounds with vastly different initial distributions. Tar, on the other hand, contains little⁴³ or no³⁵ quaternary nitrogen. As tars are subjected to higher temperatures, first pyridinic and then some pyrrolic nitrogen is converted to nitrile (cyano) nitrogen through ring opening reactions.³⁵ Kelemen et al.⁴³ interpreted the nitrile peak in coal tar to be concentrated amines, although nitrile (and not amine) nitrogen functional groups are produced upon pyrolysis of model compounds.³⁵ Specific low molecular weight aromatic compounds with nitrile attachments have been identified in the tars of several coals, in increasing concentrations with increasing pyrolysis temperature.^{42, 48} Data from a fluidized bed pyrolyzer suggest that the formation

of nitrile (ring opening reactions) begins at temperatures between 973 and 1073 K.³⁵ This is in good agreement with the temperature range in which more complex model compounds (containing an oxygen functional group or more than one nitrogen group per molecule) partially decompose.⁴⁹ Between 1073 and 1173 K, tars from a fluidized bed pyrolyzer contained almost exclusively pyrrolic and nitrile nitrogen.³⁵ Nitrogen in the 1073 K tars was 50-70% pyrrolic and 30-45% nitrile, with the proportion of pyrrolic nitrogen increasing with increasing tar fraction molecular mass. This is in contrast to chars, for which no nitrile nitrogen formation is observed.⁴³

The higher stability of pyrrolic (when compared to pyridinic) nitrogen in coal tar has been shown by more than one researcher^{35, 50} and contradicts what would be expected based on pyrolysis of pyrrole and pyridine.^{35, 51, 52} This suggests that the reactions that cause light gas nitrogen release during coal devolatilization may be mechanistically different from simple thermal decomposition of pyridine and pyrrole.

Nitrogen Release From Coal Char

During pyrolysis, coal char releases nitrogen in two ways: 1) nitrogen is transported away within the tar sites as the tar vaporizes; and 2) nitrogen is released from the char sites during ring rupture.²⁹

Nitrogen release by tar transport

Freihaut et al.^{53, 54} found that high volatile bituminous coals pyrolyzed in a heated grid reactor or a drop tube yield tar nitrogen in direct proportion to tar mass. This agrees well with the finding that high volatile bituminous coal tars closely resemble their parent coals.^{16, 25, 29, 55} In contrast, during early primary tar release, tars from low-rank coals contained a significantly lower mass fraction of nitrogen than that of the parent coal.^{11, 53, 56} Although initial nitrogen release from low-rank coals is slower than for bituminous coals on a total volatiles release basis, it has still not been established whether this

difference is due solely to differences in tar release.⁵³ Tar release generally occurs before any nitrogen is released via ring rupture in the char.¹⁵ However, several investigators have measured significant amounts of light gas nitrogen release at temperatures where primary tar yields are maximized.^{11, 39}

Nitrogen release by ring rupture

Usually nitrogen released from coal via ring rupture is mostly HCN, NH₃, HNCO, and N₂, with small amounts (less than 2%) of NO also reported.^{42, 50, 53, 56} Pyrolysis in a flow reactor of substituted pyridinic-type and pyrrolic-type model compounds produced significant amounts of both HCN and NH₃.⁴⁹ On the other hand, HCN is almost the only nitrogen containing product formed from complete pyrolysis of unsubstituted pyridine or pyrrole.^{51, 52, 57, 58}

Several researchers have performed pyrolysis tests on model compounds (for which the chemical structure is exactly known) in order to better understand nitrogen release by ring rupture. Pyrolysis at 1073 K of five different aliphatic-containing pyridine derivatives gave conversions of nitrogen to light gas of between 12 and 28%⁴⁹, conditions for which both Axworthy et al.⁵⁷ and Bruinsma et al.⁵⁸ report almost no thermal decomposition of pyridine. Thus it is possible that the presence of aliphatic material introduces a lower temperature mechanism for pyridinic nitrogen release by ring rupture. One model compound study suggested that in heterocyclic dibenzo ring systems (3-rings) such as carbazole, radical ring dimerization occurs preferential to ring system destruction.⁵⁸ This is consistent with the soot formation mechanism proposed by Badger⁵⁹, in which soot formation begins by the breaking of a C-H bond followed by dimerization, occurring most easily in the ring systems which can best stabilize aryl radicals. It is possible that such cluster dimerization reactions form a highly connected char matrix in which the ring nitrogen remaining in the char after primary pyrolysis is stable.

In general, light gas nitrogen is not seen in rapid heating rate (>1000 K/s) experiments at temperatures below 973 K.^{15, 60} Char nitrogen content can be reduced to zero under very extreme pyrolysis conditions (i.e. 20 minutes at 2100 K).⁷ Nevertheless, after pyrolysis on a heated graphite ribbon at lower temperatures, char still retained some of the coal nitrogen: 8-20% after 2 minutes at 1973 K and 30-40% after 2 minutes at 1673 K.⁵⁵ During the 1673 K tests, only 15-20% of the coal nitrogen was converted to light gas, compared to 50% released as tar nitrogen.⁵⁵ This suggests that even at high temperatures and long residence times, a large fraction of the nitrogen is stable in the char. Cai et al.⁶¹ showed that nitrogen release from an Illinois #6 coal increased from 40% to 45% as the heating rate was increased from 5 K/s to 5000 K/s, mostly due to an increase in tar (and the nitrogen therein) with increasing heating rate. Light gas nitrogen actually decreased slightly as heating rate increased. This same study found that light gas nitrogen yield during devolatilization at 1000 K/s did not vary for changes in total pressure between 1 and 70 bar.

Many researchers have observed that low-rank coals produce more light gas nitrogen than do high rank coals at the same condition.^{1, 15, 54, 62} In contrast, Nelson et al.⁴⁸ observed that HCN nitrogen as a fraction of coal nitrogen was more or less independent of coal type for four coals ranging in rank from lignite to bituminous pyrolyzed in a fluidized bed reactor. However, HCN from the char was not studied separately from HCN produced by secondary tar reactions in the gas phase.

Kambara et al.⁵⁰ found that the nitrogen released as light gas (HCN, NH_3 , and N_2) depends on the nitrogen functionality of the parent coal, although several more recent studies have shown no such dependence.^{46, 48}

Total Pyrolytic Nitrogen Release

Many studies which do not resolve the distribution of nitrogen between tar and light gas nitrogen still contain useful information. Baxter et al.⁶³ and others⁶⁴ have confirmed

the findings of Pohl and Sarofim⁷ that nitrogen release during devolatilization initially lags total mass release, after which nitrogen is released at a rate 1.25-1.5 times faster than mass. Baxter et al.⁶³ also found that this initial lag in nitrogen release was rank dependent, being shorter or non-existent for bituminous coals and higher rank. Since little or no nitrogen is thought to exist outside of the aromatic rings in coal, this lag in nitrogen release is probably driven by the release of early light gas which consists mainly of aliphatic material. A few researchers have studied coals which release a far greater percentage of nitrogen than the percentage of mass released to the volatiles.^{61, 65} Such coals do not seem to be very common.

Table 2.1 summarizes major pyrolysis studies that have been conducted to investigate nitrogen release. As can be seen, only one limited study has examined the details of both tar and char chemical structure. Therefore, as mentioned in the objectives, matched sets of tar and char were produced and characterized in this study in order to compare chemical structural changes in chars with those in the corresponding tars for five different degrees of pyrolysis severity.

Nitrogen Release Modeling

It has been suggested by some that a simple rule of thumb could be used to predict total nitrogen release during devolatilization: assume that the rate of nitrogen release is equal to the rate of mass release.⁶⁶ While this may reflect the endpoint for many high heating rate pyrolysis tests, this simple rule of thumb does not apply at low (<1300 K)^{5, 39} or very high (>1800 K)^{7, 55} temperatures nor for low-rank⁵⁴ or very high-rank⁹ coals. Furthermore, this rule of thumb does not describe anything about the split between tar nitrogen and light gas nitrogen. Thus nitrogen models have been formulated which more precisely describe nitrogen release, with the hope of improving fuel NO_x prediction capability when used with comprehensive combustion models.

Table 2.1.

Summary of pyrolysis studies for investigation of nitrogen release.

Kelemen et al. ⁴³
Kambara et al. ⁵⁰
Aho et al. ⁶⁷
Nelson et al. ^{42, 48}
Li et al. ⁶⁰
Kelemen et al. ⁴³
Basilakis et al. ¹
Solomon and Colket ²⁹
Solomon et al. ⁶⁸
Wornat et al. ⁶⁹
Fletcher et al. ⁷⁰
Watt et al. ⁷¹
Hambly ¹¹
Wu et al. ⁶²
Cai et al. ⁶¹
Chen ³⁹
Blair et al. ⁵⁵
Fletcher et al. ⁵
Friehaut et al. ⁵³
Pohl & Sarofim ⁷

Models which quantitatively predict pyrolytic nitrogen release have been formulated for use with the FG-DVC, FLASHCHAIN, and CPD network models.^{1, 9, 72} These nitrogen release models describe nitrogen release via (a) tar release and (b) light gas nitrogen release.

Each of these nitrogen release models are based on the following assumptions:

1. All fuel-bound nitrogen atoms are distributed randomly within the aromatic portion of the coal.
2. During tar release, tar aromatic clusters transport nitrogen atoms contained therein to the tar product, in an amount proportional to the number of aromatic clusters in the tar.
3. During high temperature primary devolatilization, HCN is produced from ring opening reactions in the char. However, since nitrogen represents such a small fraction of the coal, the aromatic sites/aromatic rings are still approximately conserved within the pyrolysis products.
4. During devolatilization, the rate of release of nitrogen atoms from the aromatic structure can be described as a first order process with a distribution of activation energies.

Parameters in the earliest nitrogen release models (FG-DVC and FLASHCHAIN) were tuned by matching predicted light gas and tar nitrogen values with the experimentally measured values from various coals after pyrolysis at heating rates from 0.5 to 10^4 K/s. Each model uses a distributed activation energy first-order rate expression, with one or two coal-dependent parameters, which are correlated with the ultimate analysis of the coal. Because the chemistry of nitrogen release is not well understood, no attempt is made by these models to describe the chemistry responsible for the variations in light gas nitrogen release with coal type. More recent work used parameters measured by ^{13}C NMR to predict nitrogen release by ring rupture.⁹ In doing so, Genetti found it helpful to include a “stable” nitrogen fraction (nitrogen which is not released from the char during devolatilization) to better model nitrogen release at high heating rates (10^5 K/s). This was the first nitrogen release model designed for and evaluated at the high heating rates and temperatures encountered in flat flame burner devolatilization experiments. Furthermore, Genetti was the first to evaluate the performance of his nitrogen model using measured ^{13}C

NMR char chemical structural data. However, the model was not evaluated for low heating rate pyrolysis ($<10^3$ K/s) and often greatly over-predicted nitrogen release at long residence times.

The model shown in this dissertation makes the same first three assumptions made by previous nitrogen release models. However, assumption four was modified to add a global three-step free-radical mechanism which is assumed to be the major factor causing nitrogen release from char via ring rupture. Data from this study, along with published solid-state ^{13}C NMR data were used to develop a rate equation and fit rate constants for light gas nitrogen release. The nitrogen model requires only the particle temperature history, a devolatilization model (such as the CPD model), and coal-specific chemical structural input data to predict the evolution of the char chemical structure, char nitrogen content, and total nitrogen release. Unlike previous models, the nitrogen model requires no coal-dependent parameters other than coal chemical structural data as measured by ^{13}C NMR (the same parameters required by the CPD model).

3. Objectives and Approach

The objective of this research was to develop a model that relates nitrogen release from coal during devolatilization to the changes in the chemical structural features of the char. This was accomplished in several stages: 1) expanding the database of coal chars with known particle temperature history and chemical structure; 2) analyzing this database to identify relationships between light gas nitrogen release and char chemical structure; 3) postulating a mechanism from which follows a rate expression consistent with these relationships; and 4) fitting the parameters of this rate expression by matching both nitrogen chemical structural data and nitrogen release data from pyrolysis tests. Once the model was finalized it was evaluated for data collected over a large range of heating rates, residence times, and coal rank, including many sets of data not used in the development of the model.

As part of the model development and evaluation, thirty-four high heating-rate pyrolysis tests were performed, including five different pyrolysis conditions and eight coals from a wide range of rank and origin. The products of these pyrolysis experiments were quenched with cold gas after a short time at high temperature (18-300 ms). These devolatilization products were then characterized to give a "snapshot" of information from the combustion process "motion picture." Since published ^{13}C NMR data from past pyrolysis experiments only existed for five different coals, experiments detailing the chemical structure of partially devolatilized chars from all eight coals were necessary to firmly establish the rank dependence of light gas nitrogen release. Accordingly, the eight parent coals and chars from each of these coals were characterized using elemental analysis and ^{13}C NMR. Pyrolysis experiments were performed in two BYU reactors: the drop tube

reactor (for temperatures between 900 and 1250 K) and the flat-flame reactor (for temperatures above 1600 K). At each condition, gas temperatures were measured in order to calculate particle temperature histories. These pyrolysis tests captured the characteristics of nitrogen release and char chemical structural evolution for rapid pyrolysis at two different particle heating rates for coals of varying rank. This was important for evaluating the performance of the nitrogen release model over a wide range of conditions.

A secondary objective of this work was to compare the changes occurring in the chemical structure of tar to those occurring in the char at different degrees of pyrolysis severity and establish the effect of these changes on nitrogen release. This objective was accomplished by generating matched sets of char and tar at 5 different conditions for one lignite and one high volatile bituminous coal and performing elemental and ^{13}C NMR characterization of these chars and tars.

4. Description of Experiments

Thirty-four high heating-rate coal pyrolysis tests were conducted, most of which were performed in the drop tube reactor at BYU, with some tests also performed in the flat flame reactor (FFR) at BYU. The pyrolysis products of these tests were characterized in various ways, as explained below.

Drop Tube Reactor

The drop tube reactor (Figures 4.1 and 4.2) is an electrically heated laminar flow drop tube which was operated at about one atmosphere absolute pressure, although capable of operation at pressures as high as 25 atmospheres.^{11, 73} Maximum particle heating rates were about 10^4 K/s. Separate cylindrical electrical resistance heaters were used in the pre-heater and drop tube sections, each with separate set points and control thermocouples. Each control thermocouple was kept at a constant operating temperature by a PID controller. The pre-heater section heated the (secondary) nitrogen stream to about 625 K before it entered the drop tube. A water-cooled injection probe entrained the coal particles in a small (primary) nitrogen flow and prevented the particles from being heated until they left the probe. This injection probe can be raised and lowered or the gas flow rate can be changed to vary the residence time of the particles. The particles were injected at a slow rate (~ 1 g/hr) in order to approximate single particle behavior. The secondary (pre-heated) and primary (injection probe) nitrogen flows were set so as to attempt to match their radially-averaged gas velocities (about 0.7-0.85 m/s) at the point which the coal is injected

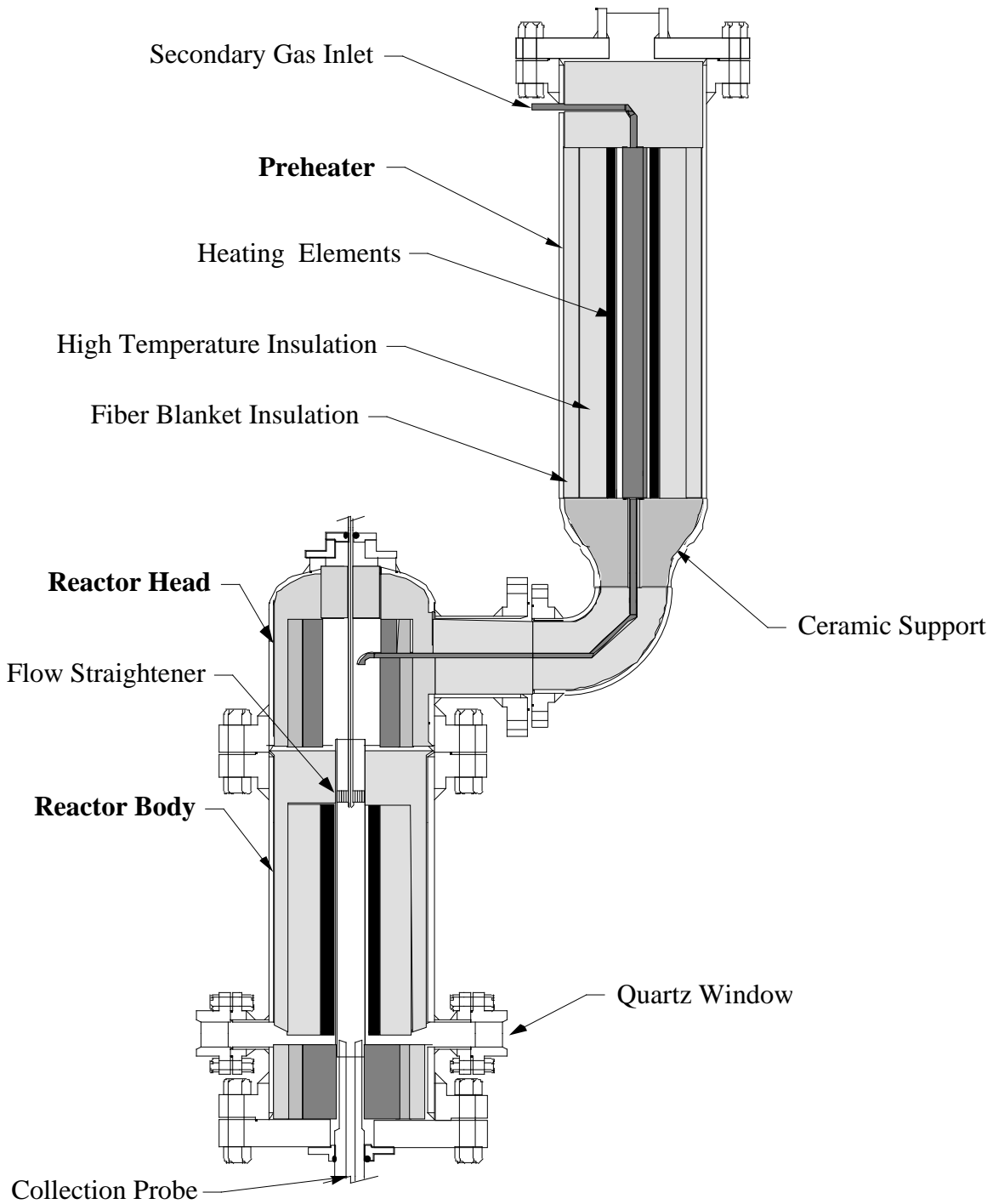


Figure 4.1. Schematic of Drop Tube Reactor with pre-heater attached (adapted from Hambly, 1998).¹¹

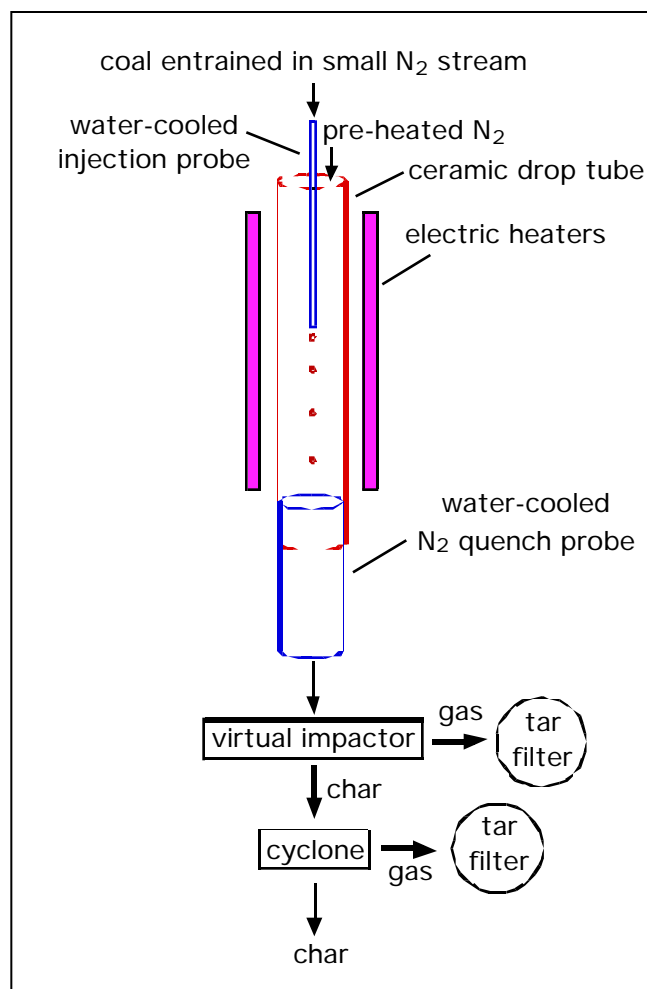


Figure 4.2. Schematic of drop tube reactor configuration.

as the two streams meet. In this way it was hoped to minimize turbulence at the point of injection so that the particles would flow down the center axis of the drop tube with minimal dispersion. Since the walls of the ceramic drop tube do not permit optical access, the radial centering of the particle path could not be verified. Gas temperatures along this center axis were carefully measured with the injection and collection systems in place (except the cyclone) using a type S thermocouple inserted from beneath the virtual impactor. Measured gas temperatures were corrected for radiative losses from the thermocouple bead as described in Appendix A. Pyrolysis products in the drop tube were immediately quenched by dilution with cool (300 K) nitrogen gas upon entering a water-cooled collection probe. Char was separated from most of the tar by a virtual impactor in

series with a one-inch cyclone. About 20-30% of the tar condensed on the sides of the collection system. These tar losses were estimated after each run by scraping and wiping the inside of the collection system and weighing the scrapings. A detailed description of the standard procedures used to operate and maintain the drop tube reactor is given in Appendix B.

Flat-Flame Reactor (FFR)

The flat-flame pyrolyzer (Figure 4.3) used in this study is the same as that used by Ma.⁴¹ Because the flat flame reactor uses the hot products of methane combustion to heat the particles, it more closely approximates a true pulverized coal combustion environment, both in temperature and gas composition. Pyrolysis temperature can be adjusted by changing the equivalence ratio or fuel composition. Residence time can be changed by raising or lowering the burner relative to the collection probe. Maximum particle heating rates in the flat flame reactor were about 10^5 K/s. Coal particles were injected up the center axis of a 5.1 cm by 5.1 cm cross section quartz tower, within which the combustion products from a fuel-rich high temperature methane-air flat flame flow in a laminar fashion. In order to approximate single particle behavior (no particle-particle interactions), the coal particles were fed at a rate of less than 1 g/hr by entrainment in a small stream of nitrogen. Particle velocities were measured previously using a high-speed video camera⁴¹ for the conditions which were used in this project. For the FFR pyrolysis tests of this study a 0% post flame oxygen condition was used, as further detailed in Appendix C.

Coal Selection

The eight coals used in this study cover a wide range of coal rank, and come from several locations around the world. Study of Pacific Rim coals is becoming increasingly important as many Asian countries expand their use of coal combustion for power

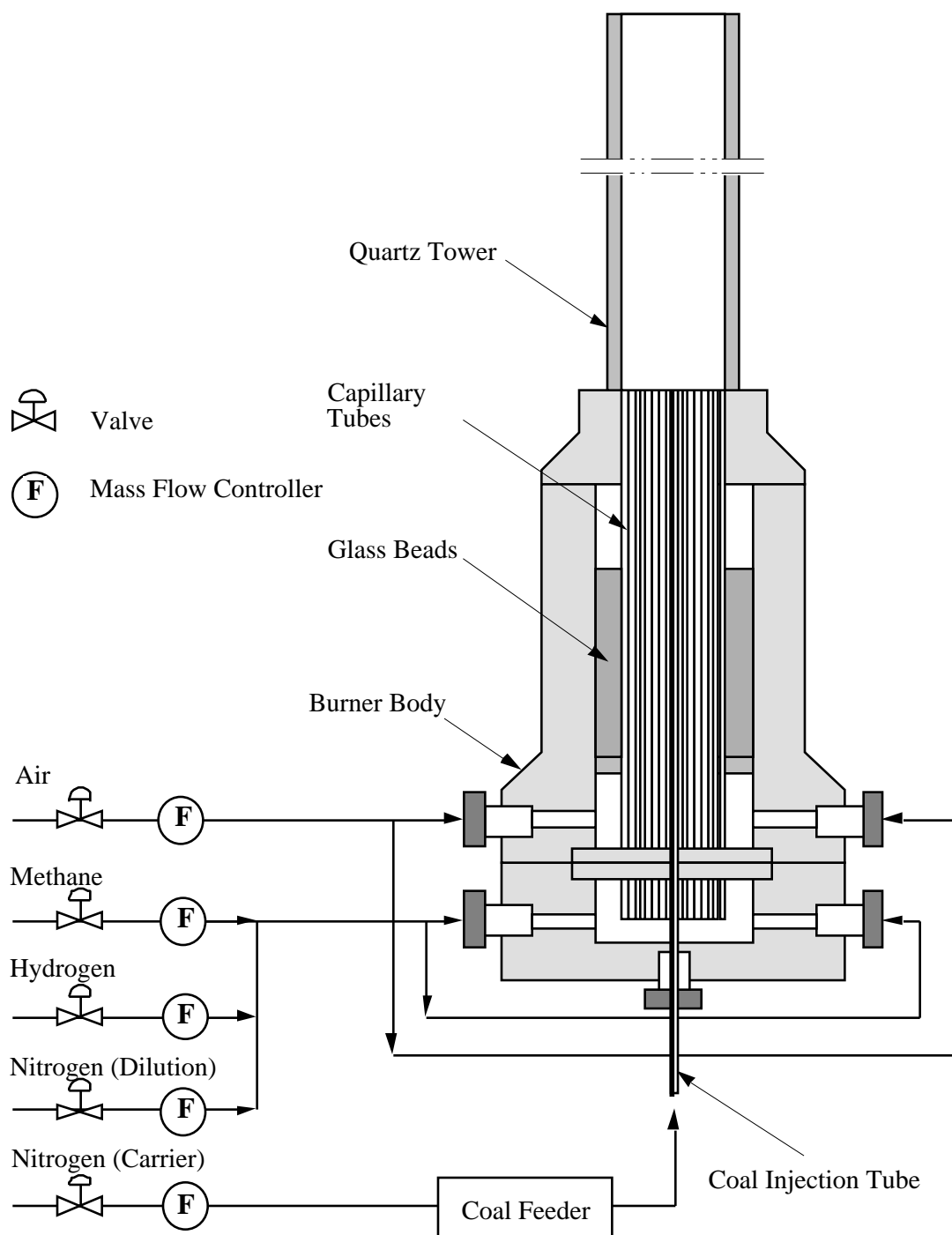


Figure 4.3. Schematic of Flat Flame Burner (FFB) (adapted from Ma).⁴¹

generation. Hence, two coals from Japan (Miike and Taiheiyo), two from Australia (Yallourn and Hunter Valley), and one from Indonesia (South Banko) were used in this study. Three well characterized U.S. coals from the Argonne premium sample bank were also used: Pittsburgh #8, Pocahontas #3, and Upper Freeport. The Pacific Rim coals (circles in Figure 4.4) fall within a narrow H/C range of 0.8 to 1.1, while the O/C varies greatly among these coals. The three U.S. coals (squares in Figure 4.4) represent a broader range of H/C, having a higher degree of coalification.

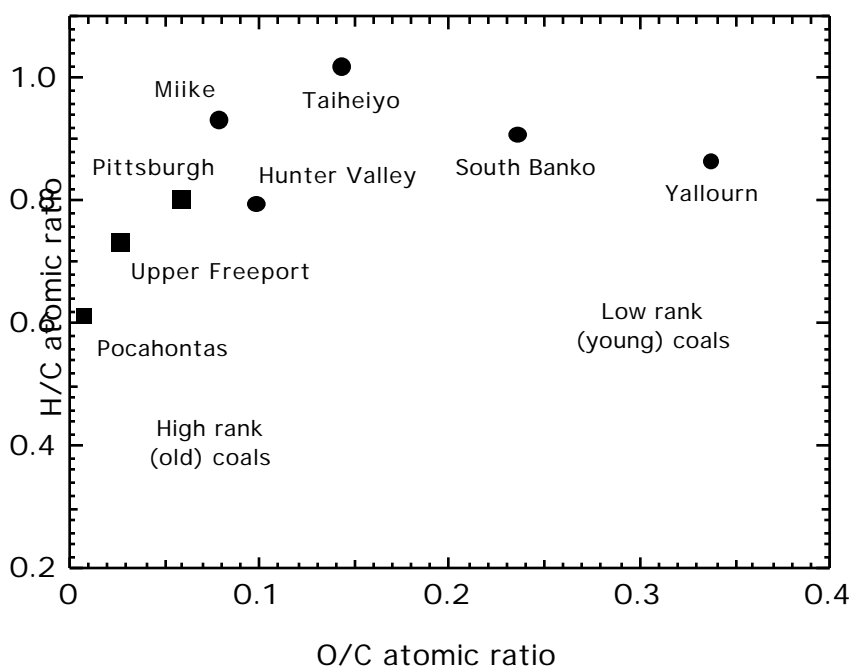


Figure 4.4. Van Krevelen coalification diagram for Pacific Rim (circles) and U.S. (squares) coals proposed for use in this study. Note the wide range of rank encompassed by these coals.

The use of such a diversity of coals was intended to help uncover the fundamental processes governing the behavior of nitrogen release during coal pyrolysis, which may not be apparent using only coals of similar rank or origin. As these processes are better understood they can be modeled in order to predict NO_x formation during combustion of any structurally characterized coal or coal blend.

Sample Preparation, Storage and Analysis

Eight parent coals were ground and sieved in an inert atmosphere to obtain coal particles of size 45-75 micron (μm) for use in the rapid devolatilization experiments. For this particle size range, a high particle heating rate can be achieved which is fairly constant over the entire range. All coal samples were stored in glass bottles with tight fitting lids, topped with argon, and kept at $-10\text{ }^{\circ}\text{C}$ until used. This prevented oxidation of the pulverized coal, preserving the characteristics that would be found in coal from most pulverized coal combustors, where coal is used immediately after it is pulverized. Each sample of coal or char taken from the bottle, whether for characterization or for pyrolysis feed material, was split off using proven techniques which preserve the characteristics of the sample in terms of particle size distribution, density, and composition.⁷⁴ A rotating single-stream sample splitter was built specifically for this purpose as part of this study.

Sample Characterization

Each parent coal, tar, soot, or char sample was characterized with the following techniques:

1. ASTM ash/moisture determination
2. Carbon, hydrogen, nitrogen, and sulfur determination on dried samples
3. Relative Ti, Si, and Al determination for char/coal pairs by Inductively Coupled Plasma (ICP) analysis for estimation of total mass release in a manner similar to Fletcher and Hardesty.⁵

Selected samples (see Figure 4.5) were also analyzed by the following techniques:

4. ^{13}C NMR (at University of Utah) to determine average chemical structural characteristics in the manner described by Solum and coworkers.⁴

Each of these characterization techniques is discussed in detail in the sections that follow in this chapter.

Determination of Elemental Composition

The elemental composition of each char, tar, and soot sample was determined using a LECO CHNS-932 elemental analyzer. This analyzer uses thermal conductivity to determine N content and infrared absorption to quantify C, H, and S after combusting and oxidizing the solid organic matter. Each sample was weighed into a tared silver crucible prior to analysis as per the operating procedure specified by the analyzer manufacturer. Five replicates of each sample were analyzed in succession and the results averaged. For samples with a large amount of heterogeneity (such as swelling chars with discrete ash particles), samples were first pulverized to a fine powder prior to analysis. Each day a coke and a coal standard with known compositions (obtained from LECO corporation) and a Pocahontas Argonne premium coal sample were analyzed to obtain average calibration factors for C, H, and N. The coal standard was also used to determine a calibration factor for sulfur. These calibration factors were used to calibrate analyses of other samples performed that day on the elemental analyzer. It was observed that both the zero and the calibration for the nitrogen analysis slowly drifted throughout each day of analyzer use and thus a calibration standard was analyzed three times throughout each day of use and a linear interpolation used to correct the calibration over time. Before analysis of each set of five sample replicates, two empty crucibles were analyzed and the values subtracted from the sample readings.

Determination of Ash, Moisture, and Volatile Matter

Dry ash and as-received moisture content were determined for all char and coal samples according to the American Society for Testing and Materials (ASTM) standards D 3173-87 and D 3174-89 using an electrically heated programmable muffle furnace. The analysis was performed in platinum crucibles, using about 0.4 grams of each char and 1 gram of each coal, except for coals with less than 5% ash, for which 2 grams were used. Volatile matter of coal was determined in a manner similar to the standard ASTM

procedure. First, 1 gram of coal was placed in a small (about 10 ml) tared ceramic crucible and dried for 1 hour at 105 °C. Then the crucible was cooled, weighed, and covered with a loose fitting cover. The covered crucible was placed inside a larger crucible to allow manipulation with tongs. Finally the crucibles were placed in a 950 °C muffle furnace for exactly 7 minutes and then cooled for 15 minutes before weighing.

Determination of Total Mass Release by Tracer

When possible, Inductively Coupled Plasma (ICP) atomic emission spectroscopy was used to determine both the titanium (Ti) and aluminum (Al) contents relative to the parent coal in a manner similar to Fletcher and Hardesty.⁵ When the ICP spectrometer was not operable, Atomic Absorption (AA) spectroscopy was used to determine Al contents. Mass release for each test was assumed to be the value obtained using the Al tracer technique, except when Ti data were available, in which case the Al and Ti results were averaged. This technique may have introduced a maximum of 3-4 % error due to release of Ti during devolatilization for a heating rates up to 10⁵ K/sec.⁷⁵ The mass release for tests in which Yallourn coal was used was calculated by overall mass balance, since the Ti and Al tracer methods gave unreasonably high values (as much as 15% absolute higher) of mass release. This is probably due to the extremely low ash content (and thus Ti, Al, and Si contents) of Yallourn coal (1.6% ash), which gives a low signal to noise ratio for ICP tracer measurements. In fact, the mass release as calculated via ash mass balance for tests using Yallourn coal was always less than the mass release as calculated by overall mass balance, giving further reason to suspect the tracer results for these tests.

¹³C NMR Chemical Structure Determination

Accepted solid-state ¹³C NMR spectroscopic techniques were used to characterize the average chemical features of selected coals, chars, and tars in this study. Cross-polarization (CP), magic angle spinning (MAS) and dipolar de-phasing techniques were

utilized in a manner similar to that described by Solum.⁴ These techniques allow characterization of a variety of average chemical structural features in a solid organic sample. Such features include the carbon aromaticity, the number of bridges and loops per cluster, the number of side chains per cluster, the fraction of carbons that are bridgeheads, and the average number of aromatic carbons per cluster. In addition, the average mass per cluster and the mass of an average aliphatic attachment can both be calculated if the carbon content of the sample is known. Aliphatic chains containing a methyl group are assumed to be side chains. Dr. Mark Solum at the University of Utah performed the ¹³C NMR characterization experiments under the direction of Dr. Ronald J. Pugmire.

HCN and NH₃ Quantification

Hydrogen cyanide (HCN) and ammonia (NH₃) concentrations were measured in the light gases immediately after passing through the tar filters using a Zelweger Analytics model 7100 Toxic Gas Monitor. The analyzer uses a chemiluminescence technique to read the color of a stain formed by reaction of the gas of interest with chemicals on a pre-made chemcassette strip. This reading is converted to a gas phase concentration based on calibrated concentration-stain relationships. Low-level HCN and NH₃ chemcassettes were used to determine HCN and NH₃ gas concentrations as low as 50 and 100 ppb, respectively. Any signal below these readings was reported by the monitor as zero. Typical HCN and NH₃ gas phase concentrations ranged from 0 ppb to 150 ppb. These gas phase concentrations were so close to the detection limits that gas phase measurement accuracy and repeatability suffered greatly. The HCN readings were corrected using the calibration factor determined by Hambly¹¹ for this analyzer. A detailed calculation to convert gas phase measurements into light gas nitrogen yields was given by Hambly.¹¹

Experimental Test Matrix

Thirty-four different pyrolysis experiments were performed, including twenty-six drop tube tests and eight flat flame reactor tests as outlined in Figure 4.5. In Figure 4.5, each box represents an experiment performed at the corresponding condition using the corresponding sieved coal. The typical quantity of coal used in each pyrolysis test was 3-5 grams in the drop tube facility and 1 gram in the flat flame reactor. For each pyrolysis test, char and tar or soot yields were carefully measured.

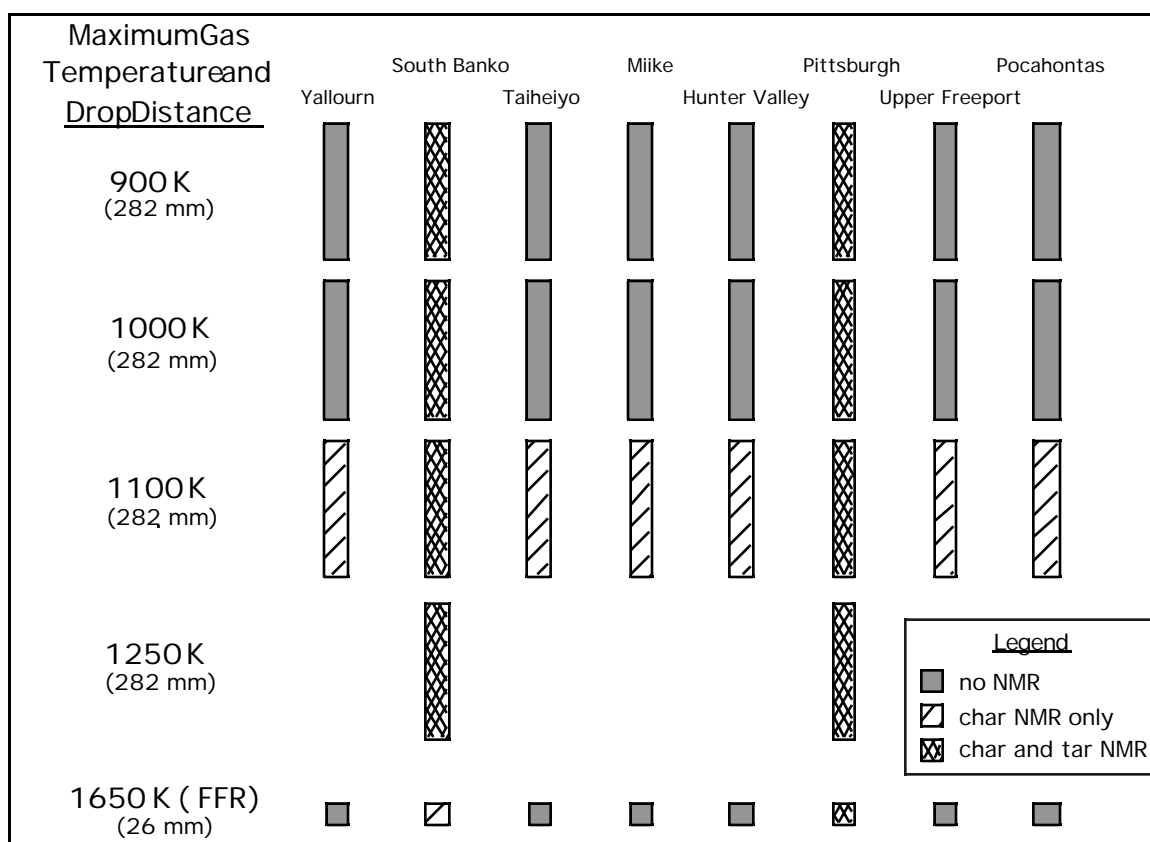


Figure 4.5 Matrix of experimental pyrolysis tests performed in the drop tube and flat flame reactor (FFR). Samples for which ^{13}C NMR analyses were performed are also indicated.

Table 4.1 further describes each condition at which experiments were performed. An additional condition, (950 K in Table 4.1) was used for one pyrolysis test with

Pittsburgh coal. Because of a net radiative heat transfer to the particles from the hot walls of the drop tube, maximum particle temperatures in this apparatus were slightly higher than maximum gas temperatures. Each condition in Table 4.1 is identified by the maximum measured centerline gas temperature. However, since it is thought that the particles did not remain on the centerline during pyrolysis, maximum gas temperatures estimated by performing a computational fluid dynamics (CFD) simulation are also shown in Table 4.1. Detailed descriptions of settings and measurements at each condition are found in Appendix C, and a detailed explanation of how gas and particle temperatures and velocities were calculated is found in Chapter 7.

Table 4.1

Summary of conditions at which pyrolysis experiments were performed in the drop tube and the flat flame reactor (FFR).

Condition	Maximum Measured Centerline Gas Temperature (K)	Maximum Calculated (non-centerline) Gas Temperature (K)	Maximum Calculated Particle Temperature (K)	Calculated Residence Time (ms)
900 K	895	1026	1040	263
950 K	960	1026	1040	263
1000 K	1000	1116	1096	252
1100 K	1085	1176	1199	234
1250 K	1245	1275	1294	294
1650 K	1640	1640 (FFR)	1560	18

Chars from sixteen of the pyrolysis tests were analyzed by ^{13}C NMR at the University of Utah, as indicated in Figure 4.5. In addition, nine tars from the aforementioned sixteen tests were analyzed by ^{13}C NMR, making nine matched tar/char sets in all with complete chemical structural characterization. Although restricted to only South Banko and Pittsburgh coals, these nine sets of matching chars and tars cover a large range of temperature conditions, giving insight into how chemical structure changes in both

tar and char as pyrolysis severity increases. The char and tar from pyrolysis of *Pittsburgh* coal at the 900 K condition was not actually analyzed by ^{13}C NMR. Instead, char and tar produced from pyrolysis of Pittsburgh coal at the 950 K condition (see Table 4.1) was analyzed by ^{13}C NMR.

Replicate pyrolysis tests were performed for Pittsburgh coal at the 950 K condition, for Pocahontas coal at the 900 K condition and for South Banko coal at the 1100 K condition. Three pyrolysis tests were also performed on chars that had already been devolatilized, rather than fresh parent coal, in order to show the effect of previously released volatiles (tar and light gas) on light gas nitrogen release. For these tests 1-2 grams of char (previously pyrolyzed in the drop tube) was split off and fed into the drop tube reactor at the 1250 K condition. This was performed using South Banko char from the 900 and 1000 K conditions and using Pittsburgh char from the 1100 K condition.

5. Experimental Results and Discussion

Proximate/Ulimate Results

A summary of the proximate and ultimate analyses as determined for the eight parent coals used in this study is presented in Table 5.1. A summary of the proximate and ultimate analyses and total mass release for the *chars* generated in this project is shown in Table 5.2, with the corresponding parent coal data also shown for comparison. An error analysis was also performed and is presented following the elemental analysis results. Except for tests using Yallourn coal, mass release values were calculated using Al and/or Ti as a tracer, as described in the previous section. Mass release values, as calculated by overall mass balance, were within 1% of the value obtained using the tracers for about half of the tests. With the exception of tests using Yallourn coal, for which the mass release

Table 5.1

Proximate/ultimate analyses of the coals used in this study.

Coal	Rank	%C (daf)	%H (daf)	%N (daf)	%S (daf)	%O (daf) (by diff.)	% ash (dry)	% moist.	VM ^a (daf)
Yallourn	brown	65.31	4.76	0.52	0.18	29.22	1.58	8.98	53.1
South Banko	brown	71.37	5.36	1.18	0.55	21.55	2.65	7.53	51.3
Taiheiyo	sub	76.72	6.35	1.13	0.21	15.59	11.12	2.64	54.7
Miike	hvb	79.91	6.13	1.18	4.48	8.30 ^b	18.79	0.88	53.0
Hunter Valley	hvb	82.82	5.43	2.08	0.48	9.18	9.25	1.39	37.2
Pittsburgh	hvb	82.77	5.48	1.64	3.38	6.73 ^b	8.83	0.72	42.5
Upper Freeport	mvb	84.15	5.13	1.55	4.56	4.60 ^b	15.75	0.31	33.4
Pocahontas	lvb	91.57	4.57	1.36	0.76	1.74	5.06	0.22	20.1

^a ASTM volatile matter

^b Sulfur values include inorganic sulfur, thus O values are somewhat under-estimated.

Table 5.2

Summary of ultimate analyses, dry ash, and mass release (%MR) for chars produced in the drop tube and flat flame reactor (FFR) pyrolysis experiments.

Coal	Condition	% C (daf)	% H (daf)	% N (daf)	% S (daf)	% O (daf) (by diff.)	% ash (dry)	% MR (daf)
Yallourn	coal	65.31	4.76	0.52	0.18	29.22	1.58	-
	900 K	75.32	3.33	0.68	0.18	20.49	3.27	46.0 ^a
	1000 K	84.09	2.95	0.73	0.14	12.09	2.95	55.0 ^a
	1100 K	87.65	2.57	0.70	0.13	8.94	3.50	57.8 ^a
	1650 K	91.84	1.27	0.58	0.14	6.18	4.46	69.0 ^a
South Banko	coal	71.37	5.36	1.18	0.55	21.55	2.65	-
	900 K	78.25	3.77	1.52	0.46	16.00	4.18	41.6
	1000 K	81.61	3.16	1.59	0.30	13.35	4.57	51.1
	1100 K	84.18	2.91	1.58	0.24	11.09	4.79	54.4
	1250 K	91.33	1.74	1.42	0.35	5.16	5.17	58.3
	1650 K	90.70	1.61	1.36	0.31	6.01	5.73	64.1
Taiheiyo	coal	76.72	6.35	1.13	0.21	15.59	11.12	-
	975 K	80.71	3.88	1.43	0.22	13.76	20.80	53.3
	1000 K	84.25	3.34	1.49	0.18	10.74	22.28	58.3
	1100 K	85.16	3.04	1.49	0.18	10.13	23.23	60.4
	1650 K	86.92	2.79	1.38	0.23	8.67	25.61	64.4
Miike	coal	79.91	6.13	1.18	4.48	8.30	18.79	-
	900 K	82.48	3.44	1.48	7.15	5.46	40.82	66.8 ^c
	1000 K	85.28	3.42	1.44	5.78	4.08	36.94	63.9
	1100 K	89.97	3.00	1.40	4.49	1.13	38.50	64.7
	1650 K	92.65	2.30	1.29	4.76	-1.00 ^b	42.52	68.9
Hunter Valley	coal	82.82	5.43	2.08	0.48	9.18	9.25	-
	900 K	87.18	4.08	2.35	0.46	5.92	13.87	38.6
	1000 K	88.05	3.42	2.47	0.31	5.74	15.47	43.8
	1100 K	89.94	2.84	2.48	0.34	4.41	16.14	47.9
	1650 K	91.29	2.27	2.22	0.71	3.52	18.58	52.4
Pittsburgh	coal	82.77	5.48	1.64	3.38	6.73	8.83	-
	900 K	80.91	4.15	1.72	6.08	7.14	14.76	45.1
	950 K	82.46	4.06	1.78	5.97	5.73	15.25	47.2
	(replicate exp.) 950 K	82.51	4.02	1.78	5.38	6.31	14.69	46.4
	1000 K	87.49	3.37	1.92	3.82	3.41	15.72	50.7

Table 5.2 (cont.)

Coal	Condition	% C (daf)	% H (daf)	% N (daf)	% S (daf)	% O (daf) (by diff.)	% ash (dry)	% MR (daf)
Pittsburgh	1100 K	87.99	3.08	1.78	3.72	3.43	16.87	54.4
	1250 K	92.18	1.72	1.76	3.68	0.66	18.76	59.8
	1650 K	88.56	2.64	1.73	4.48	2.59	19.27	59.1
Upper Freeport	coal	84.15	5.13	1.55	4.56	4.60	15.75	-
	900 K	85.47	3.09	1.61	4.82	5.01	24.68	42.9 ^c
	1000 K	85.99	3.31	1.62	8.32	0.77	N.M.	49.0 ^d
	1100 K	89.21	2.81	1.69	5.13	1.17	25.56	45.2
	1650 K	92.17	2.05	1.64	3.24	0.90	24.82	43.6
Pocahontas	coal	91.57	4.57	1.36	0.76	1.74	5.06	-
	900 K	91.54	4.32	1.35	0.73	2.05	5.79	13.4
	1000 K	93.31	3.45	1.43	0.67	1.14	6.24	21.7
	1100 K	92.45	2.96	1.42	0.61	2.56	6.34	25.8
	1650 K	95.41	2.14	1.33	0.61	0.51	6.33	24.7

^a Mass release for Yallourn chars determined by overall mass balance, not tracer mass balance.

^b Sulfur values include inorganic sulfur, thus O values are somewhat under-estimated.

^c A large proportion of the char was lost in the collection system during this test.

^d Char held up in collection system and formed large chunks

from an overall mass balance was lower than the mass release from tracer measurements, mass release values calculated by overall mass balance were 2-6% (absolute) higher than those obtained using tracers, probably due to small losses of coal and char. A summary of the ultimate analyses and yields for the corresponding *tars and soots* generated in these pyrolysis experiments is shown in Table 5.3, with the corresponding parent coal data again shown for comparison. The jet-black, very low density solid product in the gas phase of the FFR tests (1650 K) was considered to be soot, consistent with the findings of Ma.⁴¹ The solid which condensed on the tar filters from the gaseous pyrolysis products of the drop tube tests was sticky and brown or yellow in color and was considered to be tar. In Table 5.2, note that the char carbon content rises with increasing severity of pyrolysis.

Table 5.3

Summary of ultimate analyses and yields of tars/soots produced in the drop tube and flat flame reactor (FFR) pyrolysis experiments.

Coal	Condition	% C (daf)	% H (daf)	% N (daf)	% S (daf)	% O (daf) (by diff.)	% tar yield (daf) ^a
Yallourn	coal	65.31	4.76	0.52	0.18	29.22	-
	900 K	73.25	5.79	0.54	0.12	20.30	10.5
	1000 K	79.19	4.64	0.78	0.17	15.22	6.6
	1100 K	86.37	4.58	0.91	0.23	7.90	3.9
	(FFR) 1650 K	96.18	2.19	0.18	0.08	1.36	5.1
South Banko	coal	71.37	5.36	1.18	0.55	21.55	-
	900 K	78.82	6.69	1.18	0.41	12.90	15.0
	1000 K	81.48	4.82	1.69	0.54	11.46	9.0
	1100 K	84.66	4.65	1.77	0.58	8.35	7.4
	(FFR) 1650 K	98.09	2.05	0.29	0.13	-0.56 ^b	6.9
Taiheiyo	coal	76.72	6.35	1.13	0.21	15.59	-
	975 K	81.81	6.37	1.34	0.16	10.32	22.5
	1000 K	85.55	5.75	1.63	0.23	6.84	17.1
	1100 K	87.51	4.76	1.72	0.25	5.76	12.9
	(FFR) 1650 K	96.68	2.32	0.47	0.11	0.42	15.1
Miike	coal	79.91	6.13	1.18	4.48	8.30	-
	900 K	85.42	6.06	1.38	2.68	4.47	24.7
	1000 K	86.99	4.76	1.59	3.07	3.60	31.2
	1100 K	89.89	4.36	1.65	2.40	1.69	25.4
	(FFR) 1650 K	96.67	1.74	0.54	0.63	0.42	19.5
Hunter Valley	coal	82.82	5.43	2.08	0.48	9.18	-
	900 K	84.62	6.02	2.07	0.43	6.86	22.3
	1000 K	86.54	4.92	2.38	0.48	5.67	21.8
	1100 K	91.12	4.44	2.54	0.48	1.42	19.5
	(FFR) 1650 K	96.61	1.78	0.83	0.17	0.61	14.8
Pittsburgh	coal	82.77	5.48	1.64	3.38	6.73	-
	900 K	84.12	5.87	1.71	0.97	7.33	31.8
	950 K	85.50	5.65	1.76	1.02	6.08	28.5
	(replicate exp.) 950 K	86.55	5.66	1.81	1.03	4.94	-
	1000 K	86.50	4.85	1.91	1.38	5.36	28.7
	1100 K	88.92	4.43	1.99	1.47	3.20	25.1

Table 5.3 (cont.)

Coal	Condition	% C (daf)	% H (daf)	% N (daf)	% S (daf)	% O (daf) (by diff.)	% tar yield (daf) ^a
Pittsburgh	1250 K	93.31	2.87	1.51	1.24	1.06	26.6
	(FFR) 1650 K	95.02	1.75	0.81	0.40	2.01	21.0
Upper Freeport	coal	84.15	5.13	1.55	4.56	4.60	-
	900 K	87.95	5.53	1.60	0.97	3.94	18.4
	1000 K	89.51	4.73	1.79	1.15	2.82	27.7
	1100 K	92.25	4.24	1.93	1.31	0.27	27.5
	(FFR) 1650 K	94.96	1.32	0.74	0.33	2.65	17.7
	coal	91.57	4.57	1.36	0.76	1.74	-
Pocahontas	900 K	90.80	5.26	1.34	0.69	1.91	7.5
	1000 K	92.32	4.78	1.41	0.69	0.81	15.1
	1100 K	92.64	4.50	1.45	0.67	0.74	14.2
	(FFR) 1650 K	98.25	1.31	0.63	0.21	-0.40 ^b	10.7

^a Tar yields reported for FFR tests are actually soot yields.

^b Negative oxygen concentrations are not correct, but are reported for completeness.

However, the two chars from the 1250 K drop tube tests have higher carbon contents than the corresponding chars produced in the FFR. This may indicate that some of the oxygen released in the 1250 K experiments (294 ms) did not have time to be released in the 1650 K FFR experiments (18 ms).

These experimental data are also tabulated in Appendix D for convenience. Additional pyrolysis tests were also performed in the flat flame reactor and the drop tube reactor. Some of these additional tests were preliminary in nature, having been performed before a reliable procedure had been adopted. Other of these pyrolysis tests gauged the effect of volatiles on light gas nitrogen release by pyrolysis of already partially devolatilized chars, the results of which are not included in this chapter since very little effect was seen. Results from all the additional tests are found in Appendix E.

Error Analysis

An error analysis was performed to assess the variability associated with 1) sample splitting, 2) sample characterization techniques, and 3) pyrolysis test replication. Because of slight but permanent changes in the condition of the drop tube equipment just after the time when these experiments were performed, very little pyrolysis experiment replication could be performed. However, the replicate pyrolysis experiments that were performed give some indication of the repeatability of the pyrolysis tests. Furthermore, replicate samples were split off from some pyrolysis products in order to perform replicate analyses to test the repeatability of various characterization techniques. Variation introduced intrinsically in each characterization technique was coupled with the variation introduced by sample splitting.

Table 5.4 shows five replicate characterizations of a Pittsburgh char produced at the 950 K condition. Uncertainty measurements represent the standard deviation as calculated from 5 replicate elemental determinations of a single sample. This char was chosen for the

Table 5.4

Replicate sample characterization for chars produced in the drop tube at the 950 K condition using Pittsburgh coal.

	Original	CHNS replicate (same day)	Sample split replicate	Pyrolysis test replicate (next day)	CHNS replicate (not pulverized)
% Ash (dry)	14.8	-	14.6	15.3	-
% H ₂ O (AR)	0.7	-	0.7	0.8	-
% C (daf)	82.6 ± 0.2 ^a	82.4 ± 0.1	82.5 ± 0.1	82.5 ± 0.3	84.2 ± 2.3
% H (daf)	4.03 ± 0.02	4.01 ± 0.03	4.02 ± 0.01	4.06 ± 0.04	4.00 ± 0.10
% N (daf)	1.79 ± 0.02	1.77 ± 0.03	1.78 ± 0.02	1.78 ± 0.02	1.89 ± 0.06
% S (daf)	5.31 ± 0.10	5.45 ± 0.06	5.38 ± 0.10	5.97 ± 0.11	4.45 ± 0.88
N/C ratio	0.0217	0.0215	0.0216	0.0216	0.0225
MR (tracer)	46.3 %	-	46.4 %	47.2 %	-

^a Uncertainty measurements represent the standard deviation as calculated from 5 replicate elemental determinations of a single sample.

error analysis because of the very large density differences between high-ash particles and low-ash (and swollen) particles in the char that could cause large errors if inadequate sampling techniques were employed. The first column in Table 5.4 is the characterization of the original char sample. The second column contains a replicate elemental analysis of the original sample performed 30 minutes later. The third column in Table 5.4 contains the characterization of a second sample split off from the original char using the single stream sample splitter. The fourth column in Table 5.4 contains characterization of char produced in a replicate pyrolysis test one day after the original test. The fifth column contains the elemental analysis of a split from original sample that was not pulverized to a fine powder before analysis. The elemental analyses in columns 1-4 of Table 5.4 were all performed within hours of each other, while that in column 5 was performed on a different day. Comparison of columns 1, 2, and 3 in Table 5.4 show that variation introduced by the use of sample splitting is no larger than the intrinsic variation in the elemental analyzer, which is about 0.3% and 0.8% relative for carbon and hydrogen, respectively. Comparison of columns 1 and 3 in Table 5.4 gives an idea of the intrinsic variation of the ash, moisture, and mass release (by tracer) analyses. The intrinsic variation for each of these appears to be less than 1.5% (relative). Comparison of columns 1 and 4 in Table 5.4 gives an idea of the variation associated with pyrolysis test replication, which is largest as measured by ash content (about 3.5% relative) and mass release (about 2% relative). Possible sources of pyrolysis test replication variation include variations in: a) parent coal characteristics; b) particle temperature history; and c) char collection procedure. Replicate pyrolysis tests performed months later (after permanent changes had occurred in the drop tube apparatus) showed significantly larger differences in the measured gas temperature profile as well as in char characteristics. Comparison of columns 1 and 5 in Table 5.4 give some idea of the error introduced by neglecting to pulverize samples to a fine powder before performing elemental composition determinations. If char samples are pulverized to a fine powder

prior to elemental analysis, 1 mg sub-samples (required by the analyzer) can be produced which are much more representative of the entire sample.

Because it was observed that nitrogen content determination was associated with a large amount of variation, an analysis was performed to identify the nature of this variability. In Table 5.5 elemental determination replicates of a Pittsburgh char produced in the drop tube at 1100 K are shown. The coefficient of variation (CV, sometimes called the relative standard deviation) referred to in Table 5.5 is defined as:

$$CV = \frac{\sqrt{\frac{1}{n-1} \sum_{i=1}^n (x_i - \bar{x})^2}}{\bar{x}} \quad (5.1)$$

where x_i is the value of the i^{th} replicate, n is the total number of replicates, and \bar{x} is the mean value of all replicates. The effect of pulverizing samples to a fine powder prior to elemental analysis can be seen in Table 5.5, as replicates 1 and 2 (unpulverized) show inconsistent values, high coefficients of variation, and even a negative oxygen concentration (replicate 2). On the other hand, comparison of replicate 3 (pulverized) with replicate 1 shows that pulverizing the samples before elemental analysis can reduce coefficients of variation for carbon and hydrogen by as much as a factor of 10 and a factor of 4, respectively. This is due to the increased ability after pulverization to produce sub-samples of about 1 mg which are representative of the entire sample. However, the variability of the nitrogen reading seems to be high whether the samples are pulverized or not. In addition, the measured N/C ratio, which should not be affected by whether the sample was pulverized (being independent of the ash content), changes by 9% between December, 1998 and March, 1999. This is due almost entirely to changes in nitrogen content measurements over time. In fact, changes in measured nitrogen content of between

Table 5.5

Replicate sample characterization for char produced in the drop tube at the 1100 K condition using Pittsburgh coal.

	Replicate 1	Replicate 2	Replicate 3
CHNS analysis date	22-Sep-98	22-Dec-98	25-Mar-99
pulverized?	no	no	yes
Mean values:			
% C (daf)	91.50%	95.20%	87.99%
% H (daf)	3.12%	3.27%	3.08%
% N (daf)	2.03%	2.12%	1.78%
% S (daf)	2.57%	2.59%	3.72%
% O (daf, by difference)	0.78%	-3.18% ^a	3.43%
N/C (w/w) ratio	0.0222	0.0223	0.0203
Coefficients of variation:			
% C	1.70%	0.74%	0.15%
% H	2.42%	1.32%	0.62%
% N	-	1.15%	1.10%
% S	20.53%	6.56%	0.90%

^a Negative oxygen concentrations are not correct, but are reported for completeness.

0-7% (relative) were observed when three coals analyzed all on the same day were re-analyzed a week later. No such change was observed in measured carbon contents. This implies that nitrogen values as measured in this study are only good to within about 7% (relative), even though the variation in measured nitrogen contents when analyzing 5 consecutive replicates during this study was almost always less than 2%. Thus the nitrogen determination as performed on the BYU elemental analyzer is not nearly as repeatable over a long period of time as the carbon (or hydrogen) determination. The reasons for this are unclear at this time. However, if samples are analyzed consecutively in the analyzer, variations in the measured nitrogen content are much smaller, around 2% (relative).

It is estimated that the nitrogen contents (and N/C ratios) of the chars and tars are only accurate to within about 7% (relative), while carbon contents are probably accurate to within 2%, and hydrogen contents to within 3%. Organic sulfur contents are far from accurate, the measurement taken on the elemental analyzer being a combination of both organic and inorganic sulfur. Tar yields are probably accurate to within 6% (relative), with nearly all of the error coming from tar loss estimation (which losses ranged from 15%-30% of the total tar). Overall mass release values are thought to be accurate to within 3% (absolute), or about 6% relative, except for those tests (noted in table footnotes) in which anomalies were observed. The corrected temperature profiles are probably accurate to within 50°C in the drop tube and to within 100°C in the flat flame reactor.

Chemical Structure Results (¹³C NMR)

A summary of data from the ¹³C NMR analyses performed at the University of Utah on selected char and tar samples is given in Tables 5.6 and 5.7 for chars and tars, respectively. The corresponding derived structural parameters for these samples are found in Tables 5.8 and 5.9. The data in Tables 5.7 and 5.9 represent the results of some of the first extensive solid-state ¹³C NMR tar analyses ever performed, those of Hambly¹¹ being the only other data of this type. The tar data reported here differ from those of Hambly in that they include tars collected over a range of degree of pyrolysis severity. These data are also tabulated in Appendix D for more convenient access.

Analysis of Mass Release and Tar Data

In Figure 5.1, tar yield and total mass release values from the 900 K condition of this study (with particle temperatures estimated at 1040 K) for Yallourn, Taiheiyu, and Hunter Valley coals are compared to tar yield (calculated by difference) and mass release values reported by Xu and Tomita⁷⁶ for Curie-point pyrolysis at 1037 K. Although mass

Table 5.6

Parameters measured via ^{13}C NMR at the University of Utah for *chars* from the drop tube and flat flame reactor (FFR) pyrolysis experiments.^a

Coal	Condition	f_a	f_a^C	f_a'	f_a^H	f_a^N	f_a^P	f_a^S	f_a^B	f_{al}	f_{al}^H	f_{al}^*	f_{al}^O
Yallourn	coal	67	10	57	16	41	16	9	16	33	23	10	9
	2-D coal ^b	67	10	57	16	41	19	22	0	33	23	10	9
	1100 K	96	5	91	37	54	6	21	27	4	3	1	3
South Banko	coal	62	8	54	17	37	9	13	15	38	28	10	5
	Sv. coal ^c	61	8	53	16	37	9	13	15	39	30	9	5
	900 K	86	6	80	24	56	10	18	28	14	8	6	2
	1000 K	95	5	90	32	58	8	20	30	5	3	2	2
	1100 K	95	4	91	34	57	7	20	30	5	4	1	2
	1250 K	93	10	83	17	66	7	19	40	7	5	2	5
(FFR)	1650 K	91	11	80	24	56	7	17	32	9	6	3	5
Taiheiyo	coal	56	5	51	16	35	6	14	15	44	32	12	4
	1100 K	97	3	94	33	61	5	19	37	3	2	1	2
Miike	coal	66	2	64	22	42	6	17	19	34	24	10	3
	1100 K	96	8	88	30	58	9	25	24	4	3	1	2
Hunter Valley	coal	74	3	71	25	46	8	19	19	26	17	9	4
	1100 K	95	4	91	34	57	5	20	32	5	4	1	3
Pittsburgh	coal	71	1	70	27	43	6	15	22	29	21	8	4
	950 K	92	2	90	32	58	6	19	33	8	4	3	1
	1000 K	93	2	91	34	57	5	19	33	7	4	3	2
	1100 K	95	3	92	40	52	5	21	26	5	4	1	2
	1250 K	92	11	81	20	61	7	17	37	8	6	2	5
	(FFR)	1650 K	95	10	85	29	56	8	22	26	5	4	1
Upper Freeport	coal	81	0	81	28	53	4	20	29	19	11	8	2
	1100 K	97	4	93	33	60	5	21	34	3	2	1	2
Pocahontas	coal	86	0	86	33	53	2	17	34	14	9	5	1
	1100 K	97	2	95	36	59	3	19	37	3	2	1	2

^a Percentage carbon (error): f_a = total sp^2 -hybridized carbon (± 3); f_a' = aromatic carbon (± 4); f_a^C = carbonyl, $d > 165$ ppm (± 2); f_a^H = aromatic with proton attachment (± 3); f_a^N = nonprotonated aromatic (± 3); f_a^P = phenolic or phenolic ether, $d = 150$ - 165 ppm (± 2); f_a^S = alkylated aromatic $d = 135$ - 150 ppm (± 3); f_a^B = aromatic bridgehead (± 4); f_{al} = aliphatic carbon (± 2); f_{al}^H = CH or CH_2 (± 2); f_{al}^* = CH_3 or nonprotonated (± 2); f_{al}^O = bonded to oxygen, $d = 50$ - 90 ppm (± 2).

^b As analyzed by 2-D ^{13}C NMR

^c Sieved coal (45-75 μm fraction)

Table 5.7

Parameters measured via ^{13}C NMR at the University of Utah for tars from the drop tube and flat flame reactor (FFR) pyrolysis experiments.^a

Coal	Condition	f_a	f_a^C	f_a^L	f_a^H	f_a^N	f_a^P	f_a^S	f_a^B	f_{al}	f_{al}^H	f_{al}^*	f_{al}^O
South Banko	coal	62	8	54	17	37	9	13	15	38	28	10	5
	900 K	69	6	63	23	40	9	15	16	31	21	10	3
	1000 K	88	4	84	40	44	9	17	18	12	6	6	2
	1100 K	90	2	88	44	44	7	18	19	10	6	4	3
	1250 K	95	1	94	49	45	3	18	24	5	4	1	2
Pittsburgh	coal	71	1	70	27	43	6	15	22	29	21	8	4
	950 K	78	2	76	33	43	6	17	20	22	13	9	3
	1000 K	87	1	86	40	46	6	18	22	13	7	6	2
	1100 K	90	1	89	43	46	4	17	25	10	6	4	3
	1250 K	93	5	88	36	52	5	17	30	7	6	1	4
(FFR)	1650 K	91	7	84	29	55	5	14	36	9	7	2	5

^a see footer to Table 5.6.

Table 5.8

Structural parameters derived from ^{13}C NMR for *chars* produced in the drop tube and flat flame reactor (FFR) pyrolysis experiments.^a

Coal	Condition	b	C_{cl}	+1	P_0	B.L.	S.C.	M_{cl}	M
Yallourn	coal	0.281	14	6.1	0.60	3.7	2.4	452	46
	2-D coal [†]	0.000	6	4.3	0.76	3.3	1.0	189	27
	1100 K	0.297	14	4.2	0.96	4.0	0.2	211	9
South Banko	coal	0.278	13	5.3	0.55	2.9	2.4	405	46
	Sv. coal [‡]	0.283	14	5.8	0.59	3.4	2.4	450	48
	900 K	0.350	17	6.0	0.79	4.7	1.3	326	20
	1000 K	0.333	16.5	5.1	0.93	4.7	0.4	270	13
	1100 K	0.330	16	4.7	0.96	4.5	0.2	251	11
	1250 K	0.482	24	7.4	0.92	6.8	0.6	380	12
(FFR)	1650 K	0.400	20	6.0	0.88	5.3	0.7	331	14
Taiheiyo	coal	0.294	14	5.5	0.40	2.2	3.3	430	47
	1100 K	0.394	19	4.9	0.96	4.7	0.2	285	10
Miike	coal	0.297	14	5.0	0.57	2.9	2.1	329	31
	1100 K	0.273	13	5.0	0.97	4.9	0.1	197	7
Hunter Valley	coal	0.268	13	4.9	0.67	3.3	1.6	266	21
	1100 K	0.352	17.5	4.8	0.96	4.6	0.2	257	8
Pittsburgh	coal	0.314	15	4.5	0.62	2.9	1.6	311	28
	950 K	0.367	18	5.0	0.88	4.4	0.6	291	14
	1000 K	0.363	18	4.7	0.88	4.1	0.6	272	10
	1100 K	0.283	14	3.9	0.96	3.7	0.2	208	8
	1250 K	0.457	22	6.5	0.92	6.0	0.5	354	13
(FFR)	1650 K	0.306	15	5.3	0.97	5.1	0.2	239	10
Upper Freeport	coal	0.358	18	5.3	0.67	3.6	1.7	317	18
	1100 K	0.366	18	5.0	0.96	4.8	0.2	261	8
Pocahontas	coal	0.395	20	4.4	0.74	3.3	1.1	305	13
	1100 K	0.389	19	4.4	0.95	4.2	0.2	260	6

^a b = fraction of bridgehead carbons, C_{cl} = aromatic carbons per cluster, +1 = total attachments per cluster, P_0 = fraction of attachments that are bridges, B.L. = bridges and loops per cluster, S.C. = side chains per cluster, MW_{cl} = the average molecular weight of an aromatic cluster, MW = the average molecular weight of the cluster attachments.

Table 5.9

Structural parameters derived from ^{13}C NMR for tars produced in the drop tube and flat flame reactor (FFR) pyrolysis experiments.^a

Coal	Condition	b	C_{cl}	+1	P_0	B.L.	S.C.	M_{cl}	M
South Banko	coal	0.278	13	5.3	0.55	2.9	2.4	410	47
	900 K	0.254	12	4.5	0.58	2.6	1.9	290	31
	1000 K	0.214	10.5	3.3	0.77	2.5	0.8	184	16
	1100 K	0.216	11	3.0	0.84	2.5	0.5	177	13
	1250 K	0.255	12	2.7	0.95	2.6	0.1	164	5
Pittsburgh	coal	0.314	15	4.5	0.62	2.9	1.6	311	28
	950 K	0.263	13	4.0	0.61	2.4	1.6	240	20
	1000 K	0.256	12	3.3	0.75	2.5	0.8	194	13
	1100 K	0.281	13.5	3.2	0.81	2.6	0.6	205	11
	1250 K	0.341	17	4.2	0.95	4.0	0.2	249	9
(FFR)	1650 K	0.429	21	4.8	0.89	4.3	0.5	316	12

^a see footer to Table 5.8.

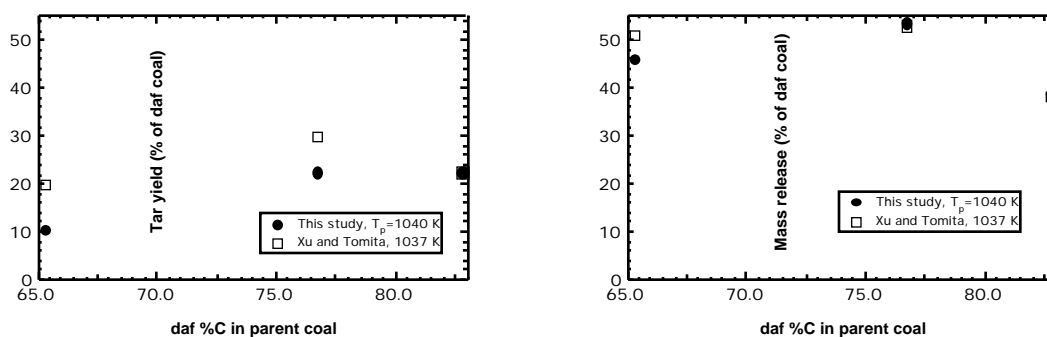


Figure 5.1. Tar yield and total mass release values at the 900 K condition are compared to values reported by Xu and Tomita⁷⁶ for Curie-point pyrolysis of Yallourn, Taiheiyu, and Hunter Valley coals. Daf %C is used as an indicator of rank.

release values agree well between the two studies, tar yields of the two low rank (low %C) coals are much lower in this study, probably due to some secondary reactions in the BYU tars and because the Xu and Tomita tar yields were calculated by difference, making them susceptible to over-estimation.

Mass release values were confirmed independently of the overall mass balance (for all coals except Yallourn) by the use of Ti and Al as tracers. For the chars produced at 1100 K, for which ^{13}C NMR structural data are available, mass release values can also be estimated as the sum of tar yields and the estimated total light gas yields. The percent of parent coal that forms light gas is estimated as the percent decay in M_{cl} (the molecular weight per cluster) in the char relative to the parent coal. This can be calculated as:

$$\text{Estimated light gas yield} = \% M_{cl} \text{ decay} = 1 - \frac{M_{cl, \text{char}}}{M_{cl, \text{coal}}} \frac{M_{\text{site, coal}}}{M_{\text{site, char}}} 100\% \quad (5.2)$$

where M_{site} is the molecular weight of the aromatic portion of an average cluster, including protons attached to aromatic carbons. M_{site} is defined as:

$$M_{\text{site}} = C_{cl} \left[12.01 \left(1 - \frac{f_a^H}{f_a} \right) + 13.02 \frac{f_a^H}{f_a} \right] \quad (5.3)$$

where C_{cl} is the average number of aromatic carbons per cluster, f_a^H is the fraction of carbon which is both aromatic and protonated, and f_a is the fraction of carbon which is aromatic. In Equation 5.3, protonated aromatic carbons are assigned a molecular weight of 13.02, while all other aromatic carbons are assigned a molecular weight of 12.01. In equation 5.2 the char molecular weight decay is adjusted to eliminate scatter in measured M_{site} values, since M_{site} is thought to remain constant at the parent coal value throughout primary pyrolysis. This adjustment is explained in detail in chapter 6.

This method of mass release estimation assumes that the chars and tars have approximately the same percentage of mass that is aromatic. This assumption can be evaluated at the 1100 K condition by comparing the fraction of mass which is aromatic in the tars and the chars for the tests using South Banko and Pittsburgh coals. For the

1100 K tests the fraction of mass that is aromatic is 0.794 and 0.780 for the South Banko char and tar, respectively, and 0.854 and 0.828 for the Pittsburgh char and tar, respectively. Once the estimated light gas yield has been calculated (Equation 5.2), the daf mass release can also be estimated as the sum of the estimated light gas yield and the measured tar yield. As can be seen in Figure 5.2, the resulting estimated values of the mass release are very close to the measured values for all eight parent coals pyrolyzed at 1100 K. Thus the ^{13}C NMR analyses, together with the tar yield measurements, independently validate the experimental mass release values. Conversely, the mass release measurements (via Ti and Al tracer) validate the tar yield and ^{13}C NMR aromaticity measurements.

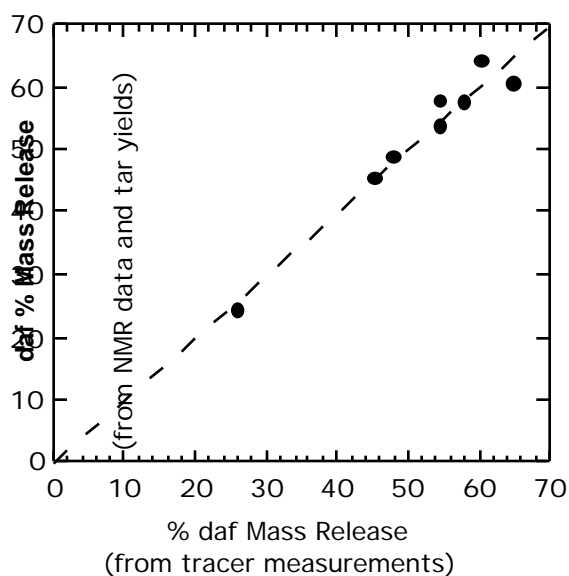


Figure 5.2. Validation of % daf mass release calculated from tracer measurements at 1100 K condition using tar yield and ^{13}C NMR data.

Ultimate (FFR) mass release values compare well with values reported for rapid pyrolysis of similar coals reported in the literature. Figure 5.3 compares ASTM volatile matter (as % of daf coal) and the measured ultimate total volatiles release for various coals

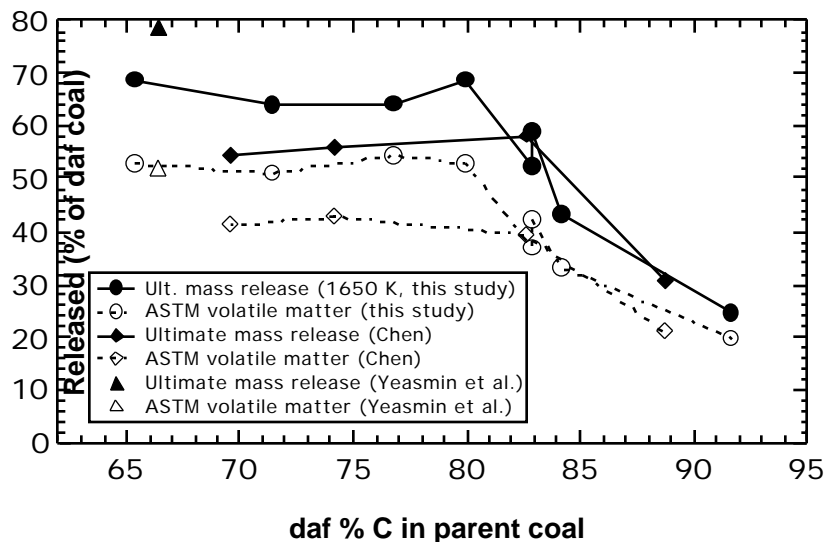


Figure 5.3. Comparison of ultimate mass release values from the 1650 K flat flame reactor experiments with daf ASTM volatile matter contents. Also shown are ultimate mass release values and ASTM volatile matter contents reported by Chen³⁹ and by Yeasmin et al.⁷⁷ Parent coal carbon content is used as an indicator of rank.

reported in the literature and as reported in this study. It can be seen that the high ultimate mass release values measured in the flat flame reactor (FFR) for this study show the same relationship to volatile matter content as those reported by Chen.³⁹ Furthermore, it is possible that the Yallourn coal pyrolyzed in the FFR has not yet reached the ultimate (highest possible) mass release, as suggested by comparison with the data of Yeasmin et al. (for char produced at 1273 K, 1.5 sec.).⁷⁷ Although the ASTM volatile matter contents measured in this study for the low rank coals are significantly higher than those reported by Chen for coals of similar carbon content, some researchers have measured even higher values for various low rank coals. For example, Smith et al.¹⁹ report daf ASTM volatile matter contents for a Wyodak subbituminous C (PSOC-1520) and a Lower Wilcox lignite A (PSOC-1443) of 62.5 and 78.7% respectively. In Figure 5.4, flat flame reactor mass release values reported by Ma for a North Dakota lignite at a variety of residence times and temperatures are compared to those measured for Yallourn and South Banko coals in this

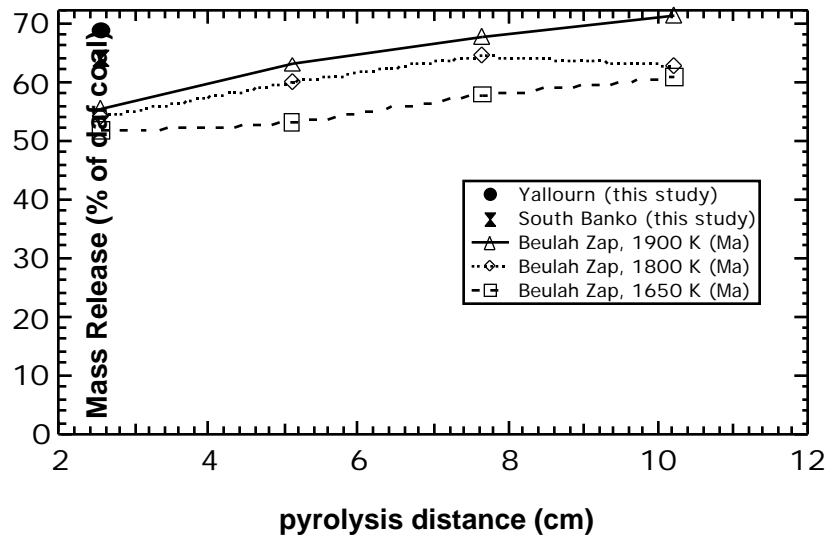


Figure 5.4. Comparison of measured flat flame reactor total volatiles release reported by Ma⁴¹ for a North Dakota lignite and those measured for Yallourn and South Banko coals in this study.

study. It can be seen in Figure 5.4 that high temperature rapid pyrolysis conditions exist which can cause low rank coals to lose much more mass than expected based on pyrolysis tests at slightly milder conditions. The Yallourn, South Banko, and Taiheiyo mass release data show the same trend, increasing significantly as conditions become more severe (see Figure 5.6). The soot yield for Pittsburgh hva bituminous coal at 1650 K (Table 5.3) matches that reported by Ma for the same residence time.⁴¹

A graphical summary of total volatiles yields from all of the pyrolysis tests grouped by rank is shown in Figure 5.5. Total volatiles yields from low rank coals increase by about 20 % daf (absolute) with an increase in temperature from 1100 K (drop tube) to 1650 K (flat flame reactor), while those from sub-bituminous and high volatile bituminous coals increase by less than 5 % daf (absolute); those from high rank coals do not increase at all. The greatly increased total mass release from low rank coals at 1650 K is evidence of either an increase in the light gas yield or an increase in the primary tar yield as early cross-linking reactions (which restrict tar release) are minimized. A similar effect was reported by Ma⁴¹ for severe pyrolysis of a North Dakota lignite (see Figure 5.4).

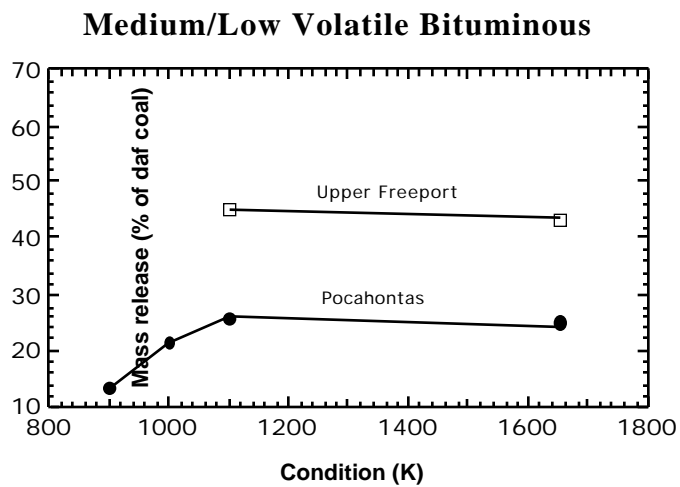
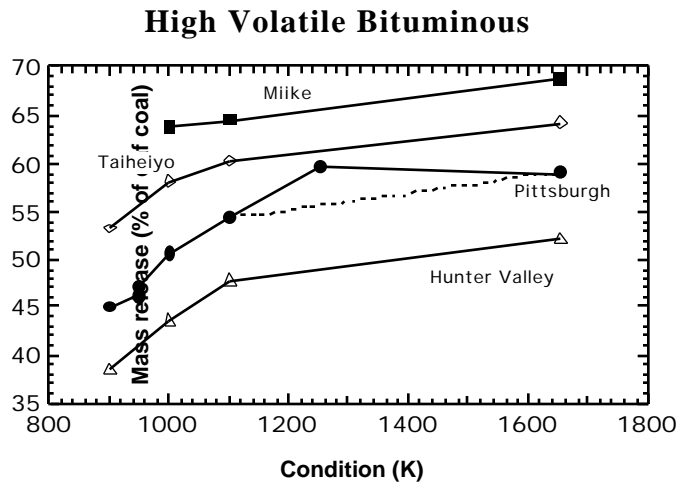
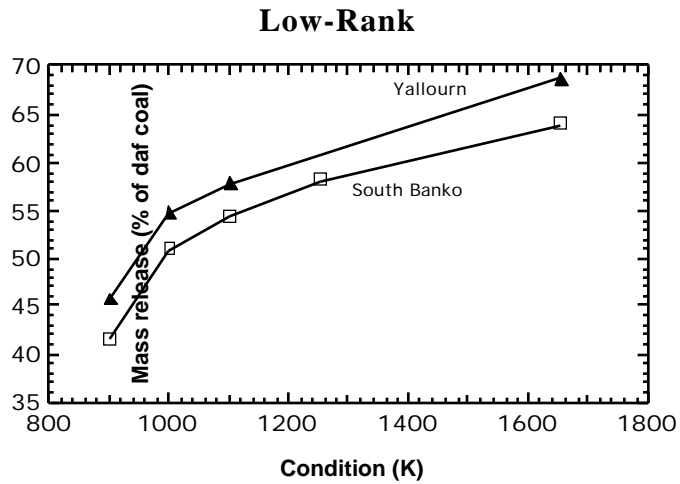


Figure 5.5. Variation of measured **total volatiles** yields with pyrolysis severity grouped by coal rank. Pyrolysis conditions are summarized in Table 4.1.

Examination of the trend with rank of tar yields shows that, except for high rank coals such as Upper Freeport and Pocahontas, tar release is essentially complete at the lowest (900 K) condition. A graphical summary of measured tar and soot yields from all of the pyrolysis tests grouped by rank is shown in Figure 5.6. Note that coals of similar rank exhibit the same trends with increasing severity of pyrolysis, both in terms of tar/soot yields and total volatiles yields. Tar yields from low rank coals reach a maximum early on, then decay as aliphatic material is lost during secondary reactions while tar yields from high rank coals (medium/low volatile bituminous) reach a maximum much later, at pyrolysis temperatures of 1000 or 1100 K. Tar yields from high volatile bituminous coals show characteristics of both effects, generally decreasing with increasing severity of pyrolysis. Comparison of these data with Chemical Percolation Devolatilization (CPD) model tar and total volatiles predictions can be found in Appendix F.

Analysis of Nitrogen Distribution Data

Table 5.10 shows the distribution of nitrogen among the pyrolysis products of each test as a percentage of parent coal nitrogen. Measured HCN and NH₃ concentrations are shown, as well as the total light gas nitrogen as calculated by difference. Note that despite the quantitative measurement of both HCN and NH₃, there is a large disparity between the measured total light gas nitrogen values and those calculated by difference. This problem was also experienced by past researchers using the BYU drop tube in the case where ammonia analysis was not performed. Preliminary Fourier Transform Infra-red (FTIR) measurements of gas phase HCN and NH₃ indicate problems with the current method of NH₃ analysis. For example, the South Banko test at 1000 K was repeated several months later with FTIR measurement of HCN and NH₃ performed by Haifeng Zhang.³¹ In this case the HCN and NH₃ nitrogen yields measured via FTIR were 6.4 and 13.6% of coal nitrogen, respectively, while the analyzer used for the original pyrolysis test gas analysis

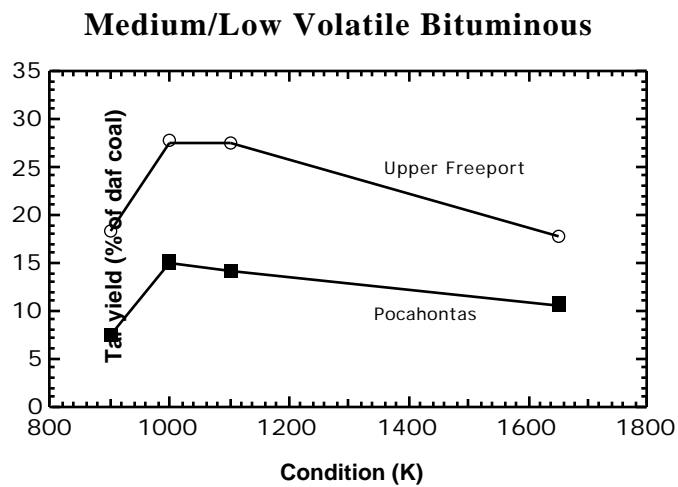
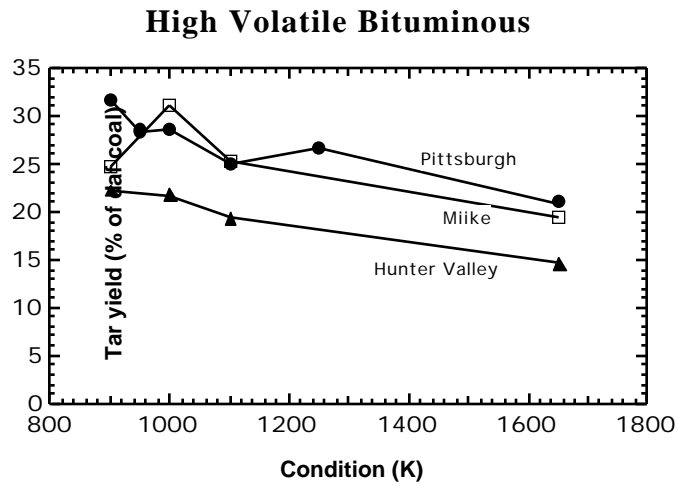
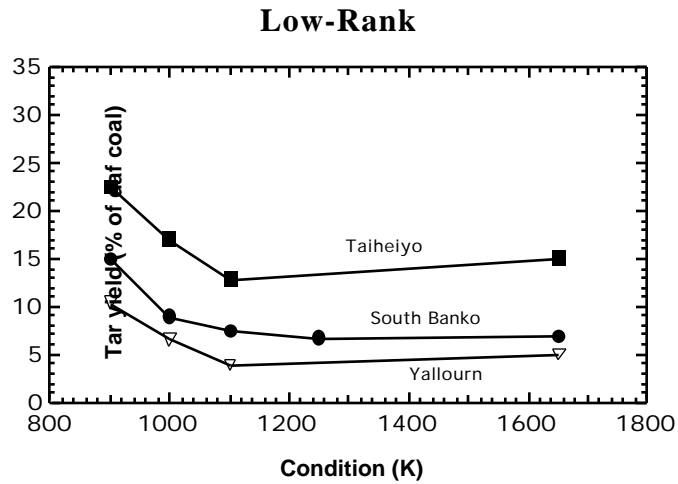


Figure 5.6. Variation of measured tar and soot yields with pyrolysis severity grouped by coal rank. Pyrolysis conditions are summarized in Table 4.1.

Table 5.10**Distribution of nitrogen in pyrolysis products for drop tube and flat flame reactor (FFR) tests.**

Parent Coal	Condition	Nitrogen yield (as % of coal N)					Char N _{site} decay
		Tar	Char	HCN	NH ₃	Light gas ^a	
Yallourn	900 K	10.9	70.5	5.3	0.0	18.6	N.M.
	1000 K	9.8	63.3	9.3	0.0	26.8	N.M.
	1100 K	6.8	57.0	19.1	0.0	36.2	37.6
	1650 K	1.8	34.5	N.M.	N.M.	63.7	N.M.
South Banko	900 K	15.1	75.4	1.1	N.M.	9.5	20.5
	1000 K	12.9	66.1	6.2	0.4	21.0	29.3
	1100 K	11.1	61.1	7.8	0.6	27.8	32.9
	1250 K	7.9	50.3	9.0	2.1	41.8	38.1
	1650 K	1.7	41.6	N.M.	N.M.	58.4	38.4
Taiheiyo	975 K	26.7	59.1	3.5	1.1	14.3	N.M.
	1000 K	24.8	55.0	6.8	0.8	20.2	N.M.
	1100 K	19.6	52.2	8.6	1.2	28.2	35.8
	1650 K	6.2	43.5	N.M.	N.M.	50.3	N.M.
Miike	900 K	28.9	41.5	6.3	N.M.	29.6	N.M.
	1000 K	42.0	44.1	8.0	0.0	13.9	N.M.
	1100 K	35.6	42.0	7.0	0.0	22.4	23.1
	1650 K	8.9	34.0	N.M.	N.M.	57.1	N.M.
Hunter Valley	900 K	22.2	69.4	0.0	0.0	8.4	N.M.
	1000 K	24.9	66.8	0.0	0.0	8.3	N.M.
	1100 K	23.7	62.1	5.1	0.0	14.1	14.5
	1650 K	5.9	50.7	N.M.	N.M.	43.4	N.M.
Pittsburgh	900 K	33.1	57.5	0.3	N.M.	9.4	N.M.
	950 K	30.6	57.2	0.0	0.0	12.2	15.1
	950 K	31.5	58.2	N.M.	N.M.	10.3	N.M.
	1000 K	33.5	57.6	1.6	0.0	9.0	14.9
	1100 K	30.4	49.5	3.3	0.2	20.1	22.5
	1250 K	24.6	43.1	3.3	0.1	32.3	15.9
	1650 K	10.4	43.1	N.M.	N.M.	46.5	18.7
Upper Freeport	900 K	19.0	59.1	3.3	N.M.	21.9	N.M.
	1000 K	31.9	53.1	4.9	0.0	15.1	N.M.

Table 5.10 (cont.)

Parent Coal	Condition	Nitrogen yield (as % of coal N)					Char N _{site} decay
		Tar	Char	HCN	NH ₃	Light gas ^a	
Upper Freeport	1100 K	34.1	59.6	3.5	0.0	6.2	10.7
	1650 K	8.5	59.6	N.M.	N.M.	32.0	N.M.
Pocahontas	900 K	7.5	86.4	0.0	N.M.	6.1	N.M.
	1000 K	15.7	82.5	0.8	2.9	1.8	N.M.
	1100 K	15.1	78.0	0.5	0.0	6.8	5.7
	1650 K	5.0	74.1	N.M.	N.M.	20.9	N.M.

^a Total light gas nitrogen as calculated by difference (100% - tar N - char N)
N.M. = not measured, 0.0 = below the detection limit

gave values of 6.2 and 0.4%. While the HCN measurements agree fairly well for the two tests, it seems that NH₃ is not being properly quantified by the analyzer. The light gas nitrogen as measured by FTIR may be much more reliable and it is likely that FTIR analysis of HCN and NH₃ could be used to better close the measured nitrogen balance in carefully performed drop tube pyrolysis tests.

Figure 5.7 compares the tar nitrogen as a fraction of coal nitrogen to the tar yield as a fraction of daf coal. Data from the 900 K condition confirm that the tar nitrogen yield is nearly equal to the tar mass yield, similar to the results of Friehaut et al.[Friehaut, 1982 #117] for heated grid pyrolysis of a variety of coals. At the 1100 K condition primary tar release appears to increase, as evidenced by the increase in tar nitrogen, while at the same time measured tar yields decrease as secondary reactions in the tar become significant. For this reason primary tar release may be better estimated from tar nitrogen yield than from tar yield if secondary tar reactions have occurred, although both techniques underestimate primary tar release. Even at the 900 K condition, it is possible that secondary reactions have already begun, as evidenced by the shift away from the values reported by Chen.³⁹ However, it should be noted that the tar samples in the experiments reported by Chen were

recovered using a solvent (tetrahydrofuran), which may have affected measured tar yields and nitrogen contents.

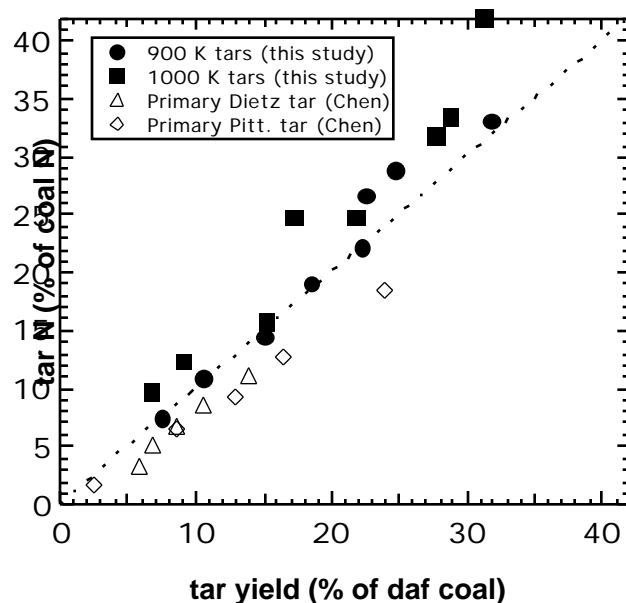


Figure 5.7. The measured fraction of coal nitrogen found in the tar for pyrolysis experiments of all eight coals at the 900 K and 1000 K conditions. The dashed line represents parity between tar nitrogen yield and tar yield. Also shown are values reported by Chen for tars produced in a radiantly heated drop tube reactor.³⁹

It should also be noted that even coals which are of similar rank and composition may vary greatly in tar yield (and thus tar nitrogen) for a given pyrolysis condition. For example, tar nitrogen yields for Hunter Valley and Pittsburgh coals at 900 K are 22% and 33%, respectively, accounting for much of the difference in total nitrogen release between the two coals.

Analysis of Chemical Structure Data

Data from ¹³C NMR analysis of matched tar and char sets for the South Banko and Pittsburgh coals allows comparison of the chemical structure of these pyrolysis products at various stages of devolatilization. For example, the number of bridges and loops (B.L.,

Figure 5.8) is 17% and 52% higher than in the parent coal for the early South Banko (900 K) and Pittsburgh (950 K) chars. This means that the char clusters are more interconnected after tar release. This early increase in the number of char bridges and loops was also seen in all 3 chars produced by Watt at 900 K¹⁰ and all 5 chars produced by Hambly at a more severe pyrolysis condition (1080 K).¹¹ Primary tar clusters (900 K) appear to have 10-17% less bridges and loops (Figure 5.8) and 0-11% less side chains (Figure 5.9) than are found in the parent coal. In contrast, the number of bridges and loops in all of the tars produced by Hambly at 1080 K were 3-35% higher than the initial parent coal value.¹¹ It is not clear why this difference exists.

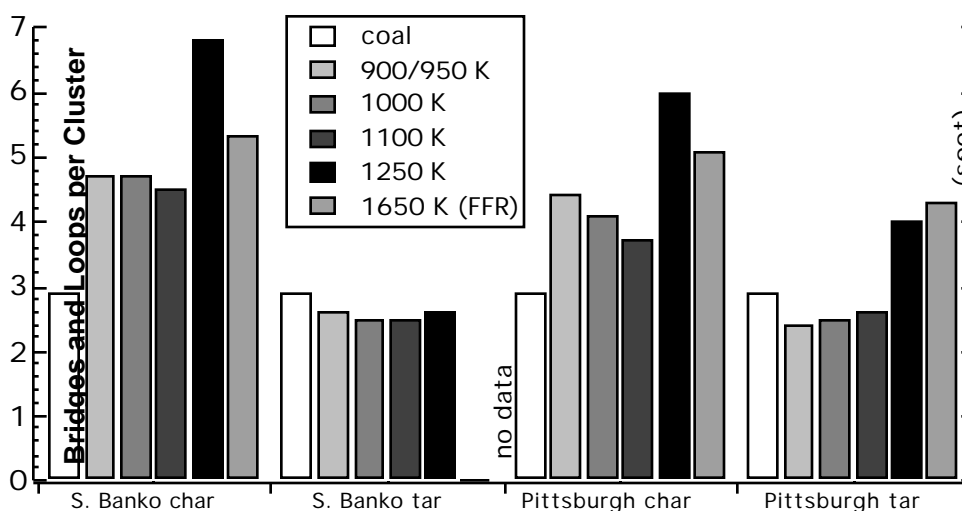


Figure 5.8. Trend with temperature of bridges and loops per cluster (B.L.) for South Banko and Pittsburgh drop tube and flat flame reactor (FFR) chars and tars.

Char and tar average cluster sizes can also be compared throughout devolatilization. At temperatures below 1250 K, chars and tars appear to have nearly the same number of aromatic carbons per cluster as their parent coals, an important assumption of most major devolatilization models (see Figure 5.10). A more quantitative comparison reveals that the

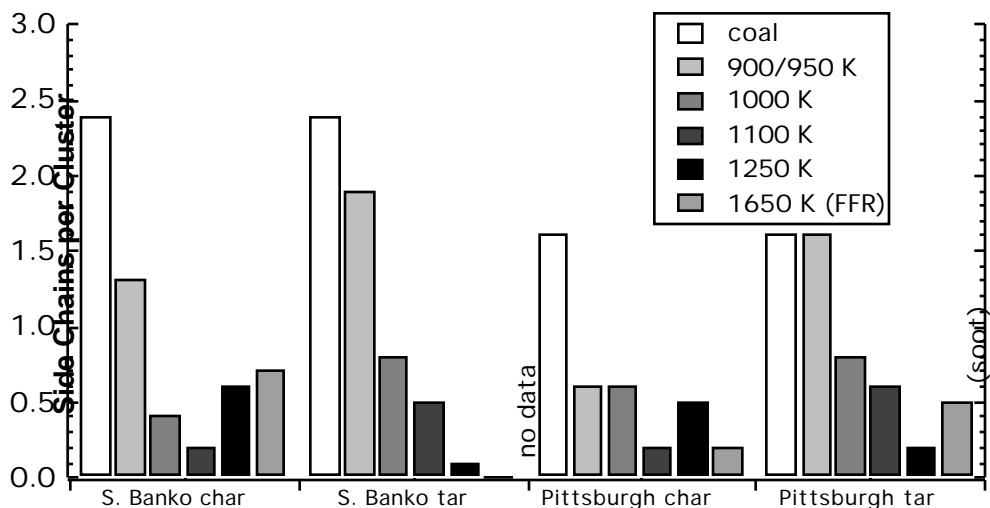


Figure 5.9. Trend with temperature of side chains per cluster (S.C.) for South Banko and Pittsburgh drop tube and flat flame reactor (FFR) chars and tars.

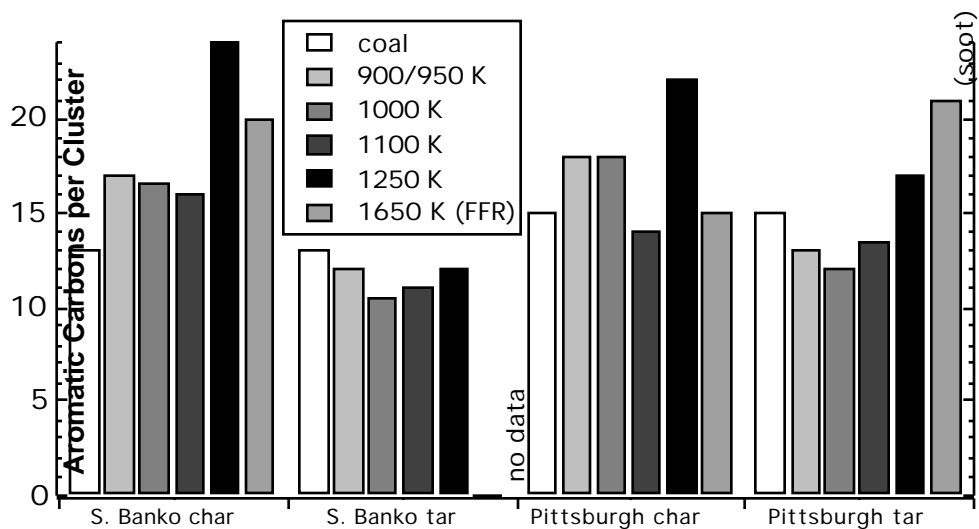


Figure 5.10. Trend with temperature of aromatic carbons per cluster for South Banko and Pittsburgh drop tube and flat flame reactor (FFR) chars and tars.

number of aromatic carbons per cluster in the early chars is actually 20-30% higher than the coal value, consistent with the findings of Watt.¹⁰ Tar, on the other hand appears to initially have 10-20% less aromatic carbons per cluster than the parent coal, a phenomenon also seen in 3 of 5 tars produced in a recent study by Hambly.¹¹ The 21 aromatic carbons per cluster for the Pittsburgh soot (FFR, 1650 K) is surprisingly low, similar to the 22

aromatic carbons per cluster observed in the 1250 K Pittsburgh char. This suggests that a large portion of the soot is formed from char bridges formed between existing tar clusters, consistent with the mechanism of Badger.^{59, 78}

It appears that there are three types of changes generally occurring in the South Banko and Pittsburgh tars and chars over the course of pyrolysis. First, tar is released, and the primary tar and char lose aliphatic material as pyrolysis severity increases. This is evidenced in both the chars and the tars by the decrease in number (S.C., Figure 5.9) and mass (M) of side chains, while the number of bridges and loops remains nearly constant (Figure 5.8).

If the particle temperature exceeds about 1200 K, a second change occurs in some of the chars and tars as ring opening reactions cause the formation of what appears to be carbonyl carbon (f_a^C) at the expense of aromatic carbon. Such a hypothetical reaction is shown in Figure 5.11 (although this is not a formal reaction, as the hydrogen abstraction step has been omitted). Ring opening reactions are evidenced by a dramatic (up to ten-fold) increase in carbonyl carbon (Figure 5.12) with increasing pyrolysis severity at temperatures above 1100 K, accompanied by nearly equal and opposite changes in the fraction of aromatic carbon (Figure 5.13). A similar phenomenon was also seen in chars produced using in a flat flame reactor at Sandia with 1600 K maximum gas temperature and 43 ms residence time.⁵ Thus after high temperature (>1200 K) rapid coal pyrolysis, evidence of ring opening reactions is often seen in both the tar and the char.

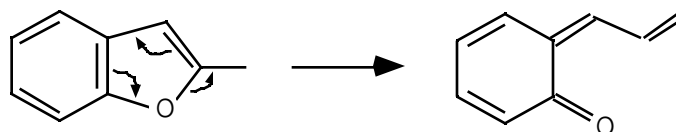


Figure 5.11. A hypothetical reaction for carbonyl formation in coal char via ring opening of aromatic rings during severe pyrolysis. In this hypothetical reaction four aromatic carbons are converted to non-aromatic carbons.

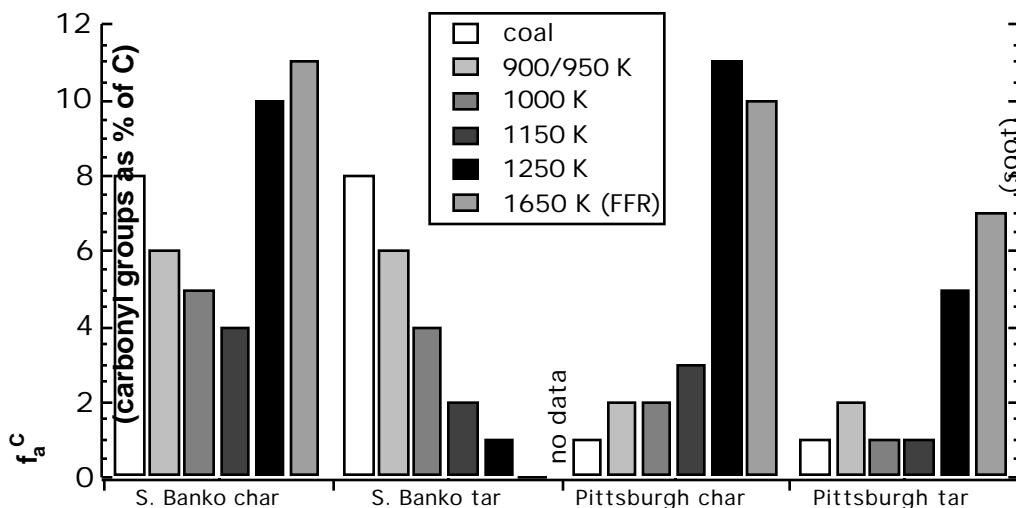


Figure 5.12. Trend with temperature of fraction of carbon which is carbonyl for South Banko and Pittsburgh drop tube and flat flame reactor (FFR) chars and tars.

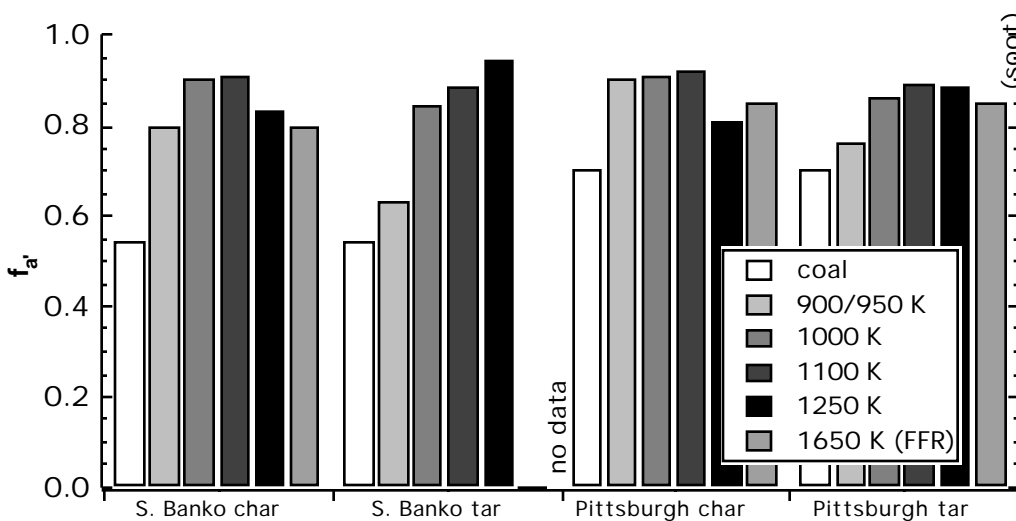


Figure 5.13. Trend with temperature of the fraction of carbon which is aromatic (f_a) for South Banko and Pittsburgh drop tube and flat flame reactor (FFR) chars and tars.

A third change, cluster coalescence, is sometimes also seen at particle temperatures above 1200 K. Cluster coalescence is evidenced by a significant increase in the number of aliphatic and aromatic (see Figure 5.10) carbons per cluster and the number of bridges and

loops per cluster (see Figure 5.8). In Figures 5.8 and 5.10, increases of 200-240% and 45-80% can be seen in the bridges and loops per cluster and the aromatic carbons per cluster, respectively, for the 1250 K chars when compared to the parent coal. In other words, the tar and char clusters become both larger and more interconnected. This cluster coalescence is minimal in the Pittsburgh flat flame reactor char, consistent with the flat flame reactor chars produced by Fletcher and Hardesty.⁵ This may be due to the shorter residence times or the higher heating rates used in flat flame reactor experiments compared to the 1250 K drop tube experiments. Solum et al.⁷⁹ also reported evidence of cluster coalescence, showing that at a heating rate of 0.5 K/s aromatic carbons per cluster in a lignite coal were 9, 10.5, 12, and 14 for tests with maximum temperatures of 500, 600, 700, and 800 K, respectively. In contrast, at higher heating rates (10^4 K/s), cluster growth was not significant except at a very high temperatures (1373 K), for which aromatic carbons per cluster doubled in both a lignite and a bituminous coal.⁷⁹

The 1650 K Pittsburgh char demonstrates that under certain conditions ring opening reactions can occur without causing cluster coalescence. This is evidenced by the ten-fold increase in carbonyl carbon (f_a^c , Figure 5.12) relative to the parent coal value, while the number of aromatic carbons per cluster (Figure 5.10) remains identical to that in the parent coal. On the other hand, every tar and char sample showing evidence of cluster coalescence (increased B.L. and C_{cl} , Figures 5.8 and 5.10) also appeared to have undergone ring opening reactions (increased f_a^c and decreased f_a , Figures 5.12 and 5.13), suggesting that ring opening reactions may be prerequisite to cluster coalescence. In an investigation of anthracene pyrolysis, Wornat et al.⁸⁰ reported an acceleration of cluster coalescence reactions at around 1300 K, with soot formation occurring between 1250 and 1350 K. This is consistent with particle temperatures of between 1250 and 1300 K calculated for the 1250 K condition of this study.

It is significant that no evidence for either ring opening or cluster coalescence reactions is seen in the South Banko tar produced at 1250 K. This may be related to the

low tar yield from South Banko coal (1/3 the yield of tar from the Pittsburgh coal). This means that under identical pyrolysis conditions, interactions between (gaseous) South Banko tar molecules would occur much less often than they would occur between Pittsburgh tar molecules (about 1/9th as often). The absence of these reactions in the South Banko tar could also be due to the slightly smaller cluster size (12.5 carbons per cluster at 1100 K) as compared to the Pittsburgh tar (15.2 carbons per cluster at 1100 K). This would be consistent with the soot formation mechanism of Badger^{59, 78}, in which soot formation begins by aryl radical formation followed by dimerization, occurring more easily in larger ring systems, which can better stabilize aryl radicals.

These data represent the first time matched sets of chars and tars from both lignite and bituminous coals pyrolyzed at increasingly severe conditions have been analyzed by solid-state ¹³C NMR. The data confirm much of what has been reported by previous investigators about the structural progression of coal chars during pyrolysis. Evidence of three types of structural changes were seen in both chars and tars during rapid pyrolysis: loss of aliphatic material, ring opening, and cluster coalescence. Understanding of such changes may contribute to the development of better soot formation models or improve modeling of char devolatilization at extreme pyrolysis conditions.

6. Nitrogen Chemical Structure Analysis

Detailed chemical structural measurement can provide valuable insights into how nitrogen is released from coal during devolatilization. In this chapter, a parameter for gauging the extent of light gas nitrogen release is defined (nitrogen mass per aromatic mass, or N_{site}). The use of N_{site} is justified and chemical structural changes that may relate to light gas nitrogen release are identified.

Definition of N_{site}

It is believed that in most coals nearly all nitrogen is contained within the aromatic rings.^{4, 37, 38} As described by Genetti,⁹ a useful parameter to describe the aromatic ring nitrogen concentration throughout devolatilization is N_{site} , defined as:

$$N_{site} = y_N \frac{M_{cl}}{M_{site}} \quad (6.1)$$

where y_N is the mass fraction of nitrogen in the sample on a dry ash free basis, M_{site} is the measured average aromatic mass per cluster, and M_{cl} is the measured average total mass per cluster. The term cluster means a group of aromatic carbon atoms plus any aliphatic attachments, while a site refers to only the aromatic portion of a cluster. M_{site} and M_{cl} are defined as:

$$M_{site} = C_{cl} \left[12.01 \left(1 - \frac{f_a^H}{f_a} \right) + 13.02 \frac{f_a^H}{f_a} \right] \quad (6.2)$$

$$M_{cl} = \frac{C_{cl} \cdot 12.01}{f_a \cdot y_c} \quad (6.3)$$

where f_a^H is the fraction of carbon which is aromatic and protonated, f_a is the fraction of carbon which is aromatic, and y_c is the daf mass fraction of carbon in the sample. The units associated with N_{site} are as follows:

$$N_{site} [=] \frac{gN}{gchar} \frac{\left(\frac{gchar}{molofclusters} \right)}{\left(\frac{garomaticchar}{molofclusters} \right)} = \frac{gN}{garomaticchar} \quad (6.4)$$

N_{site} is defined on a per-aromatic-mass basis because aromatic mass per cluster in the char is fairly stable during rapid primary pyrolysis, remaining essentially unchanged during both tar release and light gas release. This is important because if the average aromatic mass per cluster in the char is assumed to remain constant during devolatilization and the tar N_{site} value is assumed to be the same as the char value at the time of tar release, then any decrease in the value of N_{site} must be due to the release of light gas nitrogen via ring rupture. Since nitrogen is a relatively small fraction of the total aromatic mass (usually less than 3%), light gas nitrogen release can be assumed to have only a small effect on the aromatic mass per cluster (possibly up to three times the mass of the nitrogen released via ring rupture).

For the pyrolysis products analyzed for chemical structure in this study, the relative decay of N_{site} and the relative decay of N/AC (nitrogen mass per mass of aromatic carbon) are interchangeable. This is demonstrated in a parity plot in Figure 6.1 with a slope of 1.0 and a correlation coefficient of 0.999. Thus in instances where only N/AC data are available, these might be used in place of N_{site} data.

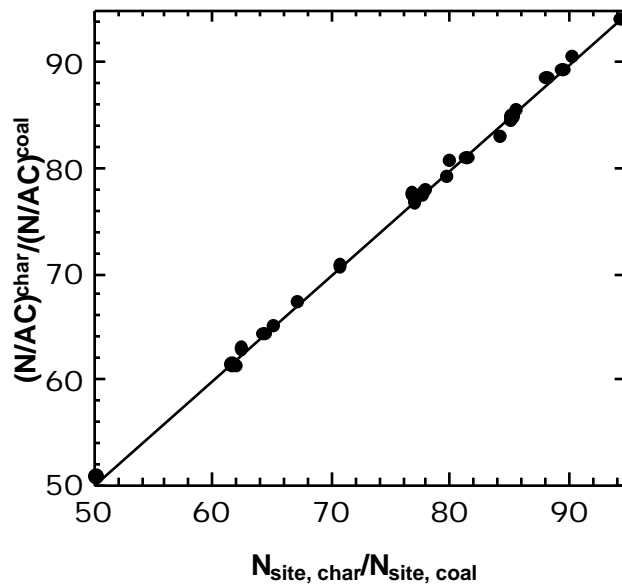


Figure 6.1. Parity plot comparing char N/AC value (normalized to parent coal value) and char N_{site} value (normalized to parent coal value) for all drop tube and flat flame reactor chars, tars, and soot generated in this study for which ^{13}C NMR characterization was performed.

Justification of the use of N_{site}

In using N_{site} (Equation 6.1) to describe the release of nitrogen as light gas, it was assumed that aromatic mass was conserved in the pyrolysis products throughout devolatilization. When ^{13}C NMR data are available for matching tar/char sets, a balance on the mass of aromatic carbon (AC, a parameter analogous to aromatic mass) in the pyrolysis products can be performed as follows:

$$AC \text{ balance} = \frac{mass_{char} \% C_{char} f_{a, char} + mass_{tar} \% C_{tar} f_{a, tar}}{mass_{coal} \% C_{coal} f_{a, coal}} \quad (6.5)$$

where % C is the daf mass percent carbon and f_a is the fraction of carbon which is aromatic in the tar, char or coal. Matched tar/char data sets from this study have been used to perform a balance on aromatic carbon at high heating rates, as shown in Figure 6.2. It can be seen that the aromatic carbon balance ranges from 116% to 106% for the South Banko

drop tube tests between 900 and 1100 K. This may mean that the measured char yields are 5-15% too high for these tests. It is also possible that at the lowest temperature (900-1100 K) conditions of this study, some aromatic carbon is created during pyrolysis of low-rank coals such as South Banko. For each of the Pittsburgh tests below 1250 K, the aromatic carbon balance is within the error of the data (about $\pm 7\%$). At or above 1250 K, aromatic carbon is not conserved, with 5-15% less aromatic carbon in the pyrolysis products than in the parent coal.

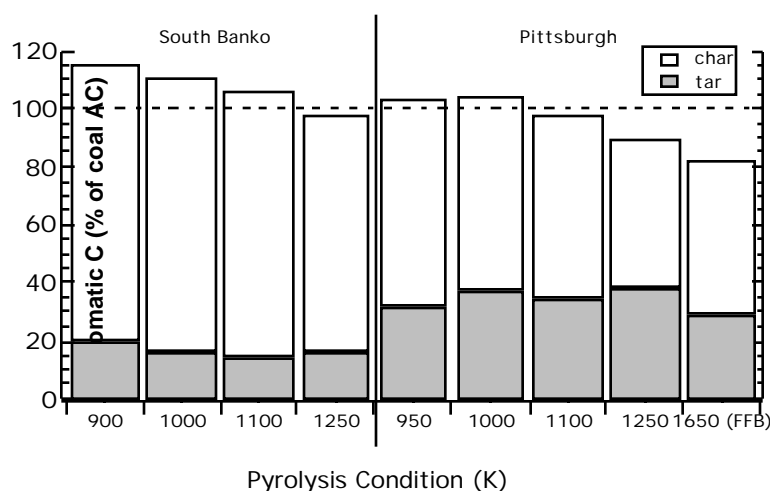


Figure 6.2. Balance on aromatic carbon for pyrolysis experiments using South Banko and Pittsburgh parent coals.

For tests in which no tar ^{13}C NMR analysis was performed, an estimate of the aromatic mass balance can still be made if the fraction of mass which is aromatic (f_{AM}) in the tar is assumed to be equal to the char value. The fraction of mass which is aromatic is defined as:

$$f_{AM} = \frac{M_{site}}{M_{cl}} \quad (6.6)$$

This appears to be a good assumption for tests performed at the 1100 K condition, as evidenced by the South Banko and Pittsburgh matched chars and tars, for which the tar f_{AM} value was only 1.5% (absolute) less than the char value. The aromatic mass balance is estimated as follows (assuming $f_{AM, tar} = f_{AM, char}$):

$$AM\ balance = \frac{mass_{char} f_{AM, char} + mass_{tar} f_{AM, tar}}{mass_{coal} f_{AM, coal}} = \frac{(mass_{char} + mass_{tar}) f_{AM, char}}{mass_{coal} f_{AM, coal}} \quad (6.7)$$

This balance also assumes that no aromatic mass escapes with the light gas. Some aromatic species are light enough not to condense at room temperature (such as benzene). However, these are not thought to be major products of coal devolatilization. For the pyrolysis products from every coal at the 1100 K condition, the balance closes to within 8%, and to within 1.5% in the majority of cases (see Figure 6.3). This demonstrates the approximate validity of the assumption that aromatic mass is conserved during primary pyrolysis, which is the major assumption adopted in using N_{site} to track light gas nitrogen release during primary pyrolysis.

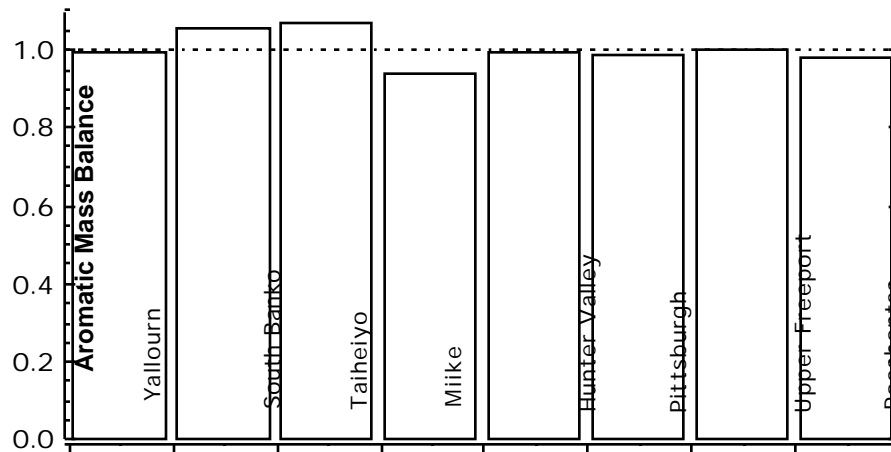


Figure 6.3. Estimated aromatic mass balance for drop tube experiments at the 1100 K condition calculated according to Equation 6.7.

At low heating rates, the assumption of conservation of aromatic mass may not be very good. Solum et al.⁷⁹ showed that for a North Dakota lignite pyrolyzed at 0.5 K/sec with a final hold time of 3 minutes, the number of aromatic carbons per cluster in the char increased monotonically with pyrolysis temperature, from 9 in the parent coal to 14 at 800 K. This does not necessarily mean that N_{site} cannot be used to *model* light gas nitrogen release at low heating rates, but rather that the *measured* value of N_{site} in the char might be significantly reduced by an increase in the mass of aromatic carbon per cluster after low heating rate pyrolysis.

It is clear from tests performed at temperatures of 1250 K and higher that aromatic carbon is not conserved at these temperatures. However, the extrapolated use of N_{site} beyond particle temperatures of 1200 K may still be appropriate for prediction of light gas nitrogen release from char. Once aliphatic release from the char is nearly complete (i.e. at or above the 1000 K condition of this study), N_{site} decay can be approximated by the decay of the nitrogen to carbon ratio (N/C), since almost all the carbon in the char is aromatic. Since aromatic mass is directly proportional to the carbon aromaticity (as seen in Figure 6.1), increases in aromaticity with increasing pyrolysis severity will cause slightly less decay in the N/C ratio decay than in N_{site} . As can be seen by the solid lines in Figure 6.4, the N/C ratio of the Pittsburgh and South Banko *chars* changes nearly linearly with changes in char mass (or yield) between 1000 and 1650 K. Thus the rate of nitrogen release from the char is probably not significantly altered by the ring opening and cluster coalescence reactions which occur above 1200 K (due to the low concentrations of N and O). On the other hand, *tar* N/C ratios (dashed lines in Figure 6.4) change drastically above 1200 K, with little change in the tar mass (yield).

Since the tar and the char chemical structure appear to be quite similar at the 1100 K condition, it is surprising that the nitrogen release from tar and char are so different during severe pyrolysis. It may be significant that large decreases in the tar N/C ratio occur

between the 1100 and 1250 K condition, even in the South Banko tar, which has undergone neither ring opening reactions nor cluster coalescence (see chapter 5).

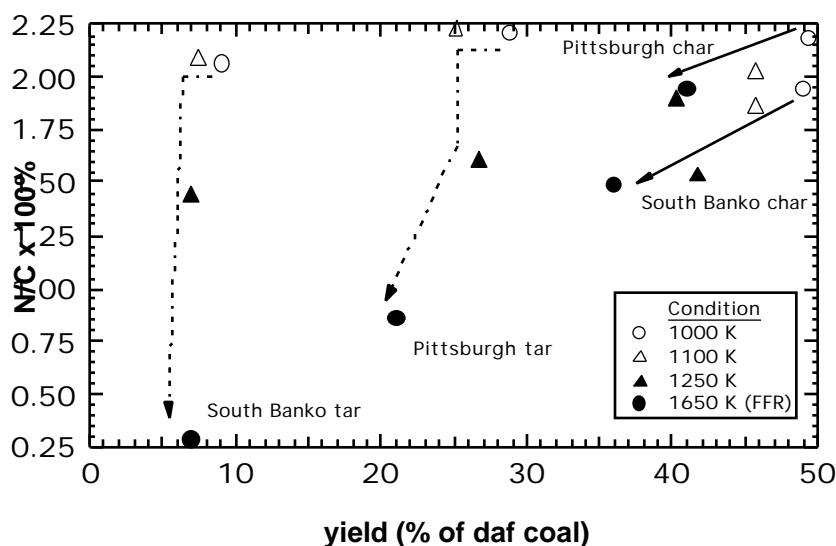


Figure 6.4. Comparison of N/C ratios for South Banko and Pittsburgh chars and tars. Arrows indicate direction of increasing severity of pyrolysis.

Nitrogen Functionality Analysis

There is some evidence that nitrogen functionality (i.e. pyridinic or pyrrolic) may not play a significant role in the rank dependence of nitrogen release during coal devolatilization. First of all, XPS studies show that the ratio of nitrogen in five membered rings to nitrogen in six membered rings only varies between 55/45 and 65/35 over the entire range of rank spanned by the Argonne premium coals.³⁷ Using the average nitrogen functionality ratio (60/40) for all coals would introduce a maximum relative error of only 10% in predicted total light gas nitrogen behavior even if the two functionality types behaved very differently from each other. Secondly, data have been reported for rapid devolatilization of a Wyodak coal at five different conditions which show nearly identical changes in the mass of nitrogen in five and six membered rings per mass of aromatic carbon in the char as measured by XPS.⁴³ These data are shown in Figure 6.5. In Figure 6.5, it is assumed that nitrogen in six membered rings is the sum of quaternary and

pyridinic nitrogen, while nitrogen in five membered rings is simply pyrrolic nitrogen. Note that although the shapes of the curves are non-linear, the two curves have similar shapes. This apparent similarity between the rate of release of nitrogen from six-membered and from five-membered rings suggests that the functional form of the nitrogen in an aromatic ring may not have a significant effect on the susceptibility of the ring to rupture during rapid pyrolysis.

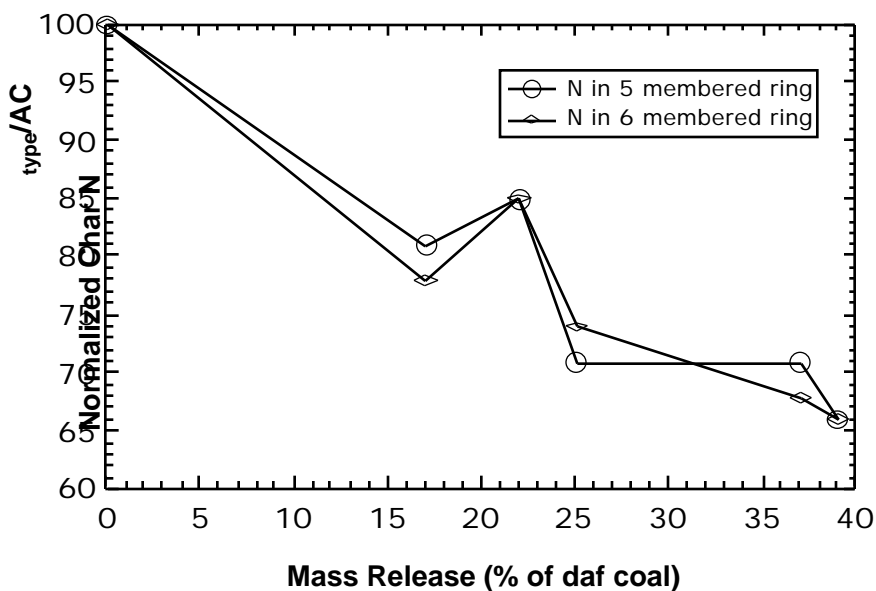


Figure 6.5. Comparison of the change in nitrogen mass per aromatic carbon mass by nitrogen functionality type as measured by XPS for chars produced in a drop tube reactor and chars produced in a flat flame reactor from a Wyodak coal.⁴³ Nitrogen in six membered rings is assumed to be the sum of quaternary and pyridinic nitrogen. All N/C and carbon aromaticity values were measured by XPS.⁴³

Relationship of N_{site} and M_{cl}

Changes in N_{site} were compared to changes in other chemical structural parameters to see whether simple relationships exist which might give clues as to the mechanisms responsible for pyrolytic nitrogen release from coal. For the chars produced in the drop tube at 1100 K of this study, an especially strong relationship was observed between relative changes in N_{site} and relative changes in the fraction of carbon which is aromatic

(f_a). Further analysis showed that increases in carbon aromaticity directly corresponded to decreases in the fraction of mass which is aromatic (f_{AM}) and the molecular weight per cluster (M_{cl}) as aliphatic material is released from the clusters as light gas. Since char molecular weight per cluster is already incorporated into the CPD model, it was a logical variable to use for further analysis. However, scatter in the measured molecular weight per aromatic site (M_{site}) and molecular weight per cluster (M_{cl}) values is much greater than for the ratio of the two (that is, f_{AM}). This is because both M_{site} (Eq. 6.2) and M_{cl} (Eq. 6.3) are directly proportional to the estimated number of aromatic carbons per cluster (C_{cl}), while f_{AM} is not, adding an extra source of data variability to M_{site} and M_{cl} values. If the definitions for M_{site} (Eq. 6.2) and M_{cl} (Eq. 6.3) are substituted into the definition of f_{AM} (Eq. 6.6), it can be seen that f_{AM} is independent of C_{cl} , depending mainly on f_a and y_C as follows:

$$f_{AM} = \frac{M_{site}}{M_{cl}} = f_a \cdot y_C \frac{12.01 \left(1 - \frac{f_a^H}{f_d}\right) + 13.02 \frac{f_a^H}{f_a}}{12.01} \quad (6.8)$$

Since char f_{AM} values should have less variability than char M_{cl} values, they can be used to calculate *adjusted* M_{cl} values if the char M_{site} value is assumed to remain constant at the coal value throughout pyrolysis, as follows:

$$M_{cl,adjusted} = \frac{M_{site,coal}}{f_{AM,char}} \frac{M_{site,char}}{f_{AM,char}} = M_{cl} \quad (6.9)$$

This assumption is thought to be valid during rapid primary devolatilization.²⁵ Random changes in C_{cl} (and thus M_{site}) char values during rapid primary pyrolysis, can probably be attributed to scatter in the measured NMR data. In fact, the CPD model assumes that M_{site} is constant throughout devolatilization,⁸¹ so adjusting measured M_{cl} data by assuming

constant M_{site} may be appropriate when comparing data to CPD model M_{cl} predictions. Figure 6.6 shows the effect of adjusting measured M_{cl} values according to Equation 6.9 for chars from two coals pyrolyzed at Sandia.⁵ In Figure 6.6, note how *measured* M_{cl} values for the chars from the Illinois #6 coal bounce randomly up and down from the coal value with increasing residence time. However, *adjusted* M_{cl} values for the same chars show much less variation, instead decreasing nearly monotonically with time. If cluster coalescence and ring opening reactions (and therefore real changes in C_{cl}) are negligible during rapid primary devolatilization, such a monotonic decrease in M_{cl} is to be expected. Thus the use of an adjusted M_{cl} (Eq. 6.9) is a useful tool for analysis of char chemical structure data.

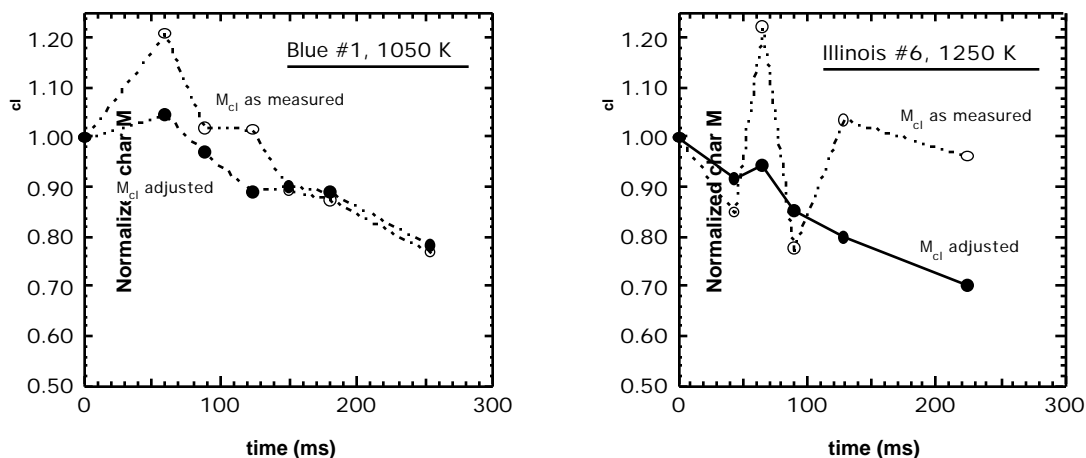


Figure 6.6. Comparison of the trend with pyrolysis time for measured and adjusted (Eq. 6.9) char molecular weight per cluster (M_{cl}) values normalized to parent coal values. Char data is from 1050 K and 1250 K drop tube pyrolysis experiments performed at Sandia.⁵

A strong correlation between N_{site} and M_{cl} in partially devolatilized chars from parent coals of a wide range of rank supports the idea that they share common chemistry, as shown in Figure 6.7 for chars produced at the 1100 K condition of this study. Although N_{site} and M_{cl} show nearly identical trends with rank, the difference between them also

shows a clear trend with rank. For this condition, the gap between M_{cl} and N_{site} narrows as coal rank increases.

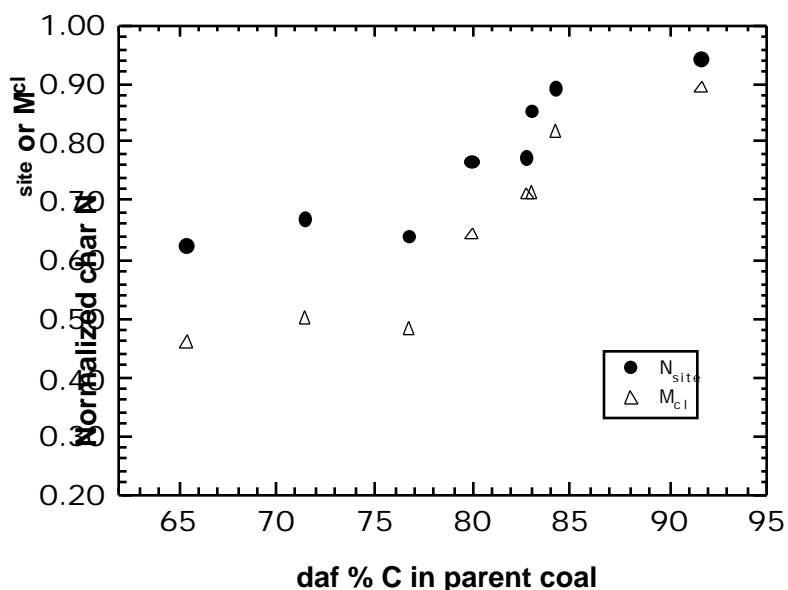


Figure 6.7. Comparison of the trend with rank for char nitrogen mass per aromatic mass (N_{site}) and char molecular weight per cluster (M_{cl}) values normalized to parent coal values. M_{cl} values were adjusted according to Equation 6.9. Chars were generated in drop tube pyrolysis experiments at the 1100 K condition. Carbon content is used as an indicator of rank.

Other evidence for a strong relationship between N_{site} and M_{cl} can be found in the published literature. Pyrolysis tests performed at Sandia in a drop tube with a 1250 K maximum gas temperature not only provide ^{13}C NMR data on chars collected at various residence times for five coals, but also report *measured* particle temperature histories.⁵ N_{site} and M_{cl} values for chars from two of the coals in the Sandia study are shown in Figure 6.8. Just as seen in Figure 6.7, char values of N_{site} and M_{cl} follow about the same trend, again implying a relationship between the two variables. Note that even though Illinois #6 (hvCb) is of a lower rank than Pittsburgh #8 (hvAb), it shows less N_{site} decay at this condition than does Pittsburgh #8, which is in disagreement with the overall trend with rank seen in Figure 6.7. However, Illinois #6 also shows significantly less M_{cl} decay than

Pittsburgh #8, which reinforces the idea that N_{site} and M_{cl} share common chemistry. The strong correlation between changes in N_{site} (a measure of the degree of light gas nitrogen release) and changes in M_{cl} (a measure of the degree of total light gas release) suggest that mechanisms of light gas *nitrogen* release and *total* light gas release share common elements.

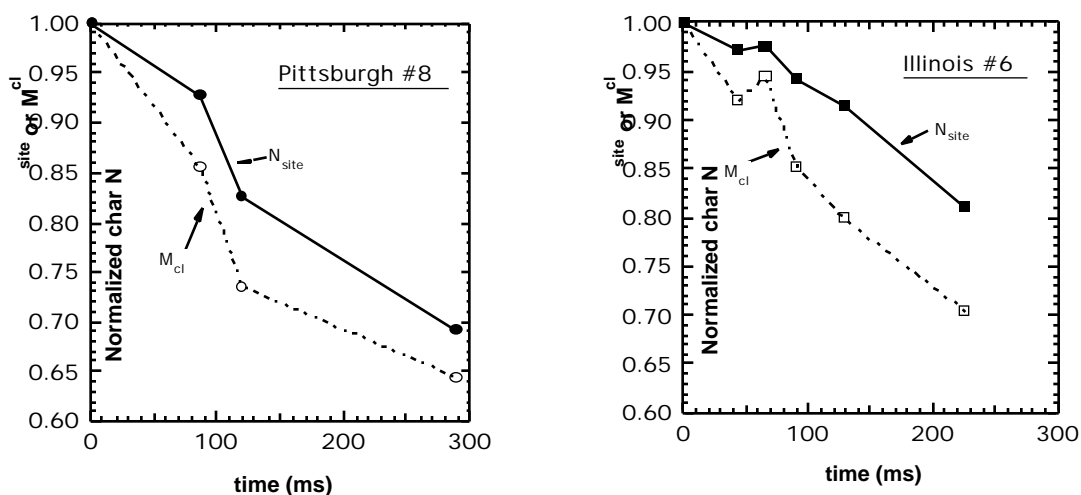


Figure 6.8. Comparison of the trend with pyrolysis time for measured char nitrogen mass per aromatic mass (N_{site}) and measured char molecular weight per cluster (M_{cl}) values normalized to parent coal values. Char data is from the 1250 K drop tube pyrolysis experiments performed at Sandia.⁵ M_{cl} values were adjusted according to Equation 6.9.

Since this study has produced only the second set of matched char/tar sets ever characterized by ^{13}C NMR, a unique opportunity exists to compare $N_{\text{site}}/M_{\text{cl}}$ relationships in the tars to those in the chars. In Figure 6.9, changes in normalized tar and char N_{site} values as a function of M_{cl} are compared for all drop tube test pyrolysis products not showing evidence of ring opening reactions or cluster coalescence. It can be seen that the tars resist release of both ring nitrogen (N_{site}) and aliphatic material (M_{cl}) until the more severe conditions of pyrolysis. Furthermore, for conditions in which the M_{cl} decay is similar in the tar and in the char, N_{site} decay is slightly less in the tar. These differences imply that the relationship between N_{site} and M_{cl} , and thus the mechanism by which nitrogen is released via ring rupture, may not be exactly the same in tars and chars. This finding could be

important to future efforts to model light gas nitrogen release from tar during soot formation.

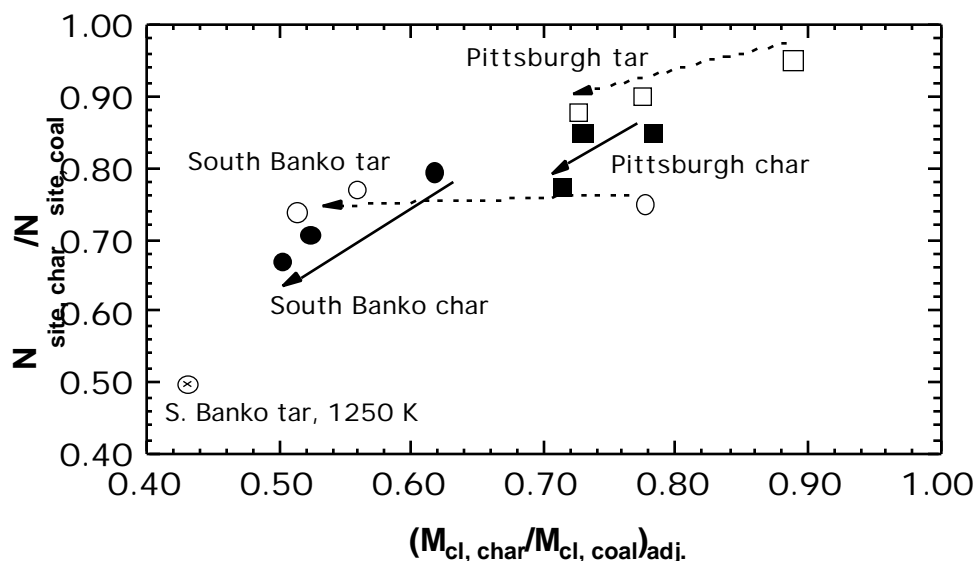


Figure 6.9. Comparison of normalized N_{site} and M_{cl} values for drop tube chars (closed symbols) and tars (open symbols) from Pittsburgh (squares) and South Banko (circles) coals at the 900, 1000, and 1100 K conditions. Arrows indicate trends and are shown to emphasize the differences between tar (dashed arrows) and char (solid arrows) N_{site} decay. Char M_{cl} values were adjusted according to Equation 6.9.

In summary, the mass of nitrogen per aromatic mass, or N_{site} , appears to be a useful variable for tracking light gas nitrogen release from char during devolatilization as long as aromatic mass is conserved. Even when aromatic mass is not conserved, there are indications that N_{site} may still be useful for modeling light gas nitrogen release from char. Also, relative changes in N_{site} (as measured by ^{13}C NMR) are essentially equivalent to relative changes in N/AC . For at least one coal, no significant difference was reported in the decay of char N/AC for nitrogen in five-membered and six-membered rings as measured by XPS,⁴³ suggesting that nitrogen functionality does not play an important role in light gas nitrogen release from char. In contrast, changes in the molecular weight per cluster, or M_{cl} , were shown to correlate strongly with changes in N_{site} , both as a function of

parent coal rank and as a function of pyrolysis residence time. This suggests that changes in the molecular weight per cluster (due to light gas release) are somehow involved in the mechanism of light gas nitrogen release. However, the relationship between M_{cl} and N_{site} does not appear to be exactly the same in tars that have undergone secondary reactions as it is in chars, suggesting a slight differences in the mechanism of nitrogen ring rupture in tars and chars.

7. Nitrogen Release Model

A nitrogen model using a three-step free-radical global mechanism to model light gas nitrogen release was developed. Initially, a variety of light gas nitrogen release mechanisms were postulated. Of these, only the rate equation derived from the (free-radical) mechanism presented in this chapter correctly described the relationship between measured N_{site} and M_{cl} char values as a function of pyrolysis severity for a variety of coal types.

Model Development

Many researchers have observed that low-rank coals produce more light gas nitrogen than do high rank coals at the same condition.^{1, 15, 54, 62} Current nitrogen release models empirically correlate light gas nitrogen release rate equation parameters with parent coal elemental composition in order to describe this rank dependence. Because the chemistry of nitrogen release is not well understood, no attempt is made by these models to describe the chemistry responsible for the variations in light gas nitrogen release with coal type.

The temperature dependence of pyrolytic light gas nitrogen release is unusual in two ways. First, pyrolytic light gas nitrogen release from coal begins at temperatures (about 900-1000 K)^{53, 60} which are much lower than those for which thermal decomposition of nitrogen-containing aromatic rings is expected to begin. For example, thermal decomposition is not significant in pure pyrrole until about 1200 K⁵¹, and in pure pyridine until about 1300 K.⁵² Second, the rate of pyrolytic light gas nitrogen release slows

dramatically once mass release is complete, leaving a large portion of the coal nitrogen in the fully devolatilized char unless treated at very high temperatures (i.e. 2000 K) for long residence times (on the order of minutes).^{5, 7, 55} These two features of the temperature dependence of pyrolytic light gas nitrogen release have been imitated in previous models^{1, 2} by using a wide distribution of activation energies with a relatively low mean value. For example, the average activation energy used in FLASHCHAIN for light gas nitrogen release is about 50 kcal/mol,⁷² similar to those measured by Bassilakis and co-workers¹, with a standard deviation of 16 kcal/mol. In contrast, the C-N bond energy in pyrrole is estimated to be 90 kcal/mol, and the activation energy for pyrrole thermal decomposition is about 70 kcal/mol.⁵¹ Current nitrogen release models offer no explanation as to why the temperature dependence of nitrogen release via ring rupture during coal devolatilization deviates so markedly from what is expected based on model compound studies.

Although never mentioned in the published literature, a comparison of several model compound pyrolysis studies^{49, 51, 52} seems to imply that model compounds containing aliphatic material release nitrogen more easily than compounds which contain no aliphatic material. This is evidence that the presence of aliphatic attachments may change the mechanism by which nitrogen is released via ring rupture.

A nitrogen model is proposed here which includes a new low activation energy, low-temperature mechanism in which light gas nitrogen release is initiated by the thermal decomposition of aliphatic side chain material. In addition, a high activation energy pure thermal decomposition mechanism is included to explain the high temperature release of all char nitrogen at very long residence times (i.e. minutes). At shorter residence times the char nitrogen appears to stabilize once mass release ceases, since the lower activation energy nitrogen release process also ceases.

The nitrogen release model includes three pathways for nitrogen release from coal char during rapid pyrolysis:

- A) **TAR**: Nitrogen-containing tar clusters transport nitrogen away from the char during tar release.
- B) **FAST LIGHT GAS**: Reaction of ring nitrogen in the char that occurs quickly and at temperatures as low as 1000 K as a result of char stabilization reactions during light gas release.
- C) **SLOW LIGHT GAS**: Ring nitrogen is slowly broken out of the char clusters at very high temperatures in a process analogous to thermal decomposition of nitrogen-containing rings.

These three pathways for nitrogen release from char are included in a schematic detailing the various ways coal nitrogen is transformed during pyrolysis (Figure 7.1). In this model, tar clusters are assumed to have the same average structural properties as the char clusters from which they were released, including the average molecular weight per cluster, average aromatic mass per cluster, and the mass of nitrogen per aromatic mass. Although this is not strictly true, as shown earlier in this dissertation, the assumption is

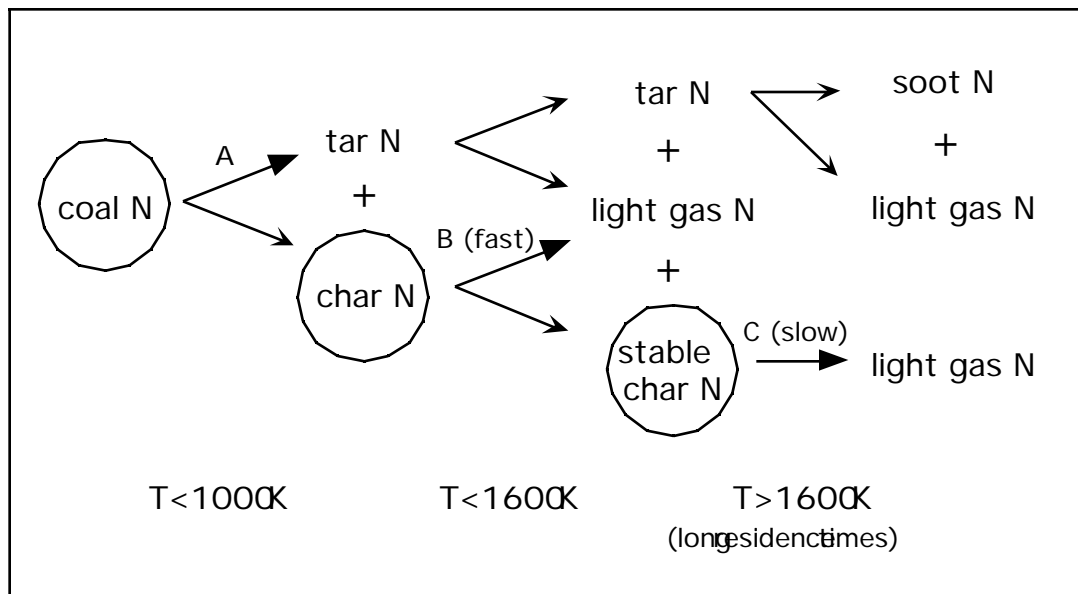
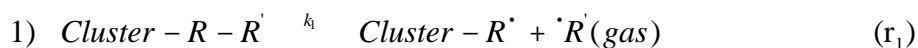


Figure 7.1. Schematic showing the fate of coal nitrogen at various stages of pyrolysis. The three pathways included in the nitrogen model of this study are indicated by bold arrows. The temperature ranges where these pathways are important are also indicated.

close enough to be practically useful. If the fraction of mass that is aromatic in the parent coal is known, any devolatilization model that can correctly predict changes in the char molecular weight per cluster throughout devolatilization may be used with this nitrogen model. In this study, the Chemical Percolation Devolatilization model⁸¹ was used to track changes in average char and tar structural properties throughout devolatilization.

Free-Radical Global Mechanism

Models which describe the kinetics of chemical reactions (such as fast light gas nitrogen release) are usually valid for a wide range of conditions only if based on a reasonable mechanism of elementary steps. Complex mechanisms with hundreds of elementary steps can often be described by much simpler global mechanisms with fewer steps (which are not elementary). In this model, fast light gas nitrogen release (pathway B) was assumed to occur via a three-step global mechanism as follows:



where Cluster-R-R' and Cluster-R-R'' are char (or coal) clusters with various aliphatic attachments (-R), Cluster-R' is a free-radical formed within the char matrix, 'R' is a light gas precursor which is also a free-radical, ring N is nitrogen contained within the aromatic portion of the char, and R'' is any material in the char which competes with ring N for char free-radicals. Steps 2 and 3 in this mechanism are not formal reactions. Additional free-radical products or reactants (not shown) must also be involved in order to either conserve or terminate (via reaction with another free-radical) the unpaired electron found in each of these reactions. Thus it should be assumed, although not specifically shown, that additional aliphatic free-radicals are formed as gas phase products in steps 2 and 3 and released as additional light gas precursors.

Some initial fraction of char free-radicals may build up and still be stabilized by resonance throughout the char network. However, once the cluster is saturated, any new radicals formed via step (1) will be reactive (unstable). At that point steps 2 and 3 compete for the unstable char free-radicals thus formed. Step 3 is a general solid-phase free-radical reaction/stabilization step which occurs very quickly and probably includes thousands of specific reactions including hydrogenation, char bridge formation, crosslinking, etc. Thus the rate of reaction of ring nitrogen depends inversely on the concentration of material available to react with free-radicals via step three.

Discussion of Free-Radical Mechanism

It is significant that the proposed global mechanism does not differentiate between types of nitrogen functional groups such as pyridinic and pyrrolic, consistent with observations made in chapter 6. This may be because high-energy reactants (such as free-radicals) tend to have lower selectivity.

Several observations of organic chemists are consistent with the postulated free-radical mechanism for light gas nitrogen release. For example, because nitrogen is more electronegative than carbon, the nitrogen heteroatom in pyridine is a net acceptor of electron density, thus causing the adjacent carbons to be more electrophilic.⁸² This might open them up to attack by a high energy nucleophile, such as an unsubstituted alkyl radical, which shows pronounced nucleophilic (electron donating) character.⁸³ The mechanism for such a reaction might be similar to the initial stages of nucleophilic aromatic substitution by addition-elimination, in which a nucleophile adds into the vacant π^* (anti-bonding) orbital of the ring, thus interrupting the aromatic system.⁸² Electron attracting groups (i.e. a nitrogen heteroatom which is more electronegative than the adjacent carbon atoms) cause this to be more easily accomplished.⁸² Another type of reaction which may be mechanistically similar to ring nitrogen attack by char or tar radicals is nucleophilic aromatic substitution by the elimination-addition mechanism, in which benzyne (a six membered

aromatic ring containing a carbon-carbon triple bond) can be formed during the initial stages of reaction. If a nitrogen heteroatom were present in the ring, ring opening and the formation of a nitrile (cyano) group (a carbon-nitrogen triple bond) might occur instead of benzyne formation. This reaction is facilitated by electronic effects that favor the removal of aromatic hydrogen from the ring.⁸² Pyrolysis probably creates conditions where removal of hydrogen from the ring is favored (i.e. hydrogen abstraction during light gas release). This second type of reaction might be more likely in tar than in char, since nitrile groups have been identified in pyrolyzed tars. Nitrile groups have a large stabilizing effect on free-radicals located at adjacent carbons.⁸³ This might explain why nitrile groups reportedly form in large proportions in tar during the initial stages of secondary pyrolysis³⁵, thus stabilizing radicals formed during release of aliphatic material. In char, nitrile groups are not observed, possibly because free-radicals can be stabilized by the char matrix of interconnected clusters or by reaction with other clusters that are nearby. In short, a variety of evidence exists which is consistent with the idea of a free-radical initiated mechanism for nitrogen release via ring rupture.

It should be remembered that light gas nitrogen formation due to tar secondary reactions is not modeled by this mechanism. There are two reasons for this: 1) N_{site} decay in the tar during primary pyrolysis exhibits somewhat different characteristics than in the char (see chapter 6); and 2) a large proportion of the nitrogen is lost from the tar during soot formation, a process which is not yet well understood. This process is currently being studied by Zhang.³¹

It may be more difficult to form free-radicals in the separated vapor phase tar clusters than in the corresponding tightly packed solid-phase char clusters. The slower decay of N_{site} in the tars (see Figure 6.5) is consistent with the free-radical mechanism, since primary tar is much more hydrogen rich than the primary char, and should promote free-radical stabilization reactions like hydrogen abstraction (step 3 in the free-radical mechanism). Since such reactions compete with ring nitrogen for unstable free-radicals,

N_{site} decay is less significant in the tar than in the char for a comparable amount of M_{cl} decay. Also, retention of tar nitrogen in the form of nitrile groups may have a stabilizing effect on unpaired electrons (radicals) in the tar clusters as aliphatic material is released. This idea is consistent with the fact that smaller molecular weight tar clusters (which have less ability to de-localize an unpaired electron) tend to have higher proportions of nitrile nitrogen relative to pyrrolic nitrogen.³⁵

Fast Light Gas Nitrogen Release

A rate equation can be developed from this global mechanism to model the rate of fast light gas nitrogen release as outlined below. The rate of disappearance of ring nitrogen is the rate of step 2 (r_2):

$$-\frac{d[\text{ring } N]}{dt} = r_2 = k_2 [\text{Cluster} - R^*][\text{ring } N] \quad (7.1)$$

where the square brackets denote concentration (grams/gram of aromatic material). Assuming no accumulation of *unstable* cluster free-radicals (steady-state approximation) gives:

$$\frac{d[\text{Cluster} - R^*]}{dt} = 0 = r_1 - k_2 [\text{Cluster} - R^*][\text{ring } N] - k_3 [\text{Cluster} - R^*][R^*] \quad (7.2)$$

Solving Equation 7.2 for $[\text{Cluster} - R^*]$ yields:

$$[\text{Cluster} - R^*] = \frac{r_1}{k_2 [\text{ring } N] + k_3 [R^*]} \quad (7.3)$$

Since experimentally we observe that released light gas *nitrogen* species make up only a very small fraction of the total light gas species released, it can be assumed that $r_2 \ll r_3$, and thus $k_2[\text{ring } N] \ll k_3[R^*]$. This assumption causes a small amount of error (~3% for a

typical coal) in the rate of ring N decay during the late stages of pyrolysis when $[R'']$ is small. With this assumption Equation 7.3 becomes:

$$[Cluster - R'] \frac{r_1}{k_3 [R'']} \quad (7.4)$$

which can be substituted into Equation 7.1 to give:

$$\frac{-d[ring N]}{dt} = k_2 \frac{r_1}{k_3 [R'']} [ring N] = \frac{k_2}{k_3} \frac{r_1}{[R'']} [ring N] \quad (7.5)$$

where k_2 and k_3 are the Arrhenius rate constants for steps 2 and 3 respectively.

This rate equation predicts that once unstable char radicals begin to form, the rate of ring nitrogen decay should be proportional (a) to the concentration of ring nitrogen, and (b) to the overall rate of light gas release (r_1). The rate of light gas formation (r_1) can be defined as the negative fractional change in the molecular weight per cluster as follows:

$$r_1 = -\frac{1}{M_{cl}} \frac{d(M_{cl})}{dt} \quad (7.6)$$

The ring nitrogen concentration is defined as N_{site} (Equation 6.1), the implications of which were described in detail in chapter 6. It is also assumed that $[R'']$ is proportional to the average total mass per cluster (M_{cl}). Since $[R'']$ competes with N_{site} for free-radicals, it must be expressed on the same basis as N_{site} , that is, per average aromatic mass per cluster as follows:

$$[R''] = \frac{M_{cl}}{M_{site}} \quad (7.7)$$

Substituting the above definitions and assumptions into Equation 7.5 yields:

$$-\frac{d(N_{site})}{dt} = \frac{k_2}{k_3} \frac{\frac{1}{M_{cl}} \frac{d(M_{cl})}{dt}}{\frac{M_{cl}}{M_{site}}} N_{site} = -\frac{k_2}{k_3} \frac{M_{site}}{(M_{cl})^2} \frac{d(M_{cl})}{dt} N_{site} \quad (7.8)$$

If the rate constants in Equation 7.8 are expanded and combined then:

$$\frac{k_2}{k_3} = \frac{A_2}{A_3} \exp \frac{-(E_2 - E_3)}{R T_p} = A_N \exp \frac{-E_N}{R T_p} \quad (7.9)$$

where R is the universal gas constant and T_p is the particle temperature. A_2 , A_3 , and A_N are the pre-exponential factors and E_2 , E_3 and E_N are activation energies for steps 2, 3 and the overall global rate expression respectively. Neglecting the linear temperature dependence of the pre-exponential factor (A) predicted by transition state theory is equivalent to a 3 °C error in temperature at 800 °C.⁸⁴ Such an error is an order of magnitude less than typical errors in calculated particle temperatures, and thus this temperature dependence has been neglected. Substituting Equation 7.9 into Equation 7.8 gives the final rate equation:

$$\frac{d(N_{site})}{dt} = A_N \exp \frac{-E_N}{R T_p} \frac{M_{site}}{(M_{cl})^2} \frac{d(M_{cl})}{dt} N_{site} \quad (7.10)$$

This differential rate equation is solved in the CPD model using a predictor-corrector numerical method, just as the other differential equations in the CPD are solved. An additional parameter, f_{stable} , was used which represents the initial fraction of decay in M_{cl} which occurs before N_{site} is allowed to decay. Thus the use of f_{stable} allows an initial fraction of *stable* free-radicals to build up in the char which do not cause any nitrogen release via ring rupture.

Changes in the average total mass per cluster in the char during devolatilization can easily be calculated from parameters predicted by the CPD model, and can also be

calculated from measured ^{13}C NMR data for chars obtained at various stages of pyrolysis. Calculation of M_{cl} in the char using the CPD model is as follows:

$$M_{cl, char} = M_{cl, coal, measured} - (1 - \ell - c_0)(M_{cl, coal, measured} - 7) \quad (7.11)$$

where M_{cl} is the cluster molecular weight, M is the attachment molecular weight, $+1$ is the total number of attachments, ℓ is the fraction of labile bridges remaining in the char, c_0 is the fraction of side chains remaining in the char and c_0 is the fraction of char bridges at time zero. Subtracting seven from the coal attachment molecular weight is an empirical correction performed internally by the CPD model to prevent the release of mass associated with char bridges during devolatilization, and is shown to clarify how the CPD performs the calculation. Changes in the predicted value of $M_{cl, char}$ at each time-step can be used to calculate $d(M_{cl})/dt$ throughout devolatilization.

Slow Light Gas Nitrogen Release

Slow light gas nitrogen release (pathway C) is assumed to be first order in N_{site} as follows:

$$-\frac{d(N_{site})}{dt} = A_4 \exp\left(\frac{-E_4}{R T_p}\right) N_{site} \quad (7.12)$$

where A_4 is the pre-exponential factor, E_4 is the activation energy, R is the universal gas constant, and T_p is the particle temperature. Although slow light gas nitrogen release is probably more realistically modeled using a distributed activation energy, the activation energy was not distributed in this model due to a lack of long residence time high temperature pyrolysis data.

Other Mechanisms

Solid-state ^{13}C NMR char and coal data were used to ensure that the fast light gas nitrogen release rate equation accurately related changes in N_{site} to changes in M_{cl} throughout primary devolatilization for coals spanning a wide range of rank. While developing this model, a large number of other options were explored in an attempt to model the rate of nitrogen release as light gas. Initially, a simple first order rate expression (with no coal-dependent parameters) for the disappearance of N_{site} in the char was tried, but this failed to describe the way in which nitrogen release stops once mass release ceases. Next, a distributed activation energy was added, but this failed to capture the trend of light gas nitrogen release with rank. Once it became clear that light gas nitrogen release was coupled with light gas release, several mechanisms were explored, but none could correctly describe the changes in measured N_{site} values as a function of measured M_{cl} values. Attempted mechanisms included: (a) reaction of char ring nitrogen with gas phase free-radicals (light gas pre-cursors); (b) reaction of ring nitrogen with char free-radicals formed from both tar and light gas release; (c) omitting the reaction which competes for char free-radicals; (d) adding a second-order free-radical destruction step which competes for char radicals; and (e) assuming that $[R^{\bullet}]$ is proportional to the aliphatic char material only. In contrast, the final free-radical mechanism rate equation (Eq. 7.10) properly describes both the manner in which N_{site} changes during pyrolysis and the rank dependence of light gas nitrogen release.

Nitrogen Distribution Calculation

When used with a network devolatilization model, nitrogen distribution predictions can be calculated from predicted N_{site} values. First the nitrogen content of the char is calculated as follows:

$$y_{N, \text{char}} = N_{\text{site, char}} \frac{M_{\text{site}}}{M_{\text{cl, char}}} \quad (7.13)$$

where $y_{N, \text{char}}$ is the mass fraction of nitrogen in the char, M_{site} is the aromatic mass per cluster and M_{cl} is the total mass per cluster. Then the tar nitrogen as a fraction of the nitrogen in the coal ($f_{N, \text{tar}}$) at any given time step i can be calculated according to the following mass balance:

$$f_{N, \text{tar}, i} = f_{N, \text{tar}, i-1} + (f_{\text{tar}, i} - f_{\text{tar}, i-1}) \frac{y_{N, \text{char}, i-1}}{y_{N, \text{coal}}} \quad (7.14)$$

where f_{tar} is the daf tar yield as a fraction of daf coal, $y_{N, \text{char}}$ is the mass fraction of nitrogen in the char (which is assumed to be equal to the value in the most recently released tar), and $y_{N, \text{coal}}$ is the mass fraction of nitrogen in the parent coal. In Equation 7.14, $y_{N, \text{char}, i}$ was substituted for $y_{N, \text{tar}, i}$, since their average chemical structural properties is assumed to be equal. Equation 7.14 is just an integrated form (on a per daf coal basis) of the following equation:

$$d(\text{masstar}N) = y_{N, \text{tar}, i} d(\text{masstar}) \quad (7.15)$$

Once the char nitrogen content and tar nitrogen yield have been predicted, the rest of the nitrogen distribution is calculated in the same manner as was used for experimentally measured nitrogen distributions in this study. Specifically, nitrogen release (NR) is calculated from a mass balance on nitrogen as follows:

$$NR = 1 - f_{\text{char}} \frac{y_{N, \text{char}}}{y_{N, \text{coal}}} \quad (7.16)$$

where f_{char} is the daf char yield as a fraction of daf coal and y_{N} is the mass fraction of nitrogen in the char or the coal. Note that nitrogen release is directly proportional to the char yield, or in other words, depends directly on the total mass release. Because of this, any error in predicted mass release will produce the same relative error in predicted nitrogen

release, even if the nitrogen model predicts the char nitrogen content perfectly. Light gas nitrogen can then be calculated from a mass balance on nitrogen in the pyrolysis products.

Devolatilization Modeling Procedure

Calculated centerline gas temperature and velocity profiles for each condition were used with the Chemical Percolation Devolatilization (CPD) model to predict time resolved particle temperature profiles and model the devolatilization process. Centerline gas velocity profiles were calculated in the drop tube by modeling the gas flow field for each condition using FLUENT. Centerline gas temperatures for these simulations matched experimentally measured values to within 50°C except that the initial temperature rise was steeper. The pyrolysis tests at the 1100 K condition produced chars with much less aliphatic material than contained in chars from coals of similar rank produced in a drop tube at Sandia at a similar condition.⁵ Hambly observed this same result for chars he produced in the BYU drop tube reactor in 1997.¹¹ One possible explanation for this observation is that the particles deviated from the centerline during the drop tube pyrolysis tests, a common problem in drop tube studies. A detailed study of the flow fields predicted by the FLUENT simulations showed turbulence at the point of particle injection and an initial maximum axial velocity far from the centerline. These factors probably caused the particles to deviate far from the centerline to a radial position where the gas temperature was much hotter. A particle trajectory was therefore chosen for the particles about halfway between the wall and the centerline in order to estimate gas temperature and velocity profiles. The use of this assumed trajectory yielded CPD predictions of M_{cl} decay that matched the experimentally measured values at the 1100 K condition fairly well. Such a procedure is consistent with the observation that CPD predictions of M_{cl} decay using *measured* particle temperature profiles matched measured values of M_{cl} decay for five coals at Sandia with maximum particle temperatures of about 1150 K. The assumed particle trajectory is shown in Figure 7.2. This same particle trajectory was also assumed for the 900, 1000, and 1250 K drop

tube conditions to obtain estimated corrected gas and velocity temperature profiles from the FLUENT simulations. Unless otherwise indicated, these estimated corrected gas and velocity profiles were used for all drop tube CPD simulations and nitrogen model evaluations. Examples of measured and predicted (FLUENT) gas temperature and gas velocity profiles for the drop tube tests are shown in Figure 7.3 and Figure 7.4, respectively. A complete set of predicted and measured gas temperature and velocity profiles for all drop tube conditions can be found in Appendix G. Gas temperature and velocity profiles for the flat flame reactor pyrolysis tests were assumed to be the same as those measured by Ma at identical conditions in the BYU flat flame reactor.⁴¹

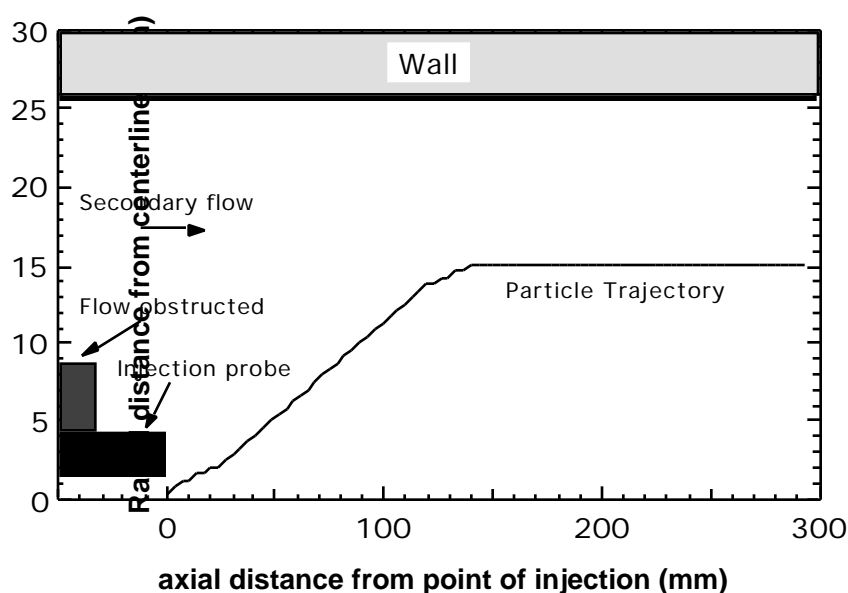


Figure 7.2. Particle trajectory assumed in modeling gas temperature and velocity profiles for all drop tube pyrolysis tests. Note the large differences in length scale between the ordinate and abscissa.

Although the 45-75 mm parent coal size fraction was used in the pyrolysis experiments, an average particle size of 55 μm was assumed for the CPD devolatilization predictions shown in this study. Although most of the model predictions use actual ^{13}C

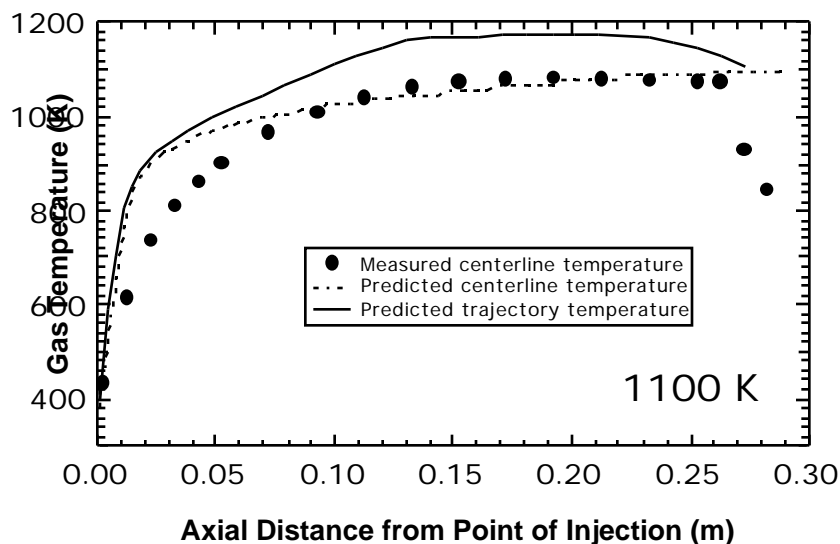


Figure 7.3. Measured (symbols) and predicted (dashed line) centerline gas temperature profiles are compared to the gas temperature profile along the assumed particle trajectory (solid line) for the 1100 K drop tube condition.

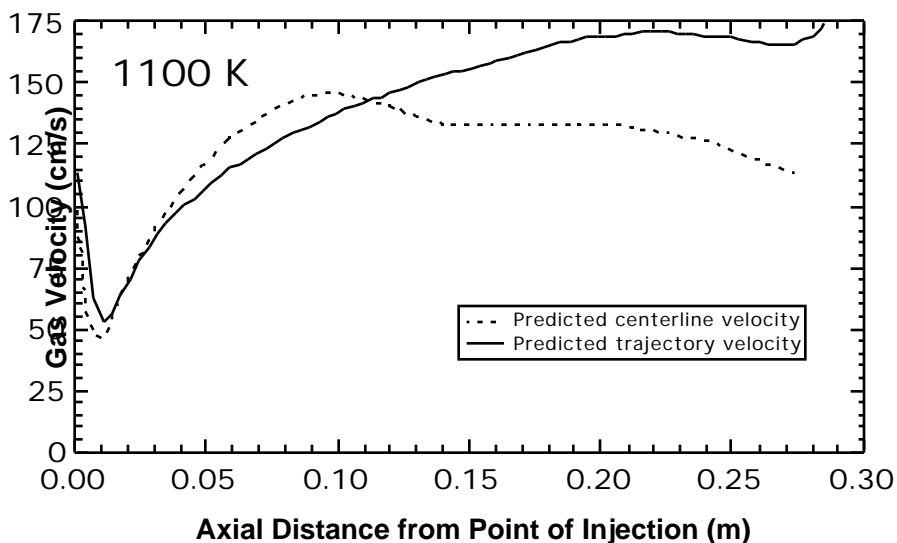


Figure 7.4. Predicted centerline gas velocity profile (dashed line) compared to the gas velocity profile along the assumed particle trajectory (solid line) for the 1100 K drop tube condition. Velocity profiles based on predicted (not measured) temperature profiles.

NMR structural data for the coal dependent CPD model input parameters, predictions were also made at the 1100 K and 1650 K conditions using a correlation reported by Genetti et al.⁸⁵ to estimate the chemical structural parameters needed by the CPD model from the

parent coal proximate and ultimate analyses. In every case the correlation developed by Genetti⁹ was used to estimate the initial fraction of char bridges in the coal (c_0):

$$c_0 = \min\{0.36, \max[(11.8 y_{C, coal} - 10.1), 0.0]\} + \min\{0.15, \max[(1.4 y_{O, coal} - 0.175), 0.0]\} \quad (7.17)$$

where $y_{C, coal}$ and $y_{O, coal}$ are the dry ash free carbon and oxygen mass fractions in the parent coal, respectively.

The CPD model in its present form predicts the retention of all aliphatic material within those bridges stabilized by early cross-linking or due to high rank (described by the empiricism c_0).⁸¹ This c_0 parameter is mainly used to describe the network structure of the coal or char, and the mass of this material was not carefully treated. Since it is thought that this aliphatic material is released with the light gases, especially at severe pyrolysis conditions such as those used in this study (i.e. Table 5.1), a correction was made to the measured mass per attachment (M) to account for this as follows:

$$M_{,corrected} = \frac{M}{(1 - c_0)} \quad (7.18)$$

where c_0 is the fraction of bridges assumed to be stable at time zero. This correction was used in all nitrogen model predictions performed for this study.

Rate Constant Regression for the Nitrogen Model

The full nitrogen model was added to the Chemical Percolation Devolatilization (CPD) model in order to predict how coal nitrogen is distributed among char, tar, and light gas products during devolatilization. In so doing, the slow nitrogen release step (eq. 7.12) was assumed to have an activation energy of 90 kcal/mol, estimated from the theoretical bond energy for the carbon nitrogen bond in pyrrole as reported by Mackie et al.⁵¹ Data

from Blair and Wendt⁵⁵ for pyrolysis of an Illinois #6 coal on a graphite ribbon at 2000 K for about 2 minutes was used to fit the pre-exponential factor for the slow nitrogen release step at $5.5 \times 10^7 \text{ sec}^{-1}$. It is possible that these rate expression parameters somewhat over-predict nitrogen release during severe, long residence time pyrolysis since 99% nitrogen release is predicted after only 3 minutes at 2100 K, whereas Pohl and Sarofim⁷ report that 20 minutes at 2100 K may be required to achieve complete nitrogen release. At any rate, the predicted slow light gas nitrogen release is not significant compared to the overall nitrogen release at the devolatilization conditions used in this study (i.e. the conditions shown in Table 5.1) or in practical combustors. More detailed high temperature long residence time data are needed to better estimate the slow nitrogen release kinetic parameters.

For the fast nitrogen release portion of the nitrogen model, decay of M_{cl} and N_{site} was also predicted in order to regress appropriate values for the pre-exponential factor (A_N) and activation energy (E_N) using experimental data (see Table 7.1). First, data published by Fletcher and Hardesty⁵ for which *measured* particle temperatures and ¹³C NMR chemical structural data were available for experiments performed at 1250 K and 1600 K were used to determine the activation energy. This was done by guessing an activation energy, calculating a pre-exponential factor by matching the N_{site} data (as a function of M_{cl}) for the Beulah Zap 1250 K test, and comparing the 1600 K nitrogen release predictions (made using the guessed E_N and A_N) with measured values. This procedure was performed iteratively until the activation energy that gave the best agreement was found. Data from the Beulah Zap test was used to fit the pre-exponential factor because doing so gave reasonable predictions (in the author's judgement) for the other coals at 1250 K. The activation energy thus determined was then used to iteratively solve for the pre-exponential factor which gave predictions most closely matching (in the author's judgement) the N_{site} vs. M_{cl} data from experiments performed for all eight coals at the 1100 K condition of the present study. The pre-exponential factor thus determined was averaged with the (slightly higher) pre-

exponential factor which best fit the 1250 K Sandia data. This regression procedure gave values of $A_N=18.4$ (unitless) and $E_N=6$ kcal/mol. The relatively low apparent activation energy is not unreasonable because it represents the *difference* between the activation energies of competing steps 2 and 3 of the free-radical mechanism.

It was assumed that the radicals formed during the initial 3% of light gas release were stable (i.e. $f_{\text{stable}} = 0.03$). This means that N_{site} was assumed to remain at the value in the parent coal until the molecular weight per cluster had decayed to 97% of the coal value. It is not clear whether this empiricism is really necessary, although it seems to fit the available data for high rank coals somewhat better, consistent with the concept of the formation of a pool of free-radicals before steady-state is reached.

A summary of the five coal-independent parameters for the free-radical mechanism nitrogen release model is shown in Table 7.1. The parameters in Table 7.1 are used in all free-radical nitrogen model predictions found in this dissertation. Sample input files for both the CPD and the CPDCP versions of the code are found in Appendix H.

Table 7.1.

Summary of free-radical mechanism parameters as used in this study.

A_N (fast light gas)	18.4 (unitless)
E_N (fast light gas)	6.0 kcal/mol
A_{slow} (slow light gas)	$5.5 \times 10^7 \text{ sec}^{-1}$
E_{slow} (slow light gas)	90 kcal/mol
f_{stable} (fraction of M_{cl} decay with no N_{site} decay)	0.03

Evaluation of the Nitrogen Release Model

The nitrogen model was used with the CPD model to make predictions of M_{cl} , N_{site} , tar yield, tar nitrogen, total mass release, and total nitrogen release for all the pyrolysis tests performed in this study, as well as for literature data. The model is also evaluated against data from pyrolysis tests using parent coals spanning a wide range of rank and heating rates

ranging from 0.5 to 10^5 K/s. Unfortunately, because of the high cost of the FG-DVC and FLASHCHAIN devolatilization models, it was not possible to purchase copies of these models with their corresponding nitrogen models for direct comparison of nitrogen model predictions.

N_{site} Predictions

Comparisons of predicted and measured M_{cl} and N_{site} are shown in Figure 7.5 for chars produced in a drop tube⁵ with a maximum gas temperature of 1250 K quenched at various points along the pyrolysis path. Char values for M_{cl} and N_{site} are normalized to the parent coal values for ease of comparison. For the data shown in Figure 7.5, it appears that the higher the coal rank, the more steep the slope of N_{site} decay, a trend which is correctly predicted by the nitrogen model. Although the final change in M_{cl} is not always perfectly predicted by the CPD model, the model correctly predicts the relationship between N_{site} and M_{cl} for each test rather than simply matching the endpoint N_{site} value. For example, although the predicted endpoint M_{cl} value is lower than the measured value (0.63 vs. 0.70) for the Illinois #6 coal at this condition (and thus the predicted endpoint N_{site} is also lower than the measured value), the trajectory follows the experimental data fairly well. Note that the nitrogen model has no effect on predictions of M_{cl} , which are calculated separately by the CPD.

Chars produced in this study at 1100 K (see Figure 7.6) showed the same trend with rank for N_{site} decay as the Sandia data shown in Figure 7.5. Again, the nitrogen model captures the trend with rank quite well, although the devolatilization model slightly under-predicts the amount of M_{cl} decay for most of the coals. It is noteworthy that the dependence of N_{site} decay on M_{cl} decay for the chars in Figure 7.6 was *weaker* than the dependence observed for the chars in Figure 7.5, even though particle temperatures were *higher* for the chars of Figure 7.6. This discrepancy may be due to the assumption made

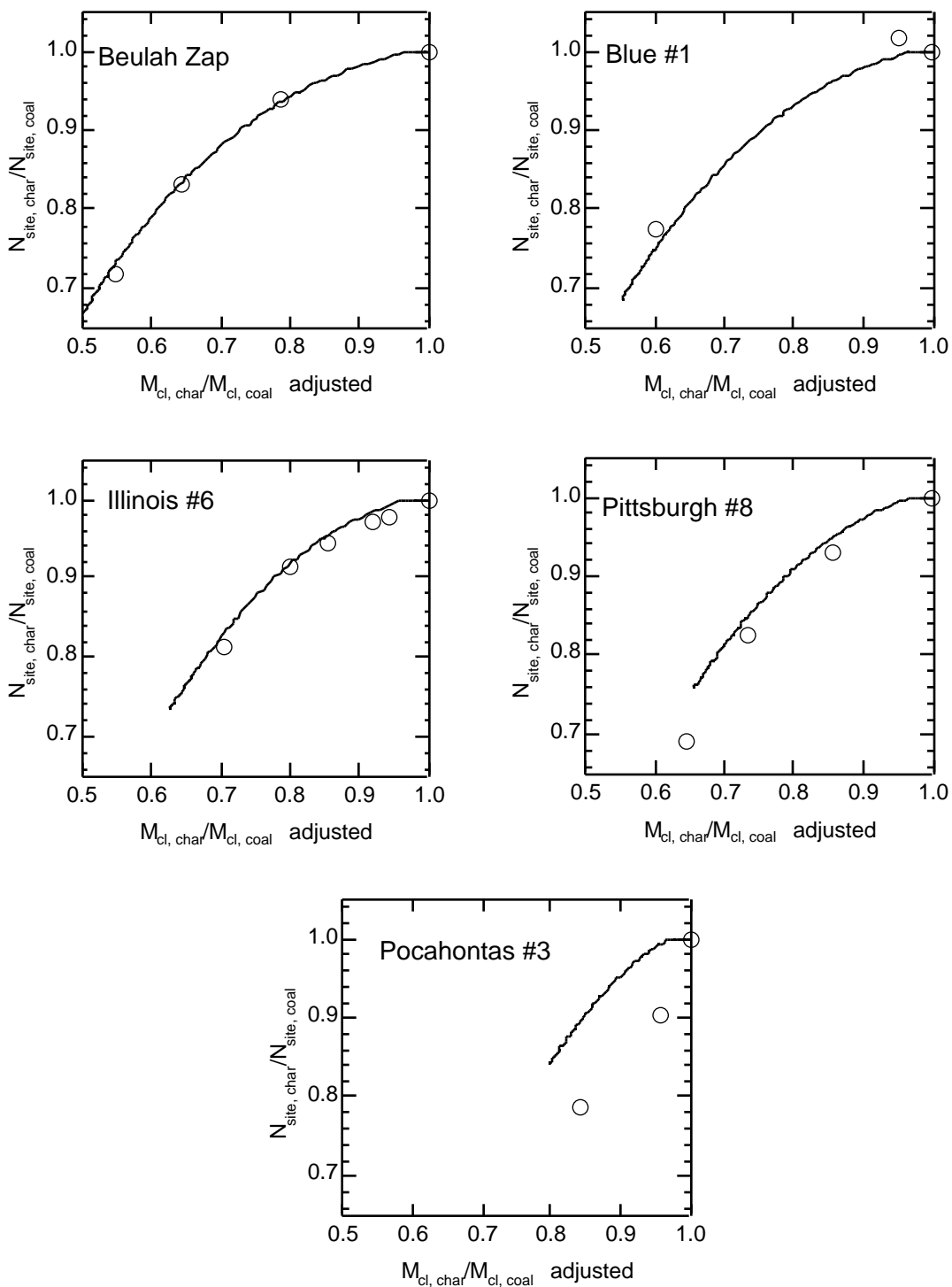


Figure 7.5. Predicted decay (lines) of N_{site} compared to values calculated from measured chemical structural data (symbols) published by Fletcher and Hardesty⁵ for drop tube pyrolysis of five coals at 1250 K maximum gas temperature and 250-300 ms residence time. Char M_{cl} values are adjusted for changes in measured M_{site} values (see eq. 6.9).

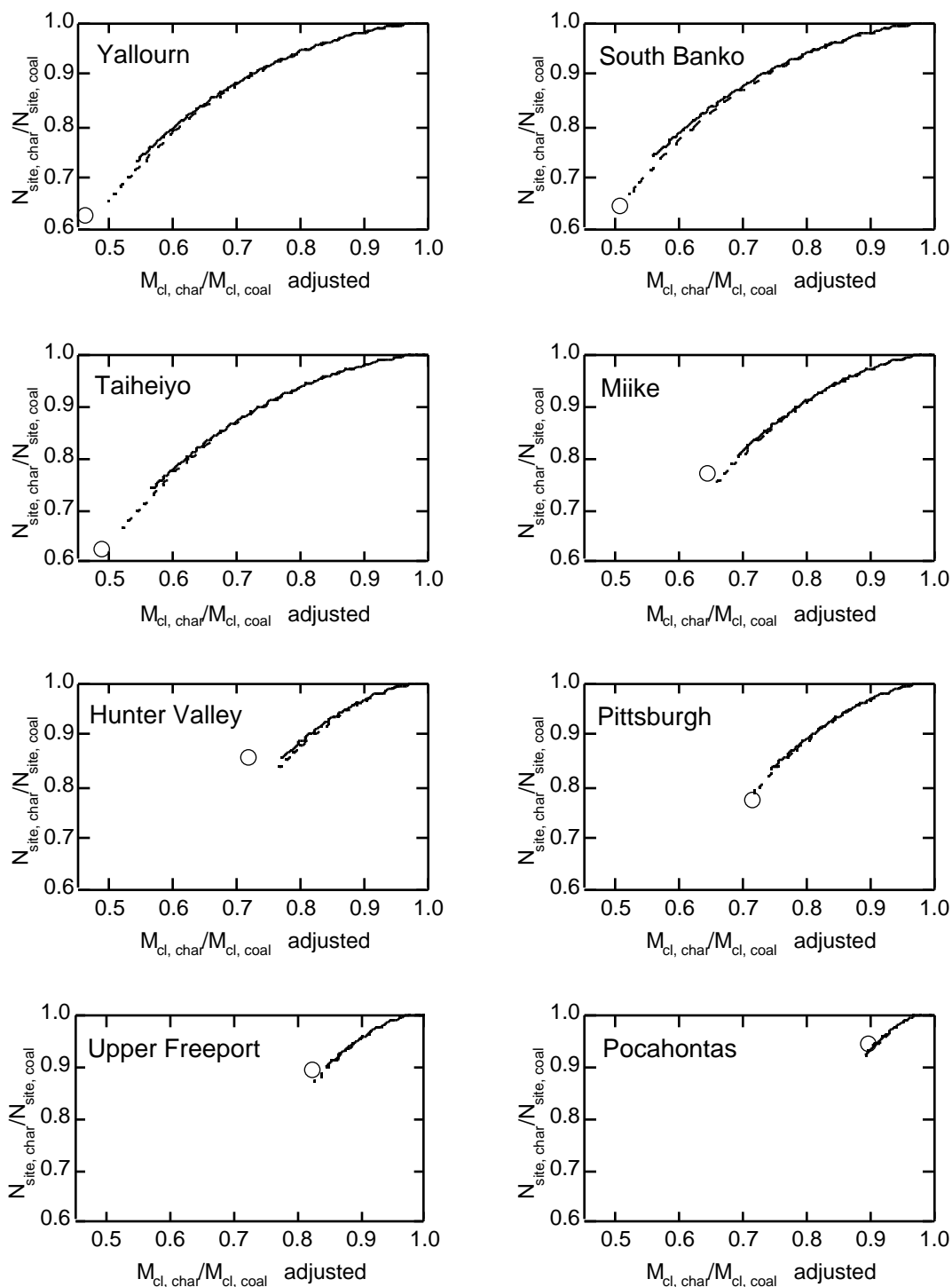


Figure 7.6. Predicted (lines) decay of N_{site} compared to values calculated from ^{13}C NMR data (symbols) for chars generated at 1100 K condition in this study. Solid lines are predictions made using the measured centerline temperature profile and dashed lines are predictions made using the temperature profile adjusted using drop tube gas simulation. Char M_{cl} values are adjusted for changes in measured M_{site} values (see eq. 6.9).

(in deriving the rate equation) that the rate of step two (ring N reaction) was much slower than the rate of step three (competing reaction), which assumption causes over-prediction of N_{site} decay dependence on M_{cl} decay for highly devolatilized chars. Thus N_{site} decay would be over-predicted in the chars of Figure 7.6 relative to the less severely pyrolyzed chars of Figure 7.5.

Figure 7.7 summarizes the amount of measured and predicted N_{site} decay for all chars at the 1100 K condition, revealing a strong trend with rank for char N_{site} decay. Note that predictions are not continuous functions of parent coal rank or daf % C, and thus predictions shown as a function of daf % C are discrete points which are represented as lines only for ease of comparison with data (i.e. Figure 7.7). The model of Genetti³ does not predict any trend with rank for char N_{site} until above 86% carbon, but it is easily seen that the free-radical mechanism model predictions follow the trend quite well. Thus the free-radical mechanism asserts that low-rank coals release more light gas nitrogen than bituminous coals, not because they have more reactive aromatic nitrogen, but rather

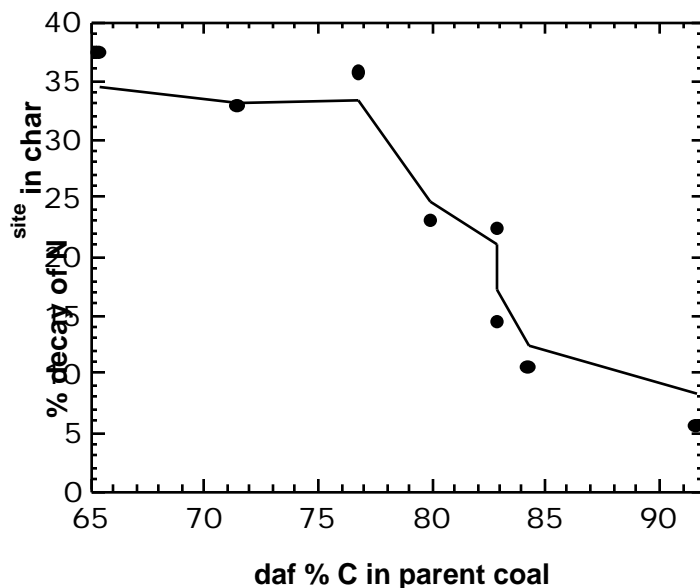


Figure 7.7. Trend with rank of measured (symbols) and predicted (line) N_{site} decay for chars produced in the drop tube at the 1100 K condition of this study. Parent coal carbon content is used as an indicator of rank.

because they release a larger fraction of aliphatic material, creating more free-radicals in the char during devolatilization.

The free-radical mechanism model may not completely explain why coals of similar composition and rank release different amounts of nitrogen. For example, although both Hunter Valley and Pittsburgh have parent coal carbon contents of 82.8% and show 28.5% char M_{cl} decay at 1100 K, Hunter Valley releases only 14% of coal nitrogen as light gas while Pittsburgh releases 20% (see Table 5.10 or Figure 7.7). The lower parent coal carbon aromaticity of Pittsburgh coal (70% versus 71% for Hunter Valley) only accounts for a small part of this difference. The difference between Pittsburgh and Hunter Valley light gas nitrogen release seems to be much less at the 900 K, 1000 K and flat flame reactor conditions, for which the light gas nitrogen yields differ by only 1 to 3%. This suggests that some of the difference may be due to data scatter. In spite of such discrepancies, the free-radical mechanism does an excellent job describing the trend with rank based only on the parent coal chemical structure, especially considering the greatly simplified chemistry assumed by the global mechanism.

The nitrogen release model in FLASHCHAIN correlates the pre-exponential factor for light gas nitrogen release with the O/N ratio in the parent coal, predicting an *exponential* dependence on O/N.⁷² Figure 7.8 shows the trend in N_{site} decay (left axis) as a function of O/N ratio in the parent coal for the 1100 K drop tube chars. Also shown are values of the corresponding pre-exponential factor used by the FLASHCHAIN model (right axis). The highest and lowest values of the O/N ratios in the parent coals were outside the range used in the FLASHCHAIN correlation. Analysis of the trend of the measured N_{site} data with O/N shows that, for the coals used in this study, a piecewise linear dependence of the A factor on O/N ratio might be a better approximation than an exponential dependence. Again, predictions made using the free-radical mechanism model describe even the deviations from the piecewise linear trend with O/N.

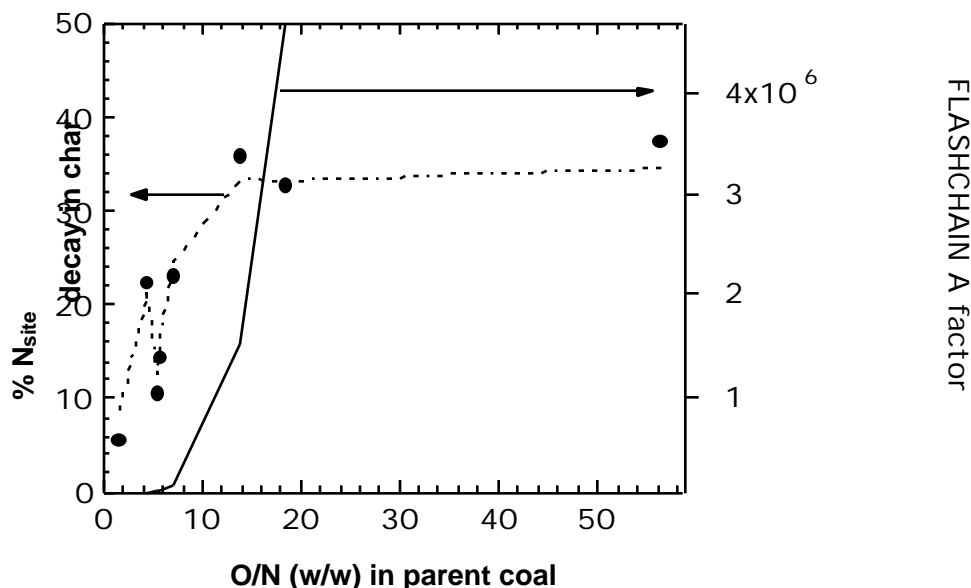


Figure 7.8. Trend with parent coal O/N ratio of measured (symbols) and predicted (dashed line) relative N_{site} decay from parent coal value (left axis) for chars produced in the drop tube at the 1100 K condition of this study. Also shown is the corresponding A factor for light gas release used by the FLASHCHAIN model (right axis).⁷²

Predictions of N_{site} decay have also been made for pyrolysis tests performed by Hambly in a drop tube reactor at 1080 K. These predictions are compared to measured values in Figure 7.9, with data from chars generated at 820 K also shown for comparison. Although the decay of M_{cl} is under-predicted by the CPD model, the relationship between N_{site} and M_{cl} seems to be very good for the 1080 K chars. The data also show a phenomenon not predicted by the free-radical mechanism model, in that the chars produced at 820 K (open symbols in Figure 7.9) have much lower values of N_{site} than expected. This phenomenon was also seen in normalized N/AC values of the majority of chars (as measured by XPS) produced at 783 K by Kelemen with a 0.23 K/sec heating rate (Figure 7.10). Most of the char data in Figure 7.10 are below the predicted values. This may be due to an increase in char aromatic mass per cluster associated with low heating rates.⁷⁹ In contrast, no such behavior was observed in the drop tube experiments performed at Sandia (Figure 7.5).

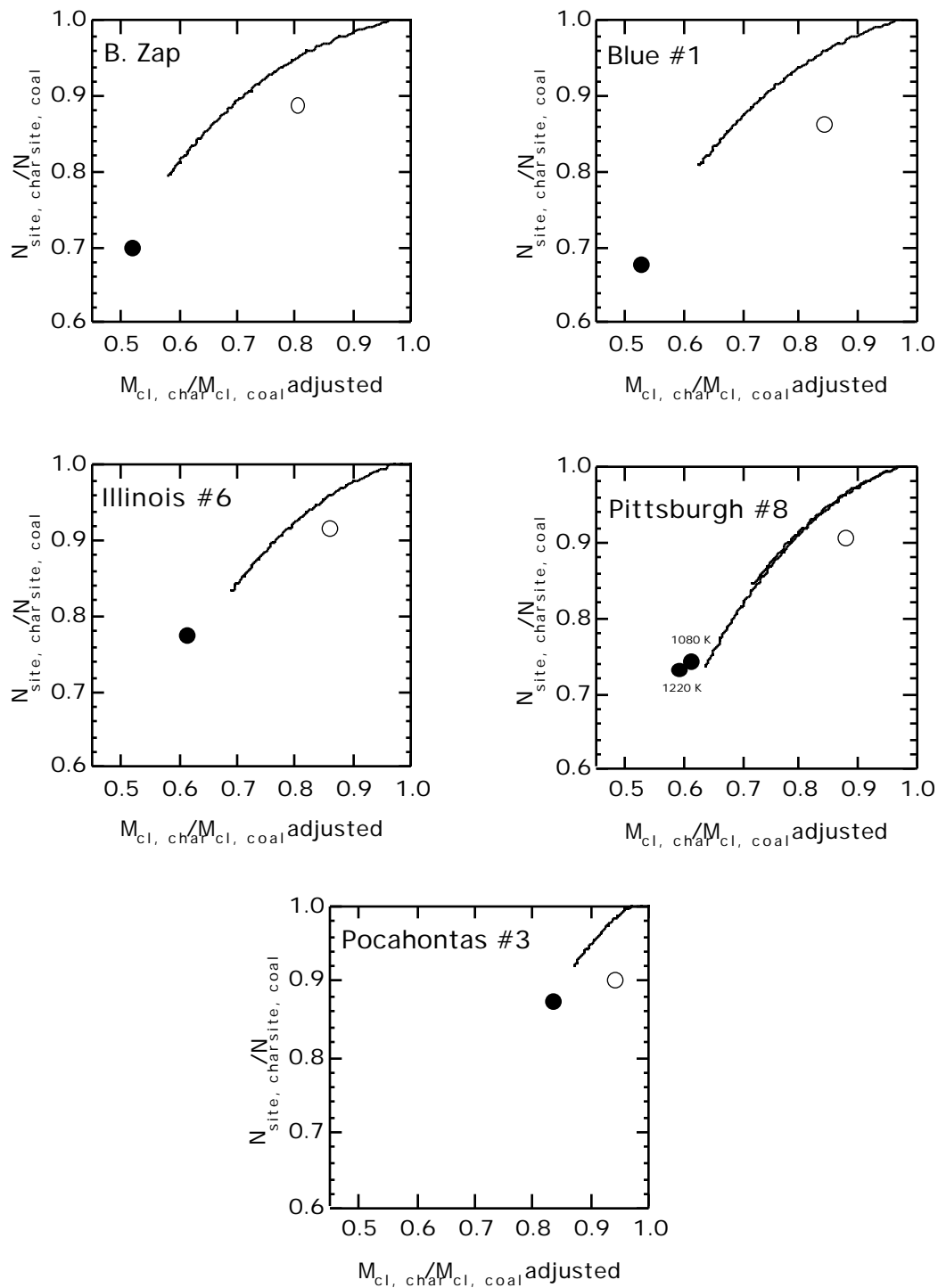


Figure 7.9. Predicted decay (lines) of N_{site} compared to values calculated from published¹¹ and unpublished¹² measured chemical structural data of Hamby for drop tube pyrolysis of five coals at 1080 K and 285 ms (closed circles) and 820 K and 170 ms (open circles). Char M_{cl} values are adjusted for changes in measured M_{site} values (see eq. 6.9).

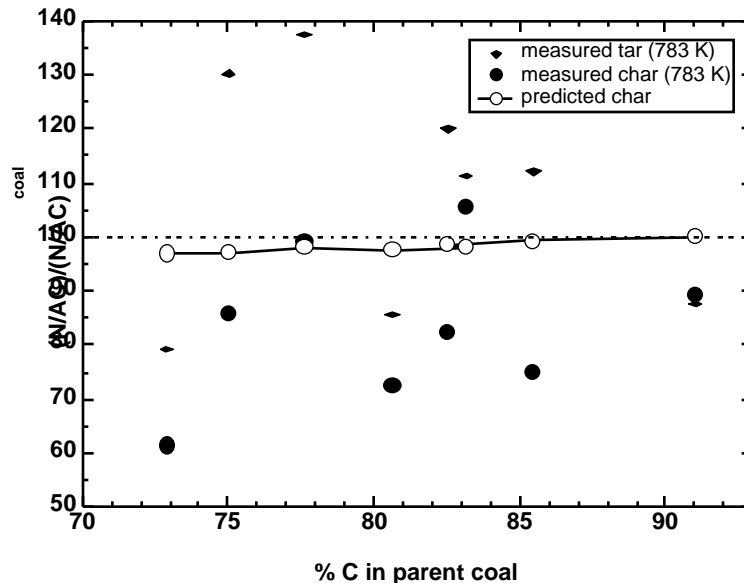


Figure 7.10. Predicted final char N/AC values (lines and open symbols) compared to values calculated from chemical structural data as measured by XPS (filled symbols) reported by Kelemen et al.⁴³ for chars (circles) and tars (diamonds) produced by pyrolysis of the Argonne premium coals at 783 K (0.23 K/sec heating rate).

Nitrogen Distribution Predictions

Figure 7.11 shows measured light gas nitrogen release ($\text{NH}_3 + \text{HCN}$) as a fraction of initial coal nitrogen for pyrolysis of the Argonne premium coals with a maximum temperature of 1173 K, a heating rate of 0.5 K/s and a hold time of 3 minutes, as reported by Basilakis and co-workers.¹ The data are shown as a function of coal type using the parent coal daf oxygen content. Predictions made of these data using both the free-radical mechanism model and the stable nitrogen fraction model of Genetti are shown. The nitrogen model of Genetti predicts the release of all nitrogen except the “stable fraction” for the long residence time used in this experiment. However, the free-radical mechanism adequately describes the light gas nitrogen release at this low heating rate for each of the Argonne coals except possibly the two low-rank coals (i.e. high %O in the parent coal). It is possible that early crosslinking in the low-rank coals at low heating rates is indicative of fast reactions which compete more effectively for free radicals (step 3 of the mechanism), thus attenuating the

N_{site} decay. Despite the omission of such effects from the nitrogen model, agreement is still fairly good.

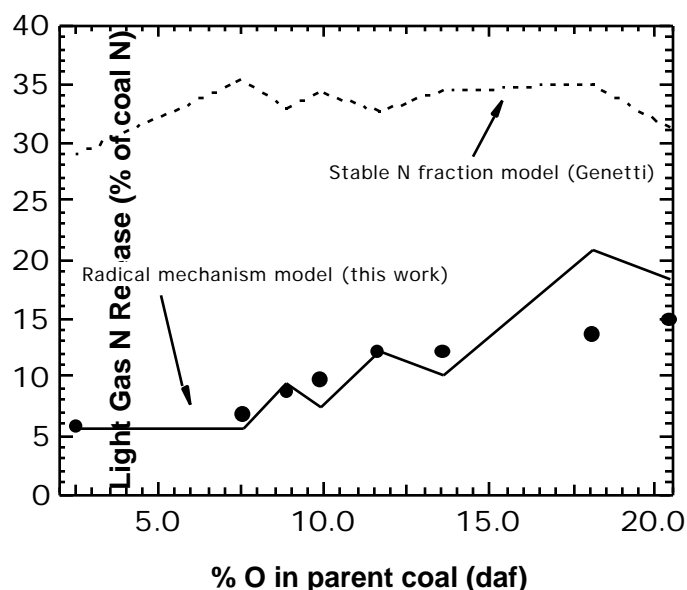


Figure 7.11. Comparison of predicted total light gas nitrogen yields with the measured $\text{HCN} + \text{NH}_3$ yields reported by Bassilakis et al.¹ for 0.5 K/sec pyrolysis of the Argonne premium coals with a maximum particle temperature of 1173 K. Predictions made using parent coal ^{13}C NMR structural parameters reported by Smith et al.¹⁹

Predictions from the nitrogen model were also compared to predictions published by Niksa⁷² for the FLASHCHAIN nitrogen model. In Figure 7.12, comparisons are made between the predictions of both models and the experimental data of Frieht et al.⁸⁶ as reported by Niksa⁷² for vacuum pyrolysis of a Pittsburgh coal in a heated grid apparatus. For the data in Figure 7.12, each calibration temperature represents a different temperature profile, with maximum particle temperatures generally 80-100 K lower than the calibration temperature. Heating rates ranged from 20 to 460 K/s and residence time was about 10 s for each test. Both models tend to predict too little tar nitrogen, especially below 1200 K. Both models also predict too little light gas nitrogen above 1100 K. However, the FLASHCHAIN nitrogen model shows much larger discrepancies in these areas and

predicts light gas nitrogen formation at unrealistically low particle temperatures (718 K or 445 °C). Thus for this coal at these conditions, the advantages of using a nitrogen model based on chemical structure and simplified light gas nitrogen release chemistry can clearly be seen.

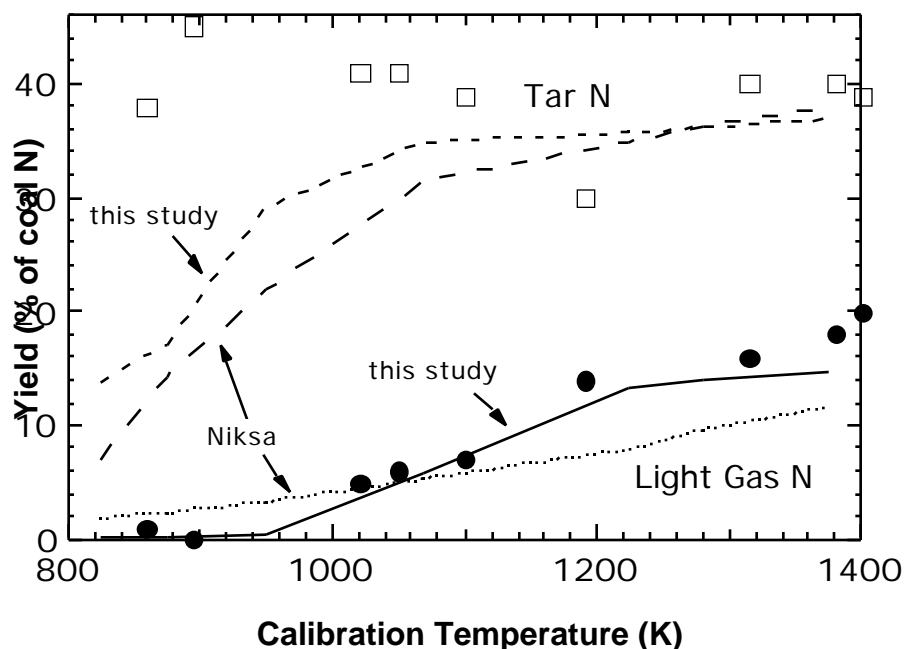


Figure 7.12. Comparison of predicted (lines) light gas nitrogen and tar nitrogen yields with measured HCN (circles) and tar nitrogen (squares) yields observed by Friehaut et al.⁸⁶ for vacuum pyrolysis (0.015 Mpa) of a Pittsburgh coal at 20-460 K/s heating rate using a heated grid apparatus. Measured data, predictions of Niksa, and particle temperature profiles used are those reported by Niksa.⁷² Predictions of this study made assuming that the parent coal ¹³C NMR structural parameters are those reported by Fletcher and Hardesty for Pittsburgh #8 coal.⁵

The model was also found to perform well for Curie point pyrolysis tests at moderate (~3000 K/s) heating rates. In Figure 7.13 model predictions of mass and nitrogen release are compared to values measured by Nomura et al.⁸⁷ for 5 coals at a variety of temperatures, with a 5 second total pyrolysis time. Both the mass and nitrogen release predictions in Figure 7.13 show good agreement with the data, except at the highest

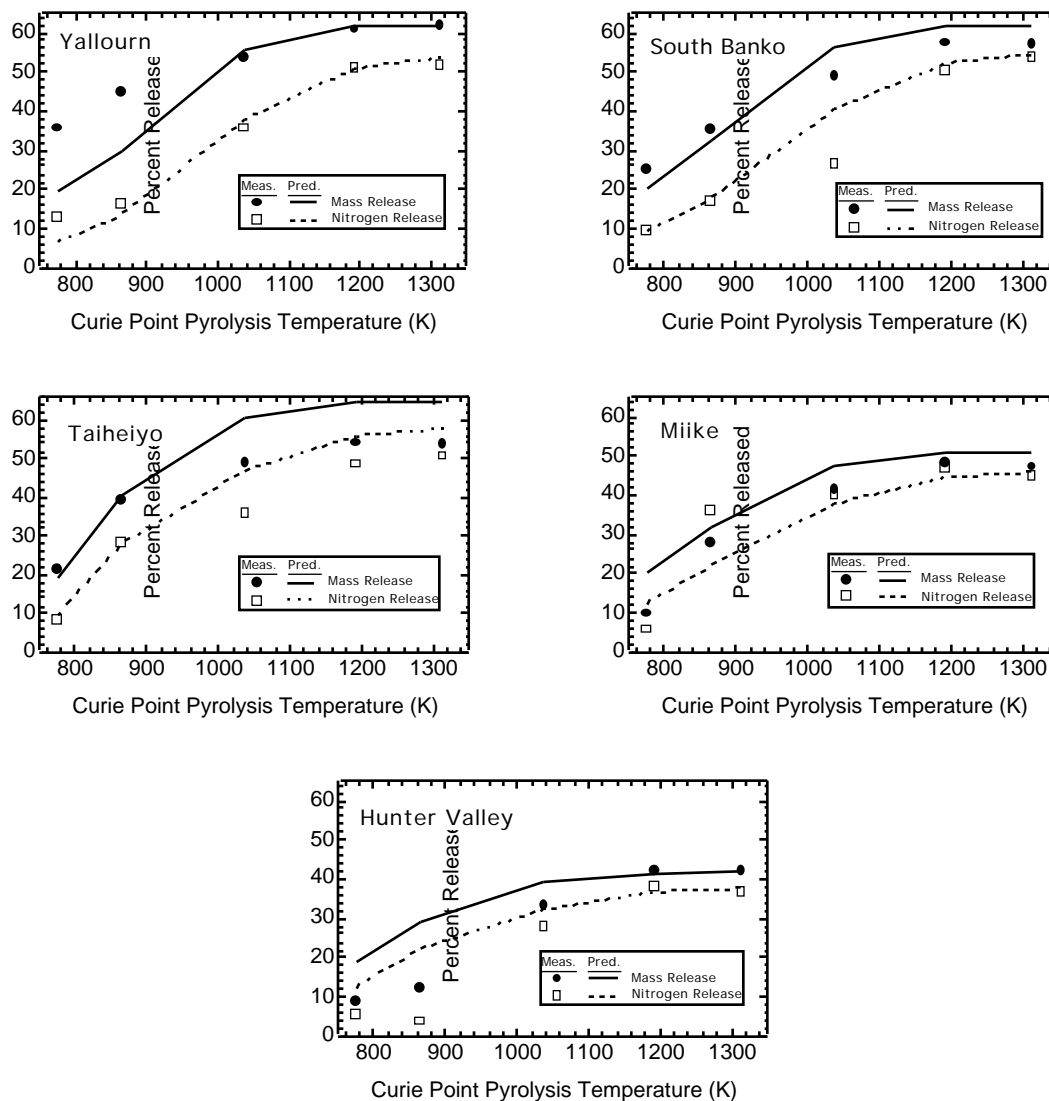


Figure 7.13. Comparison of predicted (lines) and measured (symbols) mass and nitrogen release for Curie point pyrolysis experiments reported by Nomura et al. (5 second pyrolysis time).⁸⁷

temperature, where nitrogen release seems to be slightly under-predicted (relative to mass release) for some coals. In Figure 7.14 light gas nitrogen predictions for eight coals at two different temperatures are compared to HCN yields reported by Nomura et al.⁸⁷ during Curie point pyrolysis tests. Agreement between predicted and measured values is good at 943 K, but at 1313 K, predictions are significantly higher than measured values for the lowest-rank (lowest % C) coals. This might be because light gas nitrogen measurements

were only made for HCN, although NH_3 is also known to form during pyrolysis of low-rank coals.^{1, 88}

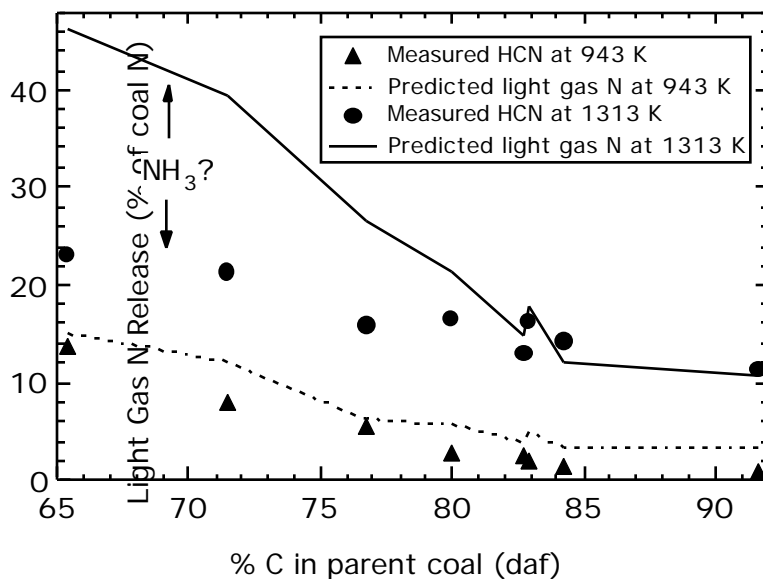


Figure 7.14. Comparison of predicted *total light gas release* (lines) and measured *HCN release* (symbols) for Curie point pyrolysis experiments reported by Nomura et al. at 943 K and 1313 K (3 second pyrolysis time).⁸⁷

At particle heating rates found in drop tube pyrolysis experiments ($\sim 10^4$ K/s), predictions from the free-radical mechanism model were compared to measured values using data sets from several different researchers. Examples of these comparisons are found in Figures 7.15-7.19. A complete set of these comparisons is located in Appendix I. Of these, only the data from the 1100 K condition of this study and the Sandia tests at 1250 K (drop tube) and 1600 K (flat flame reactor) were used in the development and tuning of model parameters. Predictions of char nitrogen content (Figure 7.17) were normalized to the parent coal values to provide a more stringent comparison. Note that even at reactor temperatures as high as 2100 K (Figure 7.19), the nitrogen model performs reasonably well (note the long residence times in this figure). Predicted ultimate mass release values

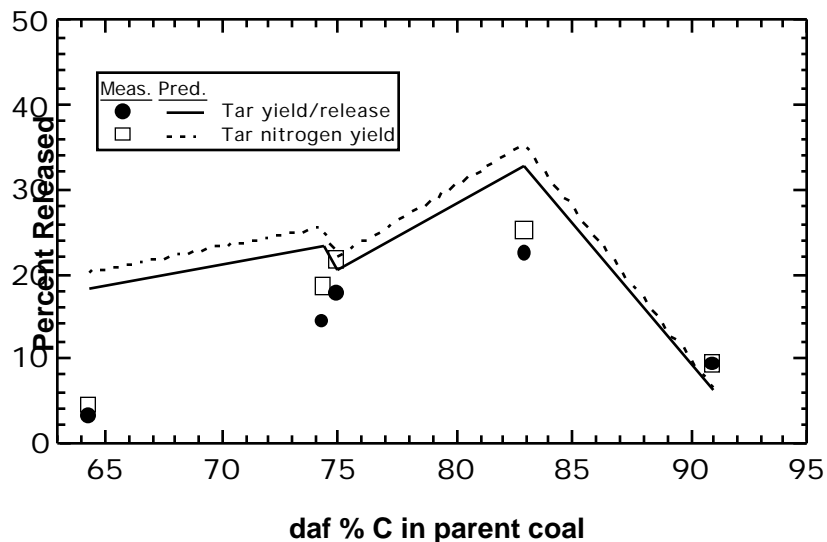


Figure 7.15. Comparison of predicted (lines) and measured (symbols) tar and tar nitrogen yields for drop tube pyrolysis experiments performed by Hambly at 1080 K (282 ms residence time).¹¹ Predictions made using measured parent coal ¹³C NMR structural parameters reported by Hambly.¹¹

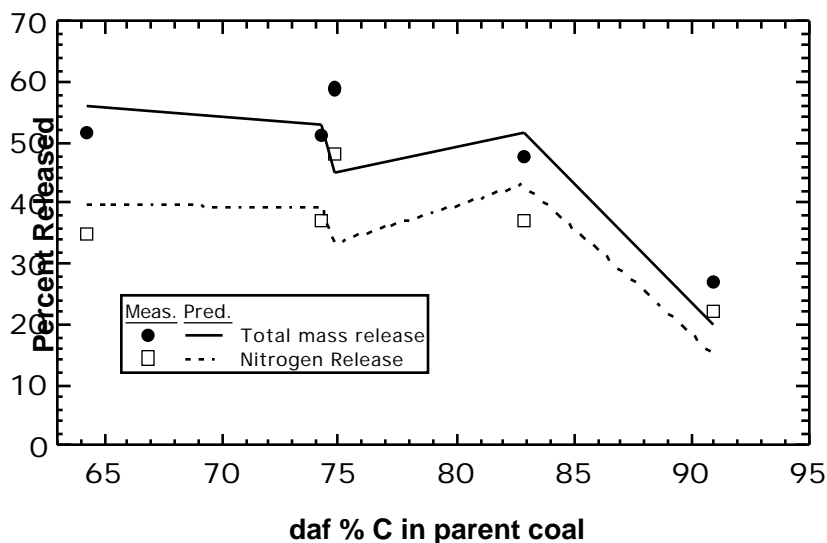


Figure 7.16. Comparison of predicted (lines) and measured (symbols) total mass and nitrogen release for drop tube pyrolysis experiments performed by Hambly at 1080 K (282 ms residence time).¹¹ Predictions made using measured parent coal ¹³C NMR structural parameters reported by Hambly.¹¹

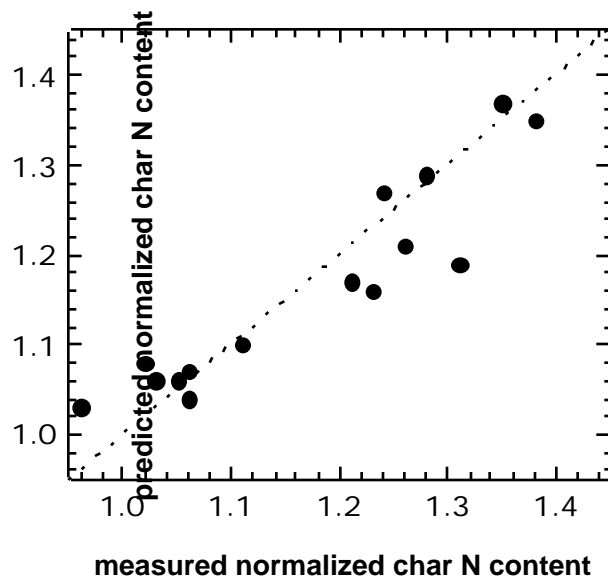


Figure 7.17. Parity plot of predicted and measured char nitrogen content normalized to the parent coal nitrogen content for drop tube pyrolysis experiments performed by Hambly at 820 K, 1080 K, and 1220 K.¹¹ Predictions made using measured parent coal ¹³C NMR structural parameters reported by Hambly.¹¹

for the data in Figure 7.19 at 2100 K were 3% higher and 5% lower than measured values for the lignite and bituminous coals, respectively. Figure 7.20 shows very long residence time nitrogen release predictions for a bituminous coal pyrolyzed at 2100 K and 1750 K, for 3 minutes and 1.5 hours, respectively. These predictions are roughly consistent with data from Pohl and Sarofim⁷ which show that a bituminous coal heated in a crucible for 20 minutes at 2100 K released *all* of the coal nitrogen, while the same coal heated for an unspecified time (between 20 minutes and 12 hours) at 1750 K released 90% of the coal nitrogen.

At higher heating rates, more typical of combustion conditions, the free radical mechanism performs reasonably well, and the nitrogen release predictions are at least as good as the mass release

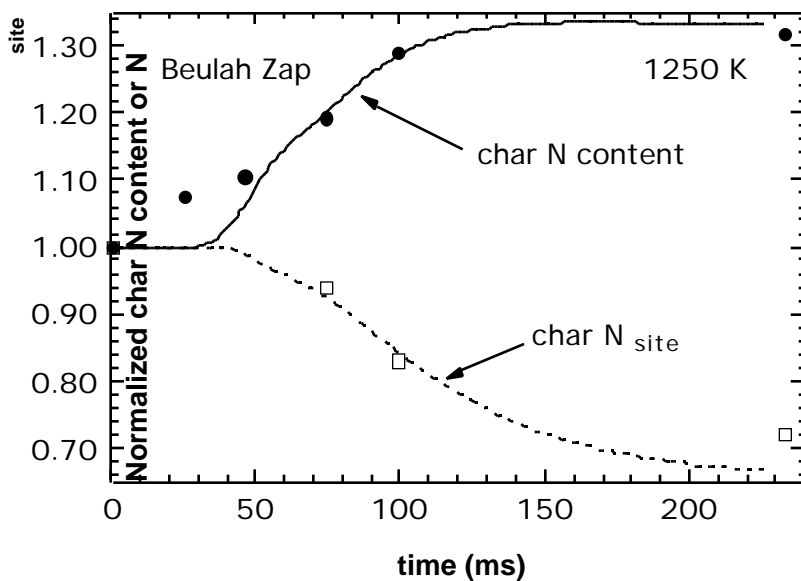
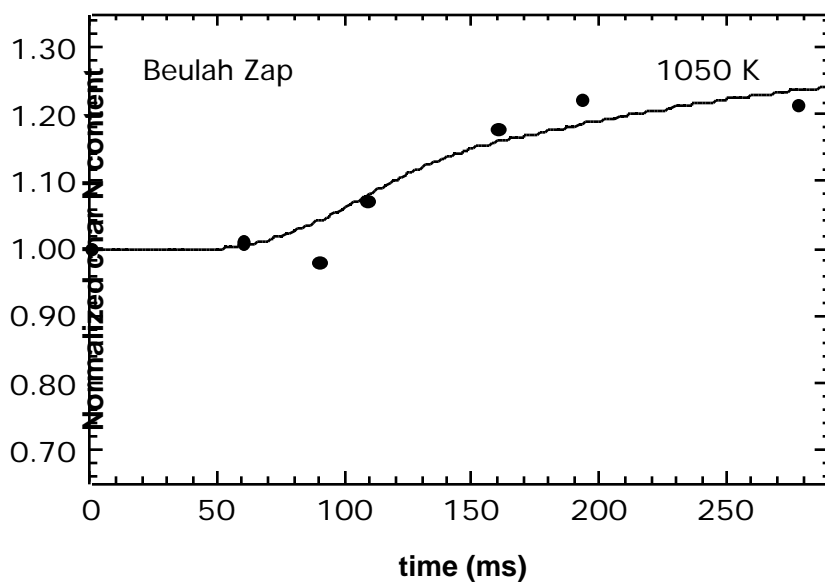


Figure 7.18. Comparison of predicted and measured char nitrogen content and char N_{site} value for a North Dakota lignite pyrolyzed in a drop tube reactor with 1050 K (upper graph) and 1250 K (lower graph) maximum gas temperatures at Sandia.⁵ Nitrogen values are normalized to parent coal nitrogen values. Predictions made using measured parent coal ^{13}C NMR structural parameters.

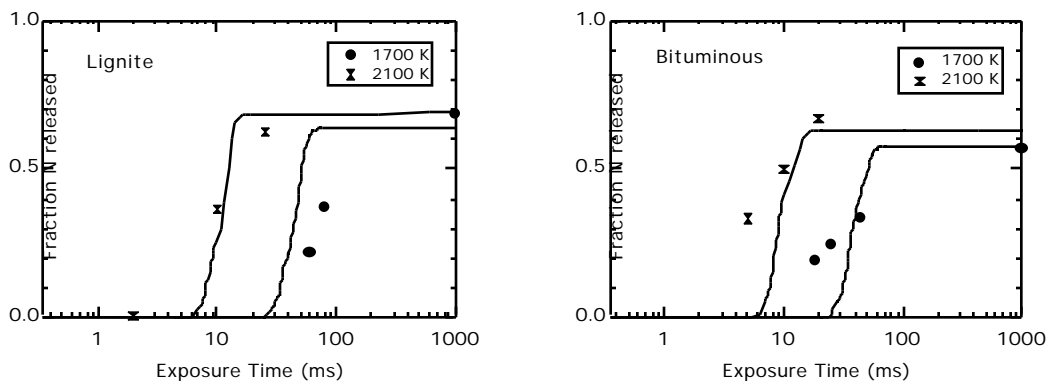


Figure 7.19. Comparisons of predicted and measured nitrogen released as a fraction of parent coal nitrogen for a lignite and a bituminous coal pyrolyzed in a drop tube or fast flow furnace. Measured data reported by Pohl and Sarofim.⁷ The chemical structures were approximated to be those of Beulah Zap lignite and Pittsburgh #8 for the lignite and bituminous coals respectively (structural data from Fletcher and Hardesty)⁵. Assumed particle temperature profiles are only rough approximations corresponding to the reported maximum gas temperatures.

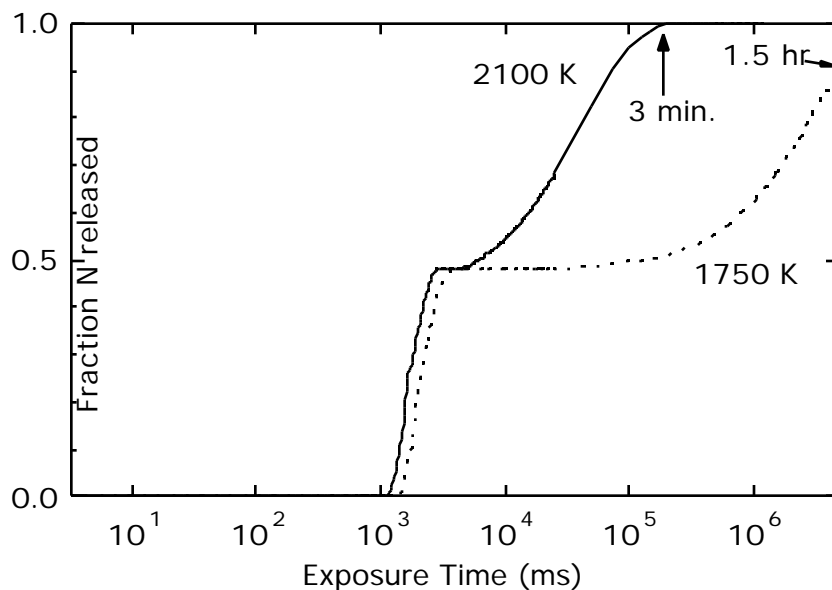


Figure 7.20. Predicted nitrogen released as a fraction of parent coal nitrogen for a bituminous coal pyrolyzed in a crucible at 2100 K and 1750 K for very long residence times. The chemical structure was approximated to be that of Pittsburgh #8 (structural data from Fletcher and Hardesty)⁵. Particles were assumed to reach the maximum temperature within 5 seconds.

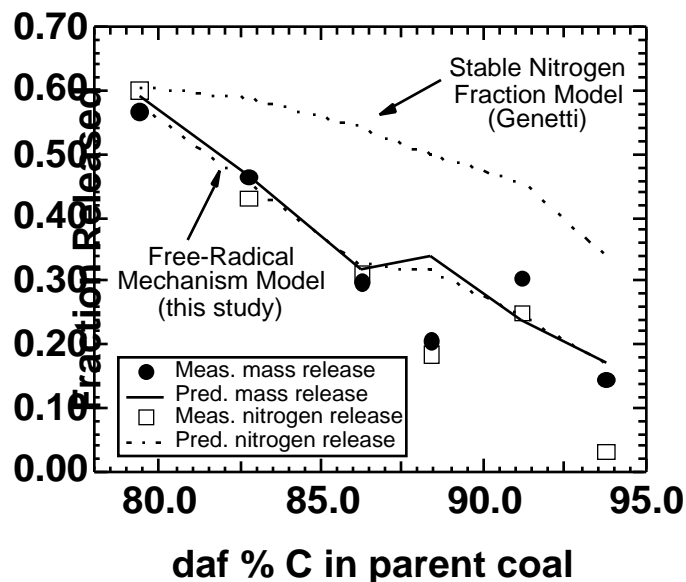
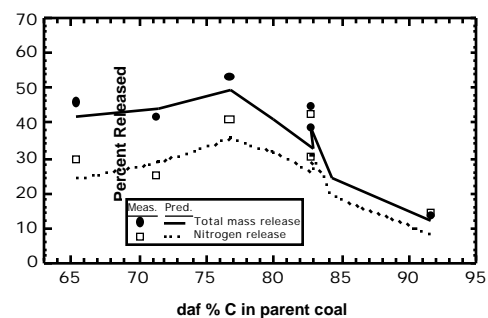
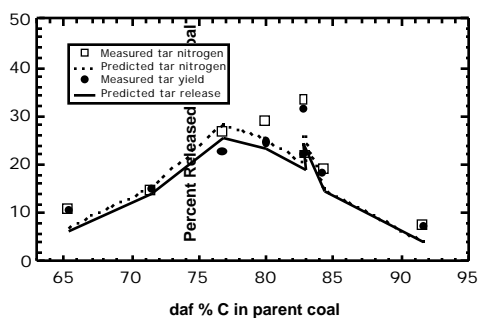


Figure 7.21. Comparison of predicted mass and nitrogen release values with measured mass and nitrogen release values reported by Genetti⁹ for flat flame reactor pyrolysis experiments at 1650 K and 78 ms residence time. Also shown are nitrogen release values predicted using the stable nitrogen fraction model of Genetti.⁹ Predictions made using measured parent coal ¹³C NMR structural parameters reported by Genetti.⁹

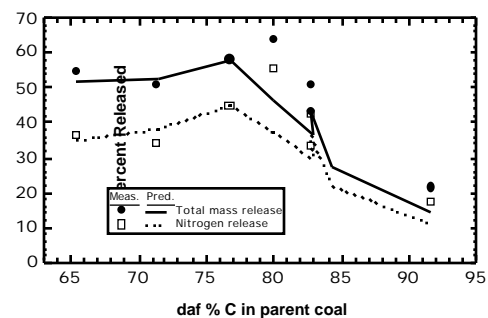
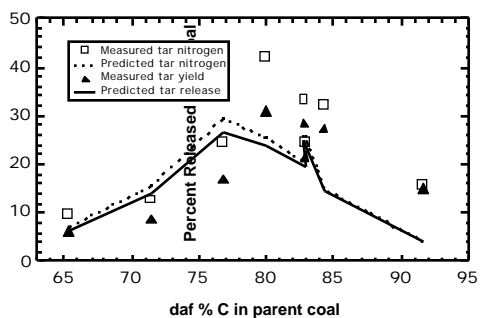
predictions for all coals except the coals with 92% and 94% carbon, where the nitrogen release appears to be retarded by some factor not taken into account by the free-radical mechanism.

The nitrogen release model was also used to predict the partitioning of nitrogen between char, tar, and light gas for each of the pyrolysis tests performed in this study. CPD predictions of tar, tar nitrogen, mass release, and nitrogen release (as a percentage of daf coal values) are compared to measured values in Figure 7.22. Trends with rank are fairly well predicted for both tar release and total mass release. The discrepancy between the predicted and measured nitrogen release is about the same as the discrepancy between the predicted and measured mass release in almost every case. Because primary tars undergo secondary reactions in this drop tube, measured tar yields are somewhat lower than the primary tar actually released. The model does not account for these secondary

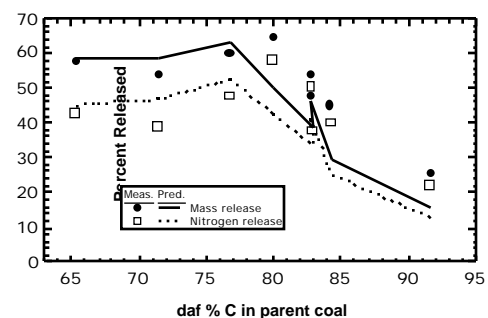
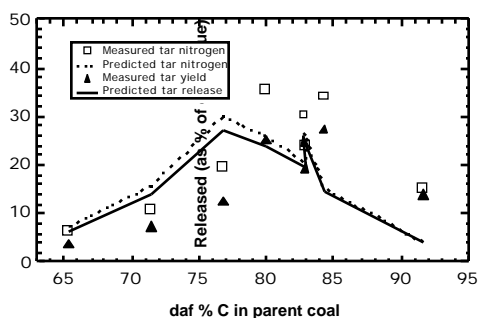
900 K



1000 K



1100 K



1650 K

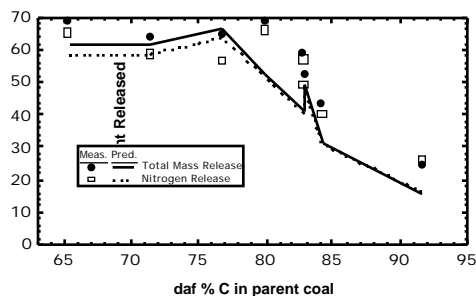


Figure 7.22. Comparison of predicted and measured tar and tar nitrogen yields and predicted and measured total mass and nitrogen release for drop tube and flat flame reactor pyrolysis experiments. Predictions made using measured ^{13}C NMR structural parameters.

reactions. Measured tar yields are at a maximum at the 900 or 1000 K condition for most coals. At 1000 K, tar release is predicted fairly well from the Yallourn and South Banko and Taiheiyo coals, but under-predicted from the bituminous coals. In fact, this under-prediction of tar release accounts for the most of the difference between measured and predicted mass release in the majority of cases. Similarly, total mass release is under-predicted at the 1650 K condition for the five highest rank (highest %C) coals. This result was surprising since the CPD model agrees with data from many other experiments.^{9, 27, 81}

One possible cause for this disagreement is that the 1250 K drop tube and 1650 K flat flame reactor tests were performed at pyrolysis conditions more severe than any used to generate data to which the CPD model parameters were originally fit. Another possible cause for this disagreement is that the activation energies for bridge breaking and side chain release may be coal dependent. Currently, the CPD model assumes that the rate coefficients are independent of coal type; future research may use these data to explore activation energies that are functions of the bridge mass.

Predictions were also made using a correlation developed by Genetti et al. for estimating the ^{13}C NMR chemical structural parameters used as input to the CPD model based only upon the elemental composition and ASTM volatile matter content of the parent coal.⁸⁵ In Figure 7.23, these predictions are compared to measured values for the tests performed at the 1100 K and 1650 K conditions. The trend with rank is again very nicely predicted by the CPD model. Except for over-prediction of the tar yields of the low rank coals, the predictions made using the correlation (which predict higher tar yields) agree slightly better with the data than the predictions made using the actual NMR values. This may be due to the fact that the measured fraction of intact bridges in the parent coal (p_0) is significantly higher in these coals than in coals of comparable rank used in the development of the CPD model. This possibility was suggested by Genetti, who left coals with unusually high p_0 out of his ^{13}C NMR parameter correlation so that the correlation would

not predict unusually high p_0 values which, in turn, would give abnormally low CPD tar predictions.⁹

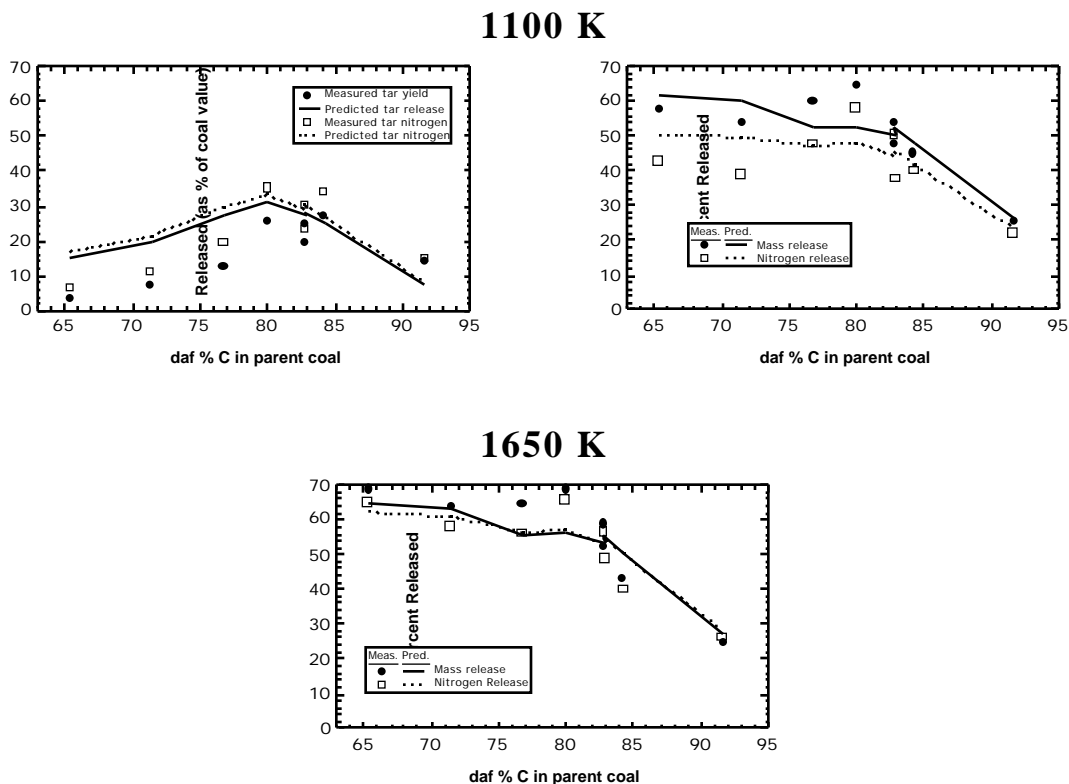


Figure 7.23. Comparison of predicted and measured tar and tar nitrogen yields and predicted and measured total mass and nitrogen release for 1100 K drop tube and 1650 K flat flame reactor pyrolysis experiments. Predictions made **using correlation of Genetti et al.**⁸⁵ to estimate parent coal structural parameters.

Another measure of the performance of a nitrogen release model is the ability to predict char nitrogen content during devolatilization. For the coals and conditions of this study, generally good agreement was observed between measured and predicted daf nitrogen contents (see Figure 7.24). In Figure 7.24, char nitrogen mass fractions have been normalized to the parent coal value to better show trends with rank. Note that the nitrogen model correctly describes the trend with rank of the nitrogen content, generally

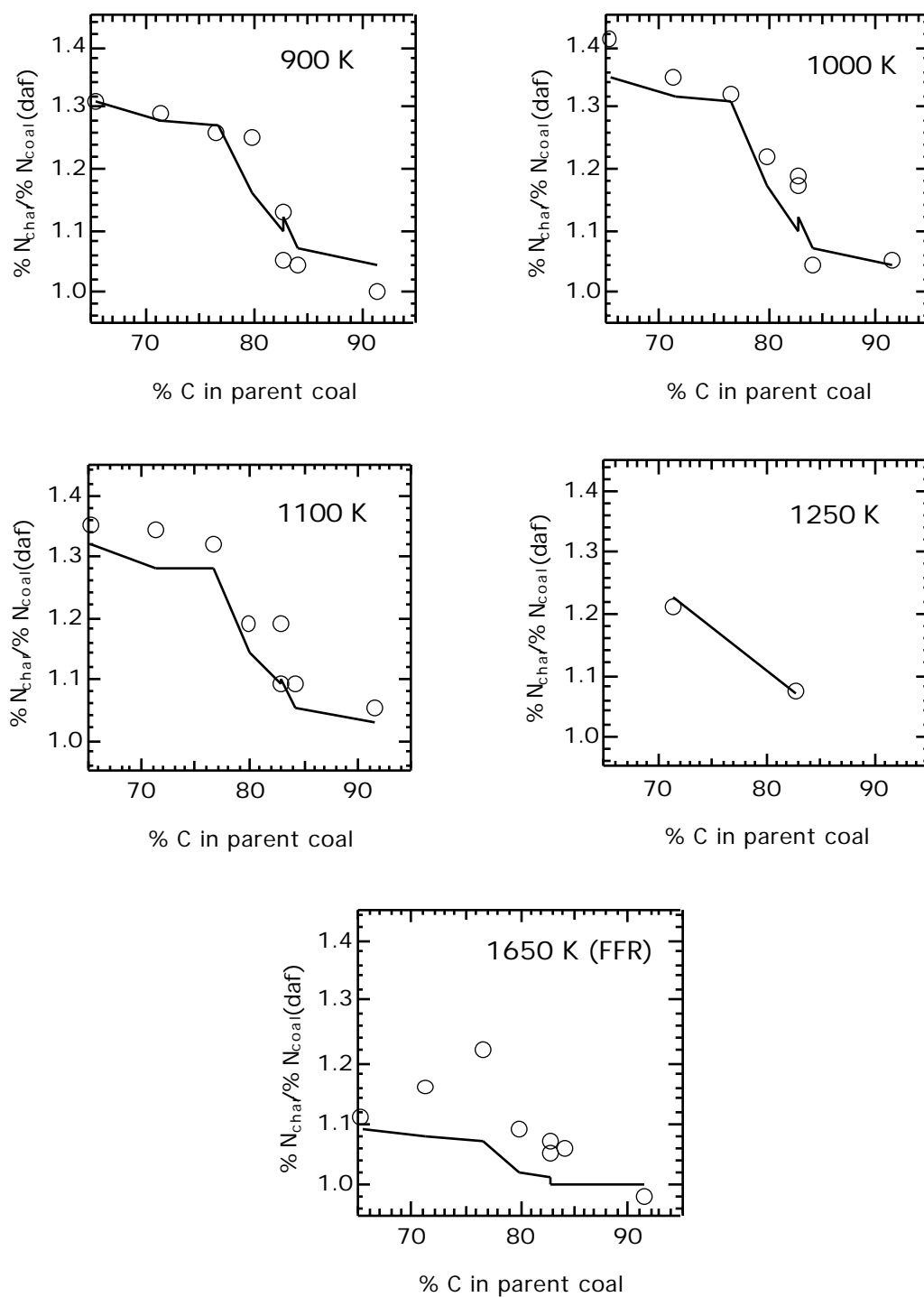


Figure 7.24. Predicted (lines) and measured (symbols) values of char nitrogen content normalized to the parent coal nitrogen content for drop tube and flat flame reactor pyrolysis experiments. Carbon content is used as an indicator of rank.

predicting nitrogen contents within experimental error (about $\pm 7\%$ relative) for every coal. However it appears that nitrogen contents for chars produced in the flat flame reactor are under-predicted in almost every case. One possible explanation for this is that the light gas nitrogen release activation energy assumed in this study is too high. Since the activation energy was regressed by matching the total nitrogen release in the flat flame reactor data taken at Sandia⁵, it is possible that CPD predictions of tar release at these conditions (i.e. 10^5 K/s heating rate) are too low. This would be consistent with the under-prediction of total mass release from 7 of 8 coals pyrolyzed in the flat flame reactor of this study, where conditions were even more severe than in the Sandia flat flame reactor. Under-prediction of tar release would in turn require overestimation of the activation energy in order to match measured total nitrogen release values.

8. Summary and Conclusions

The objective of this research was to develop a model that relates nitrogen release from coal char during devolatilization to the changes in the chemical structural features of the char and tar. A secondary objective of this work was to compare the changes occurring in the chemical structure of tar to those occurring in the char at different degrees of pyrolysis severity and establish the effect of these changes on nitrogen release. These objectives were successfully reached through the following accomplishments:

- Thirty-four pyrolysis tests were completed, spanning two different high heating rates, 5 different gas temperatures, and 8 different parent coals (from brown coal to low volatile bituminous) from around the world. The nitrogen split between tar and char was quantified for each test.
- ^{13}C NMR and elemental analyses of a selected subset of samples from these pyrolysis tests provided chemical structural data for many new coals, chars, and tars with known particle temperature histories.
- The first ever global mechanism for light gas nitrogen release during devolatilization was developed, and a corresponding rate expression was derived. The rate equation predicts light gas nitrogen variations with time, temperature, and coal rank using only three coal-independent rate constants, the transient particle temperature history, and the transient char cluster molecular weight.
- The light gas nitrogen release rate equation was incorporated into a complete nitrogen release model which was evaluated using data from a wide range of heating rate, temperature, time, and coal type. Data used for evaluation included

both chemical structural data as well as data describing nitrogen distribution among tar, char, and light gas.

Pyrolysis Tests

Trends with maximum gas temperature between 900 and 1650 K in measured tar yields and total volatiles yields were distinctly different for lignites, bituminous coals, and medium or low volatile bituminous coals. The higher the parent coal rank, the lower the temperature at which the maximum total volatiles yields was reached. In contrast, measured tar yields showed just the opposite trend, requiring increasingly high temperatures to obtain the maximum tar yield for increasing coal rank.

Char and Tar Chemical Structure

These data represent the first time matched sets of chars and tars from both lignite and bituminous coals pyrolyzed at increasingly severe conditions have been analyzed by solid-state ^{13}C NMR. The data confirm much of what has been reported by previous investigators about the structural progression of coal chars during pyrolysis. Soot produced from a bituminous coal at 1650 K had surprisingly few aromatic carbons per cluster (21), consistent with the mechanism of Badger for soot formation.⁵⁹ Evidence of three types of structural changes were seen in both chars and tars during rapid pyrolysis. First, tar is released, and the primary tar and char lose aliphatic material as pyrolysis severity increases. This is evidenced in both the chars and the tars by the decrease in number and mass of side chains, while the number of bridges and loops remains nearly constant. If the particle temperature exceeds about 1200 K, a second change occurs in most of the chars and tars as ring opening reactions cause the formation of what appears to be carbonyl carbon at the expense of aromatic carbon. A third change, cluster coalescence, is sometimes also seen at particle temperatures above 1200 K. Cluster coalescence is evidenced by a significant increase in the number of aliphatic and aromatic carbons per

cluster and the number of bridges and loops per cluster as the tar and char clusters become both larger and more interconnected. Under certain conditions, ring opening reactions occurred without causing cluster coalescence. In contrast, every tar and char sample showing evidence of cluster coalescence also appeared to have undergone ring opening reactions, suggesting that ring opening reactions may be prerequisite to cluster coalescence. At the 1250 K condition, tar and char from a bituminous coal showed evidence of both ring opening and cluster coalescence reactions, while only the char (not the tar) from a lignite coal underwent these changes. Neither ring opening nor cluster coalescence reactions appear to accelerate nitrogen release via ring rupture.

The use of *measured* nitrogen mass per aromatic mass (N_{site}) to track light gas nitrogen release was shown to be valid (at high heating rates) only for temperatures below 1200 K. However, it appears that aromatic carbon converted to carbonyl or aliphatic carbon by ring opening reactions can still be considered stable at temperatures above 1200 K. Thus N_{site} may be used to model light gas nitrogen release even at these high temperatures. In fact, based on the performance of the nitrogen release model, the use of N_{site} to model light gas nitrogen release from coal during devolatilization appears to be useful even at temperatures as high as 2100 K and for heating rates ranging from 0.5 to 10^5 K/s.

Published data were used to show that char nitrogen in five membered aromatic rings may be converted to light gas nitrogen at the same rate as nitrogen in six membered aromatic rings.

Data from this project showed that tars retained more aliphatic material and nitrogen than the corresponding chars at each temperature below 1200 K. Above 1200 K, tars seemed to undergo a shift in mechanism, losing large fractions of aliphatic matter and nitrogen simultaneously, while the corresponding chars did not.

Nitrogen Release Model

A nitrogen model using a three-step free-radical global mechanism to model light gas nitrogen release was developed. This nitrogen model requires only a network devolatilization model, such as the CPD model and coal-specific chemical structural input data to adequately predict the nitrogen distribution among pyrolysis products. Nitrogen content, tar and light gas nitrogen yields, and char chemical structure are all well described by the model for pyrolysis of coals of a wide range of rank at a variety of pyrolysis conditions. The model was found to perform satisfactorily for heating rates ranging from 0.5 K/s to 10^5 K/s, for temperatures ranging from 820 K to 2100 K, and for residence times ranging from 16 ms to more than 3 minutes. The model is the first to describe the rank dependence of nitrogen release as light gas without the use of correlations. Perhaps more importantly, the free-radical mechanism model offers reasonable explanations for the observed release of ring nitrogen at unusually low temperatures and the inherent stability of a large portion of the char nitrogen during pyrolysis. The free-radical mechanism is consistent with observations that nitrile nitrogen formation occurs in tars but not in chars.

The method by which the free-radical mechanism model was developed is significant. The database of char chemical structural data was analyzed to identify relationships between light gas nitrogen release and char chemical structure. A simplified global mechanism was then postulated, and a corresponding rate expression was derived and tested for consistency with these relationships. This was repeated until a rate expression consistent with trends in the measured chemical structural data was identified. Because the free-radical mechanism model is based on char chemical structure, it is very robust, accurately describing nitrogen release characteristics even for conditions far different from those used in the model development. This is very important since the anticipated application of such a model is to predict nitrogen release at conditions typical of coal combustion conditions, where coal particles may experience temperatures higher than 2000 K^{7, 66} and heating rates higher than 10^6 K/s.⁶⁶

9. Recommendations

Nitrogen release from coal during devolatilization has been an area of interest for over 20 years. In the course of an on-going research project such as this it is useful to reassess the situation every so often to determine whether changes should be made in the research methodology to better meet project goals or whether new goals should be developed. The completion of a dissertation or thesis, a time when new insights often are revealed, is an especially good time to do so. There are two types of recommendations that could be valuable to future researchers. The first type of recommendation involves changes that might improve the precision and usefulness of pyrolysis data. The second type of recommendation relates to ideas for future work in this area.

Improving Precision and Usefulness of Pyrolysis Data

The following steps are recommended in order to reduce errors in measurements taken during pyrolysis testing and sample characterization:

- The use of FTIR to perform gas phase analysis will better close the nitrogen balance and has already begun to be implemented here at BYU by Mr. Haifeng Zhang.³¹ This will be a valuable tool for analysis of nitrogen release during coal pyrolysis tests.
- The continued use of a sample splitter to split heterogeneous samples such as coal and char is recommended. The work presented in this dissertation is the first to have done so in a coal pyrolysis study here at BYU. The use of proper sample

splitting techniques will help minimize sample variability errors, increasing analysis accuracy and repeatability.

- The continued pulverization of samples to a fine powder (using a small mill) before performing elemental determinations. This is especially critical for char samples, which often contain particles with orders of magnitude difference in bulk density (i.e. a swollen char particle as compared to an ash particle).
- A re-design of the BYU drop tube injection probe, such that the flow straightener ends at least several inches from the point of injection of the particles. Also the injection probe inside diameter should be reduced in order to inject particles in a more precise and repeatable manner. Finally, the injection probe cooling should be re-designed, with an emphasis on removing restriction to flow, thus providing better cooling, as the present cooling water flow capacity is insufficient. Flow might also be improved by increasing the line pressure at the cooling water inlet.
- Several different primary flows should be tested at each condition used in the BYU drop tube reactor to try to minimize deviation from the centerline (and therefore severity of pyrolysis) before performing other tests. The severity of pyrolysis for char samples generated at each primary flow rate could be estimated as being proportional to the daf char carbon content or the total mass release. This would require a little extra work, but might be worthwhile in terms of determining accurate particle temperature histories. Gas phase thermocouple measurements with a quick response time might also be used to test the extent of turbulence occurring for different primary flow rates at each condition used.

Ideas for Future Work

The following ideas are recommended to further the understanding of pyrolytic nitrogen release and the corresponding chemical mechanisms or to improve modeling of coal devolatilization:

- Detailed pyrolysis tests should be conducted using high temperatures and long residence times to better estimate the slow nitrogen release kinetic parameters.
- A model compound study should be performed in which sets of nitrogen containing model compounds are used having the same aromatic structure but differing in that some contain aliphatic attachments and others do not. One example of this would be to pyrolyze pyridine and compare it to pyrolysis some form of poly(vinylpyridine). HCN and NH₃ could be analyzed in the gas phase and any tar collected for elemental analysis to close the nitrogen balance. This would help show how the presence of aliphatic material affects nitrogen release and provide further evidence for or against the free-radical mechanism presented in this work.
- A model compound study is recommended in which sets of nitrogen containing model compounds are used containing aliphatic attachments and having similar aromatic structures, but differing in that some contain pyridinic nitrogen and others contain pyrrolic nitrogen. Some model compounds might form char while other model compounds would form only tar and light gas. Similar gas and solid phase product characterization could be performed as described above. This would better establish the effect of nitrogen functionality on nitrogen release from aromatic structures during pyrolysis.
- Semi-empirical or ab-initio calculations should be performed to see how the presence of a nearby aliphatic free-radical affects the shape of the molecular orbitals of a hypothetical char or tar cluster. This might provide further evidence for or against the free radical mechanism proposed here for light gas nitrogen release from aromatic rings.
- The CPD model should be modified to better imitate the trends with coal rank reported in this study for tar yield and total volatiles yield at severe pyrolysis conditions. This might be done by correlating the strength and reactivity of labile

bridges (and hence the rate coefficients for bridge breaking) with the aliphatic oxygen content of the parent coal.

- The radical mechanism for light gas nitrogen release should be validated for pyrolysis of fuels or materials other than coal.
- The nitrogen model presented here should be integrated into PCGC-3 or another comprehensive combustion code to evaluate the effect of the new model on NO_x predictions at various conditions.

References

1. Bassilakis, B., Y. Zhao, P. R. Solomon and M. A. Serio, "Sulfur and Nitrogen Evolution in the Argonne Coals: Experiment and Modeling", *Energy and Fuels*, **7**, 710-720 (1993).
2. Niksa, S., Predicting the Evolution of Fuel Nitrogen from Various Coals; The Combustion Institute, Pittsburgh, PA, pp 537 (1994).
3. Genetti, D. and T. Fletcher, "Modeling Nitrogen Release during Devolatilization on the Basis of Chemical Structure of Coal", *Energy and Fuels (in press)*, (1999).
4. Solum, M. S., R. J. Pugmire and D. M. Grant, "¹³C Solid State NMR of the Argonne Premium Coals", *Energy and Fuels*, **3**, 187 (1989).
5. Fletcher, T. H. and D. R. Hardesty "Milestone Report for DOE's Pittsburgh Energy Technology Center," contract FWP 0709, Sandia Report No. SAND92-8209, available NTIS (1992).
6. Cooper, C. D. and F. C. Alley, *Air Pollution Control, A Design Approach*; Second ed., Waveland Press, Inc., Prospect Heights, Illinois, (1994).
7. Pohl, J. H. and A. F. Sarofim, Devolatilization and Oxidation of Coal Nitrogen; The Combustion Institute, Pittsburgh, PA, pp 491 (1977).
8. Boardman, R. and D. L. Smoot, *Pollutant Formation and Control*, In Fundamentals of Coal Combustion for Clean and Efficient Use, D. L. Smoot, Ed., Elsevier, Amsterdam, Vol. 20, pp 433-506 (1993).
9. Genetti, D. B., An Advanced Model of Coal Devolatilization Based on Chemical Structure, Chemical Engineering Department, Brigham Young University (1999).
10. Watt, M., The Chemical Structure of Coal During Devolatilization, Masters Thesis, Chemical Engineering, Brigham Young University (1996).
11. Hambly, E. M., The Chemical Structure of Coal Tar and Char During Devolatilization, Masters Thesis, Chemical Engineering Department, Brigham Young University (1998).
12. Hambly, E. M., T. H. Fletcher, M. Solum and R. J. Pugmire, Unpublished NMR chemical structural analysis of 820 K chars produced by Hambly, 1998.
13. Anthony, D. B., J. B. Howard, H. C. Hottel and H. P. Meissner, Rapid Devolatilization of Pulverized Coal; The Combustion Institute, Pittsburgh, PA, pp 1303-1317 (1974).

14. Serio, M. A., D. G. Hamblen, J. R. Markham and P. R. Solomon, "Kinetics of Volatile Product Evolution in Coal Pyrolysis: Experiment and Theory", *Energy and Fuels*, **1**, 138-152 (1987).
15. Solomon, P. R. and T. H. Fletcher, Impact of Coal Pyrolysis on Combustion; The Combustion Institute, Pittsburgh, PA, pp 463 (1994).
16. Solomon, P. R., *Coal Structure and Thermal Decomposition*, In New Approaches in Coal Chemistry, B. D. Blaustein, B. C. Bockrath and S. Friedman, Ed., American Chemical Society, Washington, D.C., Vol. 169, pp 61-71 (1981).
17. van Krevelen, D. W., *Coal: Typology, Chemistry, Physics, and Constitution*, Elsevier, New York, 514 (1981).
18. Spiro, C. L. and P. G. Kosky, "Space-Filling Models for Coal 2: Extensions to Coals of Various Types", *Fuel*, **61**, 1080-1084 (1982).
19. Smith, K. L., L. D. Smoot, T. H. Fletcher and R. J. Pugmire, *The Structure and Reaction Processes of Coal*, Plenum, New York, (1994).
20. Solomon, P. R., D. G. Hamblen, R. M. Carangelo, M. A. Serio and G. V. Deshpande, "General Model of Coal Devolatilization", *Energy and Fuels*, **2**, 405-422 (1988).
21. Given, P. H., A. Marzec, W. A. Barton, L. J. Lynch and B. C. Gerstein, "The Concept of a Mobile or Molecular Phase within the Macromolecular Network of Coals: A Debate", *Fuel*, **65**, 155-163 (1986).
22. Winans, R., *Coal Science Meeting*, Essen, Germany, (1997).
23. Miknis, F. P., T. F. Turner, L. W. Ennen and D. A. Netzel, "N.M.R. Characterization of Coal Pyrolysis Products", *Fuel*, **67**, 1568-1577 (1988).
24. Pugmire, R. J. and M. S. Solum, "NMR Analysis of Coal and Char Structure", *ACERC Annual Report*, **2**, 28 (1992).
25. Pugmire, R. J., M. S. Solum, D. M. Grant, S. Critchfield and T. H. Fletcher, "Structural Evolution of Matched Tar/Char Pairs in Rapid Pyrolysis Experiments", *Fuel*, **70**, 414 (1991).
26. Gavalas, G. R., *Coal Pyrolysis*, Elsevier, Amsterdam, 168 (1982).
27. Fletcher, T. H., A. R. Kerstein, R. J. Pugmire and D. M. Grant, "Chemical Percolation Model for Devolatilization. 2. Temperature and Heating Rate Effects on Product Yields", *Energy and Fuels*, **4**, 54-60 (1990).
28. Solomon, P. R., T. H. Fletcher and R. J. Pugmire, "Progress in Coal Pyrolysis", *Fuel*, **72**, 587-597 (1993).
29. Solomon, P. R. and M. B. Colket, "Evolution of Fuel Nitrogen in Coal Devolatilization", *Fuel*, **57**, 749 (1978).

30. Freihaut, J. D., W. M. Proscia and D. J. Seery, "Chemical Characteristics of Tars Produced in a Novel Low-Severity, Entrained-Flow Reactor", *Energy and Fuels*, **3**, 692-703 (1989).
31. Zhang, H., Nitrogen Transformations During Secondary Pyrolysis, (in progress), Chemical Engineering, Brigham Young University (2000).
32. Gibbins, J. and R. Kandiyoti, "Experimental Study of Coal Pyrolysis and Hydrolysis at Elevated Pressures Using a Variable Heating Rate Wire-Mesh Apparatus", *Energy & Fuels*, **3**, 621-626 (1989).
33. Solomon, P. R., M. A. Serio, R. M. Carangelo and R. Bassilakis, "Analysis of the Argonne Premium Coal Samples by Thermogravimetric Fourier Transform Infrared Analysis Spectroscopy", *Energy & Fuels*, **4**, 319-333 (1990).
34. Solomon, P. R., M. A. Serio, G. V. Despande and E. Kroo, "Cross-Linking Reactions during Coal Conversion", *Energy and Fuels*, **4**, 42-54 (1990).
35. Li, C.-Z., A. N. Buckley and P. F. Nelson, "Effects of Temperature and Molecular Mass on the Nitrogen Functionality of Tars Produced Under High Heating Rate Conditions", *Fuel*, **77**, 157-164 (1998).
36. Bartle, K. D., D. L. Perry and S. Wallace, "The Functionality of Nitrogen in Coal and Derived Liquids: An XPS Study", *Fuel Processing Technology*, **15**, 351 (1987).
37. Kelemen, S. R., M. L. Gorbaty and P. J. Kwiatek, "Quantification of Nitrogen forms in Argonne Premium Coals", *Energy & Fuels*, **8**, 896 (1994).
38. Davidson, R. M. "Nitrogen in Coal," IEA Coal Research, IEA PER/08 (1994).
39. Chen, J. C. "Effect of Secondary Reactions on Product Distribution and Nitrogen Evolution from Rapid Coal Pyrolysis," Stanford University, HTGL Report No. T-280 (1991).
40. Chen, J. C. and S. Niksa, Suppressed Nitrogen Evolution from Coal-Derived Soot and Low-Volatility Coal Chars; The Combustion Institute, Pittsburgh, PA, pp 1269 (1992).
41. Ma, J., Soot Formation and Secondary Reactions during Coal Pyrolysis, Ph. D. Dissertation, Chemical Engineering Department, Brigham Young University (1996).
42. Nelson, P. F., M. D. Kelly and M. J. Wornat, "Conversion of Fuel Nitrogen in Coal Volatiles to NOx Precursors Under Rapid Heating Conditions", *Fuel*, **70**, 403 (1991).
43. Kelemen, S. R., M. L. Gorbaty and P. J. Kwiatek, "Nitrogen Transformations in Coal During Pyrolysis", *Energy and Fuels*, **12**, 159-173 (1998).
44. Burchill, P. and L. S. Welch, "Variation of Nitrogen Content and Functionality with Rank for Some UK bituminous Coals", *Fuel*, **68**, 100-104 (1989).
45. Solum, M. S., R. J. Pugmire, D. M. Grant, S. R. Kelemen, M. L. Gorbaty and R. A. Wind, "15-N CPMAS NMR of the Argonne Premium Coals", *Energy and Fuels*, **11**, 491-494 (1997).

46. Pels, J. R., R. Kapteijn, J. A. Moulijn, Q. Zhu and K. M. Thomas, "Evolution of Nitrogen Functionalities in Carbonaceous Materials During Pyrolysis", *Carbon*, **33**, 1641-1653 (1995).
47. Stanczyk, K., R. Dziembaj, Z. Ptowarska and S. Witkowski, "Transformation of Nitrogen Structures in Carbonization of Model Compounds Determined by XPS", *Carbon*, **33**, 1383-1392 (1995).
48. Nelson, P. F., A. N. Buckley and M. D. Kelly, "Functional Forms of Nitrogen in Coals and the Release of Coal Nitrogen as NO_x Precursors (HCN and NH₃)", *24th Symposium (International) on Combustion*, **24**, 1259 (1992).
49. Hamalainen, J. P., M. J. Aho and J. L. Tummavuori, "Formation of Nitrogen Oxides From Fuel-N through HCN and NH₃: A Model-Compound Study", *Fuel*, **73**, 1894-1898 (1994).
50. Kambara, S., T. Takarada, Y. Yamamoto and K. Kato, "Relation Between Functional Forms of Coal Nitrogen and Formation of NO_x Precursors During Rapid Pyrolysis", *Energy & Fuels*, **7**, 1013 (1993).
51. Mackie, J. C., M. B. Colket, P. F. Nelson and M. Esler, "Shock Tube Pyrolysis of Pyrrole and Kinetic Modeling", *International Journal of Chemical Kinetics*, **23**, 733-760 (1991).
52. Mackie, J. C., M. B. Colket and P. F. Nelson, "Shock Tube Pyrolysis of Pyridine", *Journal of Physical Chemistry*, **94**, 4099-4106 (1990).
53. Freihaut, J. D., W. M. Proscia and J. C. Mackie, "Chemical and Thermochemical Properties of Heavy Molecular Weight Hydrocarbons Evolved During Rapid Heating of Coal of Varying Rank Characteristics", *Combustion Science and Technology*, **93**, 323 (1993).
54. Freihaut, J. D., W. Proscia, N. Knight, A. Vranos, H. Kollick and K. Wicks "Combustion Properties of Micronized Coal for High Intensity Combustion Applications," Final Report for DOE/PETC Contract DE-AC22-85PC80263 (1989).
55. Blair, D. W., J. O. L. Wendt and W. Bartok, Evolution of Nitrogen and Other Species During Controlled Pyrolysis of Coal; The Combustion Institute, Pittsburgh, PA, pp 475 (1977).
56. Chen, J. C. and S. Niksa, "Coal Devolatilization During Rapid Transient Heating. 1. Primary Devolatilization", *Energy & Fuels*, **6**, 254-264 (1992).
57. Axworthy, A. E., V. H. Dayan and G. B. Martin, "Reactions of Fuel-Nitrogen Compounds Under Conditions of Inert Pyrolysis", *Fuel*, **57**, 29-35 (1978).
58. Bruinsma, O. S. L., P. J. J. Tromp, H. J. J. de Sauvage Nolting and J. A. Moulijn, "Gas Phase Pyrolysis of Coal-Related Aromatic Compounds in a Coiled Tube Flow Reactor; 2. Heterocyclic Compounds, Their Benzo and Dibenzo Derivatives", *Fuel*, **67**, 334-340 (1988).
59. Badger, G. M., J. K. Donnelly and T. M. Spotswood, "The Formation of Aromatic Hydrocarbons at High Temperatures: XXII. The Pyrolysis of Phenanthrene", *Australian Journal of Chemistry*, **17**, 1138-1146 (1964).

60. Li, C.-Z., P. F. Nelson, E. B. Ledesma and J. C. Mackie, "An Experimental Study of the Release of Nitrogen From Coals Pyrolyzed in Fluidized-Bed Reactors", *Twenty-Sixth Symposium (International) on Combustion/The Combustion Institute*, 3205-3211 (1996).
61. Cai, H. Y., A. J. Guell, D. R. Dugwell and R. Kandiyoti, "Heteroatom Distribution in Pyrolysis Products as a Function of Heating Rate and Pressure", *Fuel*, **72**, 321-327 (1993).
62. Wu, Z. and Y. Ohtsuka, "Nitrogen Distribution in a Fixed Bed Pyrolysis of Coals with Different Ranks: Formation and Source of N₂", *Energy and Fuels*, **11**, 447-482 (1997).
63. Baxter, L. L., R. E. Mitchell, T. H. Fletcher and R. H. Hurt, "Nitrogen Release During Coal Combustion", *Energy and Fuels*, **10**, (1996).
64. Wendt, J. O. L. and D. W. Pershing, "Physical Mechanisms Governing the Oxidation of Volatile Fuel Nitrogen in Pulverized Coal Flames", *Combustion Science and Technology*, **16**, 111 (1977).
65. Clarke, A. G., E. Hampartsoumian and R. Sipahutar, "Conversion of Fuel-bound Nitrogen to NO During Combustion of Pulverised Coals in a Drop Tube Reactor", *Journal of the Institute of Energy*, **66**, 79-83 (1993).
66. Smoot, L. D. and P. J. Smith, *Coal Combustion and Gasification*, Plenum Press, New York and London, 443 (1985).
67. Aho, M. J., J. P. Hamalainen and J. L. Tummavuori, "Importance of Solid Fuel Properties to Nitrogen Oxide Formation Through HCN and NH₃ in Small Particle Combustion", *Combustion and Flame*, **95**, 22-30 (1993).
68. Solomon, P. R., D. G. Hamblen, R. M. Carangelo and J. L. Krause, "Coal Thermal Decomposition in an Entrained Flow Reactor: Experiments and Theory", *Nineteenth Symposium (International) on Combustion*, 1139 (1982).
69. Wornat, M. J., A. F. Sarofim, J. P. Longwell and A. L. Lafleur, "Effect of Pyrolysis Conditions on the Composition of Nitrogen-Containing Polycyclic Aromatic Compounds from a Bituminous Coal", *Energy and Fuels*, **2**, 775-782 (1988).
70. Fletcher, T. H., M. S. Solum, D. M. Grant, S. Critchfield and R. J. Pugmire, Solid State ¹³C and ¹H NMR Studies of the Evolution of the Chemical Structure of Coal Char and Tar During Devolatilization; The Combustion Institute, Pittsburgh, PA, pp 1231 (1990).
71. Watt, M., T. H. Fletcher, S. Bai, M. S. Solum and R. J. Pugmire, "Chemical Structure of Coal Tar During Devolatilization", *Twenty-Sixth Symposium (International) on Combustion*, 3153- (1996).
72. Niksa, S., "FLASHCHAIN Theory for Rapid Coal Devolatilization Kinetics. 4. Predicting the Evolution of Fuel Nitrogen from Various Coals", *Energy and Fuels*, **9**, 467-478 (1995).

73. Monson, C. R. and G. K. Germane, "A High-Pressure Drop-Tube Facility for Coal Combustion Studies", *Energy and Fuels*, **7**, 928-936 (1993).
74. Pitard, F. F., *Pierre Gy's Sampling Theory and Sampling Practice, Heterogeneity, Sampling Correctness, and Statistical Process Control*; 2 ed., CRC Press, Boca Raton, 268-272 (1993).
75. Baxter, L. L. "The Release of Inorganic Material During Coal Combustion," Sandia National Labs, SAND95-8252 (1995).
76. Xu, W. and A. Tomita, "Effect of coal type on the flash pyrolysis of various coals", *Fuel*, **66**, 627-631 (1987).
77. Yeasmin, H., J. F. Mathews and S. Ouyang, "Rapid Devolatilization of Yallourn Brown Coal at High Pressures and Temperatures", *Fuel*, **78**, 11-24 (1999).
78. Wornat, M. J., A. F. Sarofim and J. P. Longwell, "Pyrolysis-Induced Changes in the Ring Number Composition of Polycyclic Aromatic Compounds From a High Volatile Bituminous Coal", *Twenty-Second Symposium (International) on Combustion/The Combustion Institute*, 135-143 (1988).
79. Solum, M. S., R. J. Pugmire, D. M. Grant, T. H. Fletcher and P. Solomon, "Solid State ¹³C NMR Studies of Coal Char Structure Evolution", *ACS Division of Fuel Chemistry Preprints*, **34**, 1337-1346 (1989).
80. Wornat, M. J., A. F. Sarofim and A. L. Lafleur, "The Pyrolysis of Anthracene as a Model Coal-Derived Aromatic Compound", *Twenty-Fourth Symposium (International) on Combustion/The Combustion Institute*, 955-963 (1992).
81. Fletcher, T. H., A. R. Kerstein, R. J. Pugmire and D. M. Grant, "A Chemical Percolation Model for Devolatilization: 3. Direct Use of 13-C NMR Data to Predict Effect of Coal Type", *Energy and Fuels*, **6**, 414 (1992).
82. Carey, F. A. and R. J. Sundberg, *Chapter 10, Aromatic Substitution*, In *Advanced Organic Chemistry, Part A: Structure and Mechanisms, 3rd edition*, Plenum Press, New York and London, pp 560, 579-585 (1990).
83. Carey, F. A. and R. J. Sundberg, *Chapter 12. Free-Radical Reactions*, In *Advanced Organic Chemistry, Part A: Structure and Mechanisms, 3rd edition*, Plenum Press, New York and London, pp 679-687 (1990).
84. Burnham, A. K. and R. L. Braun, "Global Kinetic Analysis of Complex Materials", *Energy and Fuels*, **13**, 1-22 (1999).
85. Genetti, D. B., T. H. Fletcher and R. J. Pugmire, "Predicting 13-C NMR Measurements of the Chemical Structure of Coal Based on Elemental Composition and Volatile Matter Content", *Energy and Fuels*, **13**, 60-68 (1999).
86. Freihaut, J. D., M. F. Zabielski and D. J. Seery, "A Parametric Investigation of Tar Release In Coal Devolatilization", *Nineteenth Symposium (International) on Combustion/The Combustion Institute*, 1159 (1983).

87. Nomura, M., R. J. Pugmire, T. H. Fletcher, S. Morooka and C. Ye "International Research Grant Final Report: Molecular Level Characterization of Carbonaceous Resources for Advanced Utilization Technologies," NEDO (Japan), (1999).
88. Ledesma, E. B., C.-Z. Li, P. F. Nelson and J. C. Mackie, "Release of HCN, NH₃, and HNCO from the Thermal Gas-Phase Cracking of Coal Pyrolysis Tars", *Energy and Fuels*, **12**, 536-541 (1998).
89. Incropera, F. P. and D. P. DeWitt, *Fundamentals of Heat and Mass Transfer*; 3 ed., John Wiley & Sons, New York, (1990).
90. Nomura, M., Elemental Determination for Pacific Rim Coals, 1997.
91. Hogg, R. V. and J. Ledolter, *Applied Statistics for Engineers and Physical Scientists*; 2nd ed., Maxwell Macmillan International, New York, 472 (1987).

Appendices

Appendix A: Temperature Correction

Measured centerline gas temperature profiles were corrected to account for differences between thermocouple bead temperatures and actual gas temperatures due to radiative heat transfer. In doing so, an energy balance was used as follows:

$$h(T_{gas} - T_{bead}) = \epsilon (T_{bead}^4 - T_{surr}^4) \quad (A.1)$$

where h is the convective heat transfer coefficient, ϵ is the thermocouple bead emissivity, σ is the Stefan-Boltzmann constant, T_{gas} is the gas temperature (K), T_{bead} is the bead temperature (K), and T_{surr} is the temperature of the surroundings (K). In Equation A.1 it was assumed that the emissivity of the bead was constant at 0.2 and that the surroundings temperature was equal to the wall temperature as given by the heater control thermocouple in the drop tube. The convective heat transfer coefficient was calculated from the Nusselt number (Nu_D) as follows:

$$h = \frac{k_g \overline{Nu}_D}{D_b} \quad (A-2)$$

where k_g is the thermal conductivity of the gas and D_b is the diameter of the thermocouple bead (which was about 200 μm). The Nusselt number was estimated using the following correlation from Incropera and DeWitt:⁸⁹

$$\overline{Nu}_D = 2 + \left(0.4\text{Re}_D^{1/2} + 0.06\text{Re}_D^{2/3}\right) \text{Pr}^{0.4} \frac{\mu}{\mu_s}^{1/4} \quad (A-3)$$

where Re_p is the Reynolds number based on the bead diameter, Pr is the Prandtl number, μ is the viscosity of the gas at the gas temperature, and μ_s is the viscosity of the gas at the bead temperature. For this correlation, all properties should be evaluated at the gas temperature except μ_s . This correlation is reportedly accurate to within +/- 30% for Re between 3.5 and 7.6×10^4 , for Pr between 0.71 and 380, and for μ/μ_s from 1.0 to 3.2.

Since the gas temperature was unknown, the bead temperature was assumed in evaluating the gas properties on the first iteration. Then the gas temperature calculated in the first iteration was used to evaluate gas properties in a second iteration. Gas properties were polynomial curve fits (third order in temperature) of data published by Incropera and DeWitt⁸⁹ for molecular nitrogen gas at temperatures between 300 K and 1300 K. An example of a typical gas temperature correction is -028 °C for a 1110 K bead temperature.

Appendix B: Drop Tube Procedures

Procedures for assembling/dissassembling and operating the drop tube are detailed in this appendix. To assemble the drop tube, just follow the instructions for disassembly in reverse.

Instructions for HPCP Disassembly

1. Cool down heaters to room temperature (100 °C per hour)
2. Turn off heaters (optional)
3. Take back plate off of reactor (where heater and thermocouple leads enter). After removing all bolts you will have to use a screwdriver and hammer to pound loose the back plate. Strike in the direction of the bolts (radially outward) as much as possible.
4. Back off the thermocouples after removing insulation layer (pull them back away from ceramic drop tube so they don't get abraded when the tube slides vertically upon removal). When assembling the HPCP, use a screwdriver to pry apart the opening between the two half-cylinder insulation and heaters.
5. Carefully remove injection probe. The flow straightener is closely fit into the drop tube.
6. Remove the collection probe as follows:
 - A. Remove the nuts which hold it up. It won't fall because it will still be wedged tightly in place.
 - B. Detach the quench nitrogen inlet (the stainless steel tubing).

- C. Attach the puller and remove the collection probe. Be sure to have a second person nearby to catch the probe and gently set it down, with ceramic drop tube still attached.
- D. Gently twist the ceramic tube off of the collection probe and rest it on a plastic bucket underneath the reactor.

Instructions for operating the drop tube reactor are outlined below.

Startup

1. Check to make sure reactor is assembled and cooling water is flowing to each piece of equipment. Also make sure that the control thermocouples for the reactor and pre-heater are properly positioned.
2. Set reactor temperature.
3. Check HCN monitor (if necessary clean it, optically calibrate it, replace Chemcassette).
4. Run HCN standard gas through monitor.
5. Assemble collection system.
6. Turn cooling water on to collection system.
7. Weigh filters and put in place.
8. Check that the valve for "Filter #3" is pointing horizontally to the right, that the valve to the cyclone and the two Y valves are open.
9. Close valve on primary inlet (green).
10. Open primary bypass valve.
11. Turn on gases. You need at least 900 psi in the nitrogen tanks when using a 500 psi regulator line pressure.
12. Set flow rates of gases.
13. Put coal in the feeder.
14. Put feeder on reactor.
15. Attach the primary inlet gas to feeder
16. Attach vibrator and tighten feeder while vibrator is running.
17. Let reactor reach a steady temperature. This takes about 30 minutes from the time you turn the gases on.
18. Close bypass valve on the primary inlet and wait several seconds.
19. Slowly open injection probe valve.
20. Check for leaks of primary gas.
21. Move feeder close to coal entrance.
22. Check all flows, temperatures, and pressures.
23. Feed the coal and record time (0.3 inches/minute, do not exceed 30 inches/minute).
24. Start the HCN monitor.

To Change Tar Filters

1. Stop HCN monitor (record time).
2. Back feeder up (reverse at 30 inches/minute).

3. Close injection probe valve (green).
4. Turn off gases and make sure gas flow is 0.
5. Remove tar filters and weigh them (all 3).
6. Open primary bypass valve.
7. Repeat startup procedure (starting at step 7). It saves time to weigh out the next set of tar filters while the drop tube experiment is running.

At the End of a Run

1. Change tar filters (first 6 steps above).
2. Reassemble collection system with only glass filters.
3. Close the valve to cyclone.
4. Turn valve for "Filter #3" so it is vertical (pointing down).
5. Turn on gases.
6. Turn valve for "Filter #3" slowly (clockwise) toward horizontal to blow out char.
7. Return valve to vertical. – if it's horizontal it will blow char out!
8. Turn gases off. (Make sure there is no flow or you will lose the char.)
9. Collect any char in cyclone (before removing cyclone).
10. Remove coal feeder and weigh coal not fed remaining in feeder.
11. Turn valve for "Filter #3" horizontal (pointing to the right), open valve to cyclone, and open the two Y valves.
12. **For ONLY the removable collection system items**, turn off cooling water line (one of five lines) and disassemble pieces.
13. Estimate tar losses on pieces of collection system. I used a combination of scraping and wiping.
14. Clean each piece of the collection system with methylene chloride (this must be performed under the hood; see the MSDS for CH_2Cl_2).
15. Look for and remove any deposits seen inside the collection probe.

Appendix C: Experimental Pyrolysis Conditions

Table C.1 lists the details of the drop tube experimental pyrolysis conditions.

Table C.1

Summary of Settings Used During Drop Tube Pyrolysis Experiments

Condition	Primary flow rate (cc/min)	Secondary flow rate (SLPM)	Quench N₂ flow rate (SLPM)	Reactor Temp. (°C)	Pre-heater Temp. (°C)
900 K	334	31.8	26.8	920	1150
950/975 K	193	31.8	27.0	920	1150
1000 K	220	32.5	27.7	1022	1150
1100 K	235	31.0	26.0	1110	1150
1250 K	179	23.7	18.9	1150	1150

For each of the drop tube pyrolysis tests in Table C.1, a drop distance of 282 mm was used. Molecular nitrogen gas was used exclusively for primary, secondary, and quench flows in the drop tube reactor.

The flat flame reactor was operated at an equivalence ratio of 1.4, with 0% post-flame oxygen burning city supplied natural gas and house air. The settings for the mass flow controllers (used in the final tests) and the rotameters (used in the preliminary tests), along with the corresponding flowrates are shown in Table C.2. A staticmaster unit was attached to the inside of the feeder which greatly reduced the variability in the coal feed rate. The char leg vacuum (on the cyclone exit) rotameter was set at 60, while the soot leg

vacuum (on the virtual impactor exit) was set at 60 and allowed to increase to 70 before changing the soot filters.

Table C.2
Summary of Settings Used During Flat Flame Reactor (FFR) Pyrolysis Experiments

Gas	Flow rate (SLPM)	Mass Flow Controller (% open)	Rotameter Setting
Quench N2	64.8	64.8	123
Air	38.55	77.1	70
Methane	4.84	66.3	120
Hydrogen	2.79	55.8	35
Fuel N2	5.41	54.1	150
Carrier N2	0.04	36.7	60

Appendix D: Tabulation of Experimental Data

Measured centerline flat flame reactor temperatures and velocities as reported by Ma⁴¹ are found in Table D.1.

Table D.1

Measured flat flame reactor (FFR) centerline gas velocity and temperature profiles (corrected for thermocouple bead radiation)

Distance (mm)	Velocity (cm/s)	Distance (mm)	Temperature (K)
0	3.4	0	300
0.02	13	6.4	1591
0.33	49	12.7	1625
1.04	88	19.1	1636
2.33	128	25.4	1641
4.66	168	31.8	1641
7.56	197	33	1639
10.01	212		
13.07	233		
33	233		

Measured centerline temperature profiles are shown by condition in Table D.2. Replicate temperature profile measurements shown in Table D.2 were taken at the beginning and the end of the 1100 K drop tube experiments, showing a difference of roughly 50°C in the measured maximum centerline gas temperature.

Table D.2

Measured drop tube centerline gas temperatures by condition (corrected for thermocouple bead radiation)

distance (mm)	Corrected Gas Temperature (K)				
	900 K	1000 K	7 July 98 1100 K	20 July 98 1100 K	1250 K
10	371	459	480	438	446
20	469	610	588	618	740
30	543	705	713	741	909
40	610	762	803	812	999
50	666	808	871	866	1047
60	714	830	911	907	1079
80	772	881	975	971	1138
100	823	925	1026	1013	1190
120	852	952	1063	1042	1216
140	876	975	1086	1067	1232
160	883	989	1106	1077	1238
180	891	999	1116	1084	1242
200	893	1001	1121	1085	1243
220	894	1001	1124	1084	1241
240	894	997	1123	1080	1238
260	895	995	1122	1077	1234
270	894	993	1123	1077	1235
280	886	865	1008	932	1105
290	764	794	882	848	991

Preliminary proximate and ultimate analyses were performed for the five Pacific Rim coals. Tables D.3-D.7 compare the results of these preliminary analyses for the sieved and un-sieved coals with values measured by Murata.⁹⁰ Table D.8 shows the ultimate analyses and dry ash contents for the chars produced in the preliminary flat flame reactor pyrolysis tests.

Table D.3***Preliminary ultimate and proximate analyses of Yallourn (YL) coal samples.***

	YL reported values (from Murata)	YL as received	YL 45-75 μm
C, wt% daf basis	66.88	65.15 \pm 0.48	65.35 \pm 0.34
H, wt% daf basis	4.70	4.73 \pm 0.08	4.86 \pm 0.04
N, wt% daf basis	0.48	0.60 \pm 0.01	0.52 \pm 0.01
S, wt% daf basis	0.26	0.19 \pm 0.01	0.19 \pm 0.04
O, wt% daf basis (by difference)	29.68	29.34	29.09
ash, wt% dry basis	1.6	1.55	1.57 \pm 0.02
moisture, wt%		11.63	10.07 \pm 0.38

Table D.4***Preliminary ultimate and proximate analyses of South Banko (SB) coal samples.***

	SB reported values (from Murata)	SB as received	SB 45-75 μm
C, wt% daf basis	71.25	70.55 \pm 0.46	68.70 \pm 0.55
H, wt% daf basis	5.44	5.38 \pm 0.09	5.31 \pm 0.03
N, wt% daf basis	1.19	1.35 \pm 0.02	1.16 \pm 0.02
S, wt% daf basis	0.52	0.51 \pm 0.09	0.43 \pm 0.04
O, wt% daf basis (by difference)	21.60	22.21	22.34
ash, wt% dry basis	2.7	2.62	2.65 \pm 0.02
moisture, wt%		8.15	7.53 \pm 0.15

Table D.5***Preliminary ultimate and proximate analyses of Taiheiyo (TH) coal samples.***

	TH reported values (from Murata)	TH as received	TH 45-75 μm
C, wt% daf basis	78.72	77.20 \pm 0.72	76.41 \pm 0.70
H, wt% daf basis	6.22	6.61 \pm 0.15	6.58 \pm 0.12
N, wt% daf basis	1.17	1.18	1.16 \pm 0.11
S, wt% daf basis	0.11	0.24 \pm 0.04	0.25 \pm 0.11
O, wt% daf basis (by difference)	13.78	14.76	15.59
ash, wt% dry basis	12.50	12.39	11.23 \pm 0.10
moisture, wt%		4.59	2.84 \pm 0.08

Table D.6***Preliminary ultimate and proximate analyses of Miike (MK) coal samples.***

	MK reported values (from Murata)	MK as received	MK 45-75 μm
C, wt% daf basis	79.90	79.78 \pm 0.87	78.78 \pm 0.55
H, wt% daf basis	6.12	6.25 \pm 0.15	6.24 \pm 0.05
N, wt% daf basis	1.20	1.21 \pm 0.12	1.18 \pm 0.02
S, wt% daf basis	4.15	4.32 \pm 0.16	4.63 \pm 0.13
O, wt% daf basis (by difference)	8.63	8.44	9.17
ash, wt% dry basis	16.00	18.67 \pm 0.12	19.21 \pm 0.02
moisture, wt%		1.36 \pm 0.06	0.78 \pm 0.08

Table D.7

Preliminary ultimate and proximate analyses of Hunter Valley (HV) coal samples.

	HV reported values (from Murata)	HV as received	HV 45-75 μm
C, wt% daf basis	83.20	81.28 \pm 1.05	81.25 \pm 1.18
H, wt% daf basis	5.40	5.43 \pm 0.33	5.45 \pm 0.20
N, wt% daf basis	2.10	2.14 \pm 0.32	2.12 \pm 0.18
S, wt% daf basis	0.50	0.53 \pm 0.32	0.47 \pm 0.18
O, wt% daf basis (by difference)	8.80	10.62	10.70
ash, wt% dry basis	9.20	8.80 \pm 0.32	9.31 \pm 0.18
moisture, wt%		2.29 \pm 0.16	1.17 \pm 0.14

Table D.8

Summary of ultimate analyses and dry ash for chars produced in the flat flame reactor (FFR) preliminary pyrolysis experiments.

Char Mean/Std. Dev.	% C (daf)	% H (daf)	% N (daf)	% S (daf)	% O (daf) (by diff.)	% ash (dry)
Yallourn	94.29	1.52	0.65	0.15	3.40	4.49
std. deviation	0.85	0.16	0.09	0.02	0.58	0.09
South Banko	91.00	1.90	1.37	0.28	5.43	6.99
std. deviation	0.45	0.08	0.07	0.02	0.47	1.82
Taiheiyo	88.49	2.47	1.28	0.18	7.57	27.51
std. deviation	0.90	0.66	0.06	0.02	0.19	0.83
Miike	91.82	2.92	1.42	3.67	0.17	40.96
std. deviation	1.10	0.52	0.01	0.37	0.20	2.36
Hunter Valley	91.90	2.34	2.32	0.32	3.11	18.24
std. deviation	1.17	0.40	0.02	0.04	0.71	1.09

In order to check the accuracy of the preliminary ultimate analyses, coal standards purchased from LECO were checked on the LECO CHNS analyzer after calibration. Using

our normal calibration standard and procedure, the accuracy check standard dry values for C, H, N, and S agreed well with the values reported by LECO, with few exceptions, as shown in Table D.8. Note that none of the nitrogen standards agree closely, except the calibration standard and the 1995 coal check standard. Since the other two standards deviate in opposite directions from their reported values for N, it was assumed that the calibration standard was the most accurate. This was also the case for C, except that the 1997 coal check standard gave excellent agreement with the calibration standard. All standards are in good agreement for H. Sulfamethazine shows large deviations from the reported values, probably because it contains in excess of 20% N and 11% S, both of which are more than ten times the amount found in most coals.

Table D.9

Accuracy check of CHNS calibration for *preliminary* coals and chars.

	Calibration coal standard composition, wt % dry basis	Percent relative deviation from reported LECO values		
		1997 Check standard (coal)	1995 Check standard (coal)	Sulfamethazine (organic compound)
C	68.88	0.3	-2.9	2.7
H	4.63	0.5	-0.6	-0.39
N	1.35	6.2	-1.4	-8.6
S	1.80*	-	N/A	3.5

*Sulfur calibrated using the 1997 check standard, since the sulfur composition of our calibration standard is unknown.

Data from sample characterization of the products produced in the pyrolysis tests presented in this dissertation are summarized in Tables D.10-D.15.

Table D.10

Summary of ultimate analyses, dry ash, and mass release (%MR) for chars produced in the drop tube and flat flame reactor (FFR) pyrolysis experiments.

Coal	Condition	% C (daf)	% H (daf)	% N (daf)	% S (daf)	% O (daf) (by diff.)	% ash (dry)	% MR (daf)	
Yallourn	coal	65.31	4.76	0.52	0.18	29.22	1.58	-	
	900 K	75.32	3.33	0.68	0.18	20.49	3.27	46.0 ^a	
	1000 K	84.09	2.95	0.73	0.14	12.09	2.95	55.0 ^a	
	1100 K	87.65	2.57	0.70	0.13	8.94	3.50	57.8 ^a	
	1650 K	91.84	1.27	0.58	0.14	6.18	4.46	69.0 ^a	
South Banko	coal	71.37	5.36	1.18	0.55	21.55	2.65	-	
	900 K	78.25	3.77	1.52	0.46	16.00	4.18	41.6	
	1000 K	81.61	3.16	1.59	0.30	13.35	4.57	51.1	
	1100 K	84.18	2.91	1.58	0.24	11.09	4.79	54.4	
	1250 K	91.33	1.74	1.42	0.35	5.16	5.17	58.3	
	1650 K	90.70	1.61	1.36	0.31	6.01	5.73	64.1	
Taiheiyo	coal	76.72	6.35	1.13	0.21	15.59	11.12	-	
	975 K	80.71	3.88	1.43	0.22	13.76	20.80	53.3	
	1000 K	84.25	3.34	1.49	0.18	10.74	22.28	58.3	
	1100 K	85.16	3.04	1.49	0.18	10.13	23.23	60.4	
	1650 K	86.92	2.79	1.38	0.23	8.67	25.61	64.4	
Miike	coal	79.91	6.13	1.18	4.48	8.30	18.79	-	
	900 K	82.48	3.44	1.48	7.15	5.46	40.82	66.8 ^c	
	1000 K	85.28	3.42	1.44	5.78	4.08	36.94	63.9	
	1100 K	89.97	3.00	1.40	4.49	1.13	38.50	64.7	
	1650 K	92.65	2.30	1.29	4.76	-1.00 ^b	42.52	68.9	
Hunter Valley	coal	82.82	5.43	2.08	0.48	9.18	9.25	-	
	900 K	87.18	4.08	2.35	0.46	5.92	13.87	38.6	
	1000 K	88.05	3.42	2.47	0.31	5.74	15.47	43.8	
	1100 K	89.94	2.84	2.48	0.34	4.41	16.14	47.9	
	1650 K	91.29	2.27	2.22	0.71	3.52	18.58	52.4	
Pittsburgh	coal	82.77	5.48	1.64	3.38	6.73	8.83	-	
	900 K	80.91	4.15	1.72	6.08	7.14	14.76	45.1	
	950 K	82.46	4.06	1.78	5.97	5.73	15.25	47.2	
	(replicate exp.)	950 K	82.51	4.02	1.78	5.38	6.31	14.69	46.4
		1000 K	87.49	3.37	1.92	3.82	3.41	15.72	50.7

Table D.10 (cont.)

Coal	Condition	% C (daf)	% H (daf)	% N (daf)	% S (daf)	% O (daf) (by diff.)	% ash (dry)	% MR (daf)
Pittsburgh	1100 K	87.99	3.08	1.78	3.72	3.43	16.87	54.4
	1250 K	92.18	1.72	1.76	3.68	0.66	18.76	59.8
	1650 K	88.56	2.64	1.73	4.48	2.59	19.27	59.1
Upper Freeport	coal	84.15	5.13	1.55	4.56	4.60	15.75	-
	900 K	85.47	3.09	1.61	4.82	5.01	24.68	42.9 ^c
	1000 K	85.99	3.31	1.62	8.32	0.77	N.M.	49.0 ^d
	1100 K	89.21	2.81	1.69	5.13	1.17	25.56	45.2
	1650 K	92.17	2.05	1.64	3.24	0.90	24.82	43.6
Pocahontas	coal	91.57	4.57	1.36	0.76	1.74	5.06	-
	900 K	91.54	4.32	1.35	0.73	2.05	5.79	13.4
	1000 K	93.31	3.45	1.43	0.67	1.14	6.24	21.7
	1100 K	92.45	2.96	1.42	0.61	2.56	6.34	25.8
	1650 K	95.41	2.14	1.33	0.61	0.51	6.33	24.7

^a Mass release for Yallourn chars determined by overall mass balance, not tracer mass balance.

^b Sulfur values include inorganic sulfur, thus O values are somewhat under-estimated.

^c A large proportion of the char was lost in the collection system during this test.

^d Char held up in collection system and formed large chunks

Table D.11

Summary of ultimate analyses and yields of tars/soots produced in the drop tube and flat flame reactor (FFR) pyrolysis experiments.

Coal	Condition	% C (daf)	% H (daf)	% N (daf)	% S (daf)	% O (daf) (by diff.)	% tar yield (daf) ^a
Yallourn	coal	65.31	4.76	0.52	0.18	29.22	-
	900 K	73.25	5.79	0.54	0.12	20.30	10.5
	1000 K	79.19	4.64	0.78	0.17	15.22	6.6
	1100 K	86.37	4.58	0.91	0.23	7.90	3.9
	(FFR) 1650 K	96.18	2.19	0.18	0.08	1.36	5.1
South Banko	coal	71.37	5.36	1.18	0.55	21.55	-
	900 K	78.82	6.69	1.18	0.41	12.90	15.0
	1000 K	81.48	4.82	1.69	0.54	11.46	9.0
	1100 K	84.66	4.65	1.77	0.58	8.35	7.4
	1250 K	93.76	4.06	1.37	0.60	0.22	6.8
	(FFR) 1650 K	98.09	2.05	0.29	0.13	-0.56	6.9
Taiheiyō	coal	76.72	6.35	1.13	0.21	15.59	-
	975 K	81.81	6.37	1.34	0.16	10.32	22.5
	1000 K	85.55	5.75	1.63	0.23	6.84	17.1
	1100 K	87.51	4.76	1.72	0.25	5.76	12.9
	(FFR) 1650 K	96.68	2.32	0.47	0.11	0.42	15.1
Miike	coal	79.91	6.13	1.18	4.48	8.30	-
	900 K	85.42	6.06	1.38	2.68	4.47	24.7
	1000 K	86.99	4.76	1.59	3.07	3.60	31.2
	1100 K	89.89	4.36	1.65	2.40	1.69	25.4
	(FFR) 1650 K	96.67	1.74	0.54	0.63	0.42	19.5
Hunter Valley	coal	82.82	5.43	2.08	0.48	9.18	-
	900 K	84.62	6.02	2.07	0.43	6.86	22.3
	1000 K	86.54	4.92	2.38	0.48	5.67	21.8
	1100 K	91.12	4.44	2.54	0.48	1.42	19.5
	(FFR) 1650 K	96.61	1.78	0.83	0.17	0.61	14.8
Pittsburgh	coal	82.77	5.48	1.64	3.38	6.73	-
	900 K	84.12	5.87	1.71	0.97	7.33	31.8
	950 K	85.50	5.65	1.76	1.02	6.08	28.5
	(replicate exp.) 950 K	86.55	5.66	1.81	1.03	4.94	-
	1000 K	86.50	4.85	1.91	1.38	5.36	28.7
	1100 K	88.92	4.43	1.99	1.47	3.20	25.1

Table D.11 (cont.)

Coal	Condition	% C (daf)	% H (daf)	% N (daf)	% S (daf)	% O (daf) (by diff.)	% tar yield (daf) ^a
Pittsburgh	1250 K	93.31	2.87	1.51	1.24	1.06	26.6
(FFR)	1650 K	95.02	1.75	0.81	0.40	2.01	21.0
Upper Freeport	coal	84.15	5.13	1.55	4.56	4.60	-
	900 K	87.95	5.53	1.60	0.97	3.94	18.4
	1000 K	89.51	4.73	1.79	1.15	2.82	27.7
	1100 K	92.25	4.24	1.93	1.31	0.27	27.5
(FFR)	1650 K	94.96	1.32	0.74	0.33	2.65	17.7
Pocahontas	coal	91.57	4.57	1.36	0.76	1.74	-
	900 K	90.80	5.26	1.34	0.69	1.91	7.5
	1000 K	92.32	4.78	1.41	0.69	0.81	15.1
	1100 K	92.64	4.50	1.45	0.67	0.74	14.2
(FFR)	1650 K	98.25	1.31	0.63	0.21	-0.40	10.7

^a Tar yields reported for FFR tests are actually soot yields.

Table D.12

Parameters measured via ^{13}C NMR at the University of Utah for *chars* from the drop tube and flat flame reactor (FFR) pyrolysis experiments.^a

Coal	Condition	f_a	f_a^C	f_a'	f_a^H	f_a^N	f_a^P	f_a^S	f_a^B	f_{al}	f_{al}^H	f_{al}^*	f_{al}^O
Yallourn	coal	67	10	57	16	41	16	9	16	33	23	10	9
	2-D coal ^b	67	10	57	16	41	19	22	0	33	23	10	9
	1100 K	96	5	91	37	54	6	21	27	4	3	1	3
South Banko	coal	62	8	54	17	37	9	13	15	38	28	10	5
	Sv. coal ^c	61	8	53	16	37	9	13	15	39	30	9	5
	900 K	86	6	80	24	56	10	18	28	14	8	6	2
	1000 K	95	5	90	32	58	8	20	30	5	3	2	2
	1100 K	95	4	91	34	57	7	20	30	5	4	1	2
	1250 K	93	10	83	17	66	7	19	40	7	5	2	5
	1650 K	91	11	80	24	56	7	17	32	9	6	3	5
Taiheiyo	coal	56	5	51	16	35	6	14	15	44	32	12	4
	1100 K	97	3	94	33	61	5	19	37	3	2	1	2
Miike	coal	66	2	64	22	42	6	17	19	34	24	10	3
	1100 K	96	8	88	30	58	9	25	24	4	3	1	2
Hunter Valley	coal	74	3	71	25	46	8	19	19	26	17	9	4
	1100 K	95	4	91	34	57	5	20	32	5	4	1	3
Pittsburgh	coal	71	1	70	27	43	6	15	22	29	21	8	4
	950 K	92	2	90	32	58	6	19	33	8	4	3	1
	1000 K	93	2	91	34	57	5	19	33	7	4	3	2
	1100 K	95	3	92	40	52	5	21	26	5	4	1	2
	1250 K	92	11	81	20	61	7	17	37	8	6	2	5
	(FFR)	1650 K	95	10	85	29	56	8	22	26	5	4	1
Upper Freeport	coal	81	0	81	28	53	4	20	29	19	11	8	2
	1100 K	97	4	93	33	60	5	21	34	3	2	1	2
Pocahontas	coal	86	0	86	33	53	2	17	34	14	9	5	1
	1100 K	97	2	95	36	59	3	19	37	3	2	1	2

^a Percentage carbon (error): f_a = total sp^2 -hybridized carbon (± 3); f_a' = aromatic carbon (± 4); f_a^C = carbonyl, $d > 165$ ppm (± 2); f_a^H = aromatic with proton attachment (± 3); f_a^N = nonprotonated aromatic (± 3); f_a^P = phenolic or phenolic ether, $d = 150$ - 165 ppm (± 2); f_a^S = alkylated aromatic $d = 135$ - 150 ppm (± 3); f_a^B = aromatic bridgehead (± 4); f_{al} = aliphatic carbon (± 2); f_{al}^H = CH or CH_2 (± 2); f_{al}^* = CH_3 or nonprotonated (± 2); f_{al}^O = bonded to oxygen, $d = 50$ - 90 ppm (± 2).

^b As analyzed by 2-D ^{13}C NMR

^c Sieved coal (45-75 μm fraction)

Table D.13

Parameters measured via ^{13}C NMR at the University of Utah for tars from the drop tube and flat flame reactor (FFR) pyrolysis experiments.^a

Coal	Condition	f_a	f_a^C	f_a^L	f_a^H	f_a^N	f_a^P	f_a^S	f_a^B	f_{al}	f_{al}^H	f_{al}^*	f_{al}^O
South Banko	coal	62	8	54	17	37	9	13	15	38	28	10	5
	900 K	69	6	63	23	40	9	15	16	31	21	10	3
	1000 K	88	4	84	40	44	9	17	18	12	6	6	2
	1100 K	90	2	88	44	44	7	18	19	10	6	4	3
	1250 K	95	1	94	49	45	3	18	24	5	4	1	2
Pittsburgh	coal	71	1	70	27	43	6	15	22	29	21	8	4
	950 K	78	2	76	33	43	6	17	20	22	13	9	3
	1000 K	87	1	86	40	46	6	18	22	13	7	6	2
	1100 K	90	1	89	43	46	4	17	25	10	6	4	3
	1250 K	93	5	88	36	52	5	17	30	7	6	1	4
(FFR)	1650 K	91	7	84	29	55	5	14	36	9	7	2	5

^a see footer to Table D.12.

Table D.14

Structural parameters derived from ^{13}C NMR for *chars* produced in the drop tube and flat flame reactor (FFR) pyrolysis experiments.^a

Coal	Condition	b	C_{cl}	+1	P_0	B.L.	S.C.	M_{cl}	M
Yallourn	coal	0.281	14	6.1	0.60	3.7	2.4	452	46
	2-D coal [†]	0.000	6	4.3	0.76	3.3	1.0	189	27
	1100 K	0.297	14	4.2	0.96	4.0	0.2	211	9
South Banko	coal	0.278	13	5.3	0.55	2.9	2.4	405	46
	Sv. coal [‡]	0.283	14	5.8	0.59	3.4	2.4	450	48
	900 K	0.350	17	6.0	0.79	4.7	1.3	326	20
	1000 K	0.333	16.5	5.1	0.93	4.7	0.4	270	13
	1100 K	0.330	16	4.7	0.96	4.5	0.2	251	11
	1250 K	0.482	24	7.4	0.92	6.8	0.6	380	12
	1650 K	0.400	20	6.0	0.88	5.3	0.7	331	14
Taiheiyo	coal	0.294	14	5.5	0.40	2.2	3.3	430	47
	1100 K	0.394	19	4.9	0.96	4.7	0.2	285	10
Miike	coal	0.297	14	5.0	0.57	2.9	2.1	329	31
	1100 K	0.273	13	5.0	0.97	4.9	0.1	197	7
Hunter Valley	coal	0.268	13	4.9	0.67	3.3	1.6	266	21
	1100 K	0.352	17.5	4.8	0.96	4.6	0.2	257	8
Pittsburgh	coal	0.314	15	4.5	0.62	2.9	1.6	311	28
	950 K	0.367	18	5.0	0.88	4.4	0.6	291	14
	1000 K	0.363	18	4.7	0.88	4.1	0.6	272	10
	1100 K	0.283	14	3.9	0.96	3.7	0.2	208	8
	1250 K	0.457	22	6.5	0.92	6.0	0.5	354	13
	(FFR)	1650 K	0.306	15	5.3	0.97	5.1	0.2	239
Upper Freeport	coal	0.358	18	5.3	0.67	3.6	1.7	317	18
	1100 K	0.366	18	5.0	0.96	4.8	0.2	261	8
Pocahontas	coal	0.395	20	4.4	0.74	3.3	1.1	305	13
	1100 K	0.389	19	4.4	0.95	4.2	0.2	260	6

^a b = fraction of bridgehead carbons, C_{cl} = aromatic carbons per cluster, +1 = total attachments per cluster, P_0 = fraction of attachments that are bridges, B.L. = bridges and loops per cluster, S.C. = side chains per cluster, MW_{cl} = the average molecular weight of an aromatic cluster, MW = the average molecular weight of the cluster attachments.

Table D.15**Structural parameters derived from ^{13}C NMR for tars produced in the drop tube and flat flame reactor (FFR) pyrolysis experiments.^a**

Coal	Condition	b	C_{cl}	+1	P_0	B.L.	S.C.	M_{cl}	M
South Banko	coal	0.278	13	5.3	0.55	2.9	2.4	410	47
	900 K	0.254	12	4.5	0.58	2.6	1.9	290	31
	1000 K	0.214	10.5	3.3	0.77	2.5	0.8	184	16
	1100 K	0.216	11	3.0	0.84	2.5	0.5	177	13
	1250 K	0.255	12	2.7	0.95	2.6	0.1	164	5
Pittsburgh	coal	0.314	15	4.5	0.62	2.9	1.6	311	28
	950 K	0.263	13	4.0	0.61	2.4	1.6	240	20
	1000 K	0.256	12	3.3	0.75	2.5	0.8	194	13
	1100 K	0.281	13.5	3.2	0.81	2.6	0.6	205	11
	1250 K	0.341	17	4.2	0.95	4.0	0.2	249	9
(FFR)	1650 K	0.429	21	4.8	0.89	4.3	0.5	316	12

^a see footer to Table D.14.

Appendix E: Additional Pyrolysis Test Results and Discussion

Additional tests were performed which are not presented in the main body of the text of this dissertation. These tests were of two kinds: pyrolysis of already partially devolatilized chars and preliminary flat flame reactor pyrolysis tests.

The purpose of the tests involving pyrolysis of already devolatilized chars was to gauge the effect of volatiles on light gas nitrogen release. By using chars which had already released most of their tar and light gas as feed for pyrolysis tests at the 1250 K condition, devolatilization in an environment free of the majority of tar and light gas could be compared to devolatilization in the conventional drop tube environment (where the char remains surrounded by tar and light gases). All the tests at 1250 K were performed within the same week, thus helping to ensure that the pyrolysis environment did not change significantly from test to test. The results of the dry elemental analysis of the chars produced by pyrolysis in the drop tube reactor at the 1250 K condition of this study are shown in Table E.1. The values shown in Table E.1 are mean values based on eight replicate measurements in the elemental analyzer all measured on the same day. All of the chars produced from tests using *char* for the feed were analyzed within 1.5 hours of the chars from the corresponding tests using *coal* for the feed. In this way, the N/C and H/C ratios from these samples could be directly compared (N/C and H/C ratios are independent of ash content, and thus sample pulverization was not necessary). The H/C ratio is intended to be a measure of the degree of pyrolysis undergone in the char. The N/C ratio is intended to be a measure of N/AC in the char (and therefore the amount of light gas release) when comparing samples with the same carbon aromaticity. It might be assumed that char

samples from a given coal having no statistically significant difference in H/C ratio have the same carbon aromaticity. Based on a student's t test 95% confidence interval for the difference between the tests using *coal* as feed and the tests using *char* as feed, only the Pittsburgh test showed any statistically significant difference in the N/C ratio (that is, the interval does not contain zero). In this case, the Pittsburgh coal which was first pyrolyzed at 1100 K followed by pyrolysis at 1250 K lost more nitrogen to the light gas than the coal which was only pyrolyzed at 1250 K, as evidenced by a 6.4% (relative) lower N/C ratio. On the other hand, the measured N/C ratio values for all of the South Banko chars show no statistically significant difference at a 95% confidence level. It is not clear why tests with the two different coals gave two different results. It may have to do with the fact that the Pittsburgh 1100 K char is a swollen char (having large particles with very low density) which may behave differently in the drop tube apparatus than does a coal or an unswollen char. More tests would be necessary before drawing any firm conclusions. CPD modeling of these tests using the nitrogen model of this study predicts that N_{site} for the South Banko tests using the 900 K and 1000 K chars as feed should be 4.2% and 4.5% higher, respectively than the char from the test using coal as feed. The measured difference in the N/C ratio, although not statistically significant, were 0.3% and 1%, respectively. For the Pittsburgh test, the difference is predicted to be 1.3%, while the difference in the measured values was -6.4%. Although the predicted trend with feed type is correct (South Banko 900 K > South Banko 1000 K > Pittsburgh 1100 K), the magnitude of the difference is not correctly predicted by the nitrogen model of this study. One possible explanation for this is that the assumption that the samples from the same parent coal have the same aromaticity is not valid.

Preliminary pyrolysis tests were performed in duplicate in the flat flame reactor using the five Pacific Rim coals. The results of these tests were not included in the body of the test since the procedure used was faulty with the result that all of the char may not have been recovered after each test. Furthermore, the single stream sample splitter was not used

for these tests, so error due to sample splitting may be increased. For each of the preliminary tests, mass release was calculated based on an overall mass balance. The results of these tests are found in Table E.2 and Figure E.1. A strong correlation was

Table E.1

Dry elemental analysis of chars produced by drop tube pyrolysis of various feed types at the 1250 K condition of this study.

	Pittsburgh		South Banko		
Feed type:	coal	1100 K char	coal	900 K char	1000 K char
% C (dry)	81.78	83.64	86.61	85.78	86.38
% H (dry)	1.50	1.56	1.65	1.81	1.63
% N (dry)	1.73	1.66	1.34	1.33	1.35
% S (dry)	1.68	1.35	0.33	0.32	0.27
H/C	0.01831	0.01869	0.01909	0.02116	0.01891
H/C stdev. ^a	0.00018	0.00018	0.00016	0.00024	0.00020
H/C difference low limit ^b		-0.00128		-0.00303	-0.00076
H/C difference high limit ^b		0.00055		-0.00116	0.00110
N/C	0.02110	0.01983	0.01547	0.01552	0.01563
N/C stdev. ^a	0.00021	0.00022	0.00008	0.00018	0.00009
H/C difference low limit ^b		0.00051		-0.00058	-0.00065
H/C difference high limit ^b		0.00211		0.00037	0.00027

^a Standard deviations are based on eight replicate elemental determination measurements.

^b Low and high limits are for a 95% confidence interval⁹¹ based on a student's t test for the difference between the coal value and the char value (coal-char).

observed at the 1650 K condition between the soot mass yield as a fraction of coal mass and the soot nitrogen yield as a fraction of coal nitrogen (see Figure E.2). A strong correlation was also found between the light gas mass yield as a fraction of coal mass and the light gas nitrogen yield as a fraction of coal nitrogen for the preliminary 1650 K FFR

pyrolysis tests (see Figure E.3). Both of the variables in Figure E.3 show a nearly linear trend with parent coal carbon content.

Table E.2

Mass and nitrogen release for preliminary FFR pyrolysis tests at 1650 K condition using Pacific Rim coals.

Coal	Mass Release (% daf coal)			N release (% coal N)
	Measured	Predicted (CPD)	Difference	
Yallourn	71.2 ± 1.9	47.7	23.5	65.7 ± 4.3
South Banko	67.9 ± 1.8	55.5	12.4	64.4 ± 2.3
Taiheiyō	67.5 ± 1.5	64.1	3.4	64.6 ± 3.3
Miike	59.6 ± 0.2	52.9	6.7	51.4 ± 0.1
Hunter Valley	53.6 ± 0.2	41.2	12.4	49.3 ± 0.7

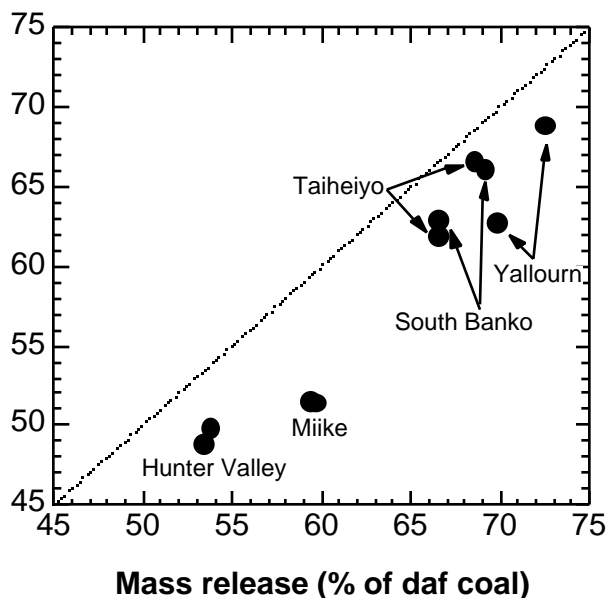


Figure E.1 Comparison of duplicate results for pyrolysis of Pacific Rim coals in a flat flame burner with 15 ms residence time and 1650 K maximum gas temperature.

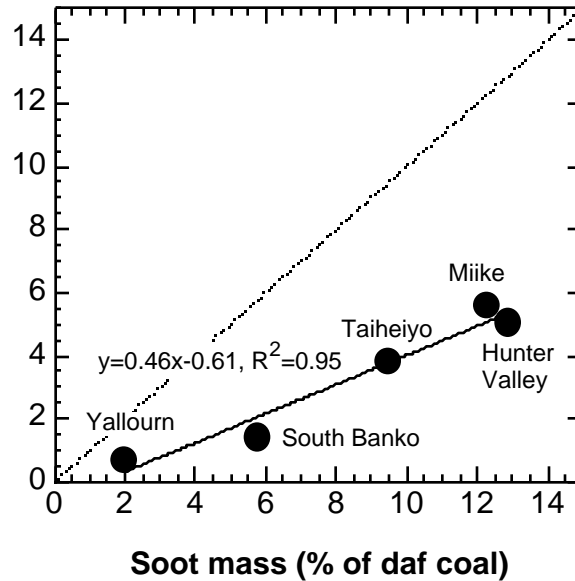


Figure E.2 Correlation of nitrogen reporting to the soot with mass reporting to the soot for pyrolysis of Pacific Rim coals in a flat flame burner with 15 ms residence time and 1650 K maximum gas temperature. Note that there is less than a 1:2 ratio of nitrogen to total mass reporting to the soot as a fraction of that in the dry ash-free coal.

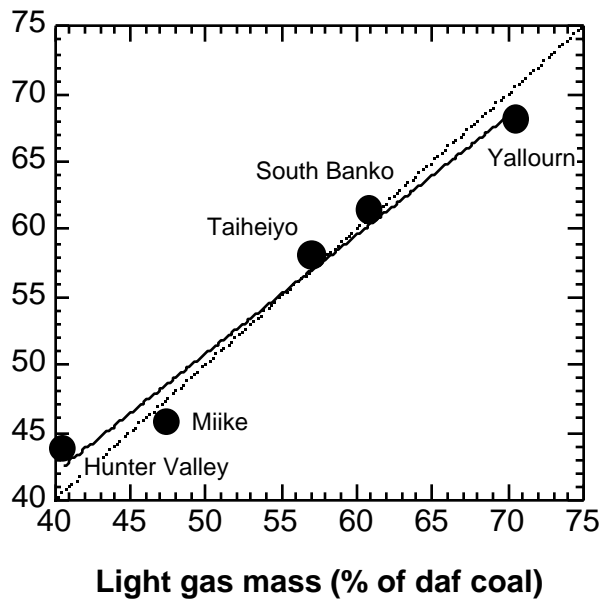


Figure E.3 Nitrogen release versus mass release to the light gases, as calculated from overall nitrogen and total mass balances, as percentages of dry ash-free coal nitrogen and mass for pyrolysis of Pacific Rim coals in a flat flame burner with 15 ms residence time and 1650 K maximum gas temperature.

Appendix F: Analysis of CPD Tar and Total Volatiles Predictions

A more detailed comparison of CPD prediction performance for tar and total volatiles release as a function of pyrolysis condition temperature is presented in this section. Figure F.1 compares CPD predictions of tar release with measured tar yields for the drop tube pyrolysis experiments of this study. Overall, the CPD does very well, matching tar yields to within about 3% (absolute) for four of the eight coals (Yallourn, South Banko, Taiheiyo, and Hunter Valley). Note that since the CPD model does not model secondary reactions in the tar, that tar release predictions should be compared with the *maximum* measured tar yield for pyrolysis tests at or below the temperature of interest. Note that five of the coals reach a maximum in tar yield at the lowest pyrolysis temperature (900 K), a trend which is nicely followed by CPD predictions. However, for three of the coals (Miike, Upper Freeport, and Pocahontas), the maximum tar yield is not reached until the 1000 K condition, a phenomenon not captured by CPD predictions. Furthermore, predictions of maximum tar release from these three coals is under-predicted by the CPD by 7%, 12%, and 11% (absolute), respectively. These two discrepancies (in 1) maximum tar yield, and 2) temperature at which it is reached) may be related and could be due to some factor not taken into account by the CPD, such as the rank dependence of the strength of labile bridges. This might be an interesting question for future work to address. Predicted maximum tar release from Pittsburgh coal is 6% (absolute) lower than the measured value, which is surprising, since predictions for the Pittsburgh high volatile bituminous coal of the Penn State Coal database (PSOC 1451) for similar pyrolysis conditions predict tar yields of over 30%.

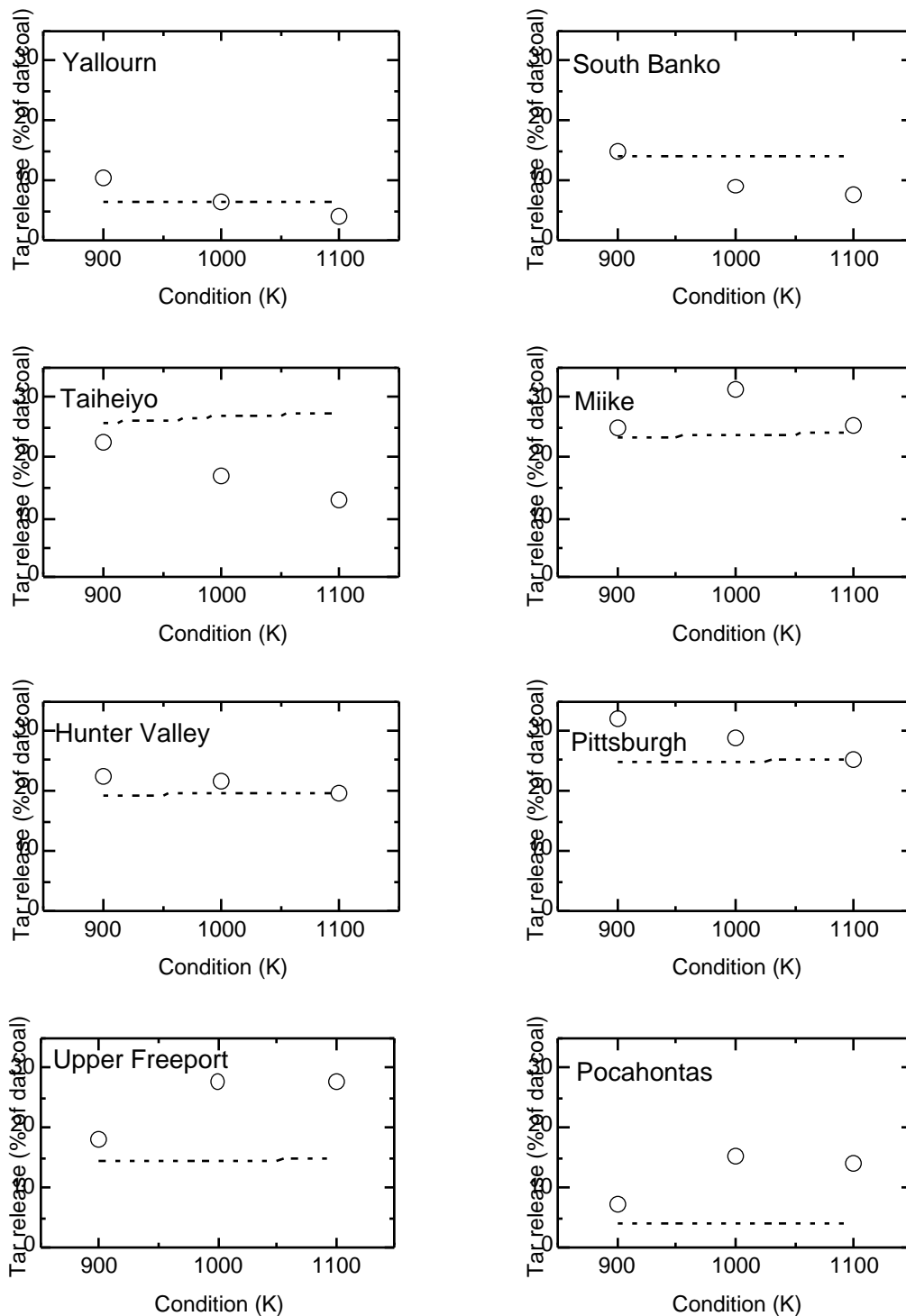


Figure F.1. Comparison of CPD predictions of tar release with measured tar yields from the drop tube pyrolysis tests of this study. Data are displayed as a function of pyrolysis condition temperature to emphasis trends with increasing pyrolysis severity.

In Figure F.2, comparisons are made between CPD predictions of total volatiles release and measured data from the drop tube and flat flame reactor tests of this study. Note that the agreement is excellent, as almost the entire discrepancy between predictions and measurements in Figure F.2 can be ascribed to the discrepancy in the tar release values.

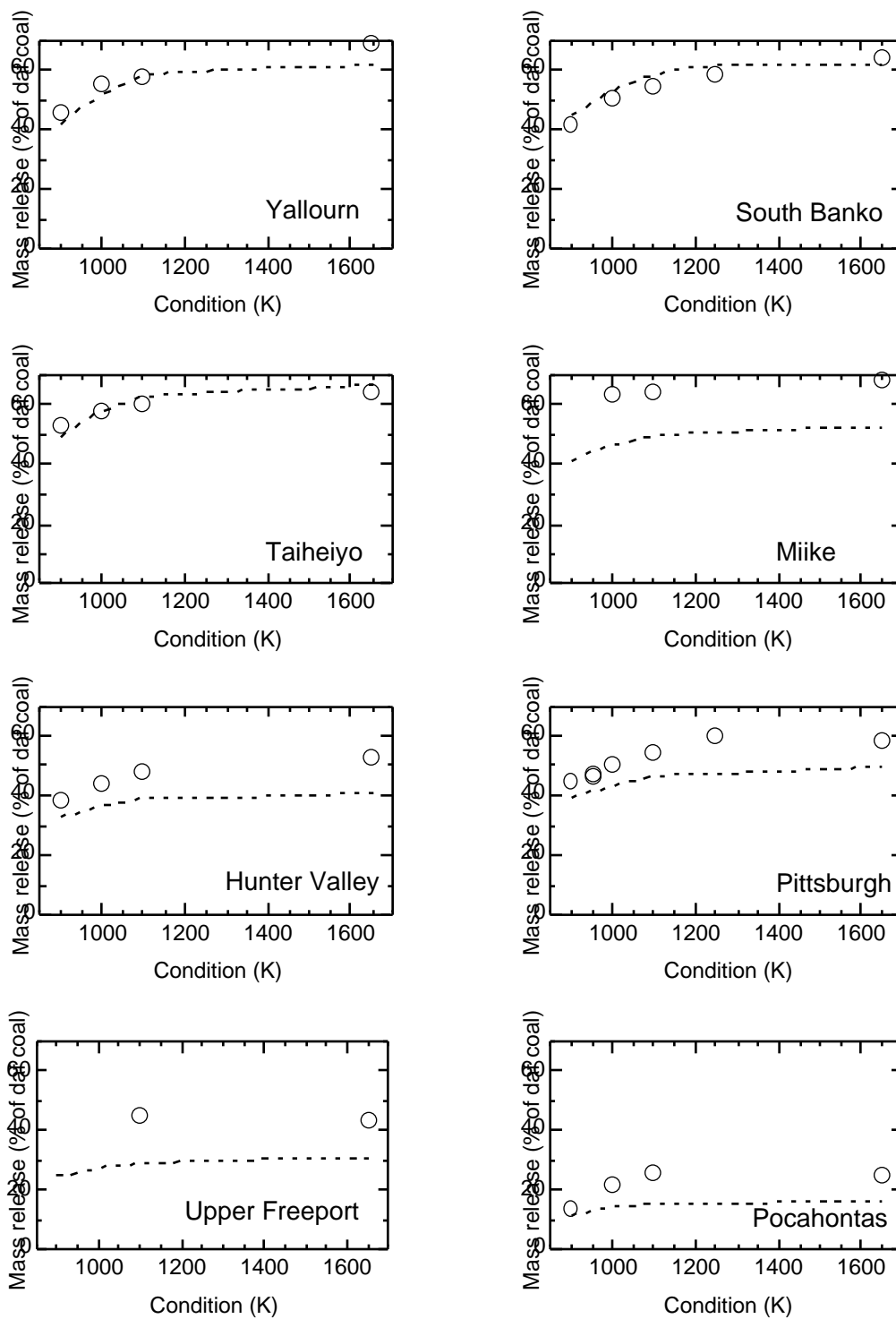


Figure F.2. Comparison of CPD predictions of total volatiles release with measured data from the drop tube and flat flame reactor pyrolysis tests of this study. Data are displayed as a function of pyrolysis condition temperature to emphasize trends with increasing pyrolysis severity.

Appendix G: Gas Field Simulations for Drop Tube Tests

In order to estimate gas velocities and temperatures for the drop tube pyrolysis experiments, gas field simulations were performed using FLUENT 4.4, a computational fluid dynamics (CFD) software program. In modeling the drop tube reactor, axi-symmetric cylindrical coordinates were used. This made the computational analysis much more simple, but eliminated the ability to model radial conduction in the flow straightener (a three-dimensional section of monolith, depicted in Figure G.1) walls without blocking the gas flow. The use of axi-symmetric cylindrical coordinates also made it impossible to properly model the array of square flow channels which comprise the flow straightener. Instead the flow straightener was modeled as a set of concentric thin-walled cylinders. This required estimation of the temperature of each of these concentric cylinders in order to simulate the radial conduction from outermost part of the flow straightener to the innermost part, which is in contact with the water cooled injection probe, setting up a large non-linear radial gradient in the flow straightener. A three dimensional simulation of the entire drop tube flow field was attempted for the 1100 K condition, but the number of grid cells required for the simulation made the calculation too slow to be practical using the computational resources available at this time at BYU. Future attempts to model the drop tube might use a 2-D axi-symmetric cylindrical case to solve for the temperature and velocity profile just prior to the flow straightener. These temperature and velocity profiles could then be used as input to a three dimensional model which focuses only on the flow straightener. This would give temperature and velocity profiles of the secondary flow at

the flow straightener exit which could then be used in a 2-D simulation of the remainder of the flow field.

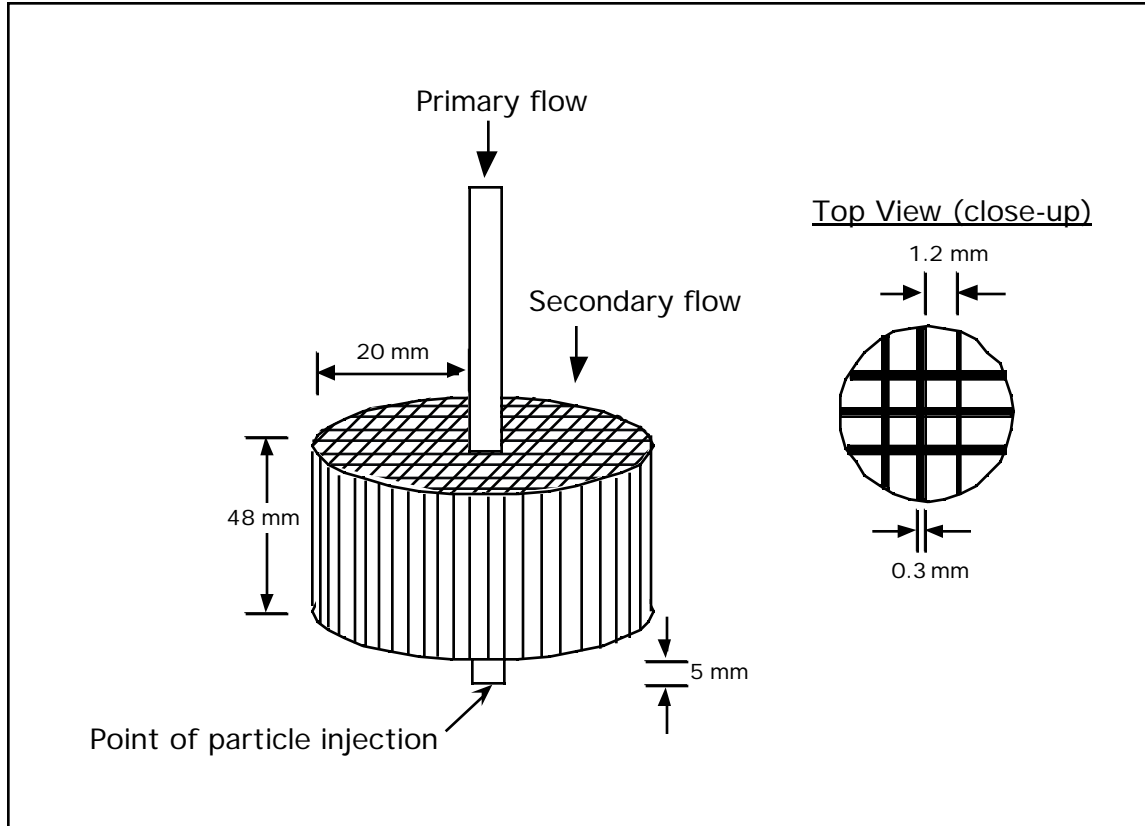


Figure G.1. Detailed schematic showing dimensions of drop tube **flow straightener**. During the FLUENT simulations, the flow straightener was modeled in two dimensions as rows of concentric cylinders with fixed temperatures, having a one radial cell wall thickness with five radial cell spaces between cylinder walls.

The geometry of the drop tube assumed for the simulations are shown in Figure G.2, with each different boundary condition region indicated. The temperature in the drop tube wall zone 2 (along the last 70 mm of the drop tube wall) were linearly interpolated between the collection probe temperature and the drop tube wall temperature in zone 1. The wall in zone 1 was assumed to be isothermal. The entire flow field was divided into 12,400 cells: 200 cells along the drop tube length and 62 cells along the drop tube radius.

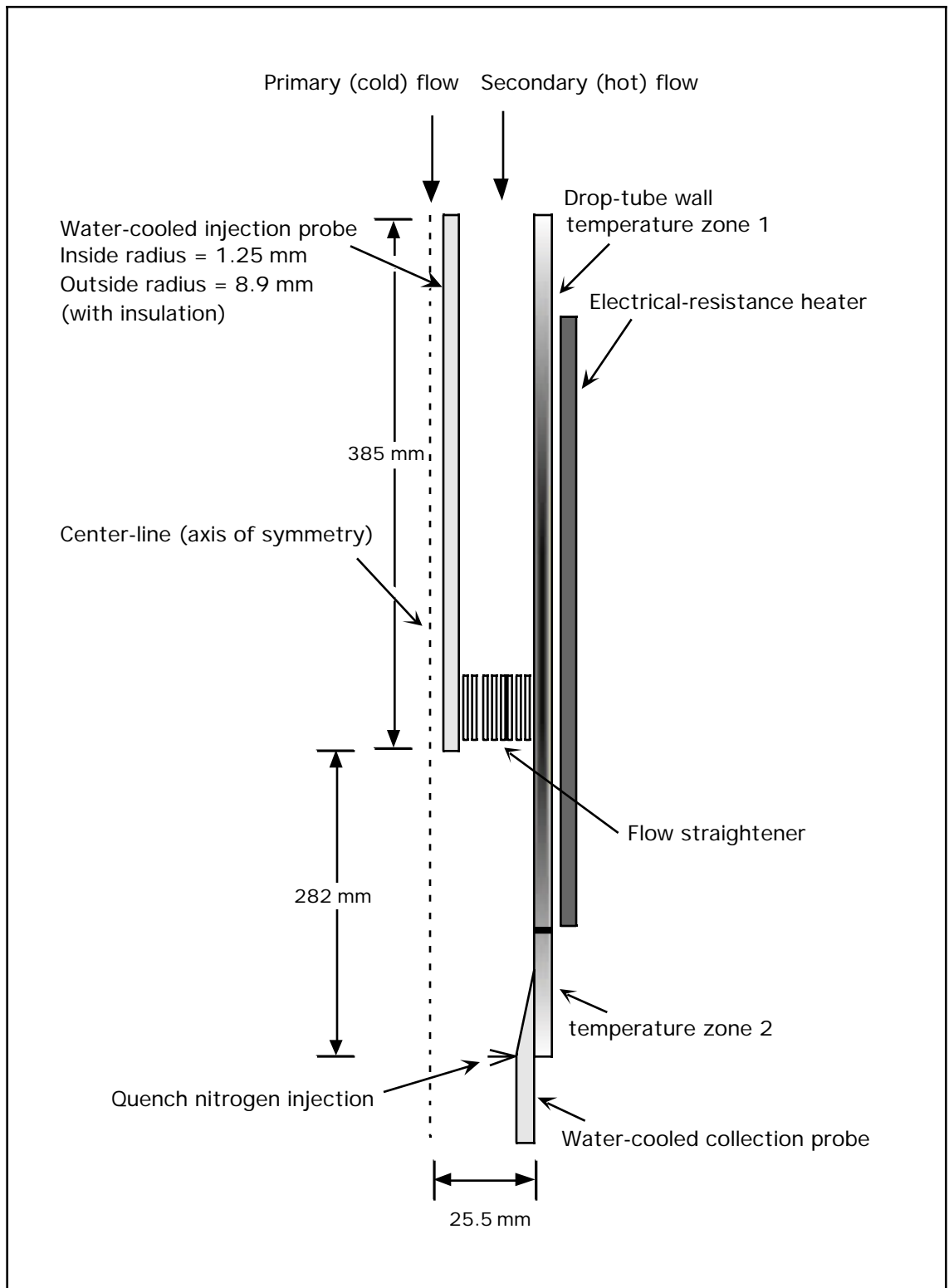


Figure G.2. Schematic of axi-symmetric slice of the drop tube reactor including the dimensions and geometry assumed in order to model gas flow field on FLUENT.

This gave the cells dimensions of 0.418 mm wide (radial dimension) by 3.38 mm long (axial dimension). Close-up schematics showing the collection probe dimensions at the drop tube exit and the injection probe radial insulation and dimensions are shown in Figures G.3 and G.4. In performing the simulations, the k-epsilon turbulence model was used with a standard wall function, and a P-1 radiation model was also used.

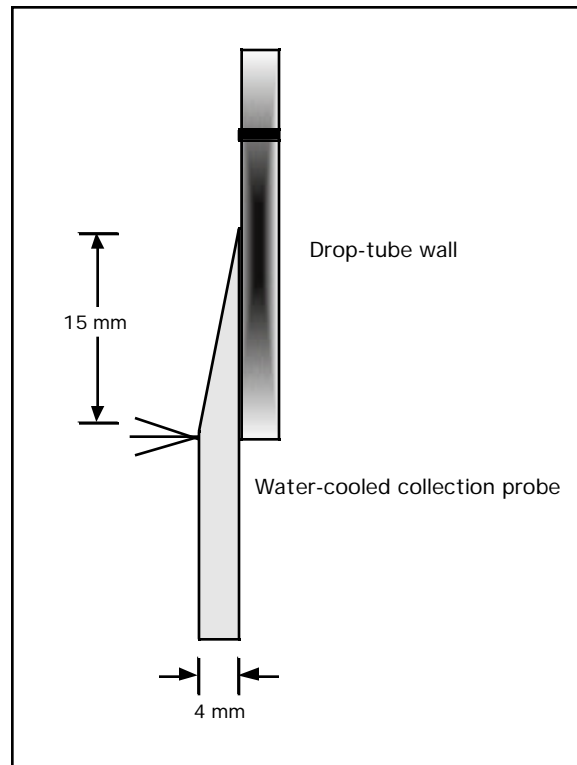


Figure G.3. Close-up schematic showing detail of dimensions used for **collection probe** in FLUENT simulations.

Material properties assumed in the calculations are given in Table G.1. Gas properties were assumed to be those of pure nitrogen as reported by Incropera and Dewitt.⁸⁹

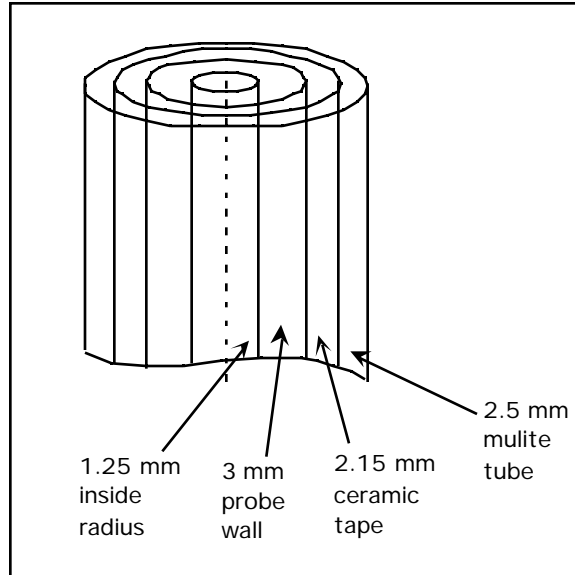


Figure G.4. Close-up schematic showing detail of radial dimensions of **injection probe** including surrounding layers of insulation, as modeled on FLUENT.

Table G.1

Summary of Material Properties Assumed for Drop Tube Gas Field Simulations

Piece	Assumed Material	Thermal Conductivity (W/m-K) ⁸⁹	Conductivity Temperature (K) ⁸⁹	Emissivity ₈₉
Injection/Collection Probe	Stainless steel (AISI 316)	-	-	0.7
Ceramic Drop Tube	Polycrystalline Al ₂ O ₃	6	1200-2000	0.5
Flow Straightener	Polycrystalline Al ₂ O ₃	6	1200-2000	0.5
Ceramic Tape	Alumina-Silica Fiber Blanket	0.15	750	-
Mulite Tube	Polycrystalline Al ₂ O ₃	6	1200-2000	0.5

The boundary conditions assumed for the FLUENT simulations are found in Table G.2. In Table G.2, flow straightener wall A is the outermost concentric cylinder, while

wall H is the innermost (closest to the injection probe) concentric flow straightener cylinder. Also in Table G.2, the drop tube wall zone 2 temperature was assumed to decrease linearly between the zone 1 temperature and the collection probe temperature.

Table G.2
Summary of Boundary Conditions Assumed for Drop Tube Gas Field Simulations by Condition

Drop Tube Condition	900 K	1000 K	1100 K	1250 K
Primary Inlet Temperature (K)	300	300	300	300
Primary Inlet Velocity (m/s)	0.87	0.80	0.85	0.70
Primary Inl. Turb. Length (m)	0.00125	0.00125	0.00125	0.00125
Secondary Inlet Temperature (K)	600	600	600	600
Secondary Inlet Velocity (m/s)	0.593	0.609	0.580	0.444
Secondary Inl. Turb. Length (m)	0.02125	0.02125	0.02125	0.02125
Wall Zone 1 Temperature (K)	1193	1295	1383	1423
Wall Zone 2 Temp. Grad. (K/m) ^a	-12,586	-13,871	-14,971	-15,443
Inject./Collect. Probe Temp. (K)	312	324	335	342
Flow Straight. Wall A Temp (K) ^b	910	1010	1110	1280
Flow Straight. Wall B Temp (K)	910	1010	1110	1280
Flow Straight. Wall C Temp (K)	905	1005	1105	1275
Flow Straight. Wall D Temp (K)	900	1000	1100	1270
Flow Straight. Wall E Temp (K)	890	990	1090	1260
Flow Straight. Wall F Temp (K)	880	980	1080	1250
Flow Straight. Wall G Temp (K)	840	940	1040	1230
Flow Straight. Wall H Temp (K)	550	650	750	900

^a Temperature zone 2 covers the last 70 mm of the drop tube wall (see Figure G.2), in which the temperature drops linearly between the zone 1 temperature and the collection probe temperature.

^b Wall A is the outermost cylinder, with walls B-H each a concentric cylinder closer to the centerline.

The particle trajectory assumed in calculating gas temperatures for use with CPD model predictions is shown in Figure G.5. The complete set of measured and predicted

(FLUENT) gas temperature and gas velocity profiles for the drop tube tests are shown in Figures G.6-G.13.

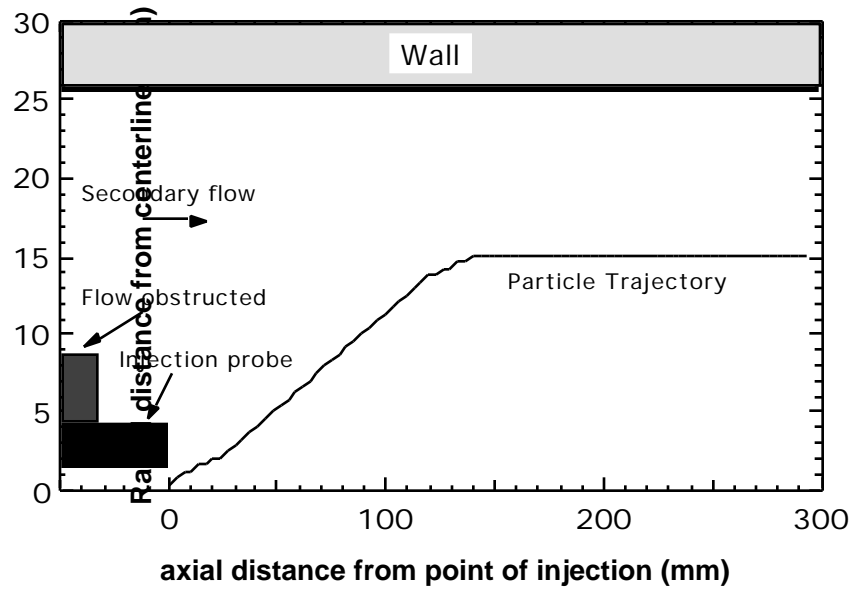


Figure G.5. Particle trajectory assumed in modeling gas temperature and velocity profiles for all drop tube pyrolysis tests. Note the large differences in length scale between the ordinate and abscissa.

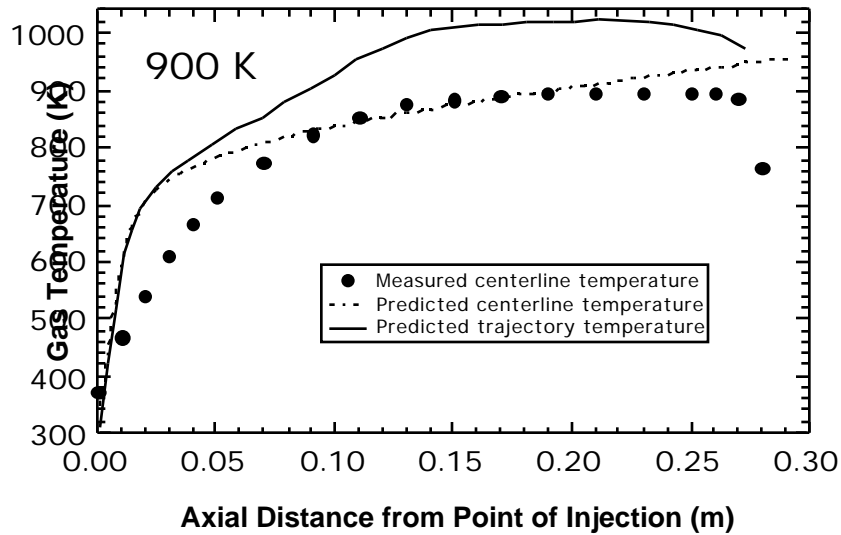


Figure G.6. Measured (symbols) and predicted (dashed line) centerline gas temperature profiles are compared to the gas temperature profile along the assumed particle trajectory (solid line) for the 900 K drop tube condition.

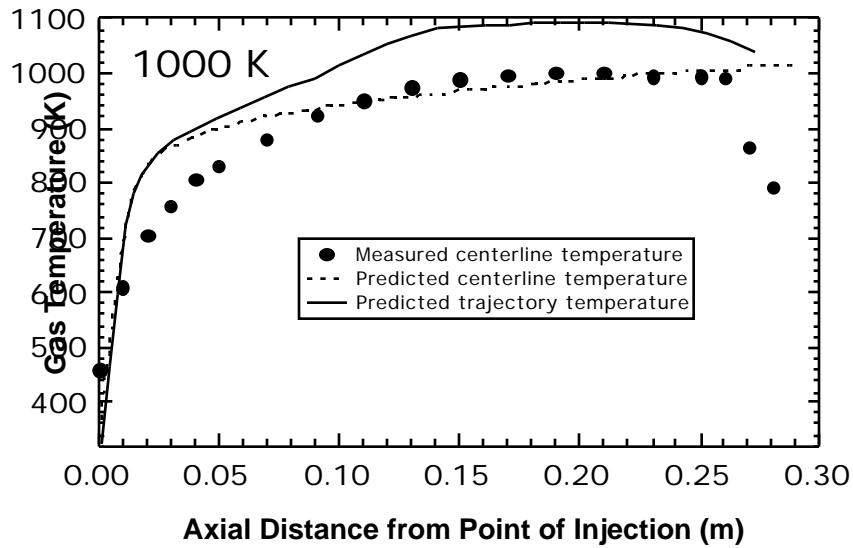


Figure G.7. Measured (symbols) and predicted (dashed line) centerline gas temperature profiles are compared to the gas temperature profile along the assumed particle trajectory (solid line) for the 1000 K drop tube condition.

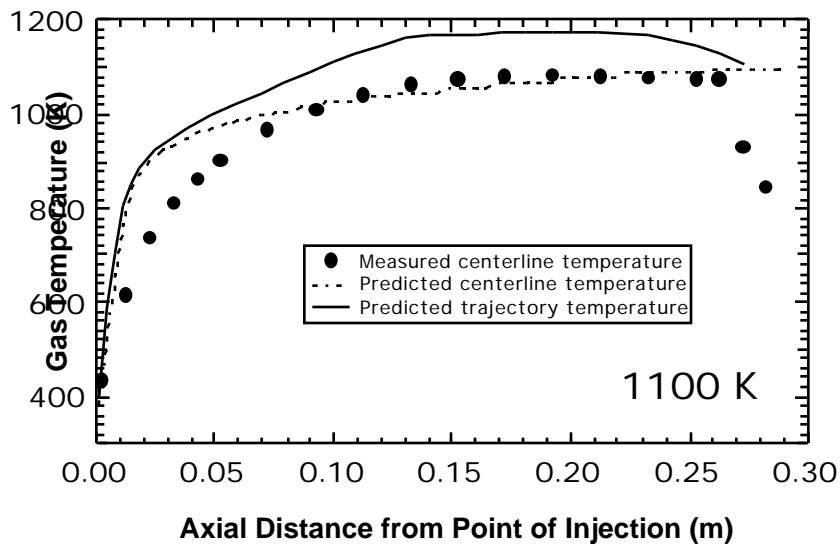


Figure G.8. Measured (symbols) and predicted (dashed line) centerline gas temperature profiles are compared to the gas temperature profile along the assumed particle trajectory (solid line) for the 1100 K drop tube condition.

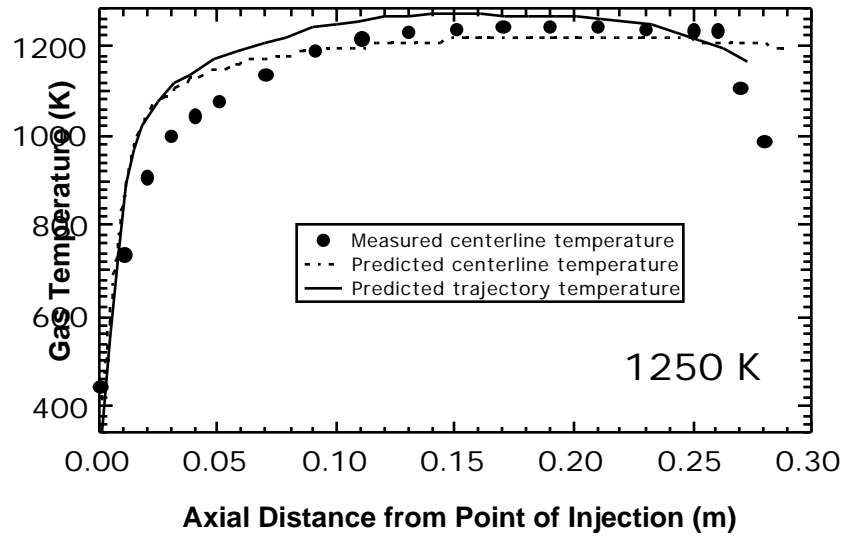


Figure G.9. Measured (symbols) and predicted (dashed line) centerline gas temperature profiles are compared to the gas temperature profile along the assumed particle trajectory (solid line) for the 1250 K drop tube condition.

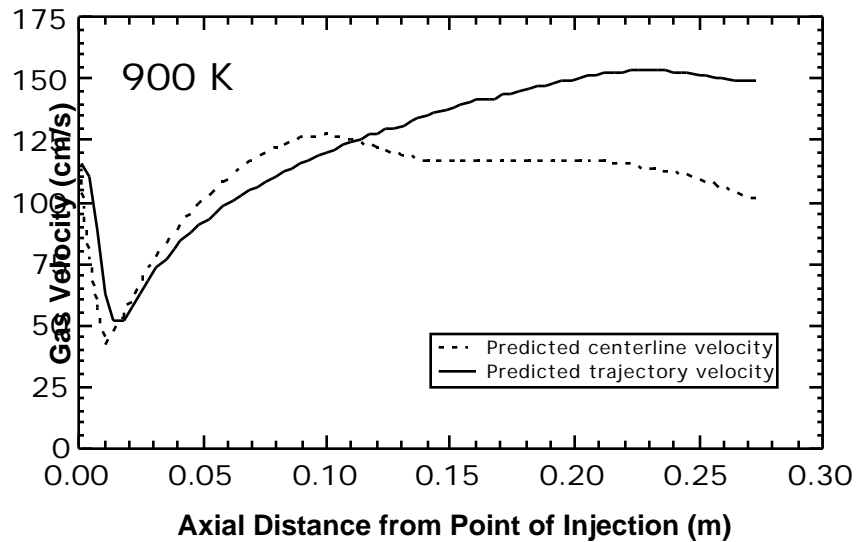


Figure G.10. Predicted centerline gas velocity profile (dashed line) compared to the gas velocity profile along the assumed particle trajectory (solid line) for the 900 K drop tube condition. Velocity profiles based on predicted (not measured) temperature profiles.

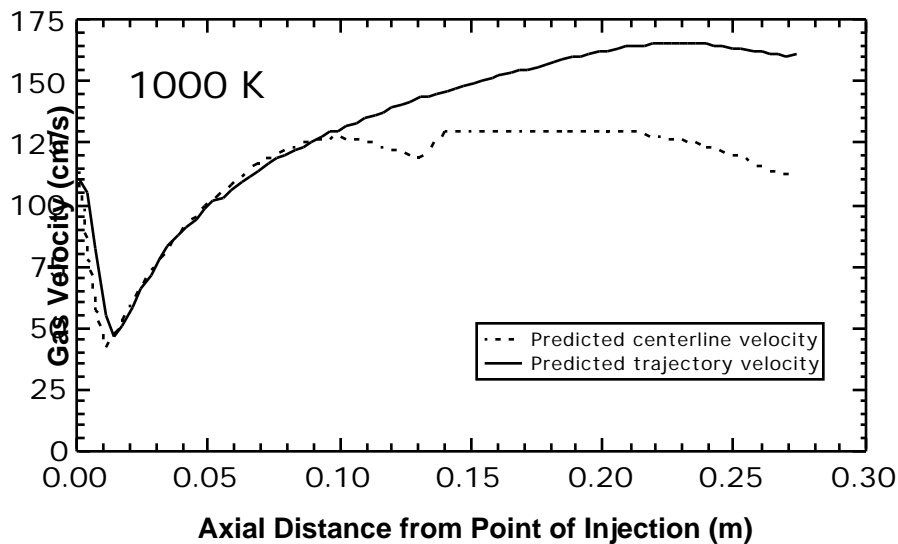


Figure G.11. Predicted centerline gas velocity profile (dashed line) compared to the gas velocity profile along the assumed particle trajectory (solid line) for the 1000 K drop tube condition. Velocity profiles based on predicted (not measured) temperature profiles.

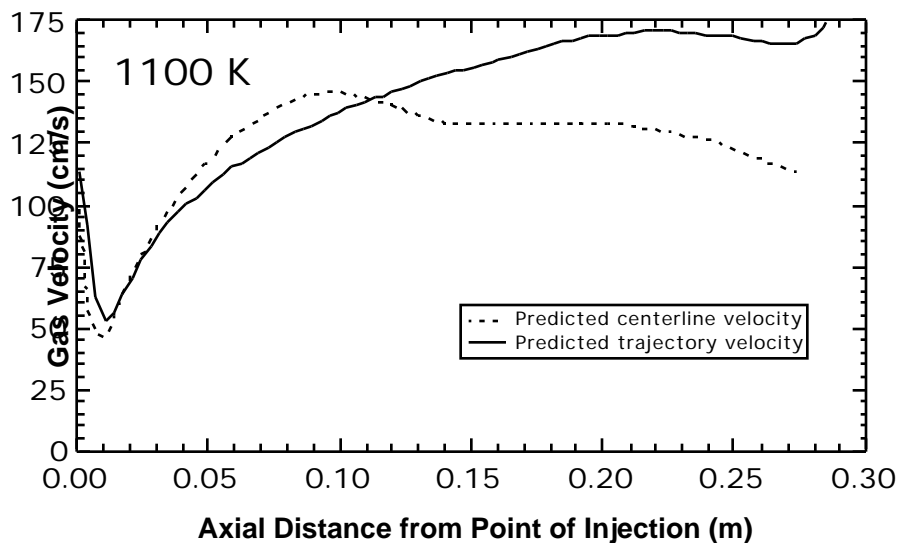


Figure G.12. Predicted centerline gas velocity profile (dashed line) compared to the gas velocity profile along the assumed particle trajectory (solid line) for the 1100 K drop tube condition. Velocity profiles based on predicted (not measured) temperature profiles.

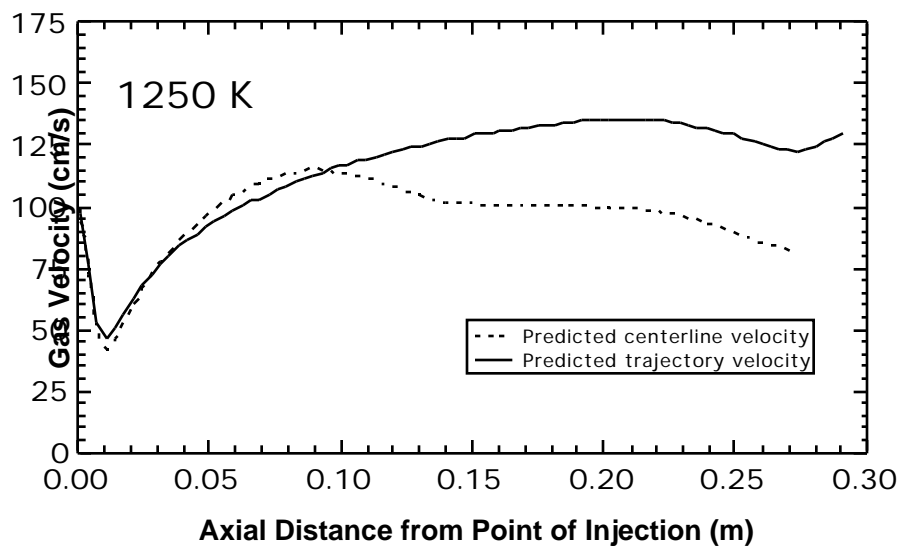


Figure G.13. Predicted centerline gas velocity profile (dashed line) compared to the gas velocity profile along the assumed particle trajectory (solid line) for the 1250 K drop tube condition. Velocity profiles based on predicted (not measured) temperature profiles.

Appendix H: Sample CPD Model Input Files

A sample input file for the CPD with the free-radical mechanism nitrogen model implemented is shown below. Free copies of the CPD source code can be found on the world-wide web (www.et.byu.edu/~tom/cpd).

```
0.535          !p0          B. Zap lignite
0.15           !c0
5.1            !sig+1
425            !mw
52             !mdel (7 will be subtracted internally to the CPD model)

2.602e15      !ab
55400         !eb
1800          !ebsig
0.9           !ac=rho
0             !ec
3.e15         !ag
69000         !eg
8100          !egsig
3.e15         !Acr (pre-exponential factor for crosslinking rate)
65000         !Ecr (Activation energy for crosslinking rate)

1.0           !pressure (atm)

18.4          !anit (Pre-exponential factor for N attack by free radical)
6000          !enit (Activation energy for N attack by free radical, cal.)
3.2e9         !aslow (slow N release pre-exponential factor)
90000         !eslow (slow N release activation energy, calories)
0.03          !fstable (initial frac. of MW decay with no radical N attack)
1.20          !yNcoal (daf mass fraction of nitrogen in parent coal)

3             !number of time points
0,300        !time(ms),temp(K)
30,2000
100,2000

5.e-5,2,5.e-4 !dt (s),print increment,max dt (s)
2.           !timax (maximum residence time [s] for calculations)
20          !nmax (maximum number of mers for tar molecular wt)
```

A sample input file for the CPD version cpdcp (which calculates particle temperatures given gas velocity and temperature as a function of distance) with the free-radical mechanism nitrogen model implemented is shown below.

```

850C_vel
850C_T
PT.out
PT8N

1.          TIMAX !maximum time (seconds)
333        TG0
72.        VG0 !cm/s
0.7        RHOP !G/CM**3
55.e-4     DP !CM
0.0        swell !(df-d0)/d0
-100.     DELHV !CAL/G (- MEANS ENDOTHERMIC)
.0072     Omegaw
.0887     OMEGAA
.75       EMIS
1383.     TWALL
1383.     THTR (1700 for high T, 1200 for Low T)
1383.     TTUBE
5.e-5,1.e-4,10      dt,dtmax,iprint

0.62      !p0 (.44)
1.0       !c0 (.16)
4.5       !sig+1
311      !mw(solum)
28       !mdel(solum)
2.602e15 !ab
55400    !eb
1800     !ebsig
0.9      !ac=rho
0        !ec
3.e15    !ag
69000    !eg
8100     !egsig
3.e15    !Acr (pre-exponential factor for crosslinking rate)
65000    !Ecr (Activation energy for crosslinking rate)
1.0      !pressure (atm)
18.4     !anit (Pre-exponential factor for N attack by free radical)
6000     !enit (Activation energy for N attack by free radical, cal.)
3.2e9    !aslow (slow N release pre-exponential factor)
90000    !eslow (slow N release activation energy, calories)
0.03     !fstable (initial frac. of MW decay with no radical N attack)

.8277    %Carbon (DAF)
.0548    %H
.0164    %N
.0673    %O
.0338    %S

```

Appendix I: Nitrogen Model Predictions

This section contains a summary of comparisons between free-radical mechanism nitrogen model predictions and experimental pyrolysis data. In making these predictions, the CPD model was used for prediction of transient tar release, total mass release, and changes in the molecular weight per cluster (M_{cl}). Furthermore, the M correction to account for the release of mass associated with c_0 was used in every case (see Equation 7.17).

Data reported by Chen³⁹ for pyrolysis of four coals in a radiatively heated drop tube reactor with a wall temperature of 1800 K was used to evaluate the performance of the nitrogen model. The results are shown in Figures I.1-I.4. Since gas temperature profiles were not measured for this experiment, the temperature profiles estimated by Genetti were used in the model predictions. In addition, since ¹³C NMR data were not available for the parent coals, the chemical structural input parameters for the CPD model were estimated using the non-linear correlations of Genetti et al.⁸⁵ In Figures I.1-I.4 it can be seen that good agreement exists between predictions and measured data, although the light gas nitrogen from experiments on the lower rank coals (Dietz and Illinois #6) is somewhat over-predicted.

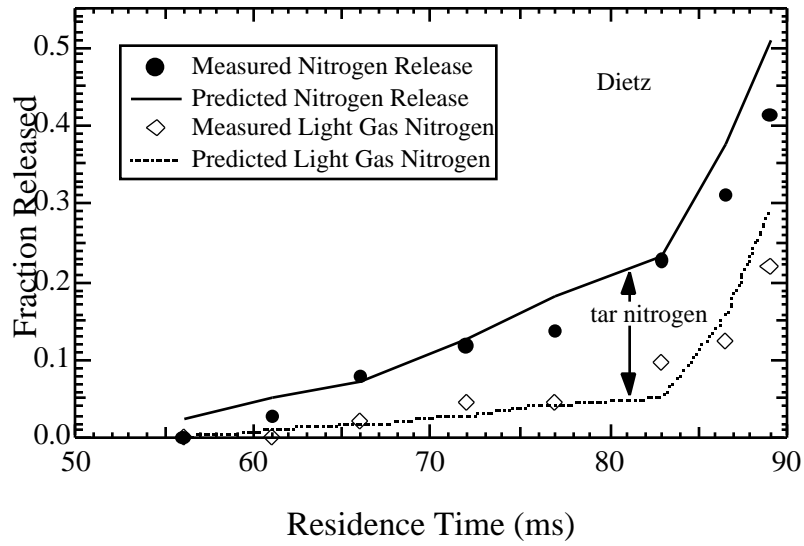


Figure I.1. Comparison of predictions of total, tar, and light gas nitrogen with experimental data from experiments conducted by Chen³⁹ on a Dietz subbituminous coal.

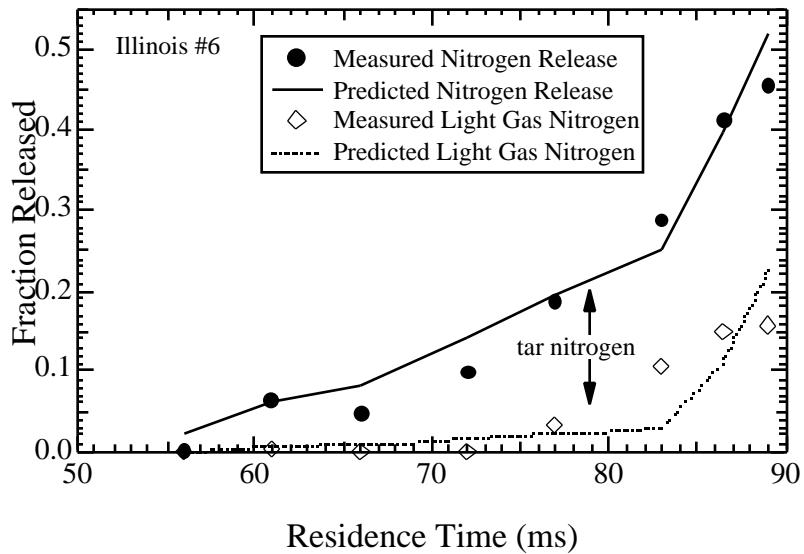


Figure I.2. Comparison of predictions of total, tar, and light gas nitrogen with experimental data from experiments conducted by Chen³⁹ on an Illinois #6 bituminous coal.

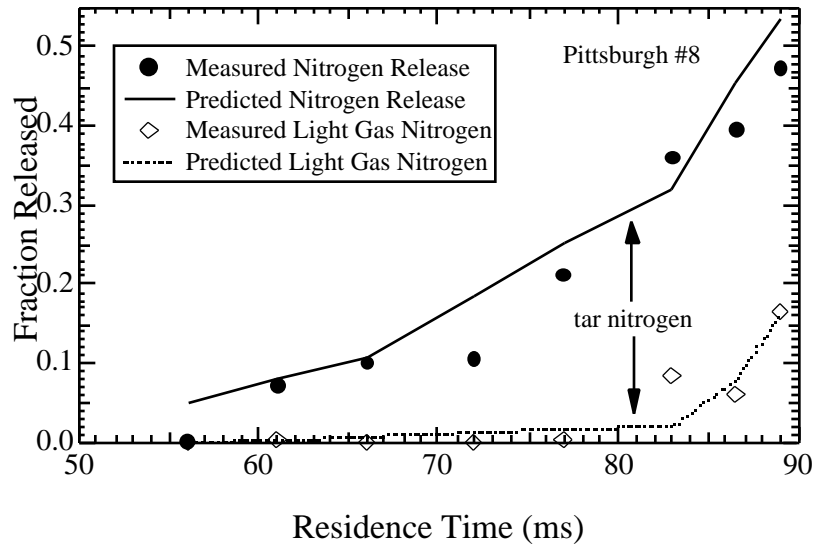


Figure I.3. Comparison of predictions of total, tar, and light gas nitrogen with experimental data from experiments conducted by Chen³⁹ on a Pittsburgh #8 bituminous coal.

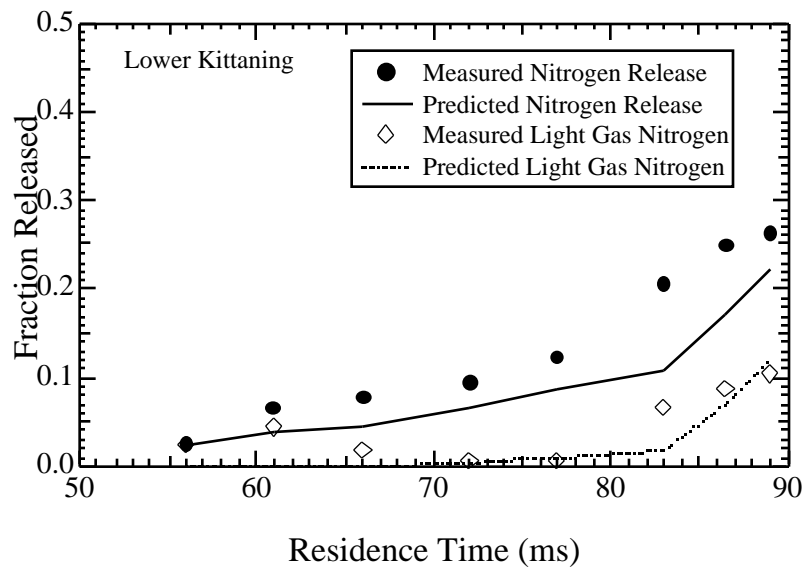


Figure I.4. Comparison of predictions of total, tar, and light gas nitrogen with experimental data from experiments conducted by Chen³⁹ on a Lower Kittanning low volatile bituminous coal.

In Figures I.5-I.7, predicted mass and nitrogen release values are compared to measured data reported by Fletcher and Hardesty⁵ for pyrolysis in a drop tube reactor with 1050 and 1250 K maximum gas temperatures and in a flat flame reactor with maximum gas temperatures of 1600 K. Figures I.8-I.17 compare predicted char N_{site} and nitrogen content values as a function of residence time for the complete set of Sandia⁵ drop tube data. The data have been normalized to the parent coal values for ease of comparison.

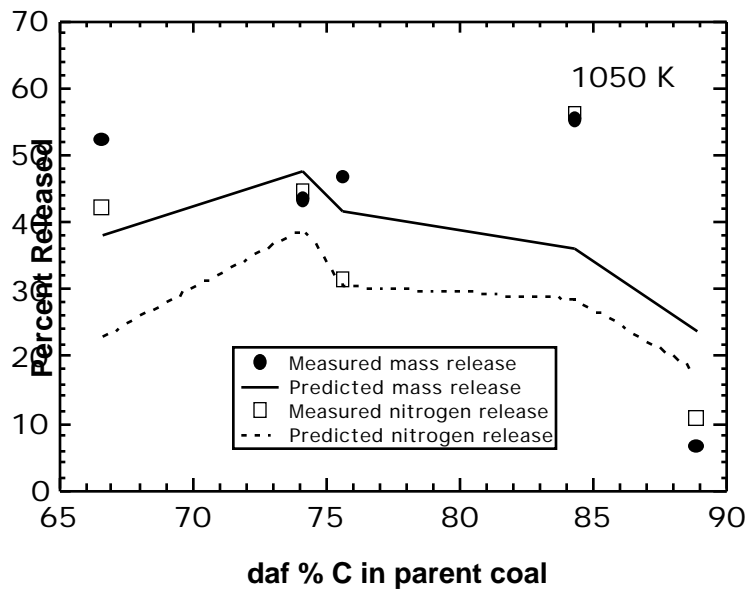


Figure I.5. Comparison of predicted and measured mass and nitrogen release for coals pyrolyzed in a drop tube reactor at Sandia with a 1050 K maximum gas temperature.⁵ Carbon content is used as a rank indicator.

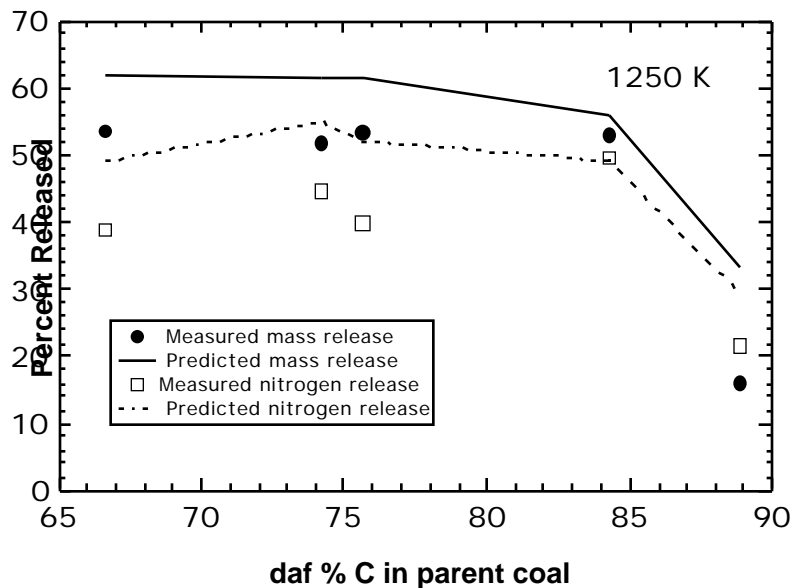


Figure I.6. Comparison of predicted and measured mass and nitrogen release for coals pyrolyzed in a drop tube reactor at Sandia with a 1250 K maximum gas temperature.⁵ Carbon content is used as a rank indicator.

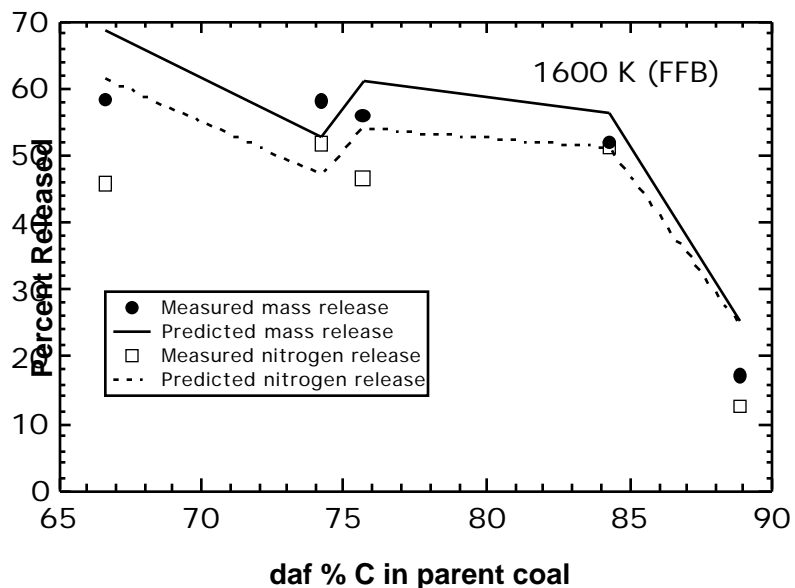


Figure I.7. Comparison of predicted and measured mass and nitrogen release for coals pyrolyzed in a flat-flame burner (FFB) at Sandia with a 1600 K maximum gas temperature.⁵ Carbon content is used as a rank indicator.

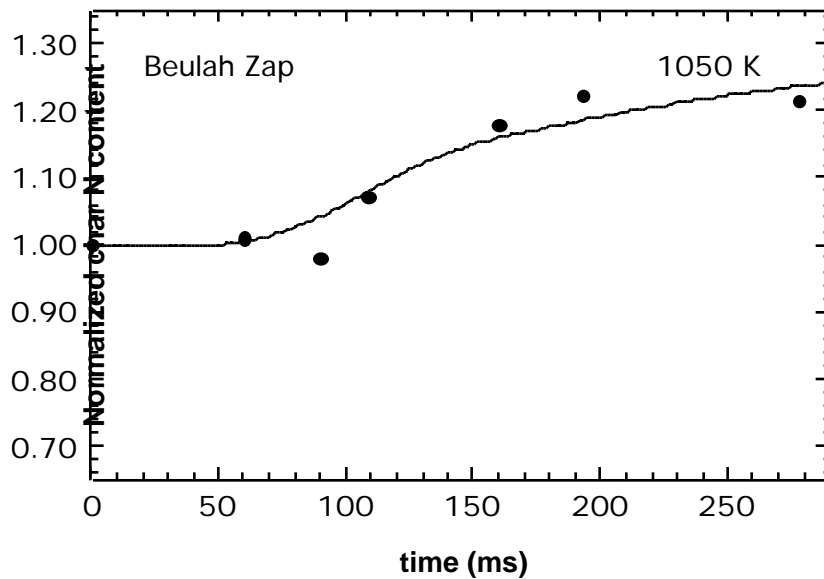


Figure I.8. Comparison of predicted and measured char nitrogen content values for a North Dakota lignite pyrolyzed at Sandia⁵ in a drop tube reactor with a 1050 K maximum gas temperature.

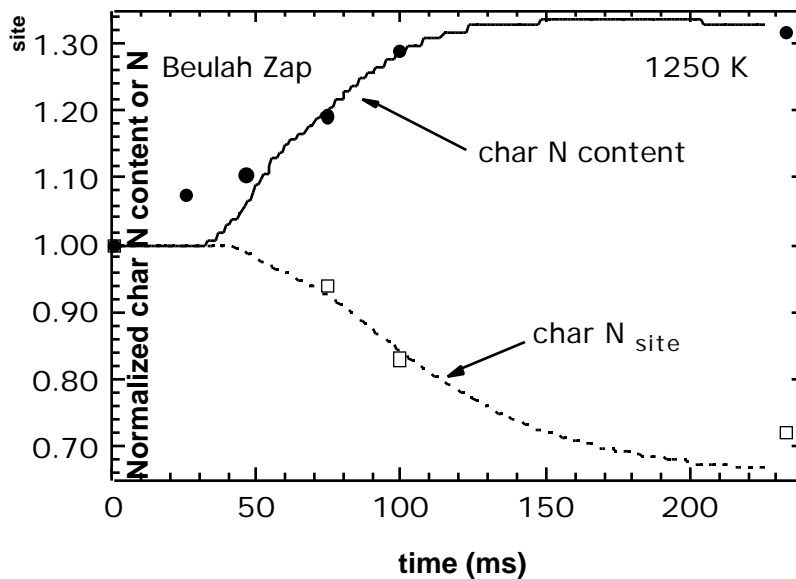


Figure I.9. Comparison of predicted and measured char nitrogen content and char N_{site} values for a North Dakota lignite pyrolyzed at Sandia⁵ in a drop tube reactor with a 1250 K maximum gas temperature.

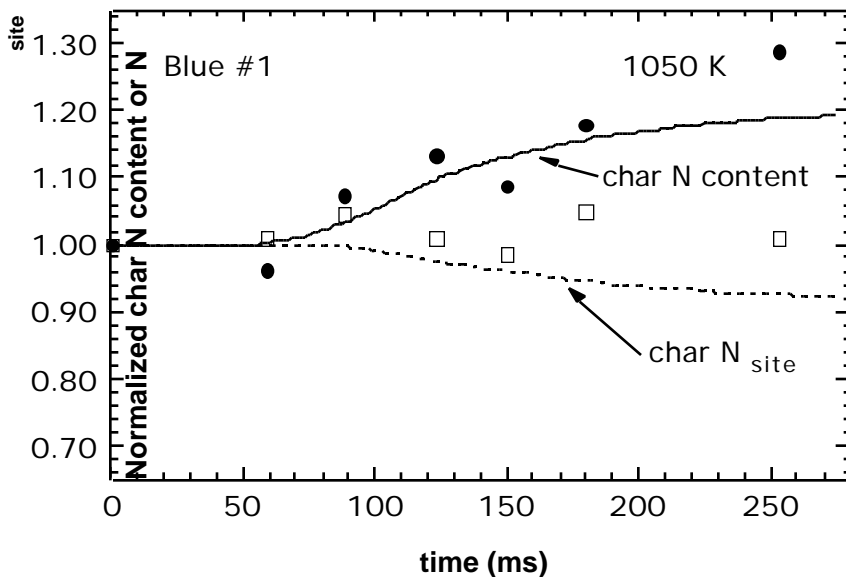


Figure I.10. Comparison of predicted and measured char nitrogen content and char N_{site} values for a Blue #1 subbituminous coal pyrolyzed at Sandia⁵ in a drop tube reactor with a 1050 K maximum gas temperature.

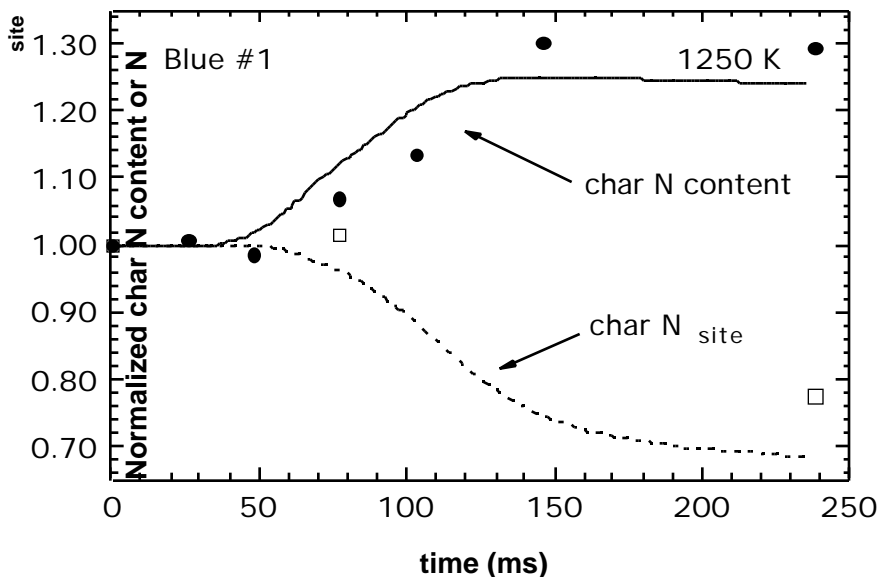


Figure I.11. Comparison of predicted and measured char nitrogen content and char N_{site} values for a Blue #1 subbituminous coal pyrolyzed at Sandia⁵ in a drop tube reactor with a 1250 K maximum gas temperature.

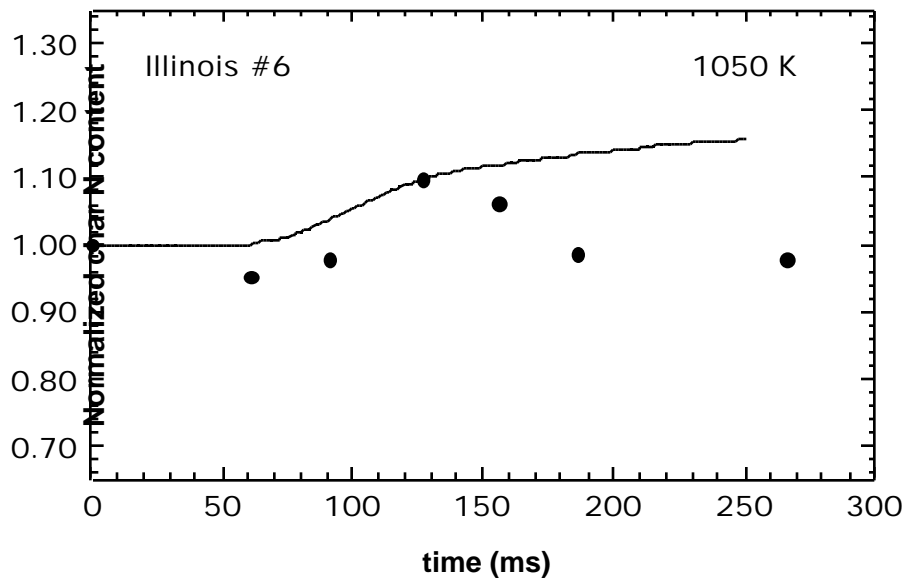


Figure I.12. Comparison of predicted and measured char nitrogen content values for an Illinois #6 bituminous coal pyrolyzed at Sandia⁵ in a drop tube reactor with a 1050 K maximum gas temperature.

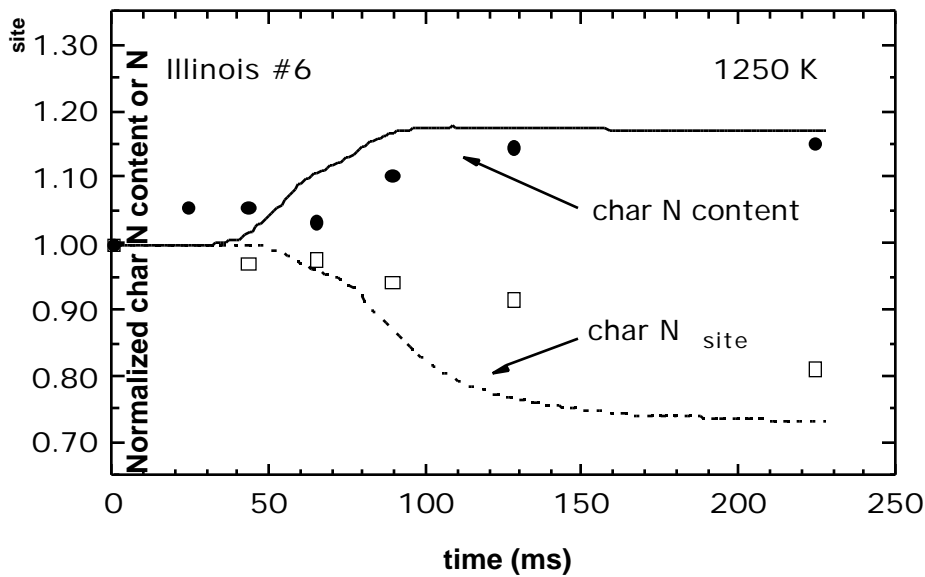


Figure I.13. Comparison of predicted and measured char nitrogen content and char N_{site} values for an Illinois #6 bituminous coal pyrolyzed at Sandia⁵ in a drop tube reactor with a 1250 K maximum gas temperature.

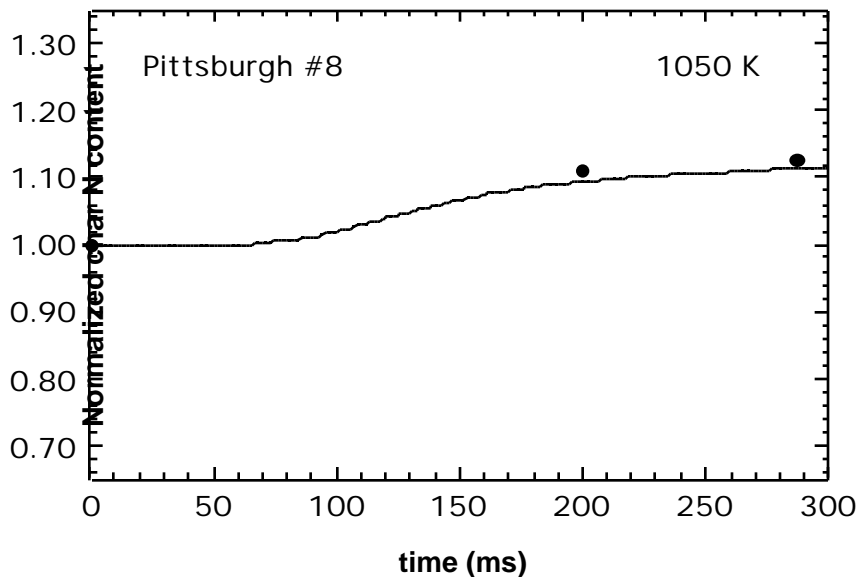


Figure I.14. Comparison of predicted and measured char nitrogen content values for a Pittsburgh #8 bituminous coal pyrolyzed at Sandia⁵ in a drop tube reactor with a 1050 K maximum gas temperature.

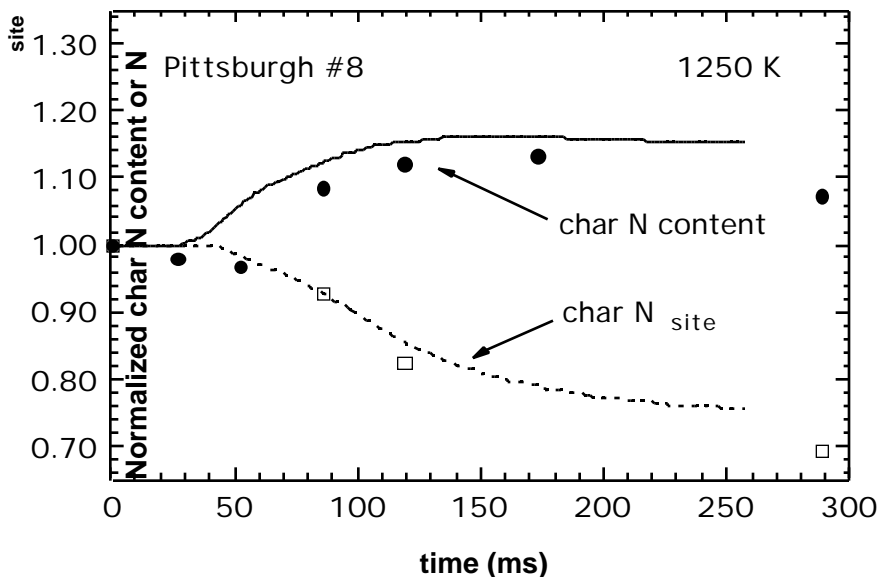


Figure I.15. Comparison of predicted and measured char nitrogen content and char N_{site} values for a Pittsburgh #8 bituminous coal pyrolyzed at Sandia⁵ in a drop tube reactor with a 1250 K maximum gas temperature.

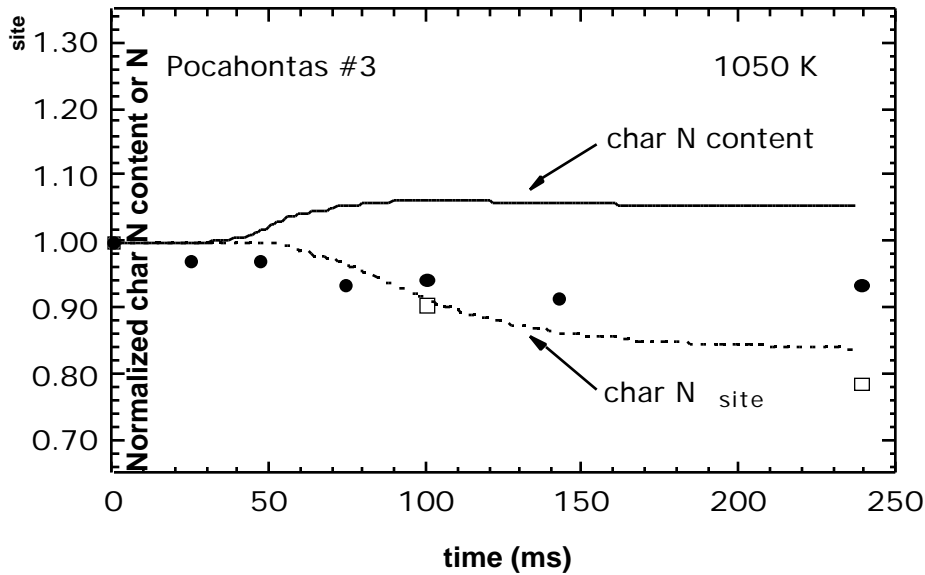


Figure I.16. Comparison of predicted and measured char nitrogen content and char N_{site} values for a Pocahontas #3 low volatile bituminous coal pyrolyzed at Sandia⁵ in a drop tube reactor with a 1050 K maximum gas temperature.

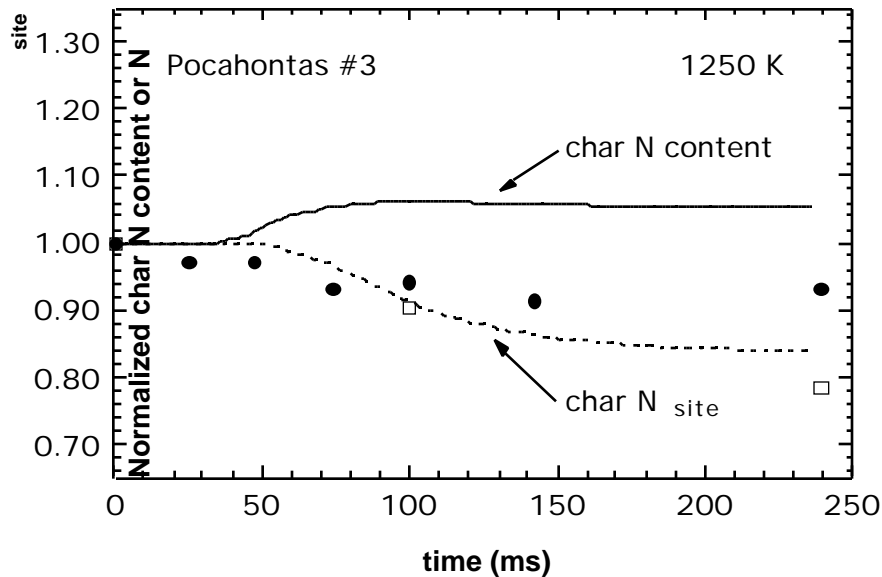


Figure I.17. Comparison of predicted and measured char nitrogen content and char N_{site} values for a Pocahontas #3 low volatile bituminous coal pyrolyzed at Sandia⁵ in a drop tube reactor with a 1250 K maximum gas temperature.

The rest of this section contains the remainder of the nitrogen release comparisons found in the body of this dissertation.

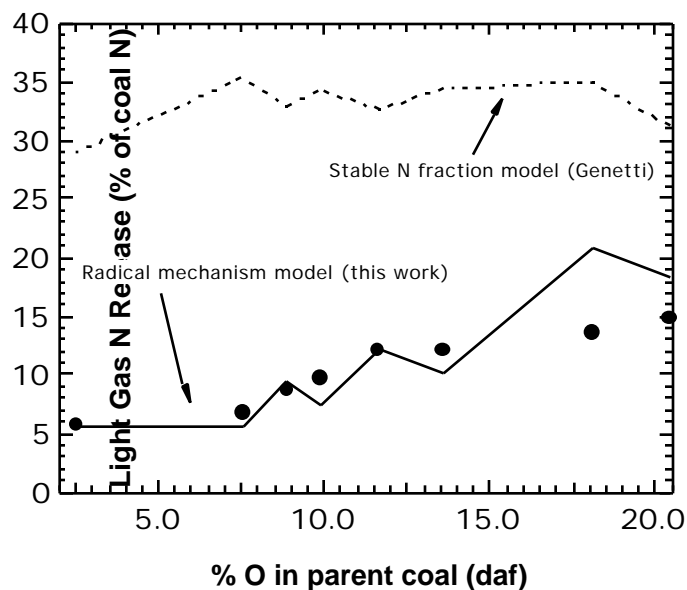


Figure I.18. Comparison of predicted total light gas nitrogen yields with the measured HCN + NH₃ yields reported by Bassilakis et al.¹ for 0.5 K/sec pyrolysis of the Argonne premium coals with a maximum particle temperature of 1173 K. Predictions made using parent coal ¹³C NMR structural parameters reported by Smith et al.¹⁹

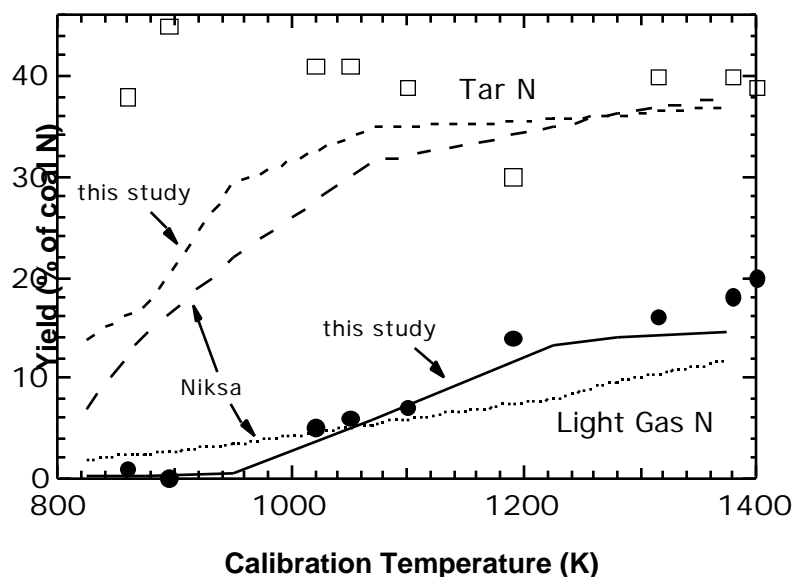


Figure I.19. Comparison of predicted (lines) light gas nitrogen and tar nitrogen yields with measured HCN (circles) and tar nitrogen (squares) yields observed by Friehaut et al.⁸⁶ for vacuum pyrolysis (0.015 Mpa) of a Pittsburgh coal at 20-460 K/s heating rate using a heated grid apparatus. Measured data, predictions of Niksa, and particle temperature profiles used are those reported by Niksa.⁷² Predictions of this study made assuming that the parent coal ¹³C NMR structural parameters are those reported by Fletcher and Hardesty for Pittsburgh #8 coal.⁵

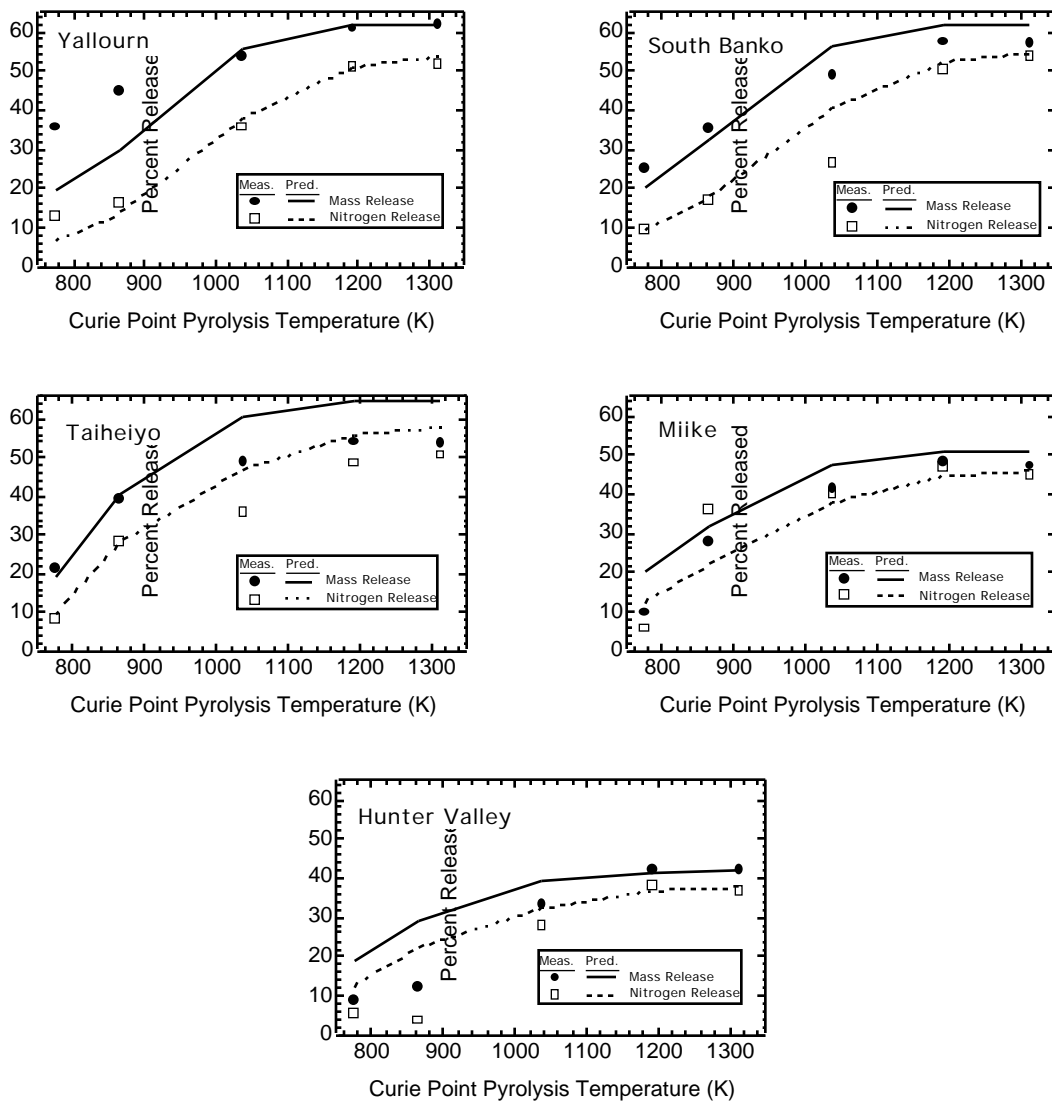


Figure I.20. Comparison of predicted (lines) and measured (symbols) mass and nitrogen release for Curie point pyrolysis experiments reported by Nomura et al. (5 second pyrolysis time).⁸⁷

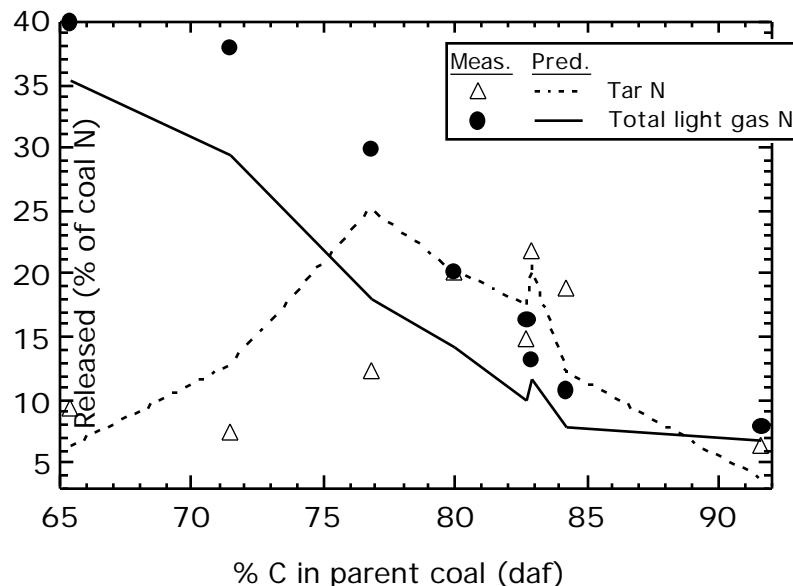


Figure I.21. Comparison of predicted (lines) and measured (symbols) total light gas nitrogen and tar nitrogen release for furnace pyrolysis of eight coals at 1273 K. Experimental data from Nomura et al. for a 10 K/s heating rate and a 10 second hold time.⁸⁷ Measured total light gas nitrogen includes HCN, NH₃, and N₂. These experiments probably experienced significant secondary reaction, which explains the disagreement.

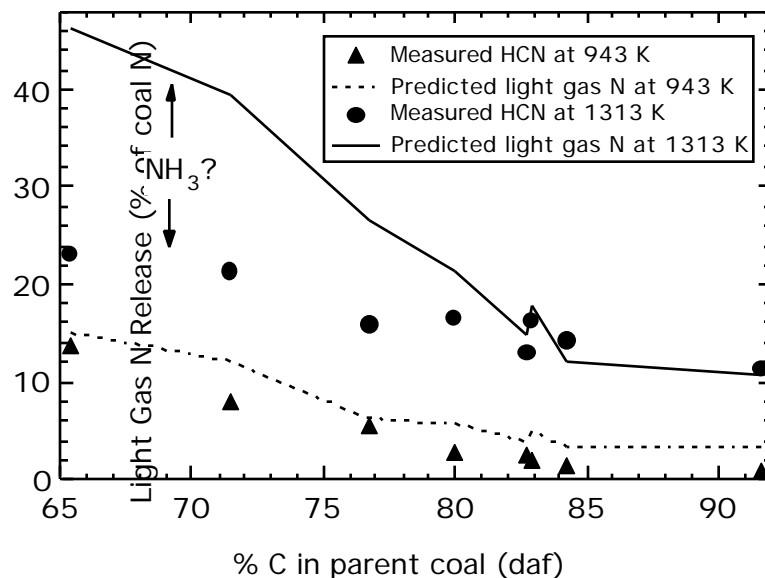


Figure I.22. Comparison of predicted *total light gas release* (lines) and measured *HCN release* (symbols) for Curie point pyrolysis experiments reported by Nomura et al. at 943 K and 1313 K (3 second pyrolysis time).⁸⁷

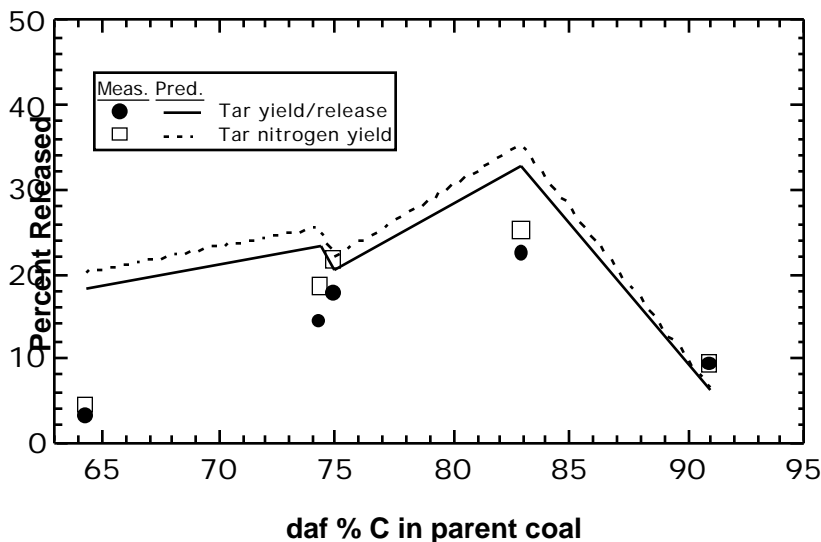


Figure I.23. Comparison of predicted (lines) and measured (symbols) tar and tar nitrogen yields for drop tube pyrolysis experiments performed by Hambly at 1080 K (282 ms residence time).¹¹ Predictions made using measured parent coal ¹³C NMR structural parameters reported by Hambly.¹¹

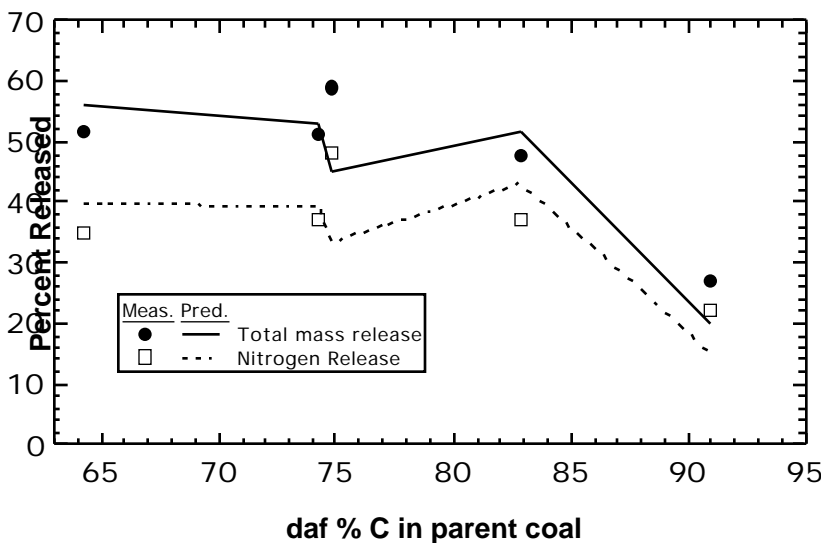


Figure I.24. Comparison of predicted (lines) and measured (symbols) total mass and nitrogen release for drop tube pyrolysis experiments performed by Hambly at 1080 K (282 ms residence time).¹¹ Predictions made using measured parent coal ¹³C NMR structural parameters reported by Hambly.¹¹

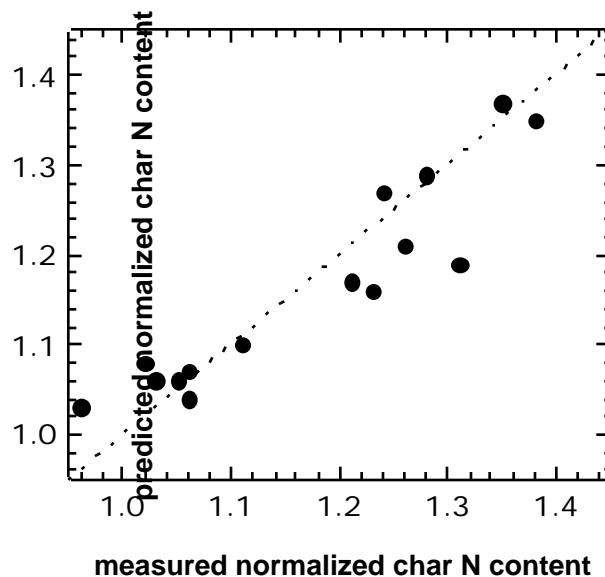


Figure I.25. Parity plot of predicted and measured char nitrogen content normalized to the parent coal nitrogen content for drop tube pyrolysis experiments performed by Hambly at 820 K, 1080 K, and 1220 K.¹¹ Predictions made using measured parent coal ¹³C NMR structural parameters reported by Hambly.¹¹

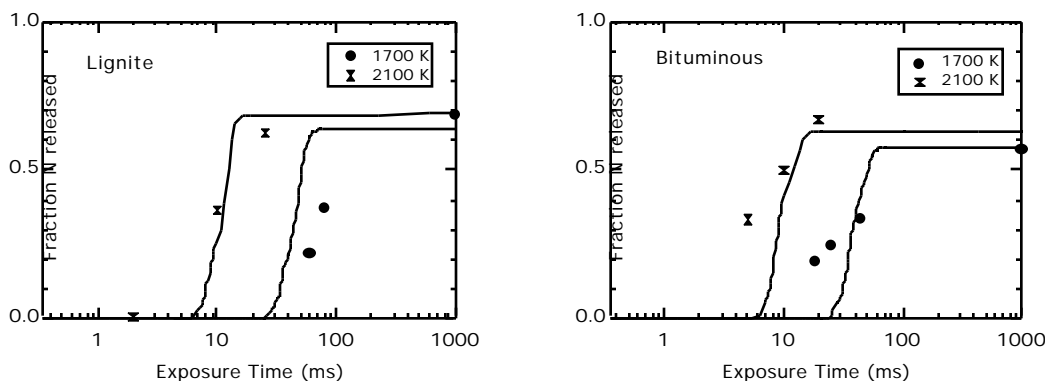


Figure I.26. Comparisons of predicted and measured nitrogen released as a fraction of parent coal nitrogen for a lignite and a bituminous coal pyrolyzed in a drop tube or fast flow furnace. Measured data reported by Pohl and Sarofim.⁷ Chemical structure approximated to be those of Beulah Zap lignite and Pittsburgh #8 for the lignite and bituminous coals respectively (structural data from Fletcher and Hardesty)⁵. Assumed particle temperature profiles are only rough approximations corresponding to the reported maximum gas temperatures.

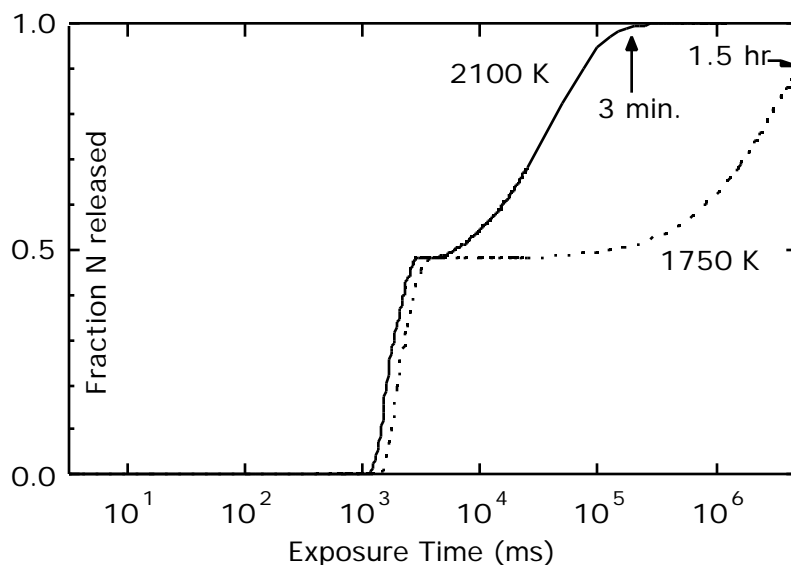


Figure I.27. Predicted nitrogen released as a fraction of parent coal nitrogen for a bituminous coal pyrolyzed in a crucible at 2100 K and 1750 K for very long residence times. The chemical structure was approximated to be that of Pittsburgh #8 (structural data from Fletcher and Hardesty)⁵. Particles were assumed to reach the maximum temperature within 5 seconds.

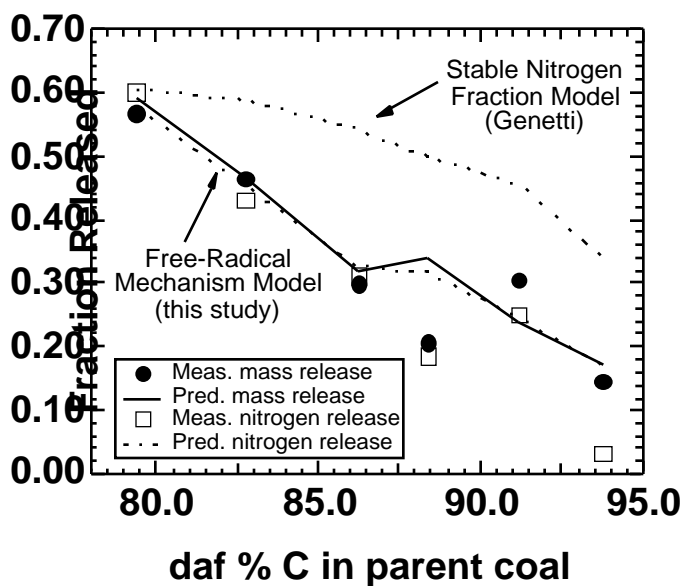
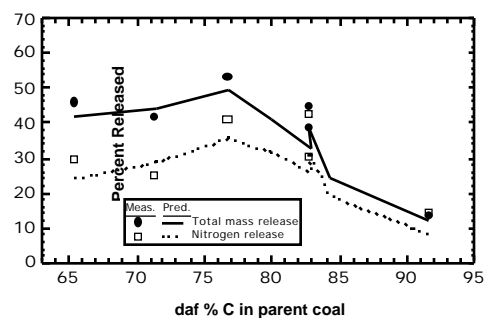
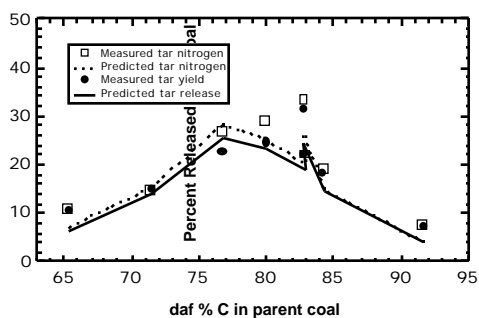
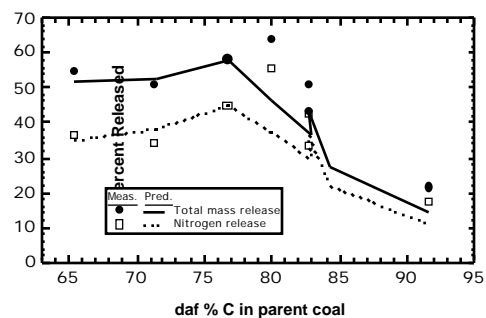
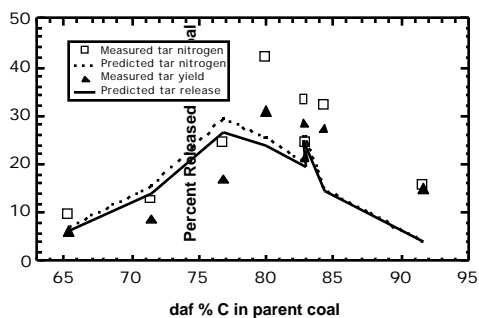


Figure I.28. Comparison of predicted mass and nitrogen release values with measured mass and nitrogen release values reported by Genetti⁹ for flat flame reactor pyrolysis experiments at 1650 K and 78 ms residence time. Also shown are nitrogen release values predicted using the stable nitrogen fraction model of Genetti.⁹ Predictions made using measured parent coal ¹³C NMR structural parameters reported by Genetti.⁹

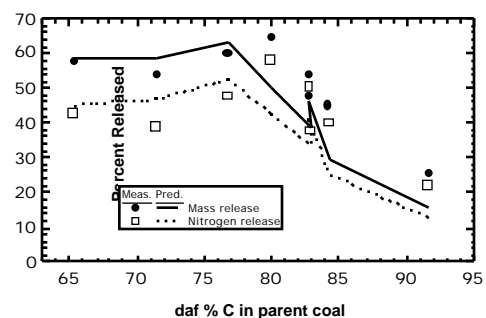
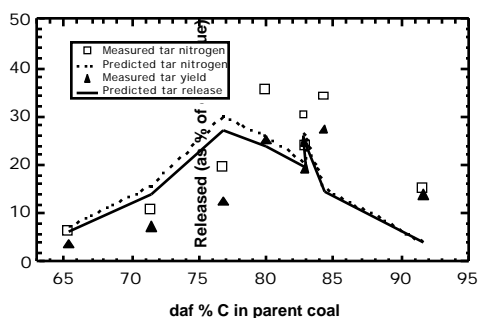
900 K



1000 K



1100 K



1650 K

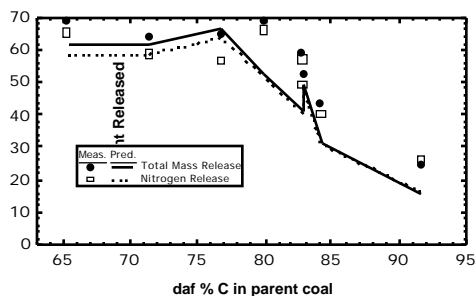
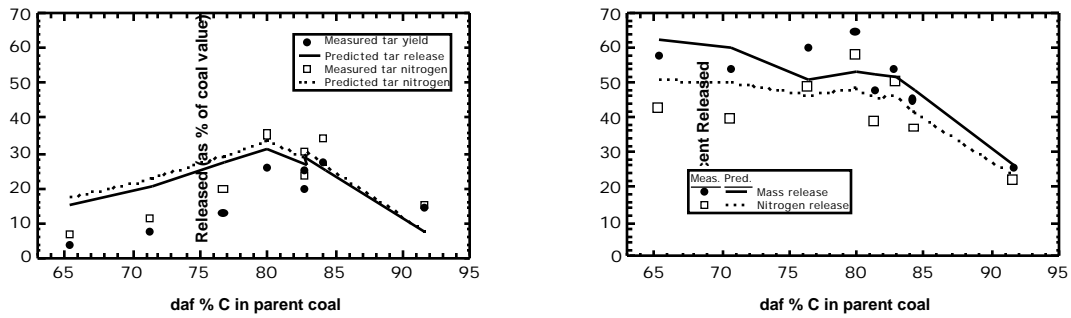


Figure I.29. Comparison of predicted and measured tar and tar nitrogen yields and predicted and measured total mass and nitrogen release for drop tube and flat flame reactor pyrolysis experiments. Predictions made using measured ^{13}C NMR structural parameters.

1100 K



1650 K

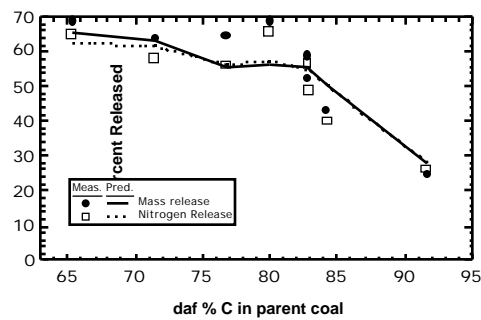


Figure I.30. Comparison of predicted and measured tar and tar nitrogen yields and predicted and measured total mass and nitrogen release for 1100 K drop tube and 1650 K flat flame reactor pyrolysis experiments. Predictions made using correlation of Genetti et al.⁸⁵ to estimate parent coal structural parameters.

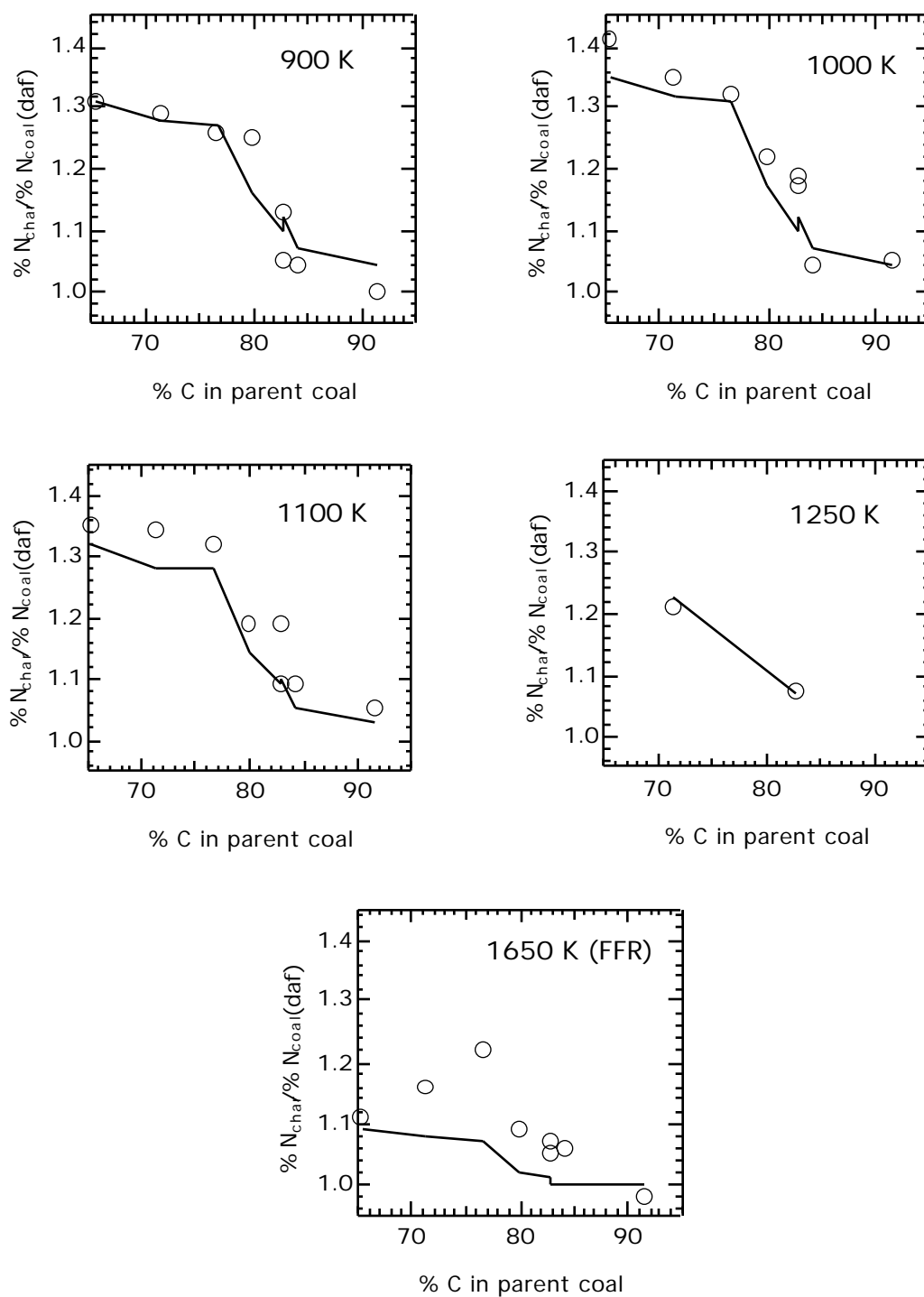


Figure I.31. Predicted (lines) and measured (symbols) values of char nitrogen content normalized to the parent coal nitrogen content for drop tube and flat flame reactor pyrolysis experiments. Carbon content is used as an indicator of rank.